Engine-Driven Synchronous Generators: Design Considerations for Grid Code Compliance

Sridhar Narayanan

Thesis submitted to the University of Nottingham for the degree of Doctor of Philosophy, December 2019



PREFACE

Between 2010 and 2015, due to the growing dependence of the European grids on renewable sources of energy, the power generation market saw a shift to regulated de-centralized power; the power-plants connected to the grids in Europe had to comply with a set of criteria intended to increase grid stability. Initially these ‘grid codes’ were only imposed on wind and solar farms but were slowly introduced to power-plants driven by reciprocating engines and hydro-power as well. These power-plants were also given a very short-notice to comply with the grid codes. In a market that had always designed for power-density, efficiency and ultimately cost, the introduction of grid-codes presented many unique challenges that would potentially impact not just competitive advantage of these power-plant owner/operators, but also their long-term survival and that of their component manufacturers. The reciprocating engines being the most expensive components in a power-plant could exercise their ‘power’ by delegating most of the grid-code compliance to other system and sub-system manufacturers, specifically the manufacturers of synchronous generators. This was the reason several synchronous generator manufacturers, including Cummins Generator Technologies invested a lot of resources to understand and develop solutions that would not only help them survive, but also potentially propel them ahead of competition.

The work presented in this thesis led to an extensive work covering all aspects of synchronous generator design specific to grid code compliance including, but not limited to understanding and articulating grid-codes and their demands from synchronous generator design, impact of the reciprocating engines on the

performance of the synchronous generator in a ‘grid-code’ environment and therefore led to numerous collaborative work with various engine manufacturers, including Cummins Generator Technologies’ parent company – Cummins Engines and the various factors that would affect the reliability of the synchronous generator and methods to improve them. All this work was led by the author Sridhar Narayanan with a cross-functional team of mechanical, electrical and thermal engineers through a program that lasted almost 5 years and resulted in numerous webinars given to customers of Cummins Generator Technologies, conference talks, white papers, a masters’ thesis, a patent and a product line that helped establish Cummins Generator Technologies as an industry leader in designing and selecting synchronous generators for grid codes. These outcomes have been listed in the next section.

KEY DELIVERABLES

WHITE PAPERS

1) '*Critical Parameters of a synchronous alternator for a grid code compliant generating set'*, www.stamford-avk.com/media/white-papers.
2) '*Fault Ride Through Effects on Alternators Connected to a Grid*', www.stamford-avk.com/media/white-papers.
3) '*Benefits and challenges of a grid coupled wound rotor synchronous generator in a wind turbine application'*, www.stamford-avk.com/media/white-papers.

CONFERENCE PROCEEDINGS & MAGAZINE PUBLICATIONS

1) S.Narayanan et.al, '*An Analytical Tool to check for static grid code compliance of generating sets'*, Proceedings of the Universities Power Engineering Conference (UPEC), 2010.
2) Sridhar Narayanan et.al, '*Low Voltage ride through performance of a 4 MVA synchronous generator – measurements and simulations*', 7th IET International Conference on Power Electronics, Machines and Drives (PEMD 2014).
3) Sridhar Narayanan, '*Critical Parameters of a synchronous alternator for grid code compliant generating set',* Proceedings of Powergen Europe, 2012, Cologne.

4) Sridhar Narayanan et.al., *'Fault Ride through effects on Alternators connected to the Grid'*, Proceedings of PowerGen Asia, 2011.
5) Sridhar Narayanan, '*Seeking Synchronicity',* Power Engineering International, 2012.

TALKS

1) '*Grid-Locked: Challenges with Designing Synchronous Generators for the Grid'* - UKMagSoc, May 24th, 2017.

MASTERS' THESIS

1) Petr Chmelicek, '*Synchronous Generator Reactance Prediction using FE Analysis',* 2010.

PATENT(S)

1) '*Reducing fault current in an electrical generator',* GB2494166 (filed: 31st August 2011, Granted: 27th November, 2018).

ABSTRACT

This thesis aims to provide a set of design criteria for designing synchronous generators (SGs) for engine driven generating sets to meet the emerging grid code requirements.

Historically, central plants have been an integral part of the electric grid, in which the power generation facilities are typically located closer to the resources or further away from the loads. Liberalization of the energy market in the early parts of the 21st century combined with stringent environmental policies and emission regulation have forced electrical energy providers to opt for renewable sources and distributed generation. While both these methods of power generation offer better efficiency and economies of scale compared to large power plants, they introduce instability in the grid. To ensure stable supply of electrical power to consumers, many transmission and distribution system operators are enforcing performance expectations on power plants connected to the grid – Grid Codes. These regulations pose great design challenges to the manufacturers and designers of generating sets and associated components, especially synchronous generator (SG) manufacturers.

In this work, relevant grid codes are analyzed and specific requirements are defined. A practical and quick analysis method is developed and then used to simulate engine driven SGs connected to electric grid. A neural network based simplification is applied to minimize the number of simulations required to provide guidelines for designing SGs for grid code compliance. Low Voltage Ride Through tests are

performed to validate the proposed guidelines. The effects of system solutions on the design parameters are also briefly analyzed.

The proposed design criteria are applied to SGs and are validated through grid code certification tests. As vessel to prove the validity of the concepts mentioned above, a 1400 KVA alternator is prototyped and experimental measurements are finally performed. The work presented in the thesis has led to a comprehensive understanding of grid codes and their effect on design and selection of engine driven SGs is obtained and a granted patent on a novel retrofit-able method to reduce fault currents in a SG.

TABLE OF CONTENTS

Contents

PREFACE 2

KEY DELIVERABLES 4

WHITE PAPERS 4

CONFERENCE PROCEEDINGS & MAGAZINE PUBLICATIONS 4

TALKS 5

MASTERS' THESIS 5

PATENT(S) 5

ABSTRACT 6

TABLE OF CONTENTS 8

ACKNOWLEDGMENTS 14

LIST OF TABLES 16

LIST OF FIGURES 18

INTRODUCTION 30

1.1 Evolution of the more distributed grid 30

1.2 Grid Codes 35

1.3 Problem Description and project objectives 38

1.4 Thesis Contributions 41

1.5 Structure of thesis 41

GRID CODES 43

2.1 Introduction to Grid Codes 43

2.2 Grid Codes – Terminology & Content 45

2.2.1 Grid Codes – Terminology 45

2.2.2 Grid Codes – Content 48

2.2.3 Compliance testing and validation 53

2.3 Impact of grid codes on performance of engine driven SGs 55

TABLE OF CONTENTS

2.4 Solutions adopted by the Renewables Industry 62

2.5 Conclusion 64

SG Modelling 66

3.1 Literature Review 67

3.1.1 Basic Theory & Construction 67

3.1.2 Equivalent Circuit Model of the SG 68

3.1.4 The Finite Element Method 70

3.1.4 Predicting Electrical Machine Reactance using Finite Element Analysis 72

3.2 Finite Element Tool Development 75

3.2.1 Overview 75

3.2.2 Computational Algorithm for SG Reactances calculation. 75

3.2.2.1 Computational Algorithm for SG Reactances calculation 76

3.2.3 Validation of SG Parameter prediction tool 90

3.4 User interface for finite element analysis tool 101

3.5 Conclusion 104

POWER SYSTEM MODEL REQUIREMENTS AND SETUP 105

4.1 Power System Simulation 106

4.1.1 Selection of the dynamic simulation tool 106

4.1.2 Modelling the components 107

4.2 Power System Model Components 108

4.2.1 Prime Mover 108

4.2.3 SG model 110

4.2.4 Transformer & Transmission Lines 112

4.2.5 Grid 113

4.3 Power System Simulation Testing 116

4.3.1 Approach 116

4.3.2 Simulation trials on a DIG142e 116

TABLE OF CONTENTS

4.3.2.1 Validation of a DIG142e model 118

4.3.2.2 LVRT simulations on DIG142e and discussions of findings 120

4.4 Selection of variables for power systems simulation 150

4.4.1 Literature Review 152

4.4.2 Critical parameter trees 153

4.4.3 Pragmatic constraints 154

4.4.4 Inputs to power systems Simulation 155

4.4.5 Pole slip prediction 156

4.5 Prediction of critical parameters for grid code compliance with neural networks 157

4.5.1 Approach 157

4.5.2 Model setup & findings 158

4.6 Grid Code Testing 159

4.7 Conclusion 163

SENSITIVITY ANALYSIS 165

5.1 Introduction to Sensitivity Analysis 166

5.2 Model Setup 168

5.2.1 Selection of model for parametrization 168

5.2.2 Selection of Parametric Variables 168

5.3 Results & Analysis 172

6.3.1 Effect of Air-gap on X_d 172

5.3.2 Effect of Tooth tip length on X_d 174

5.3.3 Effect of Slot opening 176

5.4 Conclusion 179

SYNCHRONOUS MACHINE DESIGN 180

6.1 Introduction 180

6.2 Design Specification 180

6.3 Design Constraints 181

TABLE OF CONTENTS

6.4 Baseline current product capabilities 181
6.5 Calibrating the design tool 184
6.6 Grid code compliant SG design 184
6.6.1 Electromagnetic Design 185
6.6.2 Achieving the inertia time constant target 187
6.7 Validation of the PG7S 194
6.7.1 Waveform Analysis 194
6.7.2 Open Circuit and Short-Circuit characteristics 195
6.7.3 Losses and Efficiency 196
6.7.4 Reactances and Time Constants 198
6.8 Simulation of the PG7S 200
7.9 Conclusion 202
Reliability of SGs for grid code compliance 203
7.1 Introduction 203
7.2 Design for Reliability 207
7.2.1 Temperature rise on the stator 207
7.2.2 Forces on end-windings 210
7.2.3 Limiting rotor currents during LVRT 216
7.2.4 Bearing life 222
7.3 Conclusion 223
CONCLUSION 224
FUTURE WORK 229
References 231
APPENDIX 1 246
Feasibility Studies on using various technologies towards Grid Code Compliance of Engine Driven SGs 246
A1.1 Introduction 246
A1.2 Investigation into available technologies / obvious solutions 246
A1.2.1 High Inertia 246

TABLE OF CONTENTS

A1.2.2 Transformer Reactance 247

A1.2.3 Other solutions 249

A1.2.3.1 Power Electronics 249

A1.2.3.2 Braking resistors 249

A1.3 Conclusion 249

APPENDIX 2 250

Exciter Modelling 250

A2.1 Description of the functional block “Fcn_01” 251

A4.2 Description of the functional block “Fcn_02” 252

A2.3 Description of the functional block “Fcn_03” 253

A2.4 Description of the functional block “Fcn_04” 253

A2.5 Description of the functional block “Fcn_05” 254

A2.6 Description of the functional block “Fcn_06” 254

APPENDIX 3 256

An Approximate Numerical Model of End-Winding in SGs 256

A3.1 Introduction 256

A3.2 Characterizing the behavior of end-windings under transients 259

A4.2.1 End winding geometry 259

A3.2.2 Electromagnetic loads on the end windings under transient event in consideration 261

A3.2.3 Material properties 263

A3.2.4 Boundary conditions 268

APPENDIX 4 273

An Analytical Tool to predict steady state stability of SGs 273

A4.1 Introduction 273

A4.2 Tool Development 275

A4.2 Tool Validation 276

A4.3 Discussion 279

"Bruce, why do we fall?
So that we can learn to pick ourselves up."

- Thomas Wayne & Alfred Batman Begins (2005)

ACKNOWLEDGMENTS

Vihaan, you entering this world has instilled in me a newfound energy and motivation. As I navigate through fatherhood, I am reminded of the famous American writer Clarence Budington Kelland's quote on his father: "*He didn't tell me how to live; he lived, and let me watch him do it".* My father led by example and I hope to be at least as good a father to you as my father was to me; and so Vihaan, this thesis is my first lesson to you – it proves that there are no substitutes in life for hard work and perseverance. You want something? Go get it.

Pavi, WE did it! All the sleepless nights you were awake taking care of Vihaan, all the days you have spent while I was away travelling, making sure the house wasn't on fire so I could focus on work and PhD; you have been by my side through happy and difficult times. This thesis would not have been possible without you.

Mom, Dad and my sister Srinidhi, thank you for always believing in me; even when I stopped believing in myself. Without your unwavering love and support, I wouldn't have been able to pick myself up every time I fell.

This thesis would be incomplete without me thanking Dr.Neil.L.Brown, Chief Engineer, Stamford Products at Cummins Generator Technologies, UK, for constantly reminding me of the important things, keeping me focused, and providing me with the resources needed to complete the work that has led to this thesis.

A special thanks to my advisor Dr. Michael Galea for being patient, pushing me hard and working with me to help me finish this thesis.

ACKNOWLEDGMENTS

I would like to thank Dr. Jeffrey A. Matthews, for your words of wisdom and endless motivation, Alison Snell – an amazing mentor, for your moral support and guiding me through my career, Jonathan Clegg – the most inspiring manager, for always being there for me, teaching me the '*Celestine Prophecy'* and Robin Jackson – from whom I learnt to never give up.

I would also like to thank Adrian Bell, Mark Riley, Philip Bend, Param Anpalahan and all of my engineering colleagues at Cummins Generator Technologies for valuable discussions and support with analyses.

Finally, I literally owe this experience to Cummins. Without its financial support, I would not have been able to pursue this degree. So, a big thanks to the Cummins family.

Finally, while it's really important to thank my family, supporters, mentors, advisors and guides who have been the fundamental reason for my success, it is equally important to express gratitude to those who encouraged me and helped me grow and develop by letting me know that 'I wasn't going anywhere in life'. And so, it is with a sly grin on my face that I type this message for you all: ***'check-mate'***.

LIST OF TABLES

Table 1. 1: Global access to electricity in 2017 [5] 33

Table 2. 1: Transmission System Operators by country [9] 45

Table 2. 2: Summary of grid code requirements specific to alternators globally 50

Table 2. 3: Summary of Grid Code requirements in various European countries.....51

Table 2. 4 : Timescales for enforcement of the pan-European ENTSO-e grid code.....51

Table 2. 5: Timescales for enforcement of German grid code 52

Table 2. 6: Boundaries of operation for generating set according to grid codes 56

Table 2. 7: Comparison of grid code solutions adopted by the wind industry 64

Table 3. 1: Summary of end-winding leakage measurement.....96

Table 3. 2: Summary of test results vs finite element predictions.....100

Table 4. 1: Input variables and limits set in simulation 155

LIST OF TABLES

Table 5. 1: Limits of variables for sensitivity study.....173

Table 6. 1: Summary of design specifications.....180

Table 6. 2: Summary of simulation vs test data on 3 P7 model variants 184

Table 6. 3: Summary of options for increasing inertia constant on PG7S 188

Table 6. 4: THD for the PG7S.....194

Table 6. 5: Comparison of Field currents and reactances of the PG7S between simulation and test.....196

Table 6. 6: Breakdown of losses in the PG7S.....197

Table 6. 7: PG7S reactances and time constants – test results.....199

Table A4. 1: Data for test machine 278

Table A4. 3: Validation of tool predictions 278

LIST OF FIGURES

Figure 1. 1 Conventional power-system [2] 32

Figure 1. 2 Power-System with distributed generation [2].....34

Figure 1. 3: Regional Growth of Distributed Generation [6].....37

Figure 1. 4: Current Status of Grid Codes Internationally [7].....37

Figure 2. 1 Illustration of the concepts of PCC and Point of Connection [13].....46

Figure 2. 2: Sample LVRT curve [13].....49

Figure 2. 3: Example – voltage drop at various levels in a network during a fault 50

Figure 2. 4: LVRT - German grid code 52

Figure 2. 5: LVRT - France grid code 53

Figure 2. 6: LVRT - ENTSO-e grid code 53

Figure 2. 7[34]: Proving compliance to grid code requirements 54

Figure 2. 8 [28]: Single line representation of engine driven SG connected to the grid.....55

Figure 2. 9 [32]: 3 operating regions for a grid connected engine driven generating set 57

Figure 2. 10 Representative Electrical power vs load angle curve [29] 58

LIST OF FIGURES

Figure 2. 11 [33]: Equal-Area Criterion 59

Figure 2. 12: Test Layout for emulating out of phase synchronization.....61

Figure 2. 13 [28]: Damaged keyway of shaft due to out of phase synchronization.....61

Figure 2. 14: Per Unit shaft torques measured on the UCI224F leading to the cracking of the shaft key as in Figure 2.13 62

Figure 3. 1– Axial cross-section of SG [56] 68

Figure 3. 2 a – Equivalent circuit of a SG in the d-axis.....69

Figure 3. 3 – Finite element model of a SG showing the sub-domains / finite elements.....72

Figure 3. 4 – Summary of literature review on transient and sub-transient reactance prediction using finite element method 76

Figure 3. 5 – Winding configuration for predicting d-axis reactance.....77

Figure 3. 6 – Flux plot for armature windings excited by only d-axis current 78

Figure 3. 7 – Winding configuration for predicting d-axis reactance.....79

Figure 3. 8 – Flux plot for armature windings excited by only q-axis current 80

Figure 3. 9 – Impact of saturation on the synchronous reactance values ..80

Figure 3. 10 – Contour plot of d-axis reactance plotted as functions of d and q axis currents 82

Figure 3. 11– Setup for single frequency response. A) d- axis B) q-axis ..85

Figure 3. 12– Flux plot of single frequency response simulation – note the currents induced in the damper bars and field winding. 86

Figure 3. 13 – Setup for the finite element model to run a sustained short circuit simulation 88

Figure 3. 14– Short-Circuit current trace 89

Figure 3. 15 – A) current trace processed by peak detection algorithm B) semi-log plot of peak currents vs time 89

Figure 3. 16– Automated algorithm to predict SG parameters 90

Figure 3. 17– Technical datasheet for PI734C.....93

Figure 3. 18 – Test setup for open-circuit characteristic [57].....94

Figure 3. 19– Comparison of predicted vs tested open-circuit characteristic curve showing a good match.....95

Figure 3. 20 – Test setup for measuring the end-winding leakage 95

Figure 3. 21: Test setup for single frequency response 97

Figure 3. 22: Angular position of the d and q axes 98

Figure 3. 23: Test setup for sudden short-circuit 100

Figure 3. 24: Three phase short-circuit currents in the armature winding of the test machine – PI734C. The a,b,c, phases are the same as u,v,w phases in the same sequence. 101

Figure 3. 25: Typical inputs for the user interface used to build the finite element model. 102

Figure 3. 26: Flowchart showing the functioning of the user interface of the finite element modelling tool 103

Figure 4. 1 – Pugh matrix selection of Simulation tools 106

Figure 4. 2 – Graphical representation of simulation model.....108

Figure 4. 3: IEEE [88] model of the internal combustion engine.....109

Figure 4. 4: The IEEE AC8B[89] model of the alternator excitation system with functional blocks identified 110

Figure 4. 5 – Simpowersystems model of SG [35] 112

Figure 4. 6: Model of transformer used.....113

Figure 4. 7: A generic Low Voltage Ride Through curve that is simulated 114

Figure 4. 8: Approach to two-stage power system modelling.....117

Figure 4. 9: Test setup to validate systems model of SG with short-circuit test. 119

Figure 4. 10: Results of the short-circuit test lined up against simulation results showing excellent correlation 120

Figure 4. 11: Stator peak current variations against instant of the fault for different power factors.....123

Figure 4. 12: LVRT performance of DIG14e: Pre-fault PF - unity, pre-fault terminal voltage - 1.0pu, fault duration – 110ms, retained voltage during fault – 0.0pu, and step changes in terminal voltages 125

Figure 4. 13: LVRT performance of DIG14e: Pre-fault PF - unity, pre-fault terminal voltage - 1.0pu, fault duration – 190ms, retained voltage during fault – 0.0pu, and step changes in terminal voltages 126

Figure 4. 14: LVRT performance of DIG14e: Pre-fault PF - unity, pre-fault terminal voltage - 1.0pu, fault duration – 230ms, retained voltage during fault – 0.0pu, and step changes in terminal voltages 127

Figure 4. 15: Stator peak current variation against fault duration for different power factors, pre-fault terminal voltage – 1.0pu, retained voltage during fault – 0.0pu, step voltage changes 128

Figure 4. 16: Calculation of stator rms average current during fault and post-fault condition, pre-fault terminal voltage – 1.0pu, retained voltage during fault – 0.0pu, step voltage changes and pre-fault PF – 0.8 over excited.....129

Figure 4. 17: Stator rms average current during fault and post-fault condition against fault duration, pre-fault terminal voltage – 1.0pu, retained voltage during fault – 0.0pu, step voltage changes and pre-fault PF – 0.8 over excited.....130

Figure 4. 18: Stator rms power at the terminals during fault and post-fault condition against fault duration, pre-fault terminal voltage – 1.0pu, retained voltage during fault – 0.0pu, step voltage changes and pre-fault PF – 0.8 over excited.....130

Figure 4. 19: Electromagnetic rms torque during fault and post-fault condition against fault duration, pre-fault terminal voltage – 1.0pu, retained voltage during fault – 0.0pu, step voltage changes and pre-fault PF – 0.8 over excited.....131

Figure 4. 20: Stator peak current variation against fault duration for different retained voltage, pre-fault power factor - 0.8 over excited, pre-fault terminal voltage 1.0pu and step voltage changes 132

Figure 4. 21: Stator peak current variation against fault duration for different return ramp voltages, pre-fault power factor - 0.8 over excited and fault retained voltage – 0.0pu.....133

Figure 4. 22: Stator peak current variation against fault duration for different power factor. Pre-fault terminal voltage 1.0pu, fault retained voltage - 0.3pu.....134

Figure 4. 23: LVRT performance: retained voltage during fault – 0.3pu, fault duration – 250ms, pre-fault terminal voltage – 1.0pu, pre-fault power factor - 0.8 over excited 135

Figure 4. 24: LVRT performance: retained voltage during fault – 0.3pu, fault duration – 250ms, pre-fault terminal voltage – 1.0pu, pre-fault power factor - unity 136

Figure 4. 25: LVRT performance: retained voltage during fault – 0.3pu, fault duration – 250ms, pre-fault terminal voltage – 1.0pu, pre-fault power factor - 0.8 under excited 137

Figure 4. 26: Stator rms average current during fault and post-fault condition against fault duration, pre-fault terminal voltage – 1.0pu, retained voltage during fault – 0.3pu, step voltage changes and pre-fault PF – unity 138

Figure 4. 27: Stator rms power at the terminals during fault and post-fault condition against fault duration, pre-fault terminal voltage – 1.0pu, retained voltage during fault – 0.3pu, step voltage changes and pre-fault PF – unity 138

Figure 4. 28: Electromagnetic rms torque during fault and post-fault condition against fault duration, pre-fault terminal voltage – 1.0pu, retained voltage during fault – 0.3pu, step voltage changes and pre-fault PF – unity 139

Figure 4. 29: Stator peak current variation against fault duration for under excited and unity power factors: pre and post-fault terminal voltage 1.1pu, retained voltage during fault – 0.3pu 140

Figure 4. 30: LVRT performance: pre and post-fault terminal voltage – 1.1pu, retained voltage during fault – 0.3pu, pre-fault power factor - unity.....140

Figure 4. 31: LVRT performance: pre and post-fault terminal voltage – 1.1pu, retained voltage during fault – 0.3pu, pre-fault power factor - 0.8 under excited power factor.....141

Figure 4. 32: Stator current variation against fault duration for over excited and unity pre-fault power factors: pre and post-fault terminal voltage 0.9pu, retained voltage during fault 0.3pu 142

Figure 4. 33: LVRT performance: pre and post-fault terminal voltage - 0.9pu, retained voltage during fault - 0.3, pre-fault power factor - 0.8 over excited, step change in voltages 143

Figure 4. 34: LVRT performance: pre and post-fault terminal voltage - 0.9pu, retained voltage during fault - 0.3, pre-fault power factor – unity, step change in voltages.....144

Figure 4. 35: Stator peak current variation against fault duration for different return ramp voltages, 0.8 over excited power factor and 70% drop.....145

Figure 4. 36: General LVRT profile.....146

Figure 4. 37: LVRT performance with German grid code.....147

Figure 4. 38: LVRT performance with absolute worst case and slow controller.....148

Figure 4. 39: LVRT performance with absolute worst case and fast controller.....149

Figure 4. 40: Method to determine SG design criteria for grid code compliance.....151

Figure 4. 41: Three-pronged approach to defining inputs to power systems simulation.....152

Figure 4. 42: Critical parameter tree for Steady State Load Angle.....153

Figure 4. 43: Critical Parameter Tree for shaft acceleration during transients.....154

Figure 4. 44: Process to define SG design criteria using neural network. 158

Figure 4. 45: IEC 61400-21 method of testing for grid code compliance [121].....160

Figure 4. 46: Grid code test setup for the LVSI804S generator with a Cummins QSK60 engine.....161

Figure 4. 47 Comparison of simulation (green) vs test (red) at a 70% voltage drop.....162

Figure 4. 48 Comparison of simulation (green) vs test (red) at a 30% voltage drop.....162

LIST OF FIGURES

Figure 5. 1: Model setup approach.....167

Figure 5. 2: Critical Parameter Flow Down for Steady-State Load Angle 170

Figure 5. 3: Critical Parameter Flow for Reactance and Inertia Constant 171

Figure 5. 4: Change in X_d with respect to Air-gap.....174

Figure 5. 5 a: Tooth Tip Length 175

Figure 5. 6: Change in X_d with respect to Slot opening.....176

Figure 5. 7: Electrical Steel Permeability as a function of Flux Density for various steel grades [63].....177

Figure 5. 8: Effect of steel grade (electrical steel permeability) on d-axis reactance 179

Figure 6. 1: Baseline of current product X_d capabilities 182

Figure 6. 2: Baseline of current product kVA capabilities.....183

Figure 6. 3: Baseline of current product efficiency capabilities 183

Figure 6. 4: Comparison between standard P7E baseline machine and the PG7S 187

Figure 6. 5: New PG7 Fan-inertia ring assembly drawing.....189

Figure 6. 6: (a) Burst Speed Analysis (b) Fatigue Analysis 190

Figure 6. 7: Maximum Principle Stress due to a 0.1 mm axial displacement of one of the fasteners.....190

Figure 6. 8: Maximum Principle Stress at 1800 rpm due to thermal expansion 191

Figure 6. 9: Mean Stress at 1800 rpm with LVRT loads 192

Figure 6. 10: Goodman plot for Mean Stress at 1800 rpm (MPa) 193

Figure 6. 11: Relationship between kVA, inertia constant and direct synchronous reactance for the PG7S.....193

Figure 6. 12: Harmonic analysis of the PG7S 195

Figure 6. 13: Open Circuit and Short-Circuit characteristics of the PG7S196

Figure 6. 14: No Load and Short-Circuit loss characteristics of the PG7S 197

Figure 6. 15: Tested efficiency curves of PG7S at various power factors198

Figure 6. 16: PG7S 3 phase sudden short-circuit at 400V, 50Hz.....199

Figure 6. 17: Power system model with PG7S 200

Figure 6. 18: Low Voltage Ride Through simulation on the PG7S 201

Figure 7. 1: Boundary diagram for the bracing rope showing interactions 204

Figure 7. 2: DFMEA for the boundary diagram shown in Figure 7.1 205

Figure 8. 3: A motorette sample specified by UL.....208

Figure 7. 4: Life curve of insulation system used in PG7S 208

Figure 7. 5: Axial temperature distribution on the PG7S 209

Figure 7. 6: Circumferential temperature distribution on PG7S 210

Figure 7. 7: Forces in windings of electrical machines 211

Figure 7. 8: Formed coils in the stator 212

Figure 7. 9: Random winding inserted into the stator the PG7S.....213

Figure 7. 10: Stator current during LVRT for various fault duration and power factors. 214

Figure 7. 11: Short-circuit test on the PG7S.....215

Figure 7. 12: Extension to stator core-pack to increase sub-transient reactance 216

Figure 7. 13: Rotor voltage during LVRT 217

Figure 7. 14: Snubber circuit on the PG7S 218

Figure 7. 15: Snubber Assembly (blue wires) attached to the exciter and rectifier (yellow wires) assembly 219

Figure 7. 16: Voltage transients in rotor without snubber resistor in a simulated fault in an in-house test environment 219

Figure 7. 17: Attenuation in rotor transient with snubber resistance 20 times field winding resistance 220

Figure 7. 18: Attenuation in rotor transient with snubber resistance 20 times field winding resistance 220

Figure 7. 19: Attenuation in rotor transient with snubber resistance 20 times field winding resistance 221

Figure 7. 20: Attenuation in rotor transient with snubber resistance 20 times field winding resistance 221

Figure 7. 21: Rotor winding voltage with and without snubbers during LVRT 222

Figure 8. 1: Low Voltage Grid code compliant products offered by Cummins Generator Technologies 226

Figure 8. 2: Cost per kVA comparison across all low voltage grid code compliant products offered by Cummins Generator Technologies. 226

Figure A1. 1: Inertia constant vs Critical Clearing Time.....247

Figure A1. 2: Effect of transformer reactance on critical clearing time. .248

Figure A2. 1: AC8B model of the excitation system with sub-components defined.....250

Figure A2. 2: Normalized Volt-Ampere characteristic of uncontrolled rectifier [93] 252

Figure A2. 3: Exciter Saturation Characteristics [93].....254

Figure A3. 1: Relative magnitude of forces on SG windings 256

Figure A3. 2: P7 end windings – random wound machine.....260

Figure A3. 3 DIG142 – bar wound machine.....260

Figure A3. 4: Forces on end-winding under fault conditions [125] 261

Figure A3. 5: Defining local coordinate systems on individual conductors. Axial, radial & tangential.....262

Figure A3. 6 Primary and secondary insulation on random wound machines [126].....264

Figure A3. 7: Banding tapes used on bar wound machines [124] 264

Figure A3. 8: Variation in Young's Modulus as a function of temperature [126].....265

Figure A3. 9 A multi-strand composite material, matrix and fibrous components. Chang Yan (2003) 267

Figure A3. 10 Homogenisation approach for composite materials. Chang Yan (2003) [127].....268

Figure A3. 11: Method of simulation of end-winding movement.....269

Figure A3. 12 DIG142 deflections under short circuit 270

Figure A3. 13 Deflected end winding basket under short circuit conditions. Gruning et al[125].....271

Figure A3. 14 Computed and measured values for end winding deflection. Gruning et al [125].....271

Figure A3. 15: Test method developed to measure coil mechanical properties at various temperatures. 272

LIST OF FIGURES

Figure A4. 1: Phasor diagram for salient-pole generator.....274

Figure A4. 2: Snapshot of analytical tool developed to predict static stability.....275

Figure A4. 3: Finite element models to predict reactance. 277

Figure A4. 4: Reluctance torque predicted vs tested 278

CHAPTER 1
INTRODUCTION

1.1 Evolution of the more distributed grid

The general definition of an electric grid is "*an interconnected network for delivering electricity from suppliers to consumers*". It consists of 1) generating stations that produce electrical power, 2) high-voltage transmission lines that carry power from distant sources to demand centers, and 3) distribution lines that connect individual customers [1]. Figure 1.1, which is sourced from [2] illustrates the conventional structure of electrical power systems, showing the traditional set-up of very large power plants supplying large areas. Over the last decade however, many socio-economic reasons have led to a shift towards more distributed power generation. This often consists of a vast array of interconnected systems which encourages integration (regional and otherwise) of the traditionally concentrated power generation and consumption activities. Thus, instead of limiting power generation to the classical large power plants, a number of strategically positioned smaller power plants / consumer driven generating sets are included within the distribution system. Figure 1.2, from [2] shows the general structure of power-systems with distributed generation. As summarized in the CIRED survey [4], the key factors that are leading the industry towards more distributed generation include

- Policies on reduction in greenhouse gas emissions (mainly CO2) – have led to power generation companies resorting to more renewable energy sources and smaller, more segmented distributed generation.
- Energy efficiency – the need for more efficiency systems complements the policies on greenhouse gas emission reductions. The large coal powered plants are more energy efficient than small generating sets, but less efficient operationally and cannot meet the agility requirements that the smaller distributed power plants can meet.
- Deregulation of energy market has allowed more players to enter the power generation market, thus leading to a higher competition in the energy marker. This has led to an increase in the number of electricity suppliers connected to the grid – specifically on the distribution side.
- Diversification of energy resources – the ever-increasing introduction of niche sources of energy produces a proportional segmentation of the electrical grid.

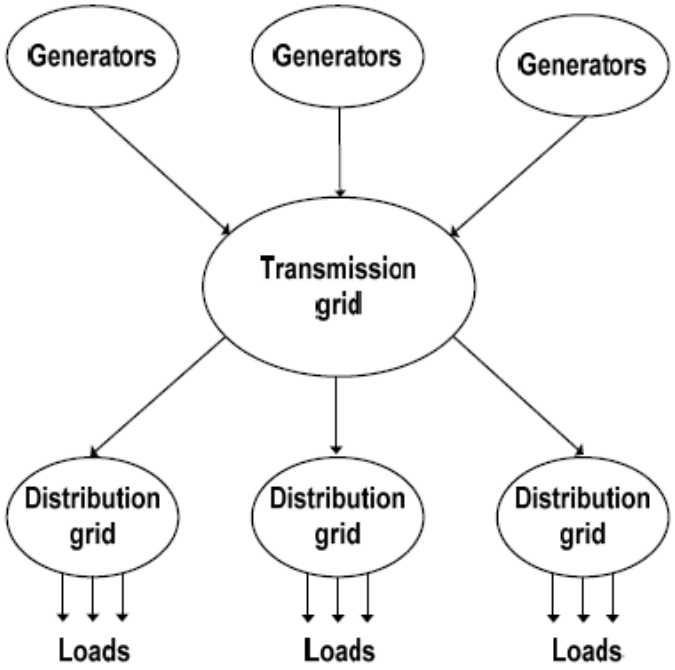


Figure 1.1

Figure 1. 1 Conventional power-system [2]

An important factor that justifies the ever-increasing need for distributed generation is that today it represents the most practical means of providing power to the remotest parts of the world. The International Energy Agency estimates that approximately 1.5 billion people lacked access to electricity in 2017, about 20% of the world's population [5]. The World Bank report on the energy gap [5] also recommends that extension of the electric distribution grid by developing mini-grids or individual systems closer to the population is often the cheapest way to new consumers and to increase access to electric power. It is also predicted that in most countries, between 80-95% of the unserved communities will receive electric power through grid extension [5]. A summary of the global access to electricity in 2017 [5] is given in Table 1.1.

Table 1. 1: Global access to electricity in 2017 [5]

	Rate of Access (%)	Population without access to electricity (millions)	Urban Electrification (%)	Rural Electrification (%)
North Africa	52	603	74	36
Sub-Saharan Africa	43	602	67	28
China	100	0	100	100
India	87	168	98	82
Other South-East Asia	88	44	97	82
Central & South America	96	20	98	86
Middle East	92	18	98	78

Besides the technology drivers for distributed generation introduced above, other important advantages related to this concept include:

- Mobility and ease of setup – distributed generation consists of many small units that can be easily transported based on power needs.
- Lower transmission losses and infrastructure costs - In distributed generation, power is normally generated closer to the load and hence the transmission losses are lower. Additionally, shorter distances to transmit power result in lower infrastructure costs.
- Low plant cost and accessibility. The modular nature of distributed generation minimizes the space required for the power plants and therefore simplifies the logistic aspects.
- However, grids made up of several small generating sets as in distributed generation have been shown to introduce instability in the power-system [12].

- Additionally, the variability in generation levels caused by the vast array of renewables in the electric grid leads to an unequivocally less reliable power system.

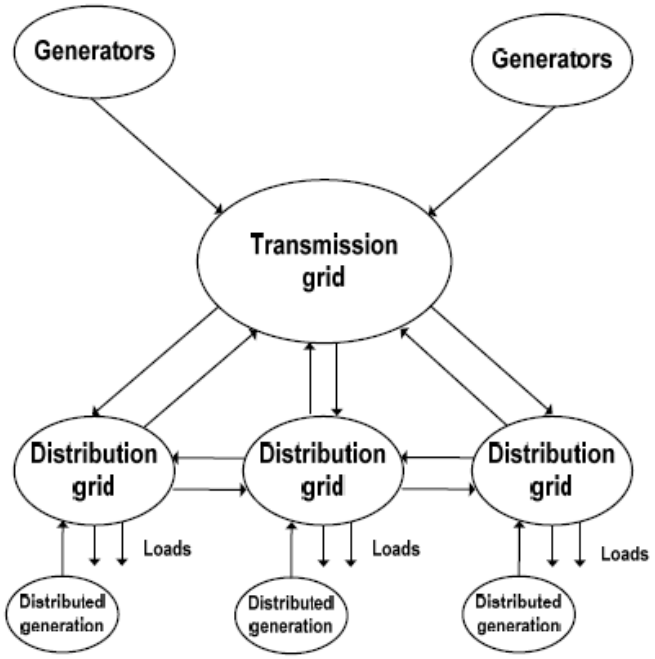


Figure 1. 2 Power-System with distributed generation [2]

This chapter describes the challenges posed by modern power-systems and the measures taken by the Transmission System Operators (TSO) and Distribution System Operators (DSO) to ensure a reliable and robust electric power supply. These measures have a significant impact on the design and operation of power plants and associated components, in particular engine driven generating sets and the SG that together form the most common source of electrical power. A brief description of the identified challenges being addressed is included in this chapter along with a summary of the layout of the thesis.

1.2 Grid Codes

As for any other system/technology, there exist a set of standards/ guidelines for grid connected systems. Grid Codes are the guidelines set out by the TSOs and DSOs that specify performance (technical and operational characteristics) expectations for power plants and all components involved in the generation, transmission, distribution and utilization of electric power [4].

Grid Codes have been around in various forms and levels of details since the first electricity transmission and distribution system. Until 2007, there were no requirements for power plants to stay connected to the grid during fault ride throughs. This meant that in the event of a small disturbance, should the power plant operators feel nervous about the integrity of their equipment, they could disconnect from the grid leading to large scale black-outs [137]. However, until 2011, no real effort in terms of enforcement of these standards had been done. At the turn of 2013, Germany became the first country to enforce Grid Codes for all electricity generating facilities. Adhering to the legislation became compulsory throughout the rest of Europe in 2015. With the projected growth of global distributed generation as shown in Figure 1.3, which is sourced from [6], an increasing number of countries across the globe are becoming conscious of the importance of these regulations. Figure 1.4 [7] illustrates the various countries that have adopted some form of grid code. The main concern related to this is that the adopted grid codes vary from country to country and this complicates enforcement.

However, the information contained in any grid code document can broadly be classified into five subsections [4]:

- Planning Code – Discusses requirements on data that needs to be presented to gain approval for power plant proposals.
- Connecting Code – Specifies the grid requirements related to the power plants' capability to maintaining connectivity protection schemes, reactance requirements, harmonic distortions, voltage fluctuations, etc. It also requires a combination of simulation and test data to prove compliance.
- Operating Code – Specifies the criteria for safe, reliable operation - i.e. maintenance and monitoring requirements, demand forecasting, contingency planning requirements, and system test requirements.

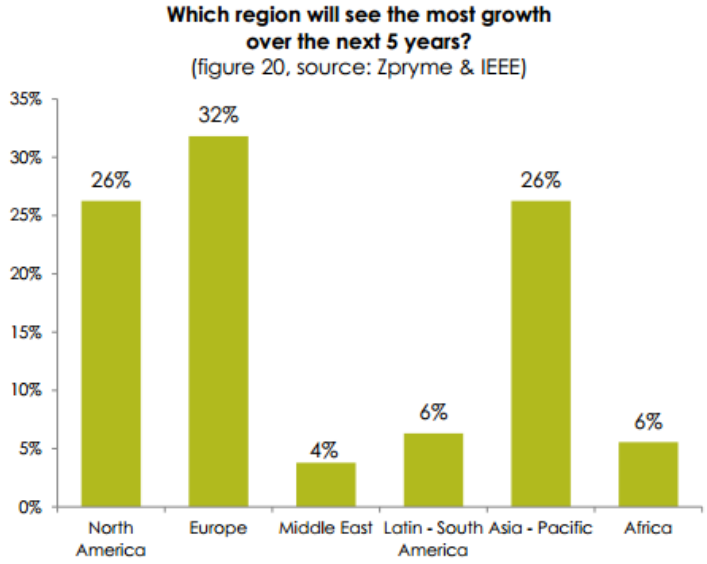


Figure 1. 3: Regional Growth of Distributed Generation [6]

- Data Communication Code – Provides guidelines on data transfer between power plants and other entities connected to the grid.
- Balancing Code – Specifies the power flow requirements in the grid, such as reactive power requirements (control system requirements), response times and voltage levels.

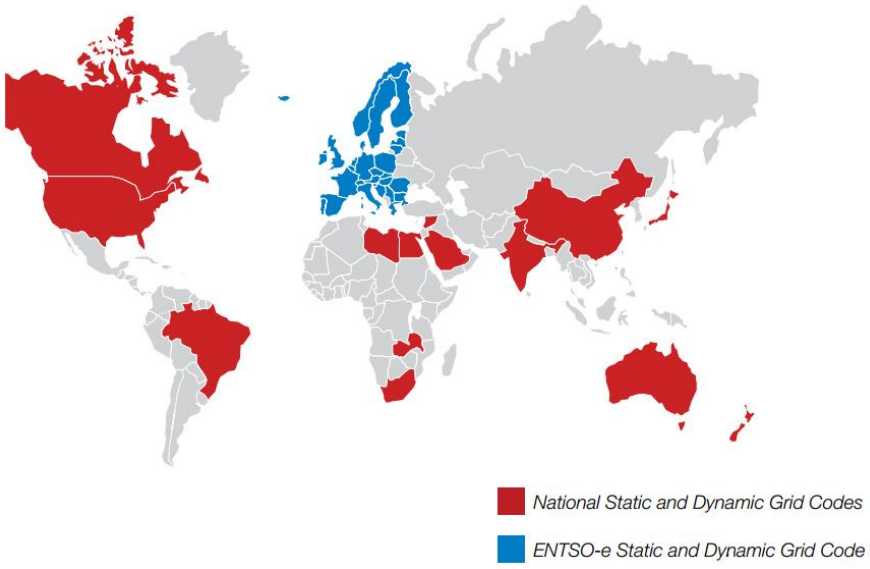


Figure 1. 4: Status of Grid Codes Internationally [7]

While the five types of codes described above, apply to all sources of electrical power connected to a grid (renewables, nuclear, hydro and fossil fuel), , the work presented in this thesis is mainly focused on the grid code compliance of engine-driven SGs (SGs). In fact, these represent the type of application that the SGs manufactured by Cummins Generator Technologies (CGT) are designed for.

1.3 Problem Description and project objectives

Cummins Generator Technologies (CGT) is one of the largest manufacturers of SGs in the world with the broadest portfolio of product ranging from $0.5kVA$ up to $20MVA$. Over US $100M worth of SGs sold in Europe for the European market are used in distributed generation / combined heat power (CHP) applications. Since early 2013 the TSOs and DSOs of countries (Germany in the lead) in the European Economic Council (EEC) have started enforcing grid codes. In fact, it is predicted that a Pan-European ENTSO-e (European Network of Transmission System Operators-electricity) grid code has been enforced starting 2015. Thus, power plants utilizing renewable sources are already implementing process to modify product and system designs to comply with grid codes. The focus of grid code compliance is currently on power plants / CHP plants that are made up of engine-driven SGs. While there are several benefits of directly connecting alternators to the grid, (e.g. reactive power compensation and voltage stability) also poses major challenges for achieving the required compliance with grid codes. This is particularly important for the conditions and requirements related to the steady state operation and to the stability demands of the low voltage ride through. Such effects are being addressed today (e.g. in the renewable industry), by deploying power electronics and associated control strategies. However, such solutions are very expensive and therefore they are not the preferred solution for SG-based power plants to comply with grid codes.

Simplistic but also potentially expensive methodologies to achieve compliance also include situations where power generation companies simply increase the inertia or significantly over-rate the main alternator. While this offers a fast and simple solution to grid code compliance, however the associated costs can be relatively high due to the traditional over-rating philosophy (over-engineering) which is behind these concepts.

A potential solution to all the above is therefore to address grid compliance requirements at every stage of the power generation system design. This means setting grid compliance as an objective function of the design of every component that will be implemented into a power generation set. Arguably, the most important component with the dominant effect on power quality is the main alternator itself (i.e. the SGs); the engine is the most expensive, but it's the alternator that connects the engine to the grid and is thus the most critical component in the genset. The alternator also becomes significant because the design of the alternator defines the level of protection the engine receives from transients in the grid. Therefore, significant benefits in terms of system level power quality and grid compliance can be achieved, if the design and development processes of the SG were to be done with grid code compliance as a main objective, 'right from the start'.

In order to achieve this, a deep understanding of the critical parameters of the SG, including its design parameters and their effects on the capability of the SG to meet grid codes is required Significant effort in terms of combining the understanding of these critical parameters with the ability of designing SGs is necessary to perform optimizations aimed at achieving design solutions for grid

code compatability, without any detrimental effects on the power density, efficiency and reliability of the machines. To the author's knowledge, no such approach to grid code compliance by radical SG design has been recorded and will represent one of the main novelties in this thesis.

The main objective of this thesis is thus to obtain a clear understanding of the design requirements of engine driven SGs for grid code compliance. To achieve this, the general methodology followed in this work will be a systematic approach in the pursuit of the following.

1) What are the relevant grid codes?
2) What aspects of the grid codes are critical to the design of SGs?
3) What are the alternator / system 'features' that would make an engine driven SG grid code compliant?

As vessel to reach the above-mentioned objectives, a 1.5MVA, SG, completely compliant with standard grid codes will be designed and developed. Firstly, grid codes from various parts of the world are summarized and the sections relevant to SGs are tabulated. These are then analyzed using power system simulations aimed at identifying the design requirements of an engine driven SG. Finally, a sensitivity study is completed to determine the most significant and least significant generator geometrical features that contribute to achieving the grid code requirements.

1.4 Thesis Contributions

The work described in this thesis led to the development and to the introduction to market of a new range of grid-compliant products by CGT. This work has enhanced the understanding of reliability of SGs relative to grid code compliant applications and contributed to entering a niche market segment through a competitive product line. Additionally, the work directly connected to this thesis led to a Masters' Thesis and a granted patent GB24949166.

1.5 Structure of thesis

This thesis is structured in the following chapters:

Chapter 1 introduces the challenges arising because of the increase in distributed generation; the need for grid codes and the challenges and opportunities that arise from mandating grid codes – particularly for SG manufacturers and finally outlines the methodology applied in this thesis.

Chapter 2 summarizes the grid codes that are applicable to engine driven SGs. The performance of an engine driven generating set in a 'grid code applicable' power system is described and analyzed and the impact of the grid codes on the machine's reliability is described. The required method of proving grid code compliance to the relevant governing bodies is presented.

Chapter 3 briefly presents the basic theory of classical SGs and then describes and the development of a numerical analysis tool (i.e. the finite-element method) for the SGs performance prediction. This chapter also describes the development

and validation of a fully automated tool to predict SG parameters with only the geometrical parameters as input in finite element analysis.

Chapter 4 summarizes the various methods of modelling and analysis of power systems. A fully automated power systems simulation model is developed and is used to run simulations of various power systems scenarios against known grid code requirements. The output of this model is combined with the matlab neural network tool to derive the design criteria for a grid code compliant synchronous generator that is validated using grid code testing.

Chapter 5 describes an approach that combines the findings described in chapter 5 with a sensitivity analysis, to relate the SG design parameters to its geometry.

Chapter 6 describes the design methodology and validation of a SG designed to meet the geometrical requirements defined in Chapter 6.

Chapter 7 summarizes the reliability aspects of a SG that must meet grid code requirements. Then the solutions identified and implemented in the SG designed in Chapter 6 are investigated.

CHAPTER 2

GRID CODES

In this chapter, the grid codes adopted by various countries, including Germany, Denmark, France, Italy, India, Australia, etc., are reviewed and summarized. A comprehensive discussion on the performance requirements according to the grid codes is presented. The implications of these expectations on the alternator durability / reliability are presented and the arguments are complimented with test evidence. This discussion is then used to review and summarize the scope of the challenges that the work presented in this thesis addresses along with an overview of the proposed methodology aimed at improving and solving these challenges

2.1 Introduction to Grid Codes

The National Grid Company [58] defines a grid code as a "*Technical specification which defines the parameters an electricity generating plant has to meet to ensure proper functioning of the electrical grid. The authority responsible for the electricity distribution specifies the grid code which may vary from country to country"*.

There are several authorities in charge of publishing such Grid codes, including

- Transmission system operators

- Distribution system operators
- Transmission system owners
- Distribution System owners
- National Electricity (or Energy) Commissions – Regulators
- Governments (as a law)
- Reliability councils – Association of operators

Grid codes apply to all power plants and associated components and protection systems connected to the electricity network. They cover the main sources of electric power, including renewables, energy storage systems, IC engine driven systems and nuclear and hydro power plants

Table 2.1, whose source is [9] summarizes some of the transmission system operators by country responsible for owning the relevant grid codes.

In Table 2.1, it can be clearly observed that there is a big diversity in the number of grid operators and therefore the number of grid codes available is relatively quite high. The table also shows the complexity and / or scale of the problem i.e. grid codes just by the number of variations available.

In addition to the transmission system operators shown above, within Europe, the ENTSO-e (European Network of Transmission System Operators – electricity) is expected to own a pan-European grid code.

Table 2. 1: Transmission System Operators by country [9]

		Transmission System Operator (TSO)		
Continent	**Country**			
		Continent	**Region**	**Responsible department**
Europe	Germany	ETSO (European Transmission System Operator)	UCTE (Union for co-ordination of Transmission - Electricity	Verband der Netzbetreiber - VDN - e. V. beim VDEW
	United Kingdom	ETSO	UCTE / UKTSOA (United Kingdom Transmission System Operator Association)	BETTA (British Electricity Trading and Transmission Arrangements)
	Denmark	ETSO	UCTE / NORDEL	Elkraft
	Sweden	ETSO	UCTE / NORDEL	Svenska Kraftnat
Africa	South Africa			NER (National Electricity Regulator)
America	USA			NERC (North American Electric Reliability Council)
Oceania	New Zealand			Transpower
Asia	India			ISTS (Inter State Transmission System)

2.2 Grid Codes – Terminology & Content

This section will focus on explaining the key terminology used in the field of grid codes and aims to summarize the elements of the five subsections described in Section 1.2 that apply to the electrical machines used in power plants.

2.2.1 Grid Codes – Terminology

- Point of Common Coupling (PCC) - IEEE [10] defines the PCC as "*the point where a local electric power system is connected to an area's electric power system*". The PCC and the point of connection are not necessarily the same point. The grid codes define the PCC

as the location where all system measurements are made and therefore the location where all the grid codes apply. Figure 2.1[13] illustrates the difference between PCC and point of connection; DER refers to a **D**istributed **E**nergy **R**esource [13].

- Agreed Active Power - Agreed Active Power or contract capacity [11] or project capacity [12] is the maximum active power allowed for export by a distribution system (power plant) and is contractually agreed between the network operator and the distribution system (power plant) owner. The agreed reactive power requirement is implicit. The specifics on feed-in tariffs, specific load requirements, load sharing requirements are covered in the contractual agreement.

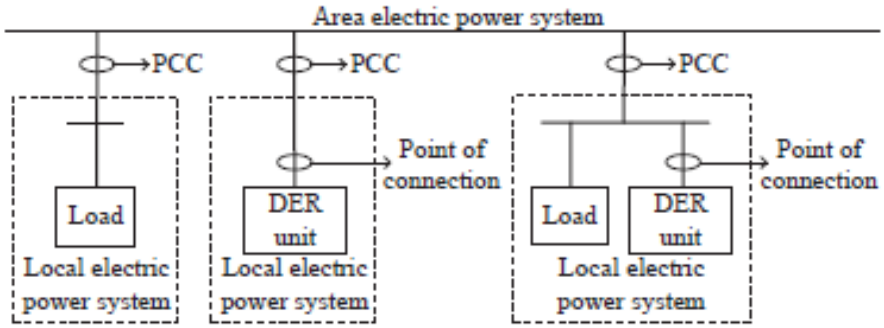


Figure 2. 1 Illustration of the concepts of PCC and Point of Connection [13]

- Ancillary Services - These encompass the support functions / roles played by the power plants / distribution system towards power system safety, security and reliability [14]. Typically, this involves:
    - Assisting in supporting local voltage
    - Assisting in regulating network frequency
    - Contribution to network spinning reserve (amount of reserve / backup power ready to be delivered to the grid upon request by the network operator)
    - Harmonic Compensation
    - Black Start Capability
- Fault Ride Through Requirements (FRT) – These specify expectations on distribution system / power plant response during and after a network fault and prohibit the distribution system / power plant from disconnecting during the network fault. The purpose of the FRT requirements according to [15] are:
    - To prevent a large distribution system / power plant to disconnect during the fault and introduce a sudden loss of generation capacity resulting in grid instability.
    - Preventing lack of voltage and frequency support (reactive and active power) to the network during and after the fault.

Depending on the power system design- system impedances, voltage levels, loads, etc. and the nature of the fault – symmetrical / unsymmetrical, the faults propagate through the network as voltage sags and this is seen by the power plant / distribution system [16]. The power plant is required to ride through these voltage sags (Low Voltage Ride Through – LVRT) and the grid codes define rules around staying connected during the LVRT and when to drop off (disconnect). Figure 2.2 illustrates a LVRT curve marking the regions where the power plant must stay connected and where it can disconnect relative to the LVRT [13]. Figure 2.3 is an example of how much voltage is retained at different parts of a network during a fault ride through.

2.2.2 Grid Codes – Content

Based on the nature of the requirements specified, grid codes can be grouped into two categories, namely

- Static Grid Codes: Enforcing the performance of power plants during steady state conditions. The Static Grid codes regulate the following parameters
    - Total harmonic Distortion (THD)
    - Voltage range the network operates within
    - Frequency range the network operates within
    - Power factor range the network range operates within

- Active and Reactive Power Requirements under the above voltage, power factor and frequency ranges.

- Dynamic Grid Codes: Regulating the performance of power plants during transient conditions. These include:
  - Low Voltage Ride Through curves
  - Pole slip conditions
  - Active and Reactive Power requirements during transients

The power plants need to prove compliance to the above requirements and the rest of the grid code document through testing and / or simulation.

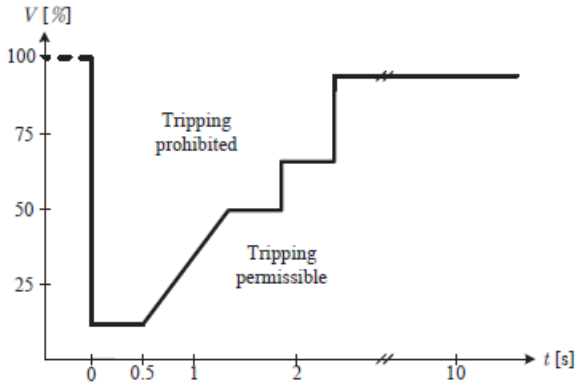


Figure 2. 2: Sample LVRT curve [13]

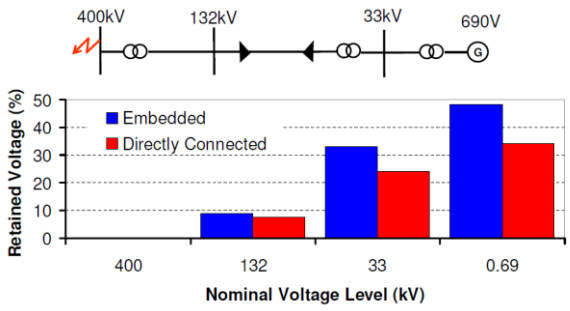


Figure 2. 3: Example – voltage drop at various levels in a network during a fault

Table 2.2 presents a summary of the grid codes relevant to power plants that use engine driven SGs and the content relevant to alternators.

Table 2. 2: Summary of grid code requirements specific to alternators globally

	Design Concept Target	Germany	Denmark	Holland	France	Spain	China	India	USA	South Africa	New Zealand	Belgium	Australia	Northern Ireland
Voltage Range	**+/- 10%**	+/- 10%	+10% to 5%	+/- 10%	+/- 10%	Dep'dent	+/- 10%	+/- 10%	+/- 10%	+/- 10%	Dep'dent	+6% to - 7.5%		
Frequency Range	**+/- 5%**	+/- 5%	+/- 2%	+/- 1%	+/- 1%	+/- 0.3%	+/-%	+/-1%	+/-1%	+/-1%	+/-1%	+3% to -5%	+/-1%	-1% to +4%
Power Factor	**0.95lag / 0.95 lead**	0.95lag/ 0.95 lead	0.9 lag / 0.95 lead	0.95lag / 0.95 lead	0.95lag/ 0.98 lead	In progress	0.95 lag/ 0.95 lead	0.95 lag/ 0.9 lead	0.95lag/ 0.95lead	0.95lag/ 0.95lead	0.95lag / 0.95lead	n/a	0.9 lag to 0.9 lead	0.95 lead to 0.98 lag
Harmonic Content	**<3%**	<3%	<5%	<5%	<3%	<3%	<3%	<6%	<6%	<8%	<6%	8%	<3%	<3.5%
Reduction of Active Power – Steady State	**No Reduction**	Yes, within 1min	15% reduction on 30min	yes after 10min	no reduction	yes outside operating points	yes after 10min	yes after 10min	yes after 10min	no reduction	yes after 10min	yes after 10min	NA	NA
Fault clearing time	**250ms**	150ms	150ms - 250ms	100ms	250ms	500ms at 20% V	n/a	n/a	100ms	150ms	150ms	200ms	430ms	

Of all the requirements captured in Table 2.2, those for Europe are being enforced in stages. The European grid code requirements specific to alternators are summarized in Table 2.3, while the ENTSO e column is emphasized in Table 2.4 which lists out the expectation of the pan-European code expected to be enforced between 2014 and 2017. Table 2.5 (data sourced from [17] – [27]) illustrates the plan and deadlines for integration and standardization of the various parts of the German grid code.

Table 2. 3: Summary of Grid Code requirements in various European countries

	Most Stringent	Design Intent	Germany	United Kingdom	Denmark	Holland	France	Spain	Ireland	Italy	ENTSO-e
Voltage Range	**+ 10% - 15%**	**+ 10% - 15%**	±10%	±10%	+10% to -5%	± 10%	± 10%	Dep'dent	±10%	+10% -15%	+10% -12.5%
Frequency Range	**± 5%**	**± 5%**	+3% - 5%	± 2%	± 2%	± 1%	± 1%	± 0.3%	-1% to +4%	+3% -5%	± 5%
PF Lag	**0.8**	**0.8**	0.95	0.85	0.9	0.95	0.95	0.85	0.95	0.9	0.85
PF Lead	**0.9**	**0.95**	0.95	0.95	0.95	0.95	0.98	0.95	0.98	0.9	0.9
Harmonic Content	**<3%**	**<3%**	<3%	<5%	<5%	<5%	<3%	<3%	<3.5%	Not specified	Not specified
Active Power Reduction – Steady State	**No Red'n**	**No Red'n**	No Red'n	Yes after 20 sec below 47.5 Hz	15% reduction on 30min	yes after 10min	No Red'n	yes outside oper'g points	N/A	No Red'n	No Red'n
Fault clearing time	**250ms**	**250ms**	150ms at 30%	140ms	150ms - 250ms	100ms	250ms	500ms at 20%	N/A	200 ms	140 to 250ms (@5% to 30%)

Table 2. 4 : Timescales for enforcement of the pan-European ENTSO-e grid code

March 2013	Final Revision Issued
December 2013	Approval, acceptance, adaptation of the regulations by the member states
2014 to 2016	Implement the code, modify the local code to be in line with the RfG
2017	Mandatory

Table 2. 5: Timescales for enforcement of German grid code

	Grid code enforcement dates	
	Wind / Photovoltaic / Fuel Cell plants	Internal Combustion Engine plants
Steady State	01/04/2011	01/01/2010
Full grid code – static / dynamic grid code	01/04/2011	01/01/2013
Certification obligation	01/04/2011	01/01/2015

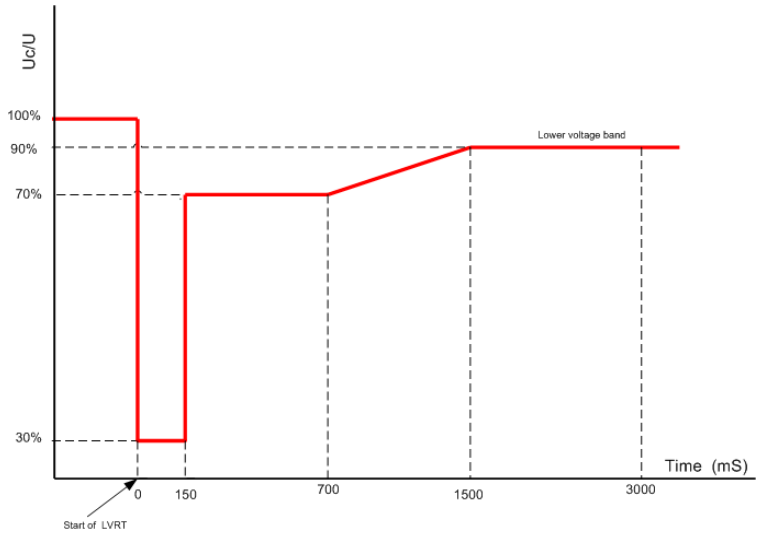


Figure 2. 4: LVRT - German grid code

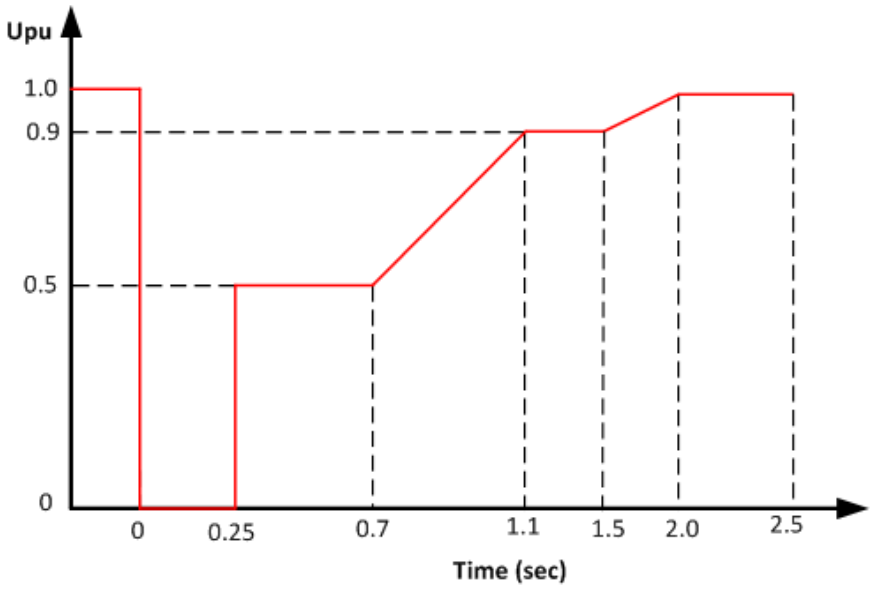


Figure 2. 5: LVRT - France grid code

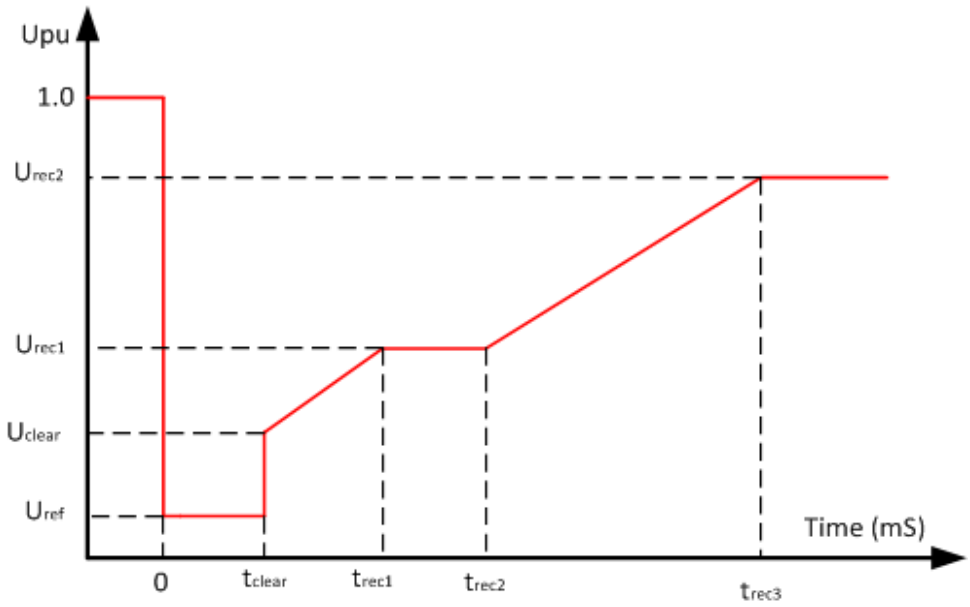


Figure 2. 6: LVRT - ENTSO-e grid code

2.2.3 Compliance testing and validation

Compliance to grid codes is proven using the test setup shown in Figure 2.7 [34]. The operating conditions, i.e. voltage, power factor and frequency levels of the

generating set can be controlled using the test setup. The steady state conditions of the generator under test are set to the required values stipulated by the relevant grid code; the steady state stability is thus assessed under these conditions. This is then followed by a low voltage ride through test. This consists in applying a fault at the terminals of the generating set by opening the circuit breaker CB2 (Figure 2.7). The low voltage ride through curve relevant to the grid code is then simulated by varying the reactance Z_2 and Z_1 that in principle operate like a voltage divider.

The load angle, reactive and active powers are measured during the test and compliance to grid codes on power transfer requirements during and after fault in addition to no pole slip occurring is checked. A certificate is then issued by the authorized grid code certifier to state compliance to the grid codes.

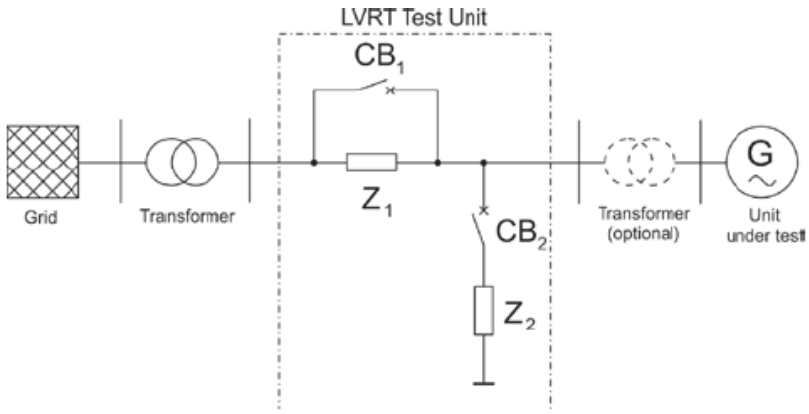


Figure 2. 7[34]: Proving compliance to grid code requirements

The outcome of the test is a comprehensive certificate of conformity approved by the test agency that confirms whether there is the capability to meet specific grid codes.

2.3 Impact of grid codes on performance of engine driven SGs

This section is aimed to study and understand the impact of the expectations set out by grid codes on engine-driven SGs. As vessel for this analysis, a system connected to the grid as shown in Figure 2.8 [28]. The grid is represented by the PCC as stipulated in various grid codes. The synchronous speed of the generating set is ω_s which corresponds to the appropriate grid electrical frequency. The SG reactance X_{gen} while $V_{terminal}$ is the voltage measured at the point of common coupling and is the reference voltage for the generator. V_{gen} is the internal electromotive force developed by the generator.

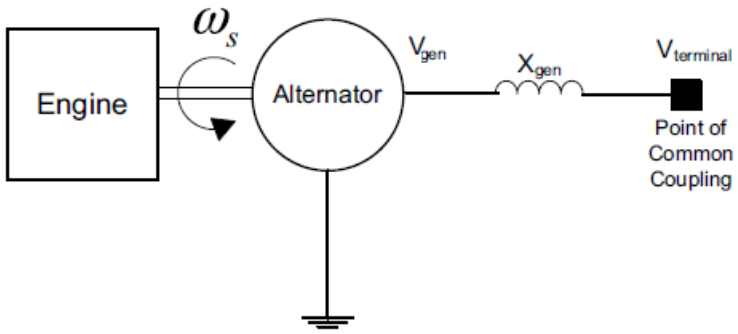


Figure 2. 8 [28]: Single line representation of engine driven SG connected to the grid

A generic grid code is imposed on the generating set of Figure 2.7. The study is focused on three specific operating regions, namely Steady State, Fault Ride Through and Post Fault Ride Through. These are shown in Figure 2.9 [32] and the major features can be summarized as follows.

- Steady State Condition: Grid codes require power plants and the generating sets to be capable of maintaining stability under a wide range of voltage levels and various power factor and frequency combinations. Using the values for frequency, power factor and voltage, shown in Table 2.3, the boundaries of operation for the generating set are defined and these are shown in Table 2.6 below, where U is given in percent of $U_{nominal}$, f is expressed in dependence $f_{nominal}$ and the power factor pf is represented with a '+' for lag and a '– 'for lead:

Table 2. 6: Boundaries of operation for generating set according to grid codes

U	f	pf
+10%	+2%	-0.95
+10%	-2%	-0.95
-10%	-2%	-0.95
-10%	-2%	+0.95
-10%	+2%	+0.95
-10%	+2%	-0.95

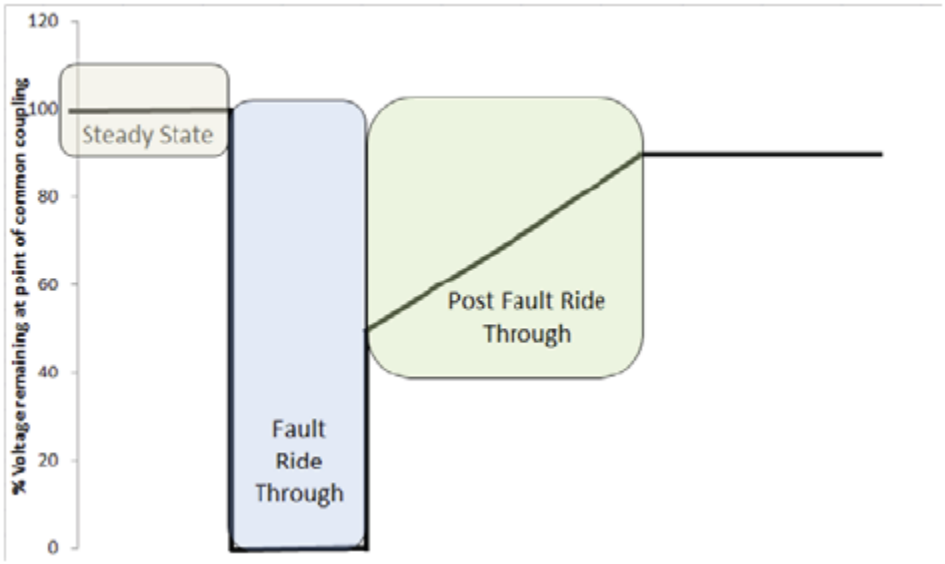


Figure 2. 9 [32]: 3 operating regions for a grid connected engine driven generating set

As shown in [29] and [30] the worst-case combination in terms of stability of any alternator operating in a power system, involves the combination of Un=-10% and pf = -0.95. These values determine the steady state load angle of the alternator for any given load demand. The steady state load angle needs to be within the design margin of the alternator for steady state stability to meet the grid code requirements under static conditions. As described by (2.1) and Fig. 2.10, the design margin for steady state stability depends on the synchronous reactances X_d and X_q. This is also substantiated further in Appendix 4. E_f is the air-gap emf in the SG, V_g is the voltage at the point of common coupling, X_d and X_q are the d and q axis reactances and δ_g is the steady state load angle.

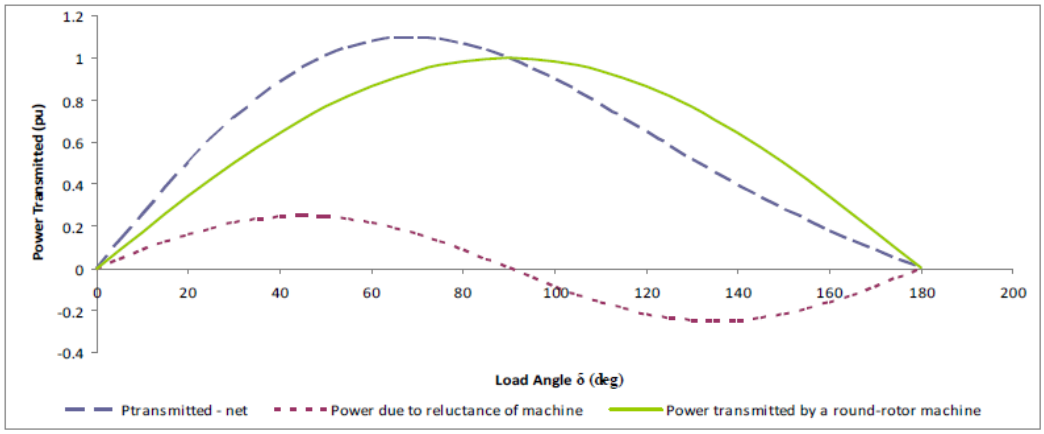


Figure 2. 10 Representative Electrical power vs load angle curve [29]

$$P_{em} = \frac{E_f V_g sin\delta_g}{X_d} + \left(\frac{V_g^2}{2}\right)\frac{X_d - X_q}{X_d X_q} sin2\delta_g \quad \text{-------- (2.1)}$$

The steady state conditions defined by the static grid codes thus regulate the steady state load angle δ_g of the SG. Equation 2.1 also confirms the need to consider an alternator design that can operate within its stability margin for the defined steady state boundary conditions.

- Fault Ride Through: During the fault ride through, the voltage at the PCC drops to a value determined by the location and intensity of the fault on the grid. If the nature of the fault is to reduce or even completely remove the active loading on the alternator, the kinetic energy stored in the shaft produces an acceleration of the rotor. The well-known technique of the equal-area criterion [33] is used to predict the ability of an alternator or a generating set to maintain stability under transient conditions. Figure 2.11 [33] describes the condition as set out by the equal-area criterion for transient stability.

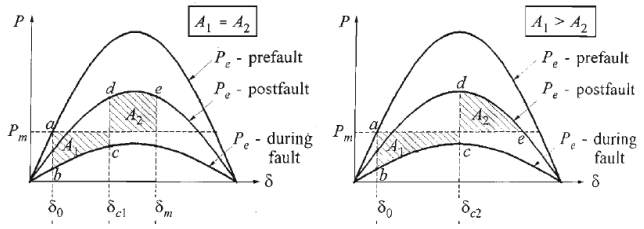


Figure 2. 11 [33]: Equal-Area Criterion

In Figure 2.11[33], the areas A_1 and A_2 represent the energy gained during the acceleration and energy lost during deceleration. The system (alternator / generating set) is said to be

- stable under transient conditions if the energy gained ≤ energy lost
- un-stable or tending towards instability if the energy gained > energy lost.

According to the grid codes summarized in Table 2.3 the alternator / generating set must remain in this 'accelerating' state for between 150 ms – 500 ms without pole slip, after which it must reconnect to the grid as seamlessly as possible before the transition into the next condition. The expectation is that the power plants provide reactive power to stabilize the grid voltage by staying connected to the grid during a fault ride through.

- Post Fault Ride Through: The alternator that had accelerated during the fault now has to connect to the grid that is now back online after the fault has been cleared. In addition to reconnecting, the generating set / power plant is expected to start delivering pre-fault active power within a

specified time. The main challenge is that, depending on the rotor position of the alternator and the speed of the rotor, the reconnection can be anywhere from a smooth uneventful synchronization potentially due to a catastrophic out of phase synchronization event.

To understand the dynamics associated with an out of phase synchronization, a test was setup at CGT. The test is performed by using a 400 V, 50Hz, 72.5 KVA alternator, electrically connected to another alternator in the 1445 KVA, designed to produce a 400V supply at 50Hz. The test setup is shown in Figure 3.2. The phase angle between the voltages of the alternators are monitored and the difference in the phase angle is controlled by varying speed of the two machines. The test emulates a small power plant (the 72.5kVA machine) connected to a grid (emulated by the 1.4MVA system). The stator and rotor currents on the smaller generator are measured and their values recorded for various phase angles between the two machines ranging from -180 degrees to +180 degrees in steps of 15 degrees. The test confirmed that depending on the phase angle mismatch between the voltages, the out of phase synchronization could lead to catastrophic outcomes. The torque produced by the event at 150° phase difference exceeded the load capability of the shaft of the 72.5kVA SG and damaged the key-way of the shaft, as shown in Figure 2.13 [28].

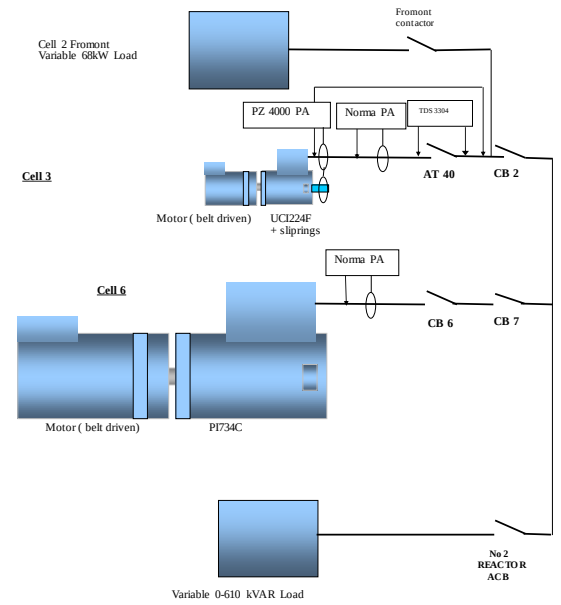


Figure 2. 12: Test Layout for emulating out of phase synchronization

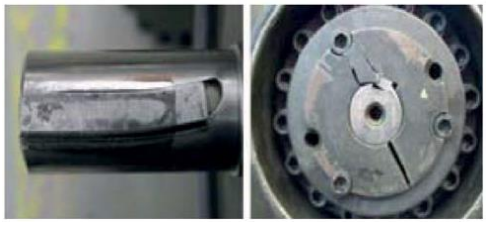


Figure 2. 13 [28]: Damaged keyway of shaft due to out of phase synchronization

In addition to the mechanical and structural damage, the rotor field voltage can register values as high as approximately 10-20 times the rated (i.e. under normal, full load operation) rotor voltage because of the current transients in the stator. Potential effects of these high voltage ‘surges’ in the rotor include degradation of the rotor insulation over time and damage to the diodes of the rotating rectifier, typically present in gensets employing brushless excitation systems.

All these potential events can lead to an inability of the alternator / generating set to meet the grid code requirements, i.e. in this case to return to pre-fault conditions within a desired time period and eventually this can lead to the power plant owner to be prevented from connecting to the grid by the power system operator.

It is clear from the above that designing for grid code compliance needs a two-pronged approach – a) Design for compliance and b) Design for robustness.

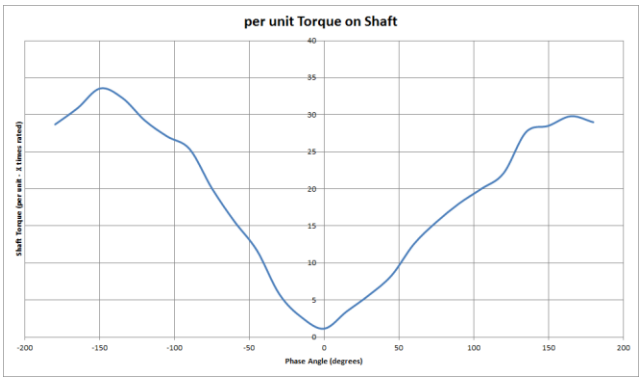


Figure 2. 14: Per Unit shaft torques measured on the UCI224F leading to the cracking of the shaft key as in Figure 2.13

2.4 Solutions adopted by the Renewables Industry

In the field of renewable energy, the wind industry was the first to be regulated towards modifying the conventional system designs to meet grid code compliance. To achieve this, wind farms adopted a combination of power electronics (full power converters), high inertia, and braking resistors. These solutions have proved to be

very effective in making wind turbines grid code compliant. Considering this, then a part of this thesis consists in an evaluation on the feasibility of using some of these solutions for the application at hand. The details of this evaluation are in Appendix 1 and the summary of the findings are shown in Table 2.6.

In summary, the main benefits and drawbacks of adopting the above solutions are:

1) Increasing the SG inertia is a good way to improve stability. However, the resulting extra weight has a detrimental effect on the system power density, which is an important factor in terms of cost and quality of the system.
2) Braking resistors are relatively very expensive, especially for larger engine driven generating sets and sometimes pose the risk of over-voltages during low voltage ride through. They also impact the efficiency of the generating set negatively during steady state operation.
3) Full Power converter / power electronics solutions are very effective; they control the active and reactive power at the output of the generating set under steady state conditions and temporarily decouples the generator from the grid during the low voltage ride through. Apart from their effect on grid power quality (switching harmonics), these converters come at a very high economical cost.

Table 2. 7: Comparison of grid code solutions adopted by the wind industry

	Inertia	Braking resistor	Full Power Converter
Functionality	Low	Moderate	High
Impact on generating set design	Low	N.A.	Moderate
Costs	Moderate	Moderate	High
Efficiency	Moderate	Moderate	Low
Market availability	Moderate	Low	Moderate

It can be seen from Table 2.7 that while several solutions exist that can be implemented on engine driven generating sets, there are practical issues associated with costs, market availability, functionality and implementation challenges that can limit the ability to use the above-mentioned solutions.

2.5 Conclusion

In this chapter, the concept of grid codes was introduced, and the various challenges posed by the ever-increasing role and importance of grid codes were described. The various solutions adopted by the wind turbines to comply with grid codes were also summarized in Section 2.4, along with the challenges that such non-invasive (to the SG itself) solutions pose to engine driven generating sets. It is therefore clear that there is a significant gap in terms of addressing the challenges related to the grid code compliance of engine driven SGs. While reciprocating engines have a impact

on the dynamic performance of the generating set through contributing to the overall inertia of the generating set, the general contribution of the reciprocating engine in distributed power plants is minimum due to the speed of the transient events being quicker than the mechanical time-constants; added to the high cost of the reciprocating engines compared to SGs and the numerous types of reciprocating engines in the market, it becomes the onus of the SG manufacturers to design their products to be grid code compliant for a wide range of reciprocating engines. As discussed above, this gap can be filled with improved design processed for SGs that establish grid code compliance as a major objective function, at the fundamental component level (i.e. the design of the alternator itself).

An important point to note is that due to the variations in grid codes published globally, it is important to develop a design and analysis tool that while being highly accurate and reliable, also allows a certain measure of flexibility, to be able to 'cater' for different grid code performance requirements.

CHAPTER 3

SG Modelling

As explained in Chapter 2, the sensitivity of the power system model to the SG's equivalent circuit parameters is quite significant and it is therefore essential to predict them in an accurate and consistent way. Traditionally, these parameters have been calculated using analytical methods or tests [96] – [106]. While the analytical methods are quick and provide the designer with the ability to try several iterations before building the prototype, they only provide approximate solutions while neglecting the geometrical details and the ensuing electromagnetic phenomena that characterize the machine.

Testing of the machines represents the most accurate method of evaluating the SG performance, but can be expensive and time consuming, when compared to virtual prototyping procedures.

Recent advances in computational resources and methods enable the use of modern analysis and design tools, that can offer a 'middle ground' for design engineers. Amongst these methodologies, numerical methods such as provided by commercial FE tools represent today's state of the art in terms of machine design and development. Considering this, an automated FE analysis tool is built using the commercial package Vector Fields Opera and its development and validation will be detailed in Chapter 4. In this chapter, the classical methods of SG analysis are discussed and presented. are implemented with an automated script that has been

used to predict the SG's equivalent circuit parameters and design the SG considered in this thesis.

3.1 Literature Review

3.1.1 Basic Theory & Construction

A generator is a device that converts mechanical energy into electrical energy. The energy conversion is controlled by a magnetic field inside the generator. Majority of the generators used in power generation currently are SGs. These are AC rotating machine in which, at steady state, the speed of the rotation of the shaft is directly related to the frequency of the armature electromagnetic quantities. The two main parts of a conventional SG are the stator and rotor. The stator consists of a magnetic core supported by a frame for structural integrity. The stator houses the armature windings usually held in slots stamped into its inner periphery. The rotor is made up of magnetic material and includes the so-called field winding, which is wound around the rotor poles. The rotor is attached to a rotating shaft that is used to mechanically couple the rotor to the prime mover and is separated from the stator by an air-gap. Based on the rotor pole geometry, there are two types of SGs – salient pole and cylindrical rotors [55]. Figure 3.1 shows the axial cross-section of a four-pole salient pole SG representative of the type that is the focus of this thesis. The part of the pole closest to the air gap is called the pole shoe. On these poles, an additional winding, known as the damper cage, which is used for multiple purposes is also usually implemented. A classical approach is used to study the operation

of the SGs is given in [54], where the direct (d-axis) and quadrature (q-axis) axes are used to model the machine behavior.

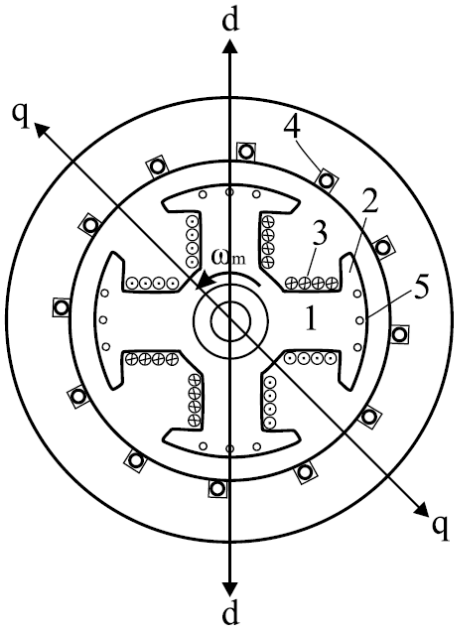


Figure 3. 1– Axial cross-section of SG [56]

3.1.2 Equivalent Circuit Model of the SG

In studies, which involve the understanding of the behavior of SGs either separately or as part of a system, a set of electrical equations are used to represent the operation of the machine under various operating conditions. Based on the level of complexity and accuracy relative to the application, the equivalent circuit models are characterized by several equations which define the order of the system. The equivalent circuit of a SG with the relevant circuit parameters are shown below in Figures 3.2 a and b. The quantities shown in Figures 3.2 a and b are: L_{fd} and R_{fd} are the field self-inductance and field resistance along the direct axis (d-axis) respectively, L_{1d} and R_{1d} are the d-axis damper circuit self-inductance and d-axis

damper cage resistance respectively, while L_{1q} and R_{1q} are the q-axis damper cage self-inductance and resistance respectively, L_{ad} and L_{aq} are the armature self-inductances along d and q axes respectively; ed and eq are the induced emfs in d and q axes respectively, while e_{fd} is the field voltage, ω the angular frequency in rad/sec, Ψ_d and Ψ_q are the d and q axes flux linkages, R_a the armature resistance and L_l the leakage self-inductance.

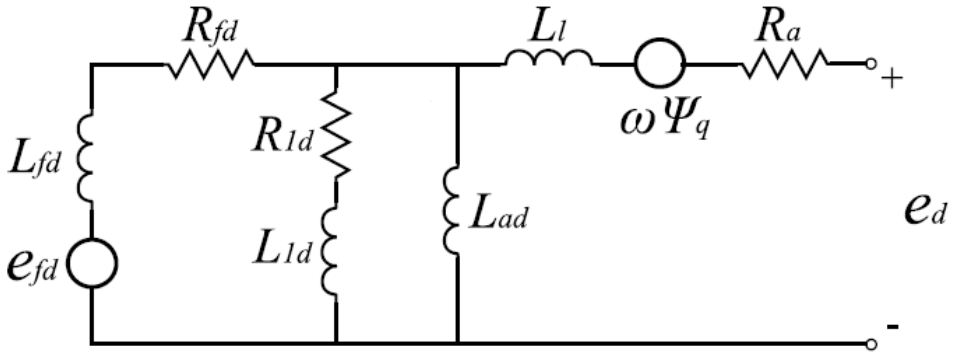


Figure 3. 2 a – Equivalent circuit of a SG in the d-axis

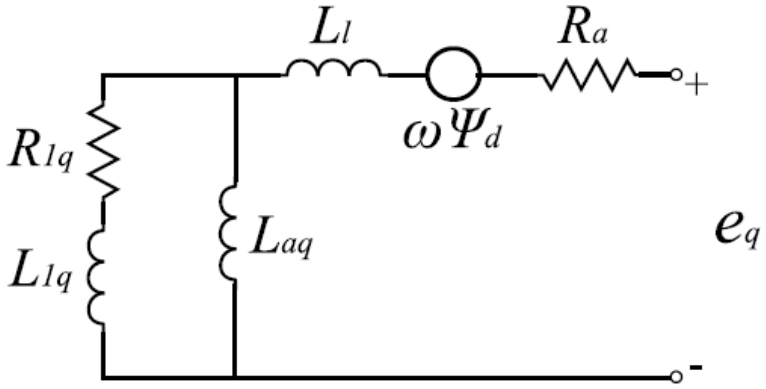


Figure 3.2 b – Equivalent circuit of a SG in the q-axis

3.1.4 The Finite Element Method

While the classical equivalent circuit analysis is well-known and consolidated, however it represents certain drawbacks, such as limited ability to predict operation under non-linear conditions (saturation), parameter variation due to geometrical features like slot and teeth geometry, graded air-gap on rotor poles, asymmetrically distributed damper cage and connection of damper bars in d and q axes. These drawbacks can be solved using more accurate techniques such as FE. The FE method, used to design and analyze electrical machines has been gaining popularity in recent years due to the availability of powerful computing systems, and because it can achieve and predict very accurate results [43].

Although FE methods are wisely utilised for predicting the performance of any electro-magneto-mechanical device, this section describes the basic concepts relative to the use of such technique for the electromagnetic analysis of electrical machines and of classical, salient-pole, SGs. An overview of the two-dimensional finite element methods is given in [43].

The finite element method consists in by segmenting the geometry / space into a number of sub-domains (the finite elements) and this concept is shown in Fig 3.3. The relevant system of equations are then applied to each of these sub-domains with the associated boundary conditions applied. The sub-division of the analysis space into small sections allows the finite element algorithm to run several problems of manageable sizes that product improvements in computational speed and efficiency.

Finite Element Analysis can broadly be summarized in 4 steps:

1. Creating ‘finite-elements’- The problem domain is divided into a number of relatively smaller, finer elements, whose size depends on computational speed and solution accuracy requirements. Increasing the number of elements provides better accuracy at the cost of increased computational resource.

2. Selecting the interpolating functions – Functions representing the unknown quantities are selected. The quantities are typically simple and the calculation of which at the small scale can be replicated at the larger scale as well.

3. Defining the system of equations – The interpolating functions and associated boundary conditions are used to formulate a system of equations that will be solved by the computational system. A detailed review of the process of selecting equations is described in [43].

4. Solving the system of equations developed using the interpolating function, then the results are obtained. The solution provides spatial and / or temporal values for the interpolating functions that can be used to glean more information about other quantities.

While, Finite Element Analysis can be done in two and three dimensions, most of the problems can be solved by employing two-dimensional analysis [43]. In applications, where the three-dimensional effects can’t be neglected, then a popular method is to implement correction factors thorough analytical formulas to compensate and take these effects into account.

3.1.4 Predicting Electrical Machine Reactance using Finite Element Analysis

A good overview of finite element analysis of electrical machines and electromechanical devices in general is given in [43], where techniques to determine and identify the main parameters for synchronous machines are discussed along with numerical algorithms to implement some of these methods.

References [44], [45] and [46] provide an exhaustive description of synchronous machine operation during steady state and transient conditions.

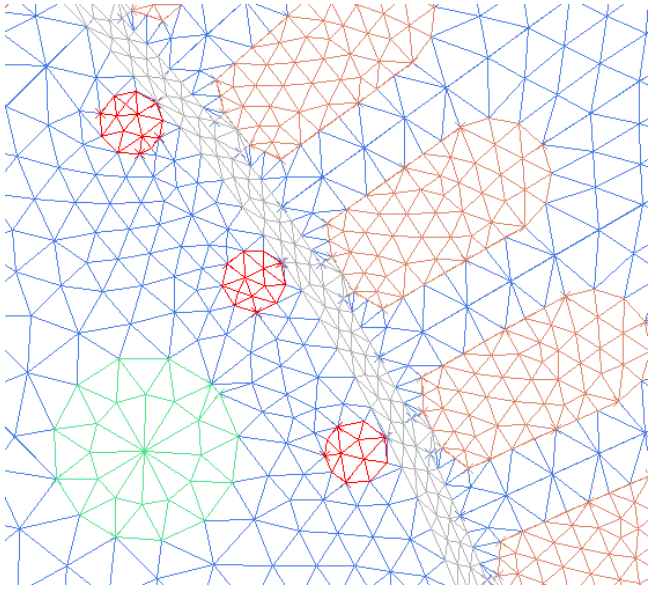


Figure 3. 3 – Finite element model of a SG showing the sub-domains / finite elements

Mathematical models of synchronous machines are compared and their pros and cons relative to steady state and transient simulations are described. In [44], several test procedures to determine synchronous machine parameters are compared and it

recommends that either sudden short circuit test or steady state frequency response test may be used to determine transient and sub-transient parameters for the SG.

A magneto-static method of predicting transient and sub-transient SG parameters using FE is elaborated in [47]. This method involves replacing currents, induced in damper cage and field winding by an equivalent boundary condition.

Stator winding currents may be chosen to represent MMF aligned with d or q axis (based on power factor or operating condition). The assumptions used in this model enable faster computation of transient and sub-transient parameters, but, this method is recommended for larger SGs, specifically, those used in hydro power plants [47].

In [48] a detailed approach to calculate reactances for SGs with cylindrical rotors is presented. The magneto-static method is used, and the methods described in [47] are applied to simulate magnetic saturation. The method is validated, and the authors observe a 10% difference between test data and predicted values. In [49], a method to calculate reactances for salient pole synchronous machines equipped with damper windings is presented. A time harmonic simulation is used to calculate transient and sub-transient reactances. The rotor position is fixed, and field currents of varying frequencies are used to simulate the rotor under different operating conditions. In this work it is observed that while a time harmonic simulation is faster and requires minimum computing resources, the results are dependent on the frequency used to simulate the rotor under fault conditions and the designer should ensure that the ‘correct’ frequency is used to minimize errors in prediction.

According to [50] and [51] actual test procedure can be replicated with time step simulations. With this technique, the electrical machine is initially running under open-circuit condition and a sudden short-circuit is then applied. Current traces are recorded and are used to calculate reactances. The time step simulation depends on how the model is setup and most importantly on how an external fault simulation circuit is setup. The short circuit in an electrical machine only involves the direct axis (d-axis) and hence the data from short-circuit test provides limited information on the quadrature parameters (q-axis) [47]. The stand-still frequency response test allows for the prediction of both d-axis and q-axis reactances. The rotor is stationary during the test and its position fixed to direct / quadrature axis as required. The armature winding is supplied an AC voltage of varying frequencies and magnitudes. The current induced in the armature winding is measured and is used to predict the reactances along the d and q axes. In [52], an approach that consists in using the stand-still frequency response to determine machine reactances is described. The main conclusion of this work is that the suggested method is viable and poses minimum risk to the electrical machine during the test.

All the above indicates the wealth of literature that exists today in terms of SG modelling and analysis. The current state of the art is however still based on defining individual techniques and methodologies aimed at describing one aspect (or a set of parameters) of the SG. The aim is therefore to develop and validate a more comprehensive a design tool and its associated GUI, whose objective is to predict the entire equivalent circuit parameters of a SG using only the geometry of the generator as input, via FE techniques.

3.2 Finite Element Tool Development

3.2.1 Overview

This section describes the various finite element techniques that are adopted to predict the SG reactances characteristics of the SG's equivalent circuit. The reactances predicted by using this method are: the d and q axes synchronous reactances – X_d and X_q respectively, the d and q axes transient reactances – X'_d and X'_q respectively and the d and q axes sub-transient reactances – X''_d and X''_q respectively. All other parameters (i.e time-constants) are then extrapolated based on the reactance values. All the methods described in this section are used to develop an algorithm that is then controlled through an appropriately designed user interface. A SG reactance calculation tool will be also developed and used into the power system simulation model. This tool will also be used to design the grid code compliant SG described in Chapter 7 of this thesis.

3.2.2 Computational Algorithm for SG Reactances calculation

Based on the literature review discussed in Section 3.1.4, an extensive assessment of the various finite element techniques used to predict the SG parameters was completed and the results are summarized in Figure 3.4.

Through the assessment completed, it was determined that a magneto-static simulation can be used to predict X_d and X_q, while several methods can be implemented for the transient and sub-transient parameters – specifically, the short-

circuit simulation vs single frequency response, to ensure that the SG machine model could be suitably validated.

Method of prediction	X_d	X_q	X'_d	X''_d	X''_q
Sudden short-circuit	×	×	✓	×	×
Single frequency response	×	×	×	✓	✓
Magneto-static simulation	✓	✓	×	×	×

Figure 3. 4 – Summary of methodologies used based on literature review to predict synchronous generator parameters.

3.2.2.1 Computational Algorithm for SG Reactances calculation

In this section, the findings presented in Figure 3.4 are explained in greater detail and a step by step approach is developed to automate the process of calculating SG parameters.

3.2.2.2 Calculation of X_d

The synchronous direct axis reactance X_d is defined as the reactance of the phase winding whose axis coincides with the direct axis of the rotor, when the three-phase currents are flowing through the armature windings [54]. The magneto-static solver is sufficient for the calculation as relative speed between the rotor and the armature reaction field is zero, thereby resembling a 'static' condition. Due to the geometrical symmetry associated with the design of salient pole machines, only one pole is modelled, and boundary conditions are assigned according to Figure 3.5. Field current is set to be zero so magnetic field is only induced by the armature currents.

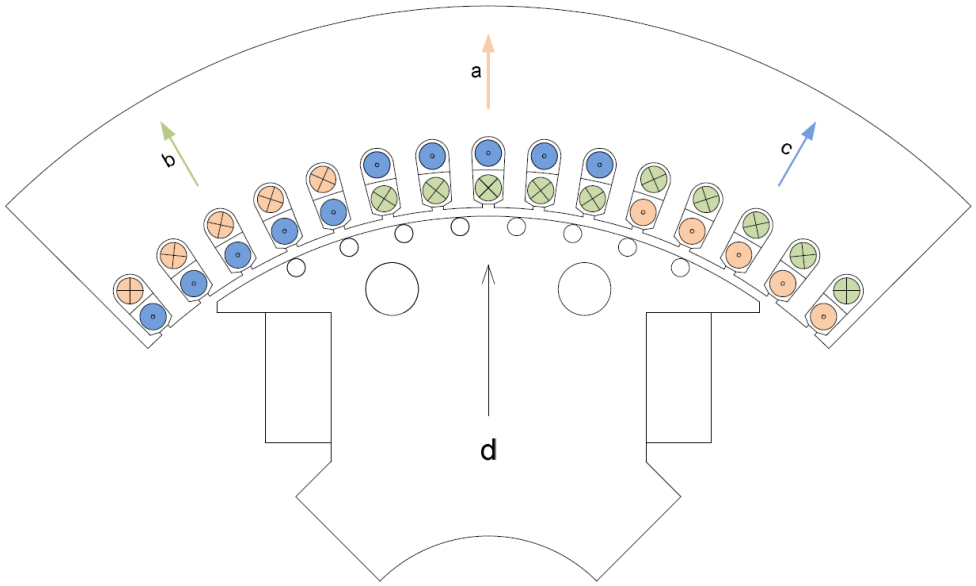


Figure 3. 5 – Winding configuration for predicting d-axis reactance

In magneto static simulations, DC currents are injected into the armature conductors when the direct axis aligns with peak mmf. This is followed by computation of the magnetic vector potential. In the FE simulation set up for this purpose, the field winding is not excited. However, it is also possible to run the simulation with the field winding excited, but the flux due to the excitation current must be subtracted from the total flux linkage of the d-axis coil to obtain the d-axis reactance.

Additionally, due to the non-linear properties of the electromagnetic materials, the simulation had to be repeated at various values of d-axis currents to plot a reactance profile and to accurately capture the saturation characteristic. In Fig. 3.6, the flux lines distribution of the salient-pole SG under analysis is shown.

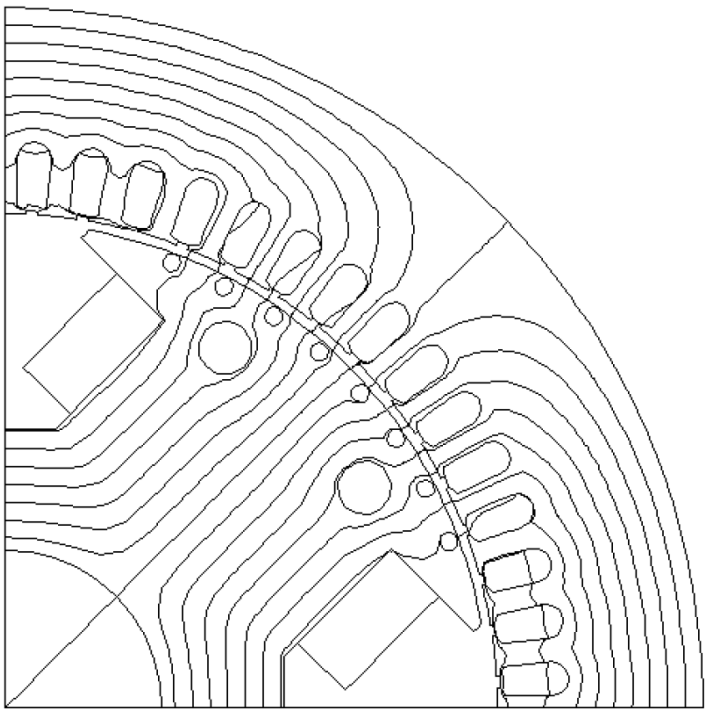


Figure 3. 6 – Flux plot for armature windings excited by only d-axis current

3.2.2.3 Calculation of X_q

The q-axis synchronous reactance prediction method is identical to that of the d-axis synchronous reactance as described in Section 3.2.1.1, with the only difference being the q-axis is aligned with peak mmf in the former. The winding configuration and flux lines distribution for the q-axis reactance prediction method are shown in Figures 3.7 and 3.8 respectively. The effect of saturation is considered, also for the q-axis reactance evaluation. shown. The synchronous reactances, evaluated along the d- and the q- axes, are shown in Figure 3.9, where the saturation effects can be observed.

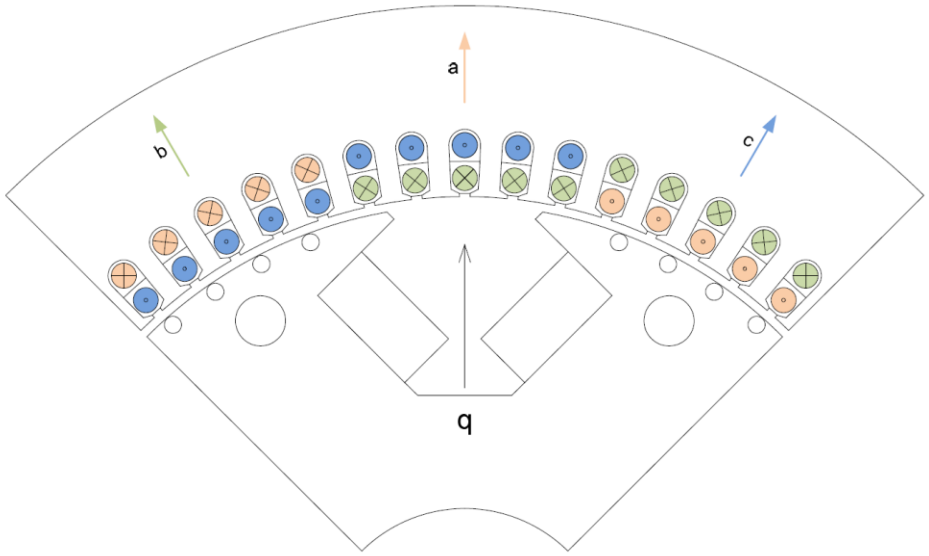


Figure 3. 7 – Winding configuration for predicting d-axis reactance

3.2.1.3 Cross-Coupling and impact on X_d and X_q values

Cross-coupling is the magnetic interaction between the direct and quadrature axes that becomes relevant to the SG performance prediction especially during saturated conditions [145] [146]. It is crucial to include the effect of cross-coupling in the calculation of synchronous reactances to be able to accurately predict load angles [146]. Equations (3.1) and (3.2) summarize the impact of cross-coupling on the flux linkages in the d and q axes. This section focuses on the phenomenon of cross-coupling and its impact on synchronous reactances. With high levels of magnetic flux, the d-axis may be saturated by flux from q-axis and vice versa and the synchronous reactance is a function of currents in both axes.

$$\varphi_d = L_d(i_d, i_q) i_d + \varphi_{dq}(i_d, i_q) \quad (3.1)$$

$$\varphi_q = L_q(i_d, i_q) i_q + \varphi_{qd}(i_d, i_q) \quad (3.2)$$

Where, the d and q sub-scripts represents the quantities along the d and q axes respectively, i the current, L the self-inductance and φ is the flux linkage.

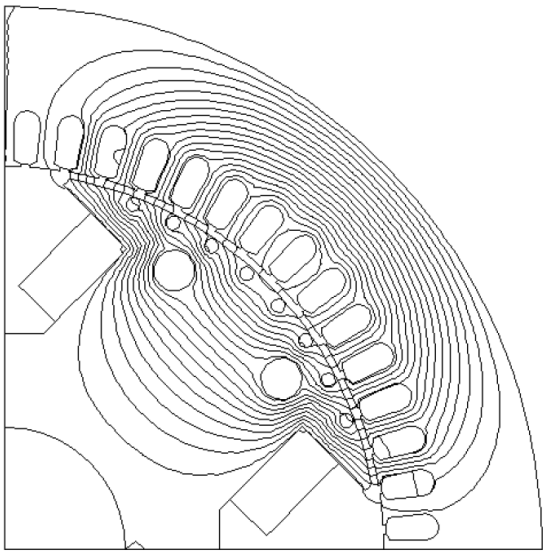


Figure 3. 8 – Flux plot for armature windings excited by only q-axis current

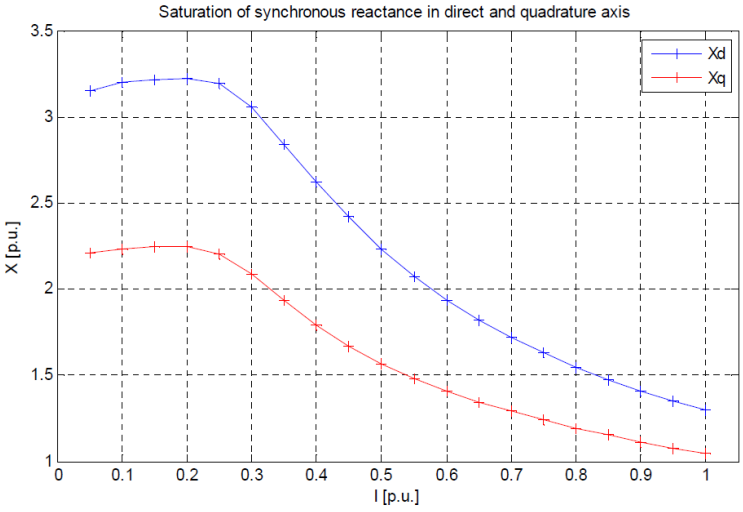


Figure 3. 9 – Impact of saturation on the synchronous reactance values

The effect of cross-coupling is included into the model by using the following procedure:

1) Inverse park transformation is used to calculate d and q axes stator currents. These currents are then introduced into the armature windings.
2) The associated flux linkage of each phase coil is then transformed in to the d-q reference using Park Transformation.
3) The flux linkages in d and q axes are then used to calculate the associated inductances / reactances using the known current values in the corresponding axes.
4) The reactances may be plotted in a contour plot, as shown in Figure 3.10, and are then used as lookup tables which are used in reactance prediction.

Figure 3.10 shows the contour plot of the d-axis synchronous reactance plotted against the d and q axes currents. It can be observed that as the current in either axes increases, the d-axis synchronous reactance reduces due to saturation in the machine. The values from the contour map can be used to create a table relating the reactances, in this case the d-axis synchronous reactance with the currents. Since the d and q axis currents for any given electrical load depend on the power factor and on the loading of the SG, the table can then be translated into a specific reactance value for the machine at any given operating point.

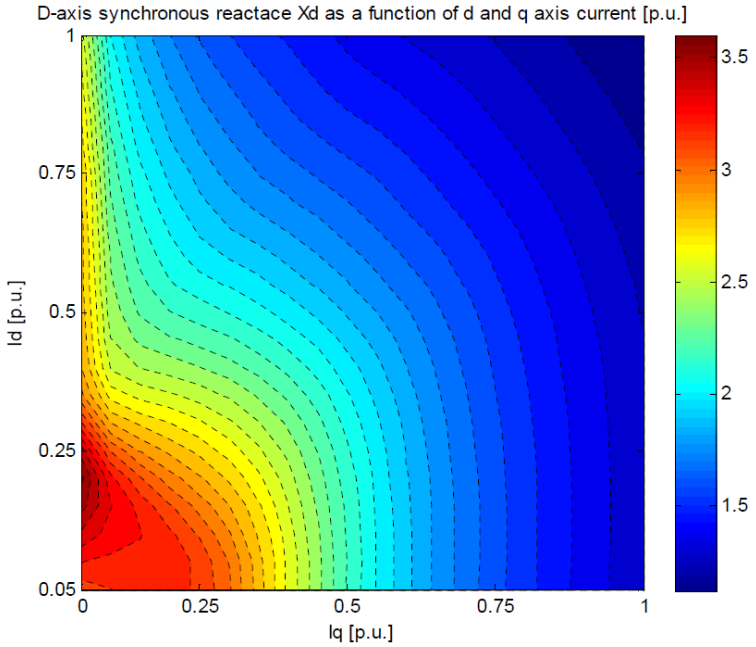


Figure 3. 10 – Contour plot of d-axis reactance plotted as functions of d and q axis currents

3.2.2.4 Calculation of end-winding leakage reactance

The datasheet in Figure 3.17, shows that the leakage inductance itself has a minimal contribution to the overall performance of the SG and the end-winding leakage inductance from [139] and [140] can be shown to contribute to not more than 5% of the overall reactance of the SG even during dynamic conditions. [138], [139] and [141] also show that during a transient event, the leakage reactances relative to the rotor and field winding dominate the performance of the SG. This means that while the end-winding leakage reactance needs to be modelled for completeness, even a 100% error in end-winding leakage would lead to a small variation in the

performance of the SG and well within the allowed tolerances according to international standards [66].

[139] lays the foundation to calculate ‘armature leakage reactance as shown in equation (3.3). where the first term in the bracket represents the slot leakage and the second term in the bracket represents the end-winding leakage. In equation (3.3), A is the maximum Ampere Turns per pole, d_1, d_2, d_3, w are the slot dimensions from [139], D if the air gap diameter, F is the no-load air-fap ampere turns per pole, K_B is the leakage constant, K_P and K_D are the pitch and distribution factors of armature winding, L is the core-length, p the winding pitch, P the number of poles, S the number of slots, X_l the armature leakage reactance and $\emptyset$ the flux per pole.

A 2D FE model of a SG includes the effects of leakage reactance due to the higher order harmonics, the slot leakage inductances, and the leakage flux between the poles. Other inherently 3D features, such as skewing (when implemented) and end winding effects, can be also considered in 2D models of SGs. The value of the end winding leakage flux may sometimes be ignored during normal operation but the saturation effect, during the short circuit can strongly influence the magnetic circuit in the teeth close to the short-circuited windings, since they may carry elevated currents. As the end windings are surrounded by air and almost unaffected by the saturation effect it gains in importance in case of a short circuit.

The end-winding leakage flux can be accurately modelled only by an accurate 3D, FE evaluation of the electromagnetic phenomena. However, these models consume

significant computing time and resources. To simplify the process of end-winding leakage flux calculation, a variation of the end-winding part of equation (3.3) can be modified to derive (3.4) can be used within the developed FE analysis code to approximate the end-winding leakage. In (3.4), l_{ew} is the effective end winding length, and λ_{ew} is the specific permeance coefficient; its value ranges between 0.35 and 0.55, according to the winding type (winding geometry, pitch, distribution) [139].

This technique is validated using an appropriate test method developed and is described in Section 3.3 of this chapter.

$$X_l = \frac{20A}{K_p^2 K_d^2 \emptyset}\left[\frac{PL}{S}(3p+1)\left(\frac{d_3}{w}+\frac{d_1}{3w}\right)+\frac{0.3(3p-1)D}{P}+\frac{1.1A}{F}\left(\frac{P}{S}\right)^2+0.6K_B\right] \quad (3.3)$$

$$L_{\sigma,end} = \mu_0 \frac{N^2}{2p} l_{ew}\lambda_{ew} \quad (3.4)$$

3.2.2.5 Prediction of sub-transient reactance

To accurately model the transient behavior of the SG, the sub-transient reactance X''_d needs to be accurately predicted. The sub-transient reactance can be predicted using finite element analysis using two methods; the single frequency response simulation and the sudden short-circuit test. Both methods have been reviewed in the below sections and the more accurate method is applied to build the tool to predict SG parameters.

3.2.2.5.1 Single frequency response simulation

T/he single frequency response method is used to predict the sub-transient reactances of the SG. In this method the rotor is at standstill and is aligned with the direct or quadrature axis depending on the specific sub-transient reactance that needs to be predicted. The rotor winding is shorted and a rated voltage at nominal frequency is applied across two stator phases. The current in the armature windings are then measured and (3.4) is used to calculate the sub-transient reactances Z''$_{d,\,q.}$ The schematic diagram of the single frequency response calculation setup is shown in Figure 3.11, while Fig. 3.12 shows the flux line paths during the test. In this figure, the currents induced in the field winding and in the damper bars can be also noticed.

$$Z''_{d,q} = \frac{V}{2I} => X''_{d,q} = \sqrt{Z''^{2}_{d,q} - R_s^2} \tag{3.4}$$

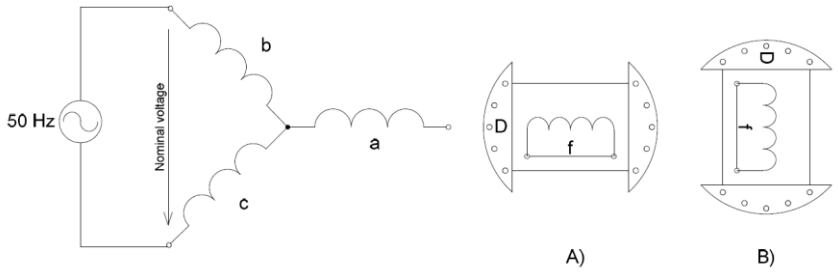


Figure 3. 11– Setup for single frequency response. A) d- axis B) q-axis

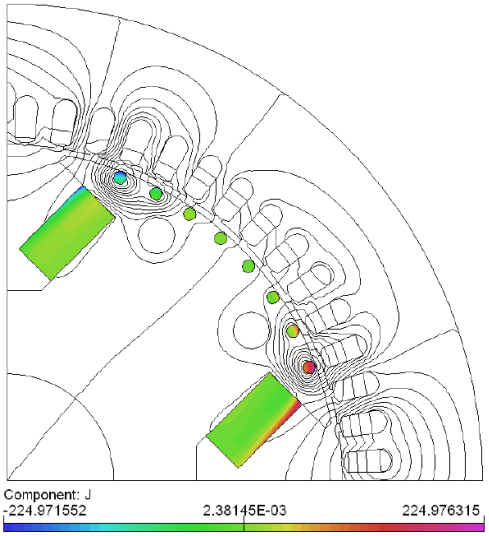


Figure 3. 12– Flux plot of single frequency response simulation – note the currents induced in the damper bars and field winding. [136]

3.2.2.5.2 Sudden Short-Circuit simulation

In addition to being capable of predicting the sub-transient reactance in the d-axis, the sudden three-phase, short-circuit simulation is also capable of predicting the transient reactance. The simulation test is carried out by using a time stepping solver in conjunction with an external electrical circuit as shown in Figure 3.13. The procedure adopted to simulate a sustained short-circuit curve can be summarized as below:

- The stator winding connections are defined by an external circuit with inductance and resistance connected in series. The resistance represents the associated values of the armature winding and the inductance value is that of the leakage inductance of the armature winding overhangs.

- The rotor rotates at rated speed and this is maintained throughout the simulation.
- The field winding is connected to an external circuit (and therefore to an external resistance and voltage source) and is coupled to the FE model. The field voltage is set to get the field current, necessary to produce the rated no-load voltage at machine terminals. The imposed field voltage is constant during the short circuit simulation, but additional currents may be induced during transient operation.
- Short circuit is applied to the armature winding using a variable resistance (parametric variable). For initial no-load run the resistance is set equal to a practical infinite value and thus only a very small current flow in the armature winding. At the chosen time instant, the resistance is switched to the value of phase resistance by an external command file.
- Short circuit current traces are recorded up to the point when they reach sustained short-circuit conditions.

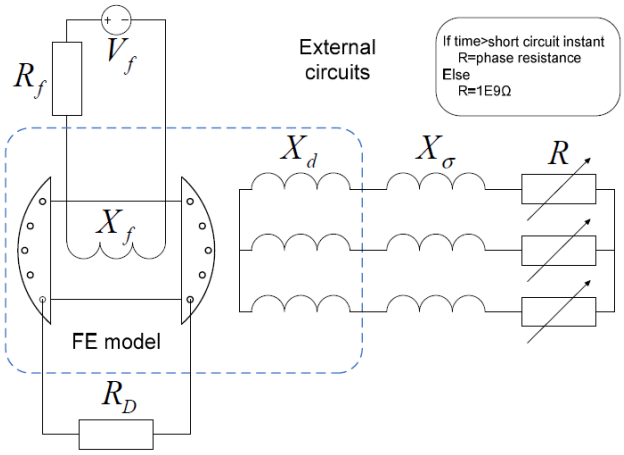


Figure 3. 13 – Setup for the finite element model to run a sustained short circuit simulation [136]

The simulation yields a short-circuit decrement curve for the currents in all three phases of the armature winding (Figure 3.14). These currents are then analyzed using a peak detection algorithm that is used to plot a graph in a semi-log plot (Figure 3.15). This is then used to calculate the transient and sub-transient reactances.

All the methods described above were automated using a script written in Vector Fields Opera. The process flowchart for this script is shown in Figure 3.16.

The next section details the testing a SG P7C that is used to validate the process developed above.

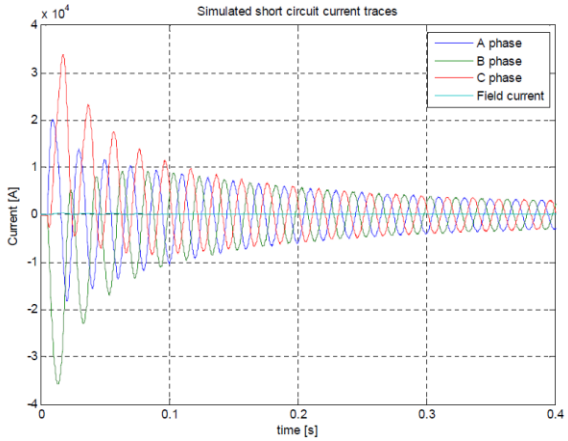
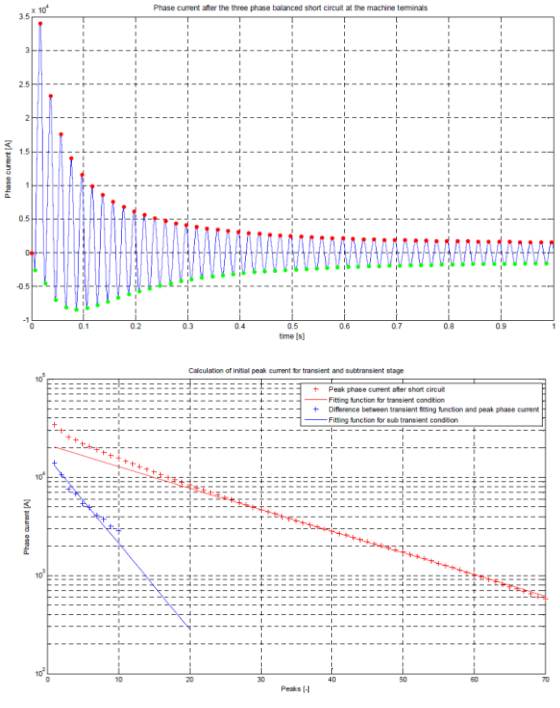


Figure 3. 14– Short-Circuit current trace



(A) (B)

Figure 3. 15 – A) current trace processed by peak detection algorithm B) semi-log plot of peak currents vs time

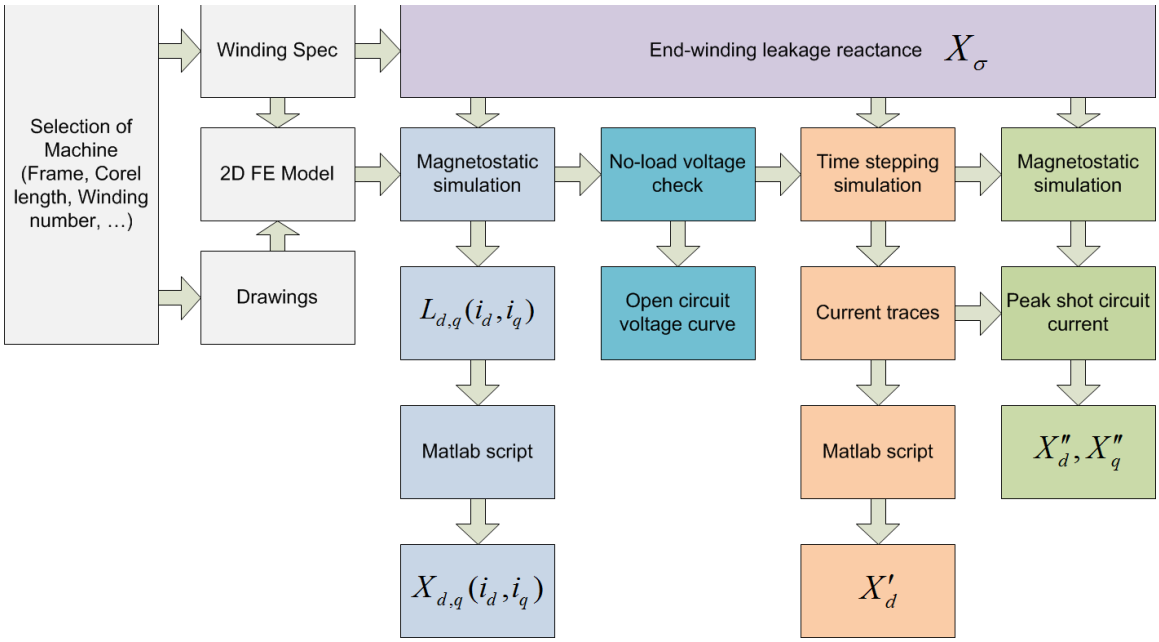


Figure 3. 16– Automated algorithm to predict SG parameters

3.2.3 Validation of SG Parameter prediction tool

To validate the process developed above, a 1.4MVA machine known as the PI734C alternator is used, whose data sheet is shown in Figure 3.17.

3.2.3.1 Validation of X_d

The characteristic reactance of a SG (i.e. the synchronous reactance) can be calculated by two tests, with the armature terminals open circuited or short circuited. The open-circuit test will be discussed in this section. The no-load voltage curve is more commonly referred to as the *open circuit characteristic* (or the *open circuit saturation curve*). The open circuit characteristic (occ) represents the connection between the *mmf* acting on the magnetic circuit when no currents flow in the stator winding and the ensuing air gap flux. As the field current increases the

magnetic material saturates and the reluctance of the flux paths along the ferro-magnetic parts of the machine increases, thus producing a reduction of the field current's ability to produce magnetic flux. The *occ* (air-gap line) represents the open circuit voltage characteristic in the machine in relation to unsaturated operation. The degree of saturation in a machine can be measured by deviations of the actual *occ* from this curve. The terminal voltage is equal to the generated voltage E_{af} when the armature terminals are open circuited. Therefore, the *occ* represents the relationship between the field current I_f andE_{af}. Therefore, comparing the open-circuit curves of the finite element analysis and test data aids with validating the finite element analysis model with respect to its ability to predict synchronous reactances. The open-circuit test on the chosen machine PI734C was performed at CGT. The test setup is shown in Figure 3.18 while Figure 3.19 shows the comparison between the FE-predicted and the experimental open circuit curves, where a good match can be observed thus validating the implemented FE model.

3.2.3.2 Validation of end-leakage reactance

A methodology is developed to estimate the end-winding leakage reactance. Two measurements are taken for this purpose:

1) The stator reactance is measured in one phase while the rotor is removed, and the other two phases are not energized. To understand the effects of saturation on end-leakage, three different voltage levels are applied, and the current is measured for the three voltages. Figure 3.20 shows the test setup.

It was confirmed that saturation does not lead to a discernible change in the end-winding leakage reactance.

2) . Replicate the test described in 1) with a 2D FE model of the PI734C generator and record the voltage/current values for the different scenarios simulated. To replicate the test with respect to rotor removal, the rotor permeability is set to 1 in the FE model, behaving then as air from a magnetic point of view.

3) The test and simulation exclude the effect of rotor position on the reactance measured / simulated. The 2D FEA model excludes end-windings and therefore the difference in the reactance obtained from the test in 1) and the 2D FEA in 2) will give the value of the end-leakage.

PI734C STAMFORD

WINDING 312

CONTROL SYSTEM	SEPARATELY EXCITED BY P.M.G.		
A.V.R.	MX341	MX321	
VOLTAGE REGULATION	± 1 %	± 0.5 %	With 4% ENGINE GOVERNING
SUSTAINED SHORT CIRCUIT	REFER TO SHORT CIRCUIT DECREMENT CURVES (page 7)		

INSULATION SYSTEM	CLASS H						
PROTECTION	IP23						
RATED POWER FACTOR	0.8						
STATOR WINDING	DOUBLE LAYER LAP						
WINDING PITCH	TWO THIRDS						
WINDING LEADS	6						
MAIN STATOR RESISTANCE	0.00126 Ohms PER PHASE AT 22°C STAR CONNECTED						
MAIN ROTOR RESISTANCE	1.85 Ohms at 22°C						
EXCITER STATOR RESISTANCE	17.5 Ohms at 22°C						
EXCITER ROTOR RESISTANCE	0.063 Ohms PER PHASE AT 22°C						
R.F.I. SUPPRESSION	BS EN 61000-6-2 & BS EN 61000-6-4,VDE 0875G, VDE 0875N. refer to factory for others						
WAVEFORM DISTORTION	NO LOAD < 1.5% NON-DISTORTING BALANCED LINEAR LOAD < 5.0%						
MAXIMUM OVERSPEED	2250 Rev/Min						
BEARING DRIVE END	BALL. 6228 C3						
BEARING NON-DRIVE END	BALL. 6319 C3						
	1 BEARING				2 BEARING		
WEIGHT COMP. GENERATOR	3018 kg				2967 kg		
WEIGHT WOUND STATOR	1445 kg				1445 kg		
WEIGHT WOUND ROTOR	1257 kg				1195 kg		
WR² INERTIA	37.3309 kgm²				36.33 kgm²		
SHIPPING WEIGHTS in a crate	3091kg				3036kg		
PACKING CRATE SIZE	194 x 105 x 154(cm)				194 x 105 x 154(cm)		
	50 Hz				60 Hz		
TELEPHONE INTERFERENCE	THF<2%				TIF<50		
COOLING AIR	2.69 m³/sec 5700 cfm				3.45 m³/sec 7300 cfm		
VOLTAGE STAR	380/220	400/231	415/240	440/254	416/240	440/254	460/266	480/277
kVA BASE RATING FOR REACTANCE VALUES	1505	1550	1550	1520	1705	1815	1855	1890
Xd DIR. AXIS SYNCHRONOUS	3.18	2.96	2.75	2.40	3.86	3.67	3.43	3.21
X'd DIR. AXIS TRANSIENT	0.19	0.18	0.17	0.15	0.23	0.22	0.21	0.20
X"d DIR. AXIS SUBTRANSIENT	0.14	0.13	0.12	0.11	0.17	0.16	0.15	0.14
Xq QUAD. AXIS REACTANCE	2.05	1.91	1.77	1.55	2.49	2.37	2.22	2.07
X"q QUAD. AXIS SUBTRANSIENT	0.29	0.27	0.25	0.22	0.35	0.33	0.31	0.29
X_L LEAKAGE REACTANCE	0.04	0.03	0.03	0.03	0.04	0.04	0.04	0.04
X_2 NEGATIVE SEQUENCE	0.20	0.19	0.18	0.15	0.25	0.23	0.22	0.21
X_0 ZERO SEQUENCE	0.02	0.02	0.02	0.02	0.03	0.03	0.03	0.03
REACTANCES ARE SATURATED	VALUES ARE PER UNIT AT RATING AND VOLTAGE INDICATED							
T'd TRANSIENT TIME CONST.	0.135s							
T"d SUB-TRANSTIME CONST.	0.01s							
T'do O.C. FIELD TIME CONST.	2.23s							
Ta ARMATURE TIME CONST.	0.02s							
SHORT CIRCUIT RATIO	1/Xd							

APPROVED DOCUMENT

Figure 3. 17– Technical datasheet for PI734C

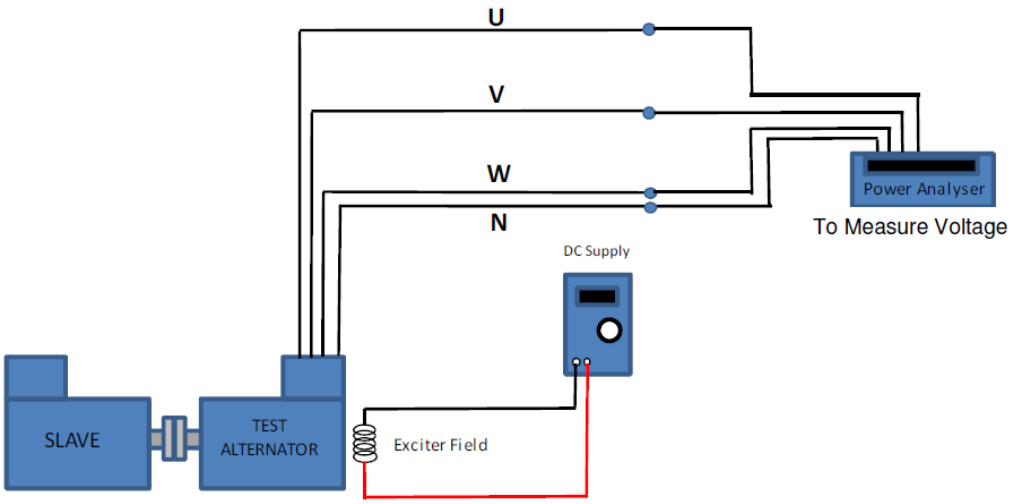


Figure 3. 18 – Test setup for open-circuit characteristic [57]

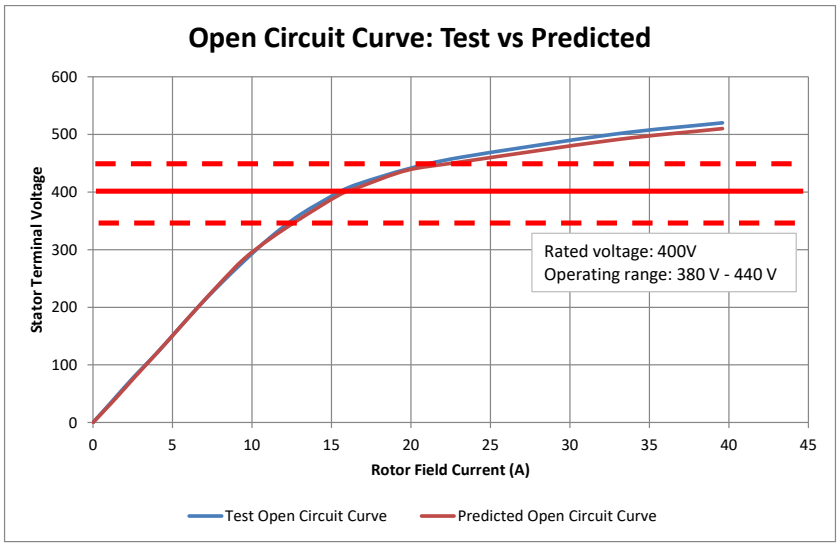


Figure 3. 19– Comparison of predicted vs tested open-circuit characteristic curve showing a good match

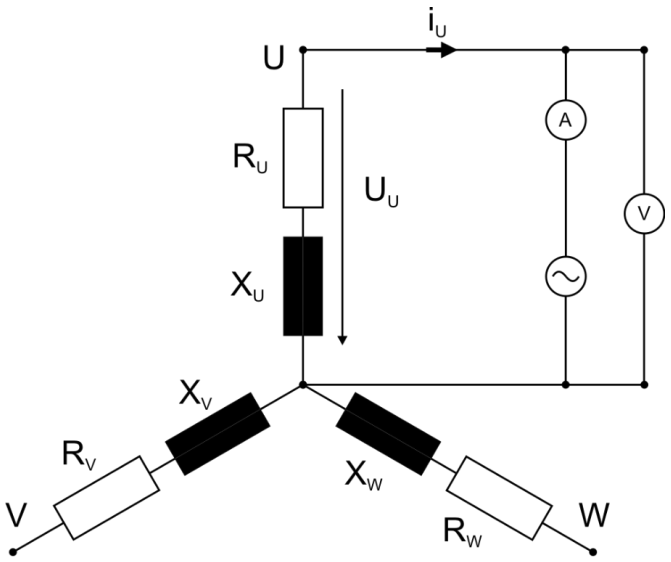


Figure 3. 20 – Test setup for measuring the end-winding leakage

As the end-winding leakage is sensitive to the alternator size and design, the above described method is applied to 3 different types of alternators manufactured by

Cummins Generator Technologies and the results are summarized below in Table 3.1.

Table 3. 1: Summary of end-winding leakage measurement

Machine Type	Analytical Leakage reactance in µH	Test Leakage Reactance in µH
UCI27E	23.8	22.1
PI7C	17.3	16.7
PI7E	18.2	17.4

As seen in Table 3.1, there is good correlation between the analytical formula used and the tested values for leakage reactances. Once the end-winding leakage analytical formula was validated, the formula was added to an automated code written to calculate the SG parameters.

3.2.3.3 Single Frequency Response test

A test methodology is developed to measure the sub-transient reactances of the SG using the single frequency response test. These values are then compared against the simulation results for the same voltage levels to confirm the validity of the finite element models. The test involves locking / holding the rotor in place, either aligned with the d-axis / q-axis as shown in Figure 3.21 while shorting the field winding and applying a voltage at the rated frequency (50 Hz) across two of the armature phases. The angular positions of the d and q axes themselves are determined at the beginning of the test by slowly rotating the rotor and recording the currents for

various angular positions; the currents at the d and q axes positions are represented by the two peaks seen in Figure 3.22. Once the angular positions of the d and q axes are known, the rotor is then locked either at the d-axis or q-axis to record the corresponding reactance value by using the current induced in the armature winding.



Figure 3. 21: Test setup for single frequency response

The test is carried out by applying voltage levels equal to 100V and 400 V, respectively to analyse the saturated and the unsaturated conditions, in terms of the values of the reactances. The summary of the comparative exercise between FE and experimental results is shown in Table 3.2.

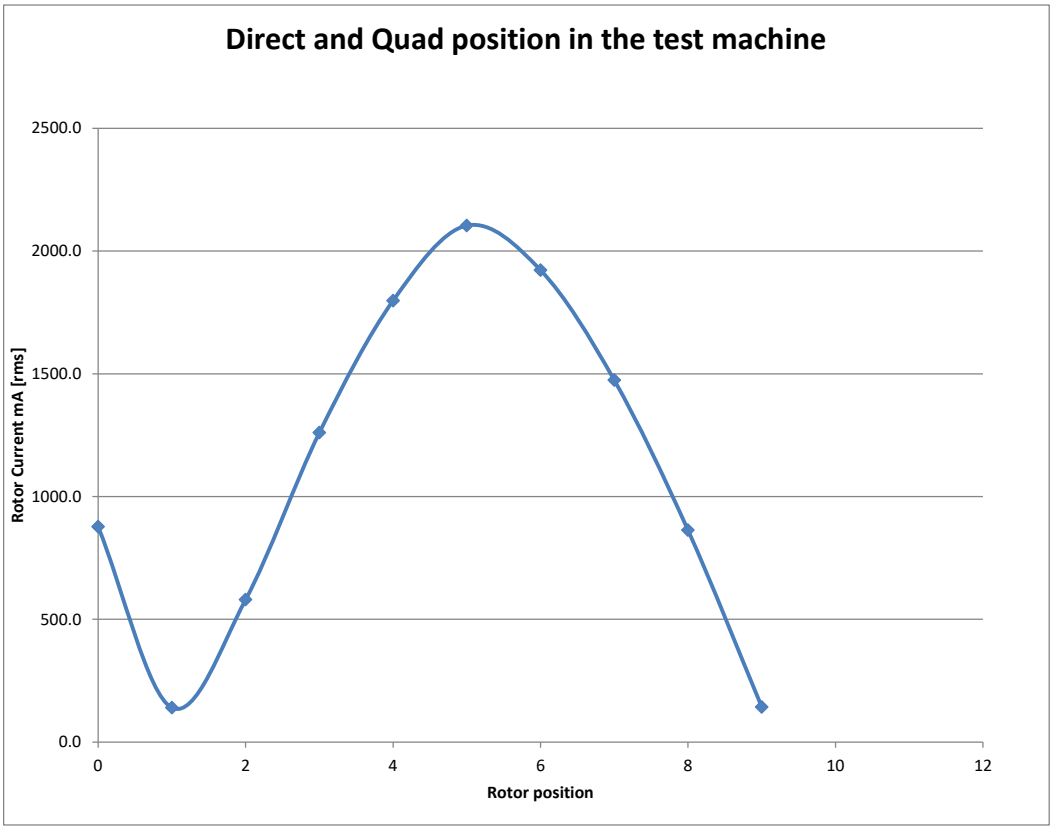


Figure 3. 22: Angular position of the d and q axes

3.2.3.4 Sudden Short-Circuit Test

The sudden three phase short circuit test is one of the main standard methods used to determine the d-axis transient and sub-transient reactances of the synchronous machine. These reactances are obtained by analyzing of the current traces occurring after having applied a symmetrical, three-phase short circuit at the machine terminals. The alternator is initially driven at nominal speed by the prime mover and terminals are open circuited. The field winding is supplied with DC current get the rated voltage at the stator terminals. At an appropriate time instant, the short circuit is applied, and current and voltage traces are registered. The schematic

diagram for this procedure is given in Figure 3.23. Analysis of the current traces is widely described in literature and international standards. This consists in creating two envelopes and mid-point curve for each trace and the resultant waveform is then decomposed into symmetrical and unsymmetrical components. The peak values of unsymmetrical component are plotted on a semi-logarithmic plot. Values of transient and sub-transient currents are identified by extrapolation of the curve on to a semi-log plot and finally the reactances are then calculated as the ratio between of the no-load voltage (before the short circuit), and to the initial asymmetrical current value. The same script is implemented and used to analyze the current trace ensuing from the test data was then used for the analysis of the results. A summary of the results comparing finite element predictions with test data is shown in Table 3.2, while a plot of the current traces are shown in Figure 3.24 for the sake of completeness.

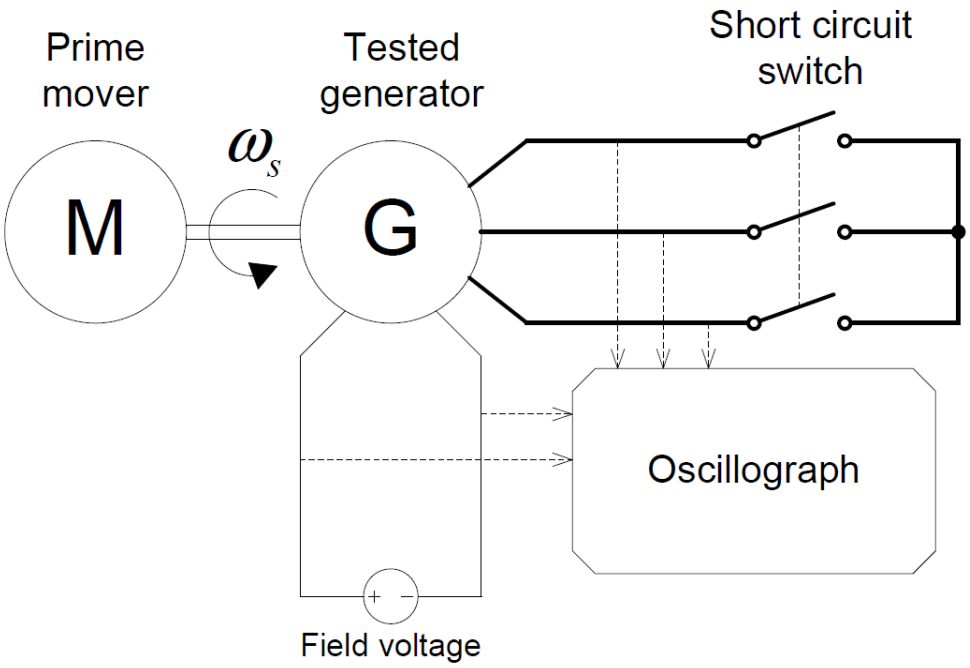


Figure 3. 23: Test setup for sudden short-circuit

Table 3. 2: Summary of test results vs finite element predictions

Analysis Methods	X'_d	X''_d	X''_q
3ph SSC test	0.2734	0.1803	N.A.
3ph SSC simulation – finite element	0.262		N.A.
Single frequency response test (unsat)	0.2872	0.2872	0.265
Single frequency response test (sat)	N.A.	0.238	0.2189
Single frequency response – finite element (unsat)	N.A.	0.2846	0.261
Single frequency response – finite element (Vector fields) (sat)	N.A.	0.236	0.22

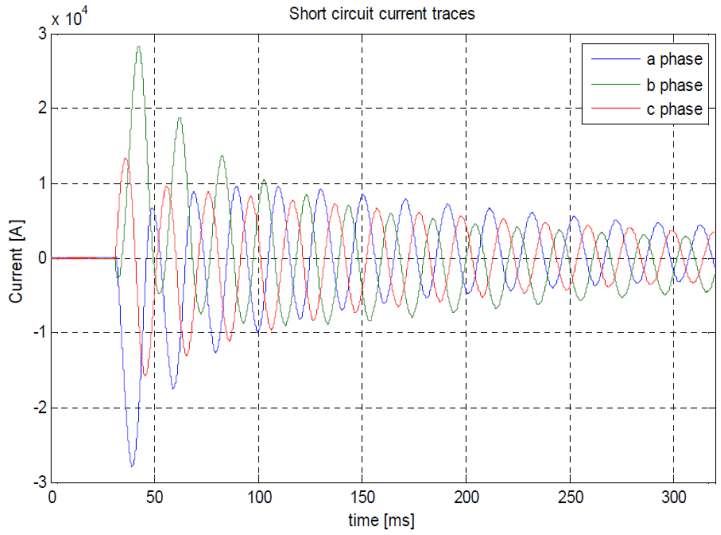
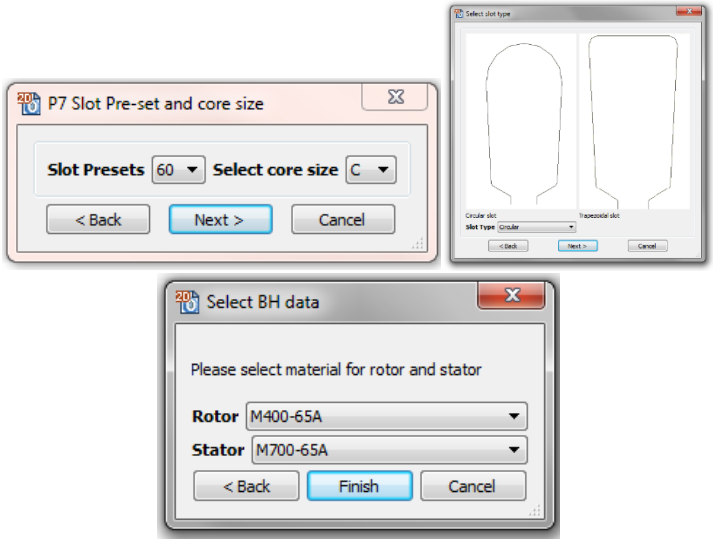


Figure 3. 24: Three phase short-circuit currents in the armature winding of the test machine – PI734C. The a,b,c, phases are the same as u,v,w phases in the same sequence.

3.4 User interface for finite element analysis tool

Having validated the tools used to determine the SG parameters, a user interface is thus developed with the aim of building a FE model that can be used to run various simulations as shown in the previous sections to predict the performance of the considered alternator. Figure 3.25 a,b,c are snapshots of some of the inputs that are required by the tool. Figure 3.26 shows the flowchart that gives a comprehensive overview of how the user interface was setup.



(a) (b) (c)

Figure 3. 25: Typical inputs for the user interface used to build the finite element model.

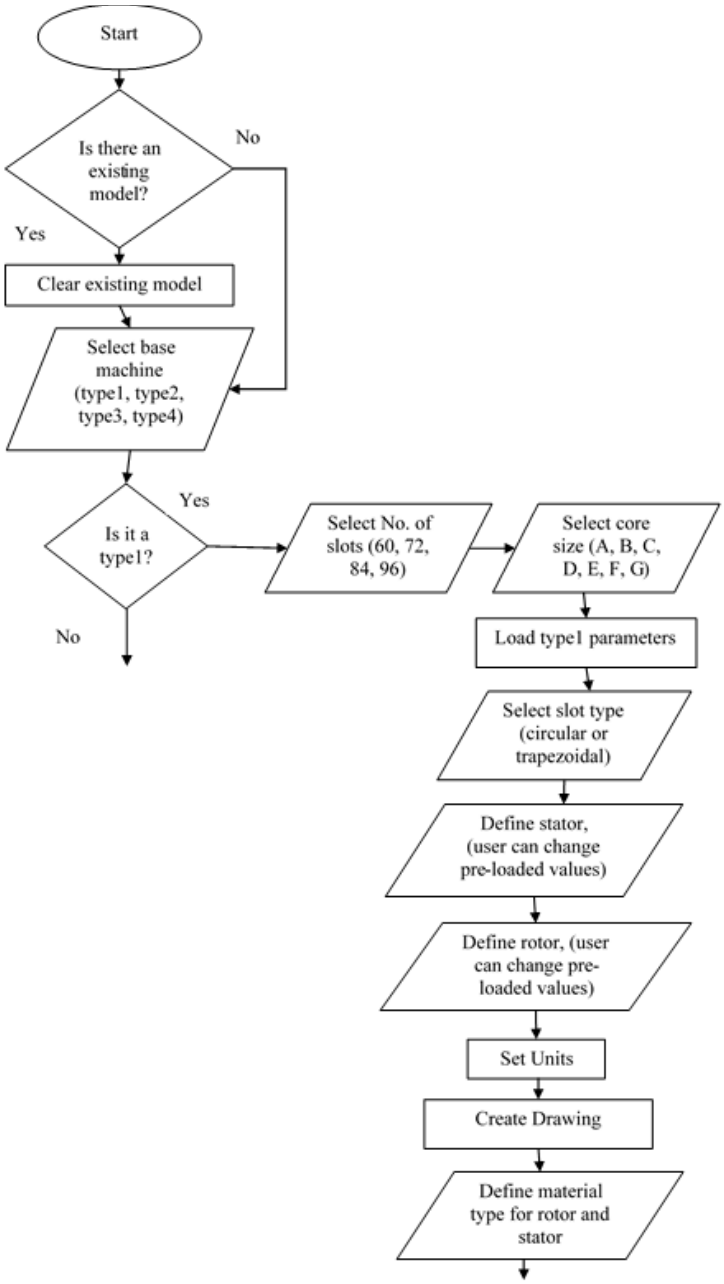


Figure 3. 26: Flowchart showing the functioning of the user interface of the finite element modelling tool

3.5 Conclusion

In this chapter, a finite element analysis tool that can predict the SG parameters, i.e. the synchronous transient and sub-transient reactances was developed. The tool takes minimal user input and builds the desired model of the SG and creates performance reports with the click of a button. Since the tool was meant to be used for analyzing / modifying existing product lines, the designs available on the tool were limited to all feasible design changes and all possible design combinations for the existing products manufactured by Cummins Generator Technologies. This also allows for easy fine tuning of the model which will have to be completed every time an entirely new model of SG is developed using the tool. A simulate – test regimen is required to ensure that the user understands the limitations of the model whilst developing new product lines; however, when driving sensitivity studies to determine SG sensitivity under various application conditions, the tool is a very quick and accurate approach. The results of the simulation tool were validated against experimental measurements.

CHAPTER 4

POWER SYSTEM MODEL REQUIREMENTS AND SETUP

The design of SGs used in power systems must include a detailed understanding of the conditions, related to the application that the generator interacts with. Building and testing generating sets for power systems may be expensive and time consuming and therefore the use of computer simulations is today an integral part of the design process. In this chapter a step-by-step approach to build and initialize a power system model to be used in grid code simulation studies is described. The boundaries / assumptions for the power system model are presented along with an extensive review of literature on power system modelling and the various tools available for such applications. The tools described and validated in Chapter 3 are used to calculate the SG parameters aimed at deriving the characteristics (reactances and time constants) of any SG based on its geometry. The parameters calculated using this approach are applied to the SG model in the power system simulation tool. Chapter 4 discusses in detail, the results of the power system simulations and the methods adopted to reduce the computation effort. A systematic modeling approach is also presented an utilise to generalize the developed models, as a contribution to the field. Several variables influence the LVRT performance and these combinations can lead to several design iterations. An automated process was setup to evaluate all possible combinations. The results from the power system simulations are fed in to a neural network model to evaluate specific requirements. The neural network development and results from analysis of power system simulation data are discussed in Chapter 5.

4.1 Power System Simulation

4.1.1 Selection of the dynamic simulation tool

To select the appropriate tool to be used for simulation purposes the tools available in the market were scored against critical criteria defined by both commercial and technical constraints. Figure 4.1 shows the 'Pugh Matrix' that was developed to compare the various simulation tools. Matlab/Simulink is an excellent simulation tool for the considered applications and is used in the simulations described in the thesis. The Vector Fields Opera package was selected with the sole purpose of calculating the SG design parameters used in the Matlab/Simulink models.

Critical Parameter Estimation				
Best way to determine critical parameter	Concept Testing	Matlab/Simulink	Opera 2D / 3D	Ansoft / Maxwell
Precision	S	S	+	+
User Friendliness	S	+	+	+
Reproducible	S	S	S	S
Speed	S	+	+	+
Cost of Setup	S	+	+	-
Cost of Training	S	+	-	-
Variation	S	+	+	+
Validation	S	-	+	+
Maintenance	S	+	S	-
Repeatable	S	+	+	+
Complexity of setup	S	+	+	-
	S			
	S			
	S			
Total Σ +	0	8	8	6
Total Σ –	0	1	1	4
Total Σ S	14	2	2	1

Figure 4. 1 – Pugh matrix selection of Simulation tools

4.1.2 Modelling the components

This section describes the various simulation components and the associated mathematical models used to effectively describe the dynamics of an Engine Driven SG connected to the grid.

4.1.2.1 System Overview

Figure 4.2 is a graphical representation of the generic power system model that was built for this thesis. Although the outcome of this thesis is to develop a 1.45 MW alternator that is capable of being used in a grid code application, the simulation's purpose is broader and is intended for use beyond the P7 (P7 is the same as the PI734 introduced in Chapter 3). For this reason, a system model is initially built, based on a generality concept. To build a model that can be used robustly on the P7, but also be extended to other CGT products, the model was tested on the largest CGT product by kVA , namely theDIG142e that is used in grid code applications. Since the SG parameters are themselves used from a validated model, the power system model results won't be tested unless deemed necessary. This approach was also adopted since a DIG 142e was readily available for testing and validation. Once the generic model is built and tested, a P7C alternator coupled to a Cummins QSK 60 Hi-Surf gas engine is simulated and the outcome of the simulations are analyzed through a Neural Network to determine the critical parameters that will enable compliance with the grid codes identified in Chapter 2.

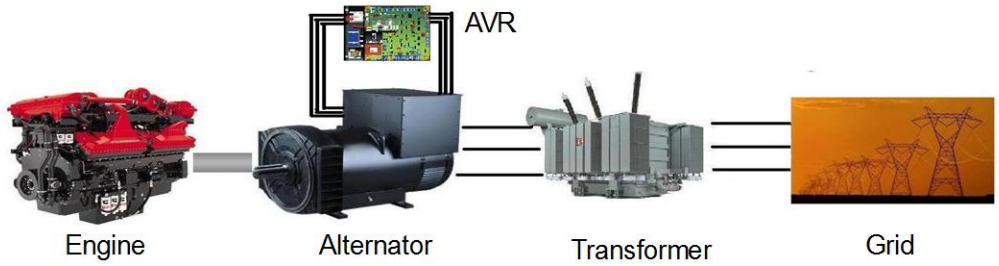


Figure 4. 2 – Graphical representation of simulation model

4.2 Power System Model Components

4.2.1 Prime Mover

The Cummins QSK 60 Hi-Surf gas engine model [60] was used to represent the Prime Mover that drives the P7C alternator. A gas engine is chosen as opposed to a diesel engine due to its slower response time to change in load conditions making it a worst-case prime mover case study. Additionally, an industry wide review of all engine inertias were reviewed and Cummins engines with inertia constants almost the same as those of the SGs they were coupled with were selected based on this arrangement being the lowest generating set inertia that the SG would encounter. A Cummins QSK 60 [133] Hi-Surf is chosen for modelling purposes and the simulation model is built based on the IEEE recommended practices for gas turbines in combination with the exact time constants representing the fuel systems and the speed governor used in the engine. Figure 4.3 below represents the simple IEEE model of a reciprocating engine based on which the Cummins Engine model was developed.

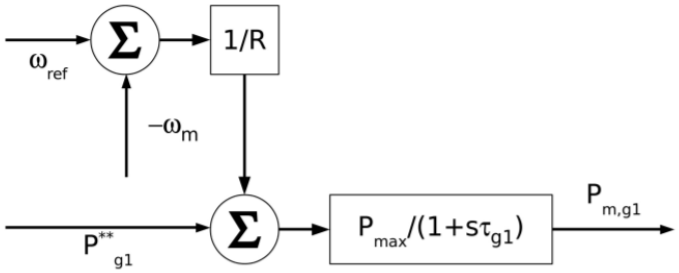


Figure 4. 3: IEEE [88] model of the internal combustion engine

4.2.2 Automatic Voltage Regulator and Exciter-Excitation system

In any engine, a governor measures the speed of the shaft relative to the reference speed and adjusts the fuel injection based on torque / power demand which is evaluated using the speed measured. The IEEE model in Figure 4.3 represents the speed measurement and power adjustment by the engine. The model is simple enough that it consolidates the entire fuel injection and governor systems into a time constant that is specific to an engine / engine class.

Figure 4.4 below illustrates the IEEE AC8B [89] model of an excitation system that is required to be used in grid code simulations. The AVR is represented using P-I-D blocks in conjunction with a voltage limiter. The functional blocks “Fcn_03”, “Fcn_04”, “Fcn_05” and “Fcn_06” represent the alternator exciter. The uncontrollable three-phase rectifier is modelled by functional blocks “Fcn_01” and “Fcn_02” which provides the field voltage that is used to provide input to the simpowersystems synchronous machines model . Variables in terms of their abbreviations follow Figure 4.4, so that they correspond to the IEEE AC8B standard [89].

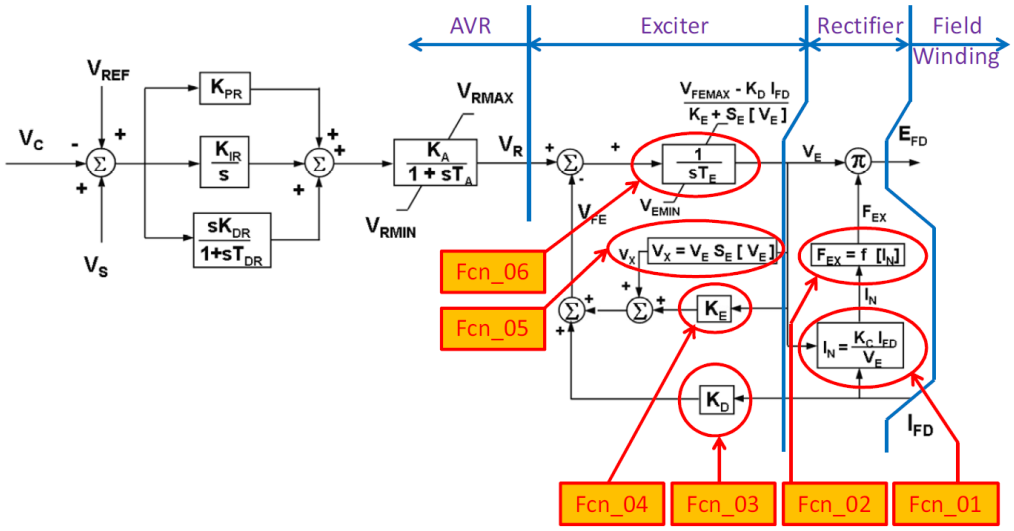


Figure 4. 4: The IEEE AC8B[89] model of the alternator excitation system with functional blocks identified

Since the model represented in Figure 4.4 follows the requirements of an international standard including the variables used within the models, the details of the various individual blocks and the associated parameters within the blocks are described in Appendix 2 which also provides a summary of the internal technical standard that was developed on modelling excitation systems directly as a result of the work presented in this thesis.

4.2.3 SG model

Five different generator models with varying levels of complexity and accuracy have been discussed in [35]. The construction, operation and derivation of the SG models have been extensively discussed in [35], [37] – [41] This section will therefore perform a review of these models and define the rationale for selecting the most adequate generator model ideal for the scope of the work defined in the

thesis. The development of all the generator models are based on the following assumptions [35]:

- The three-phase stator winding is symmetrical.
- The capacitance of all the windings can be neglected.
- Each of the distributed windings may be represented by a concentrated winding.
- The dependence of the self and mutual inductance of the stator windings on the rotational variable is assumed to have a sinusoidal trend, i.e. the higher order harmonics are neglect.

There are 5 types of SG mathematical models based on the number of state variables used [35], [42], ranging from the second to the sixth order. Details of the various SG models have been provided in Appendix A.

The power system simulations are run with the Simpower Systems toolbox. A sixth order system (Figure 4.4) is used and will be the focus of this thesis.

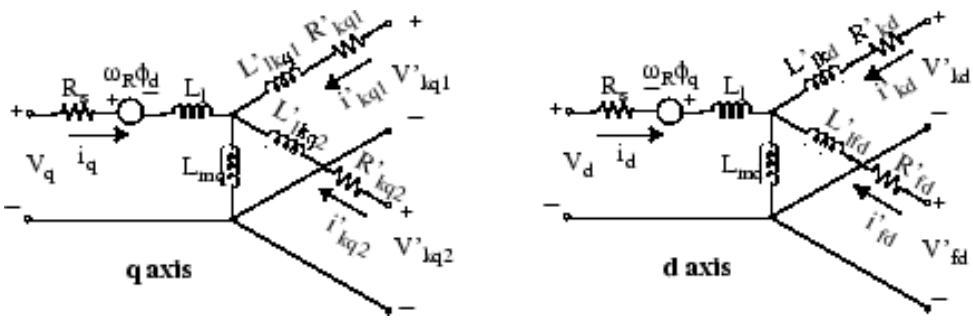


Figure 4. 5 – Simpowersystems model of SG [35]

The sixth order model represents four windings – two on the d-axis and two on the q-axis. This model neglects network and stator transients which leads to conservative predictions [35]. The sixth order is the most preferred model for stability studies. In figure 4.5, the various subscripts can be interpreted as d- and q-axis quantity, R,s – rotor and stator quantity, l, m – leakage and magnetizing inductance and f,k – field and damper winding quantity while the quantities themselves are represented as V – voltage, R – resistance, L -self-inductance, i – current, ω – angular velocity and Φ – flux.

4.2.4 Transformer & Transmission Lines

The Matlab Simpowersystems toolbox provides a model of an ideal transformer that is represented by winding resistances and leakage inductances as well as the magnetizing characteristics of the transformer core [91]. Figure 4.6 shows the typical model of a transformer used to connect an engine driven SG to the grid. The typical impedance of the transformer is 6% for the size of the generating sets that are simulated. Typical values for leakage reactances and magnetizing inductance of a transformer are used [95]. R1, R2, R3 are the winding resistances, L1, L2, L3 are leakage inductances and Rm and Lsat represent the magnetizing characteristics

of the core. This model does not include hysteresis and eddy current effects, as well as the phenomena related to the non-linear behavior (i.e. saturation) of the magnetic cores. However, for the sake of this study, it was considered enough to represent the contribution of the transformer during dynamic events on the grid, which represents the main purpose of this modelling aspect.

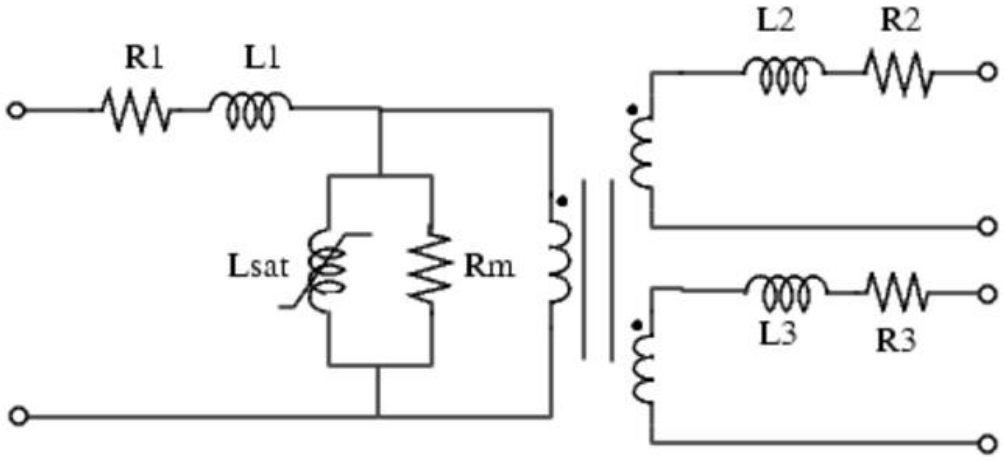


Figure 4. 6: Model of transformer used

The worse-case scenario for a generating set operating in connection to the electrical grid is simulated by neglecting the transmission line parameters. Therefore, the transformer represents the only connection between the generating set and the grid. This ensures that any voltage drop simulated on the grid is applied mostly across the terminals of themachine.

4.2.5 Grid

A Matlab model of a three-phase source which feeds a resistance and an inductance as a typical load of the grid is built. The size of the grid can be varied

by adjusting the short-circuit level and voltage level of the three-phase source model.

A fault through a voltage dip and rise is introduced using the curve shown in Figure 4.6 below and the variables, a, b, c, d and e can be changed to represent the appropriate low voltage ride through profile. For this application, the simulation consists of the profile from the France low voltage ride through requirement [20].

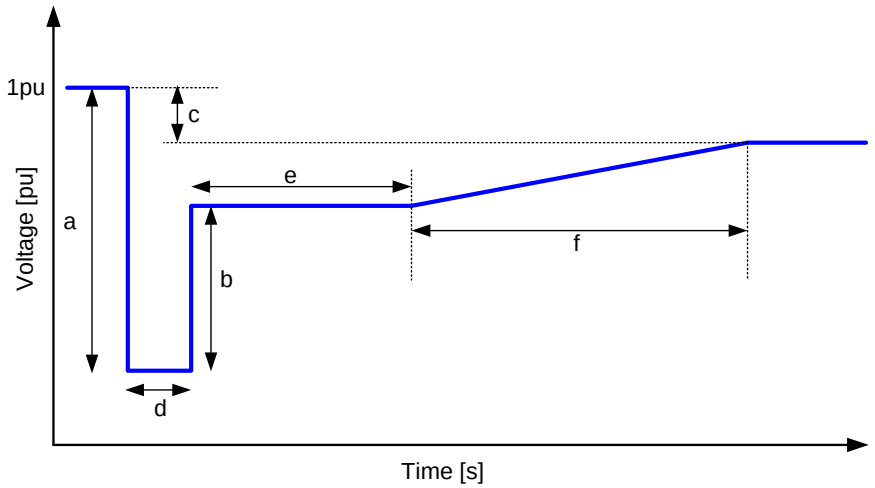


Figure 4. 7: A generic Low Voltage Ride Through curve that is simulated

4.2.2.6 Summary

In an engine driven SG, the engine is set to run at a rated speed – the synchronous speed. Under no-load operation, no current flows in the stator windings, there is no almost torque on the rotor and the engine burns a minimum amount of fuel to maintain synchronous speed. On connecting a load, the load current in the stator windings interact with the rotor current to produce an opposing torque that slows down the rotor. The engine governor picks up this reduction in speed and injects

more fuel into the cylinders thereby producing more power which works against the armature reaction to maintain synchronous speed. When the load is removed, this torque on the rotor due to armature reaction no longer exists and the rotor starts to accelerate. This increase in speed is picked up by the engine governor which in turn cuts / reduces the necessary amount of fuel injected into the SG which slows it down and allows continued operation at synchronous speed. The IEEE model of the engine introduced in the above sections accurately captures this behavior of the engine required to model dynamic performance of the SG to include engine time constants and the torque balancing action.

The method of accurately predicting synchronous reactances developed in Chapter 3 are used to drive the Simulink model of the SG which is then used to model its behavior whilst connected to the grid.

The grid model used is a simple voltage-impedance model that can be used to control the size of the grid through its kVA and short-circuit level and the voltage control program that was developed allows controlling the behavior of any voltage ride-through conditions that are being studied as part of this thesis. Since the transformer reactances are more crucial to the study of dynamic stability of SGs connected to the grid, a simple two wire model of a transformer is used for the simulation.

The entire power system model setup is an excellent approach to studying the sensitivity of SG dynamic stability to characteristics of various system elements like engine, transformers and the grid itself (Figure 4.7).

4.3 Power System Simulation Testing

4.3.1 Approach

To fully understand the SG behavior under both static and dynamic grid conditions, test simulations of the generating set itself have been done considering these two conditions. Figure 4.8 below summarizes the considered modelling approach. An analytical method is used to determine the initial states and therefore the pre-fault static stability of the SG can be determined using this approach, which is laid out in Appendix 4.

4.3.2 Simulation trials on a DIG142e

To validate the power systems model introduced in the previous sections, a 4 MVA, DIG 142e SG is modelled and simulated. The DIG 142e represents the

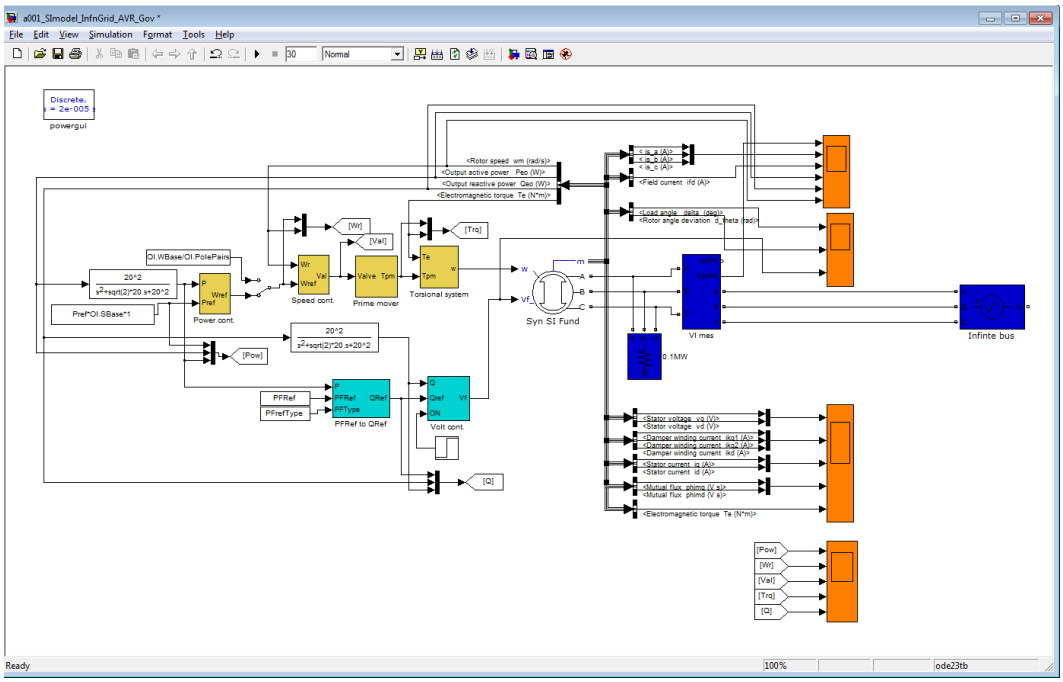


Figure 4.7: Power Systems Model developed

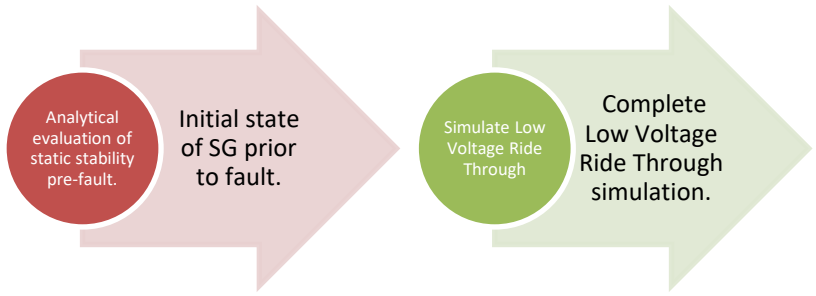


Figure 4. 8: Approach to two-stage power system modelling

largest CGT product used in grid code applications and since was readily available for testing, was used to test the model results. The results from the simulation are then validated to demonstrate the capability of the model. This section discusses

the results of the simulation that will form the basis for setting up the power systems model for the target 1.45 MVA SG (P7).

4.3.2.1 Validation of a DIG142e model

To validate the systems model developed, a short-circuit test on a 4MVA DIG142e is planned. The machine is chosen as it was available to test right away and fits in with the intent to make the model valid for a broad range of alternators. The results of this test have been discussed in [92] and therefore this section will briefly introduce the test method and validation results only. Figure 4.9 below shows the test setup to simulate a short-circuit on the DIG142e. A drive motor is used to run the test unit at synchronous speed. An excitation system provides the input required for the rotor field current in a closed loop feedback system that measures the stator voltage and adjusts the rotor field current input needed to maintain the voltage at its rated value across the terminals. The machine is loaded initially with a very large load, which is then switched to a very small load to reproduce the short-circuit across the stator terminals of the DIG142e. The value of the load used in the test is also used in the simulation to represent realistic conditions. The modelling tool developed in Chapter 3 was used to predict the parameters of the DIG142e and then used to build the synchronous machine model on Matlab.

Figure 4.10 shows the results of the short-circuit test and their comparison with the simulated short-circuit results. A good correlation between simulation and measured quantities is observed. Some variations are seen in values and this is attributed to three reasons:

- Nominal tolerance of the model which is within +/- 10%. This tolerance is due to the physical distance between the connection points in test vs the assumed resistances / line impedances in the model and due to the inherent differences in reactance values that occur due to geometrical and analytical approximations.
- Differences in speed change over time between the drive used in test and the simulation.
- The time of applying the fault; while in simulation, the time at which the fault is applied can be controlled, it is not practical to exactly match this thereby leading to some differences.

A validated synchronous machine parameter estimation tool that can predict the synchronous machine reactances within reasonable tolerances and the load from the test was accurately represented in the simulation.

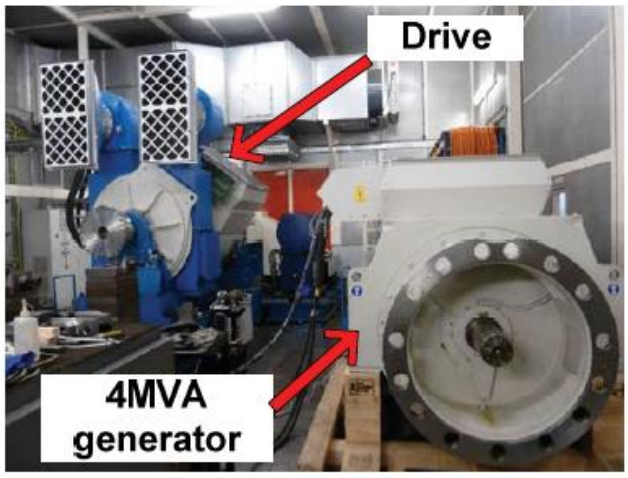


Figure 4. 9: Test setup to validate systems model of SG with short-circuit test.

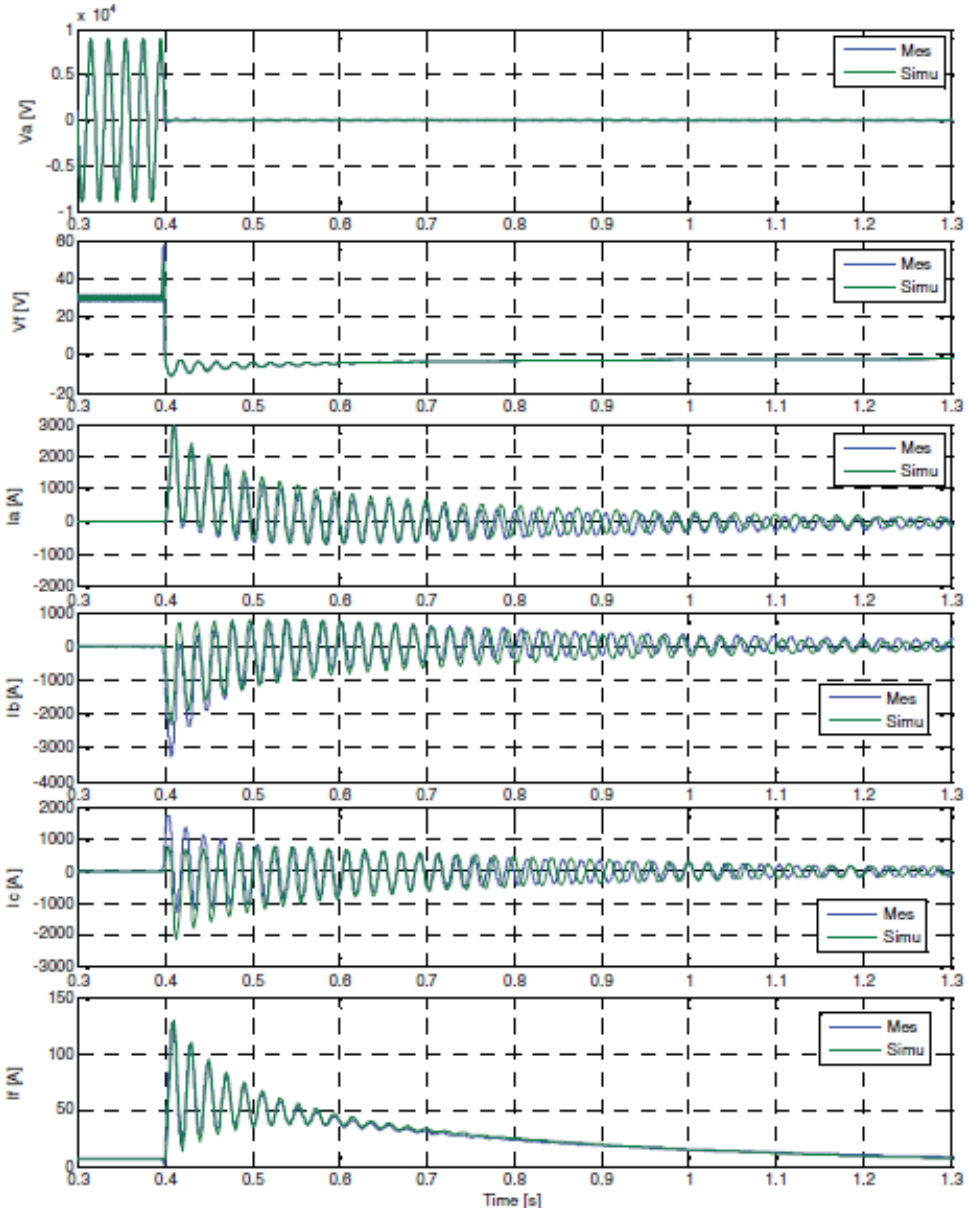


Figure 4. 10: Results of the short-circuit test lined up against simulation results showing excellent correlation

4.3.2.2 LVRT simulations on DIG142e and discussions of findings

Following validation of the DIG142e model with short-circuit tests discussed in the previous section, the systems model was then used to run LVRT simulations. A voltage following Figure 4.6 was applied at the terminals of the DIG142e and over

600 simulations were completed for various voltage ride through profiles. This section discusses the findings from the simulations.

According to [59], Simpowersystems is good for dynamic simulations and tends to be slow or to pose Sensitivity analysis of LVRT. A low voltage ride through impacts the generator at two instances, initially at the instance of the fault and then upon clearing that fault. When a fault occurs in a grid, terminal voltage of the generator drops abruptly. On the other hand, as the fault is cleared, the terminal voltage recovers rapidly. Sudden change in terminal voltage results in high amplitude current oscillations in the machine.

The peak current during fault condition is determined by several factors, such as the characteristics of the fault, operating condition of the generator, condition of the grid and the reaction of the control system. Each of those mentioned factors has several variables. Some of the important variables that affect the fault currents are given below.

Characteristic of the fault: Depth of voltage drop: Fault current increases with the depth of the fault; therefore, the worst condition for maximum fault current is 100% voltage drop.

Duration of fault: Generator speed generally increases during a fault. As a result, the angle difference between the generator rotor and the grid voltage increase. This could lead to crash resynchronization upon clearing the fault.

Condition of the generator: Operating power factor: Operating power factor determines the internal generated voltage of the generator. Internal generated voltage influences the fault current.

Operating active power output: Pre-fault active power output determines the prime mover torque. High prime mover torque during that fault leads to undesirable rotor acceleration.

Instant of fault: Instance of the fault with respect to generator voltage phase angle affects the dc offset component of the fault current.

Condition of the grid: Fault level of the grid at connection point: Effective impedance of the grid at the connection point slows down the speed of the voltage recovery upon clearing the fault. Therefore, the worst condition for generator fault current would be infinite grid at the generator terminal.

Location of the fault from generator terminal: Any impedance between the generator and the fault helps reducing the fault current from the generator. Fault occurring at the terminal of the generator would be the worst case.

Governor action for fault: Prime mover governor regulates the speed of the generator and helps maintain the rotor speed. Speed variation during the fault affects the rotor angle and thus the fault current magnitude.

Action of AVR: AVR increases the field voltage to boost the voltage drop during the fault. However, higher field voltage leads to high short circuit current.

Short circuit current at the instance of fault: The magnitude of dc current in any phase depends upon the instance at which the fault is applied. As there are three voltages mutually at 120 deg apart it is possible for only one phase to have the maximum direct current component. Numerous simulations were conducted to identify the worst time to apply the fault. In these simulations the apparent power and the terminal voltage of the generator were kept at rated before the fault.

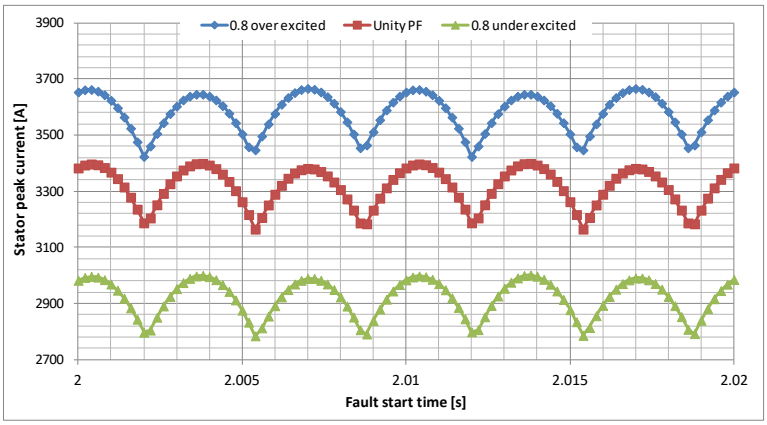


Figure 4. 11: Stator peak current variations against instant of the fault for different power factors

Duration of fault: Grid cod requirements for LVRT specify the duration of a fault in which the generator needs to retain its connection to the grid. Apart from demanding grid code requirements, it is always desirable to design a generator to withstand any fault conditions.

Duration of the fault is one of the important factors affecting the peak current upon clearing a fault. When the terminal voltage drops to a very low value, the generator is unable to transfer all the power input coming from the prime mover. During a 100% voltage drop, generator losses (mainly increased heat loss) are the only power

sink. However, the prime mover generally maintains the power output at its pre-fault value during the fault. Mismatch between the input and output torque at the generator rotor leads to unwanted acceleration.

Governor of a prime mover regulates the speed of the generator and helps to maintain the rotor at the synchronous speed. Feedback speed controller generally has low control bandwidth and cannot strictly maintain the speed during the fault. As the speed increases, the angle difference between the generator rotor and the grid voltage increase. This would lead to crash resynchronization upon clearing the fault. However, modern prime movers may include advanced feed-forward protection mechanism to stop the rotor accelerating by means of cutting off the energy input. The worst-case scenario for the maximum peak current would be without advanced feed-forward protection controllers.

Absolute worst case: A number of simulations was conducted to identify stator peak current during LVRT at the worst theoretical conditions. The voltage drop during the fault is assumed to be 100% and the generator terminal voltage changes as a step without any transients. Combination of 100% voltage drop and step change in terminal voltage would be the worst-case scenario for maximum peak current. Figures 4.12, 4.13 and 4.14 show the response of the generator during an LVRT for the fault durations of 110, 190 and 230ms. In these simulations, the power factor of the generator was maintained at unity before the fault. Each figure has several variables and an indicative rotor position diagram.

In Figure 4.12, the fault duration is small therefore there is no pole slip due the LVRT. The prime mover initially accelerates the rotor and then the grid resynchronizes the rotor. On the other hand, in Figure 4.11, the fault duration is long enough to let the rotor pass the critical mechanical angle. As the grid is restored, the stator flux is pulling the opposite pole. As a result, the rotor is experiencing motoring torque and further accelerates. Finally, rotor to pole slip occurs with high induced stator current. In Figure 4.14, the rotor shaft is shifted by around 130 deg during the fault and then the fault recovery pulls the rotor and resynchronizes.

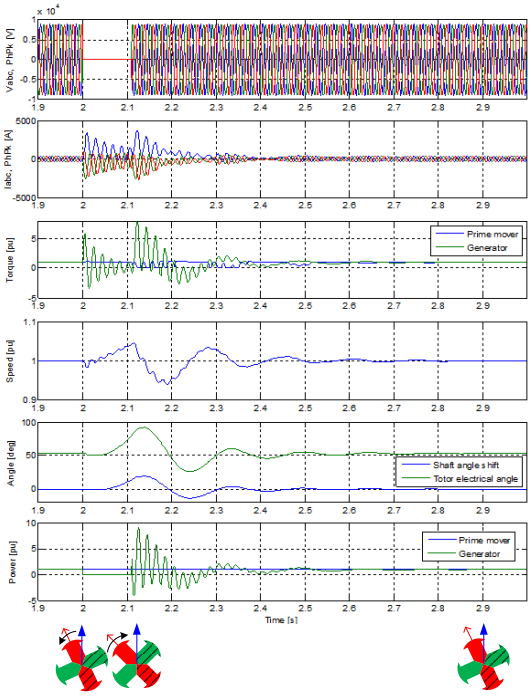


Figure 4. 12: LVRT performance of DIG14e: Pre-fault PF - unity, pre-fault terminal voltage - 1.0pu, fault duration – 110ms, retained voltage during fault – 0.0pu, and step changes in terminal voltages

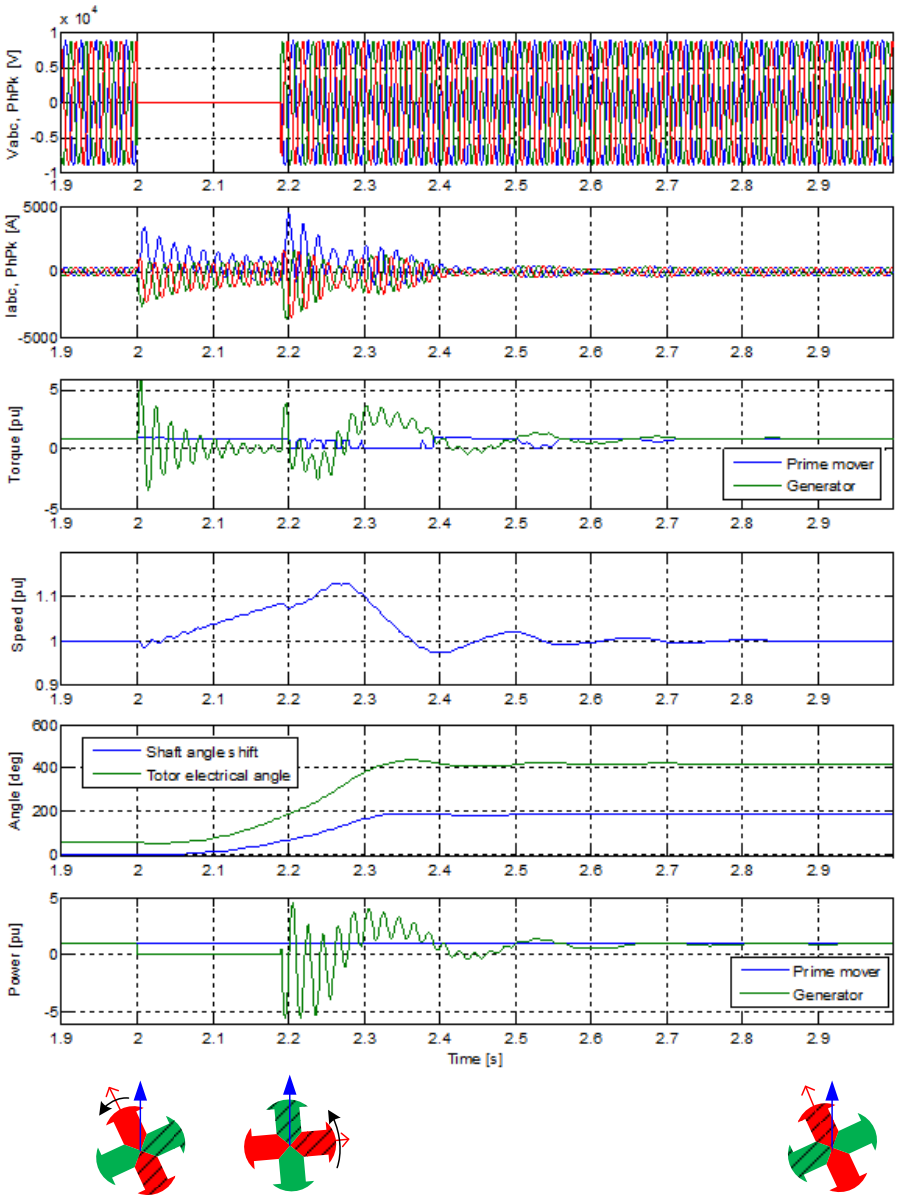


Figure 4. 13: LVRT performance of DIG14e: Pre-fault PF - unity, pre-fault terminal voltage - 1.0pu, fault duration – 190ms, retained voltage during fault – 0.0pu, and step changes in terminal voltages

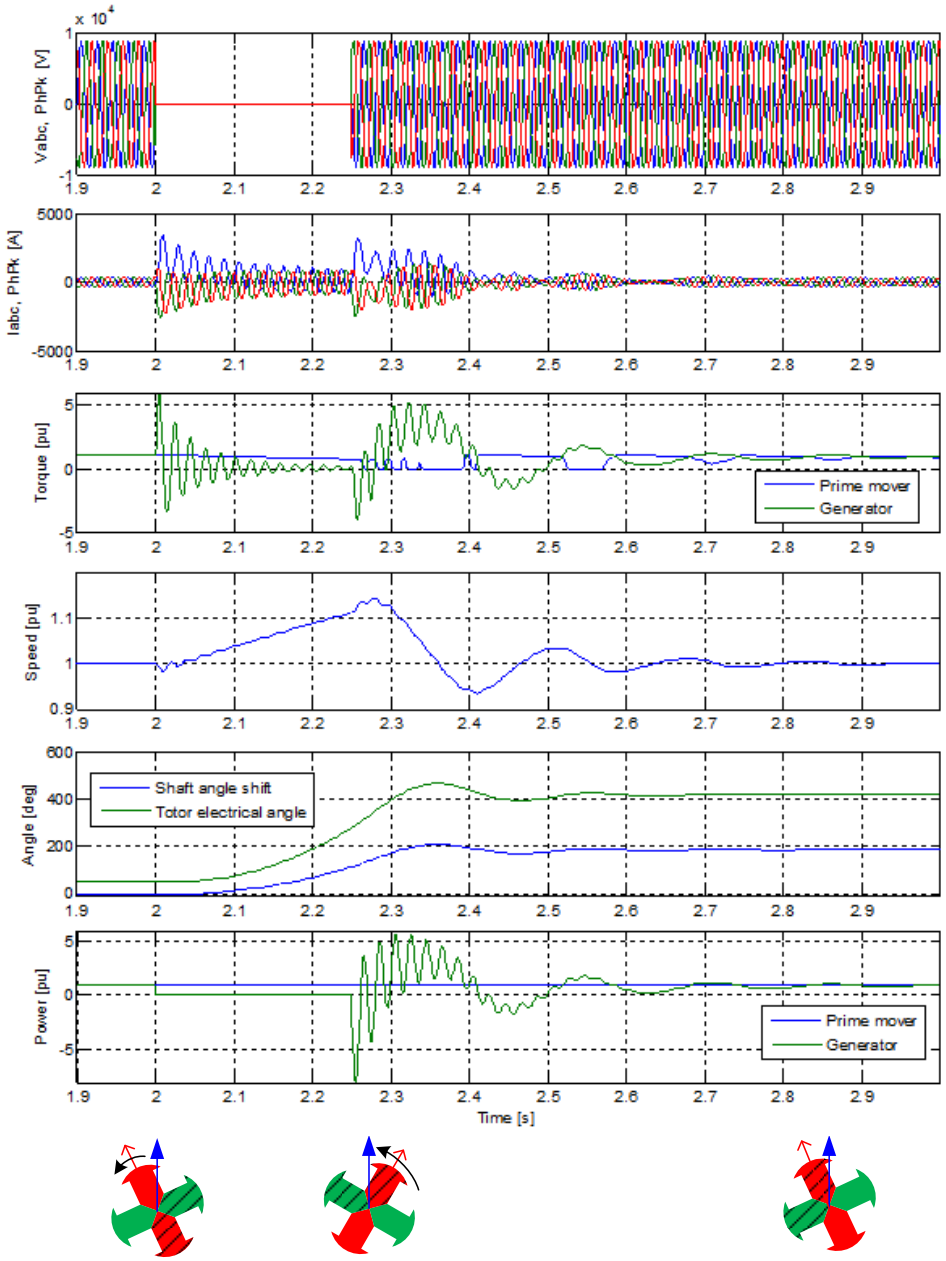


Figure 4. 14: LVRT performance of DIG14e: Pre-fault PF - unity, pre-fault terminal voltage - 1.0pu, fault duration – 230ms, retained voltage during fault – 0.0pu, and step changes in terminal voltages

More than 600 simulations were conducted at different fault durations (starting from 50ms to 300ms) and power factor settings. Figure 4.15 shows the stator peak

current variation against fault duration for different power factors. Locations of operating conditions of Figures 4.11, 4.12 and 4.13 are illustrated in Figure 4.14. In these simulations, the pre-fault apparent power and terminal voltage were kept at rated values before the fault. As the fault duration increases, the peak stator fault current also increases and the maximum peak current magnitude is identified as 4600A at 0.8 over excited power factor. The fault duration for this worst condition is 230ms.

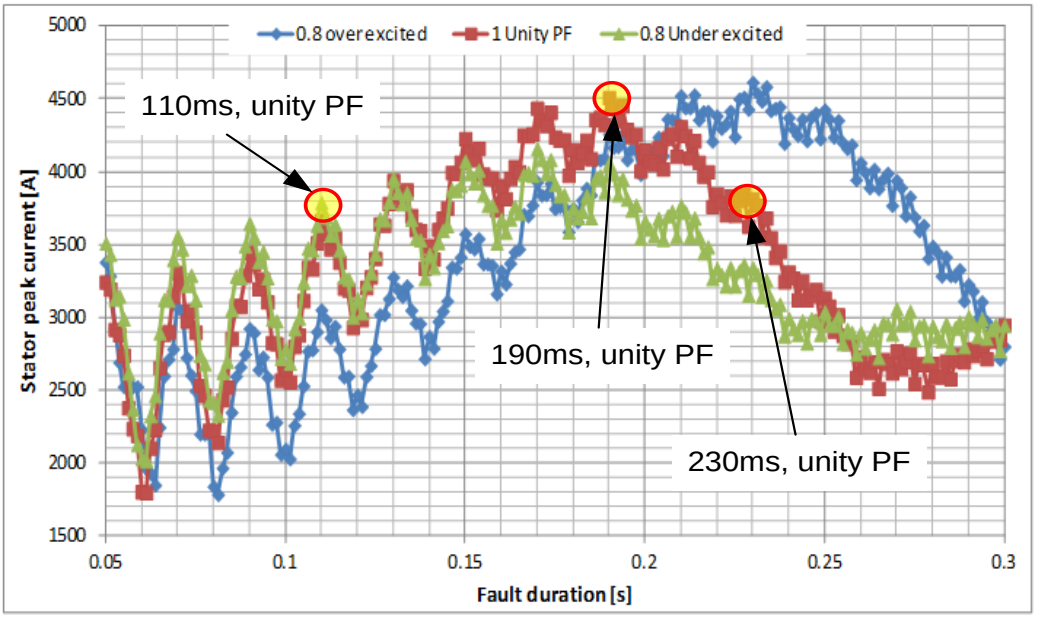


Figure 4. 15: Stator peak current variation against fault duration for different power factors, pre-fault terminal voltage – 1.0pu, retained voltage during fault – 0.0pu, step voltage changes

RMS values during and post-fault: Maximum peak current is one of the important factors that define the forces at the end winding. It is also important to understand the persistent current, power and torque variations that are generated by the LVRT event.

Figure 4.15 shows three phase current variation during a 230ms LVRT. RMS values of the currents are calculated during and post-fault for the fault duration. Comparing rms of the current during and post-fault gives useful indication of the severity of the fault recovery against the short circuit conditions.

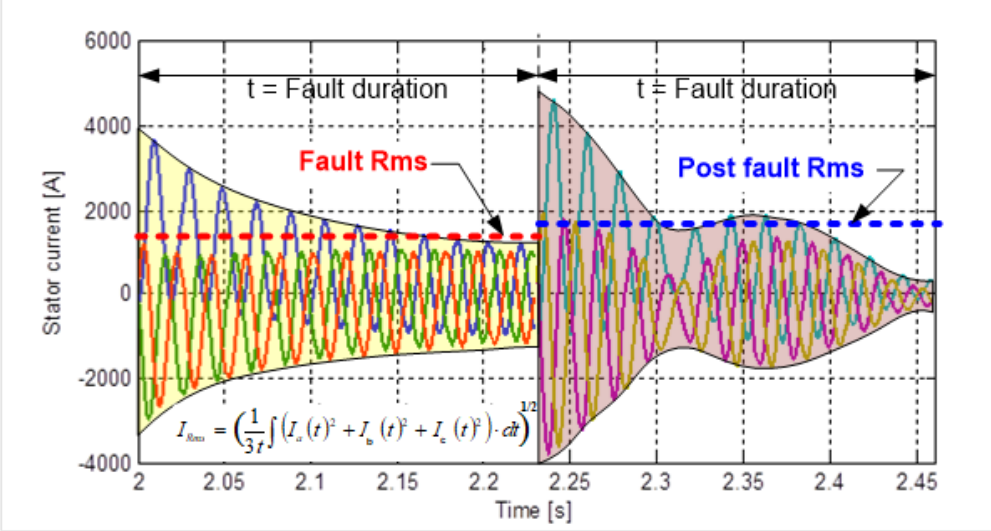


Figure 4. 16: Calculation of stator rms current during fault and post-fault condition, pre-fault terminal voltage – 1.0pu, retained voltage during fault – 0.0pu, step voltage changes and pre-fault PF – 0.8 over excited

Calculated rms values of stator current are shown in Figure 4.17 for different fault durations. The rms value of the short circuit current is higher than the post-fault value until the fault duration reaches 180ms. Then the post-fault rms current reaches a peak value of 1520A at 210ms. Post-fault rms drops below the short circuit rms current when the fault duration reaches 250ms.

The power at the terminal is shown in Figure 4.18, where it can be observed that the power during the fault is not given as it is zero during the fault. Electromagnetic torque rms variation during and post-fault is given in Figure 4.19.

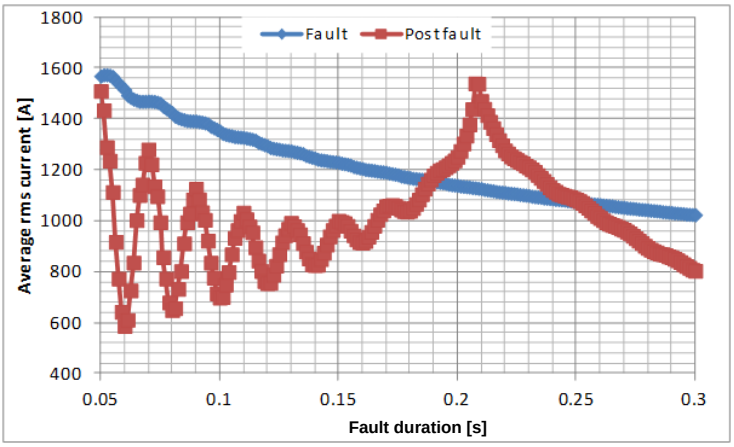


Figure 4. 17: Stator current during fault and post-fault condition against fault duration, pre-fault terminal voltage – 1.0pu, retained voltage during fault – 0.0pu, step voltage changes and pre-fault PF – 0.8 over excited

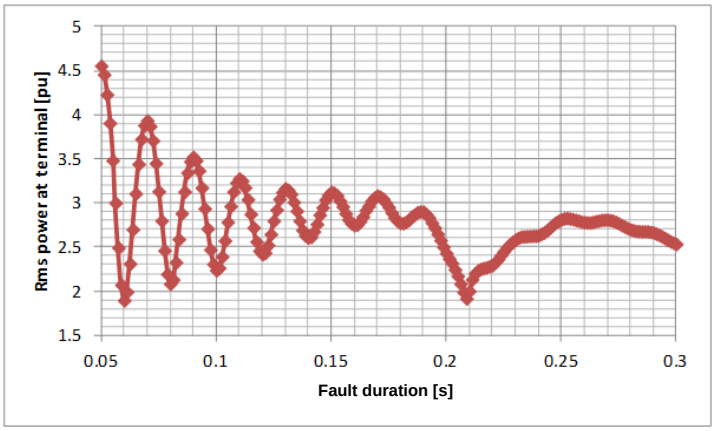


Figure 4. 18: RMS power at the stator terminals during fault and post-fault condition against fault duration, pre-fault terminal voltage – 1.0pu, retained voltage during fault – 0.0pu, step voltage changes and pre-fault PF – 0.8 over excited

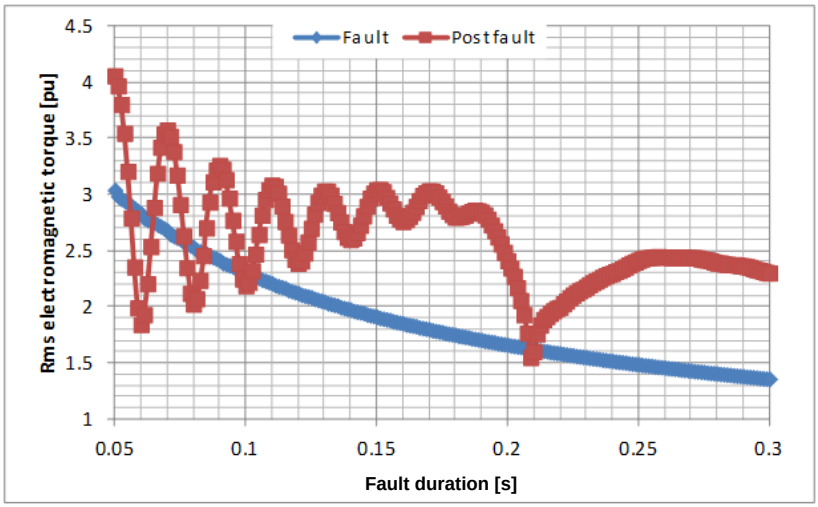


Figure 4. 19: Electromagnetic torque during fault and post-fault condition against fault duration, pre-fault terminal voltage – 1.0pu, retained voltage during fault – 0.0pu, step voltage changes and pre-fault PF – 0.8 over excited

Practical considerations: It was identified in the previous section that the worst-case scenario occurs when the peak current is 4600A. Designing an electrical machine for this absolute worst case could lead to an over engineered system that rarely experiences the theoretical worst case. Therefore, it is desirable to consider some practical scenarios. Non-zero retained voltage during a fault and finite slope of voltage changes are the two most important factors that reduces the peak current during an LVRT.

Non-zero retained voltage: Retained voltage during a fault enables the generator to transfer some active power to the grid thus maintains useful electromagnetic torque. As a result, rotor acceleration is reduced and helps to reduce the peak current.

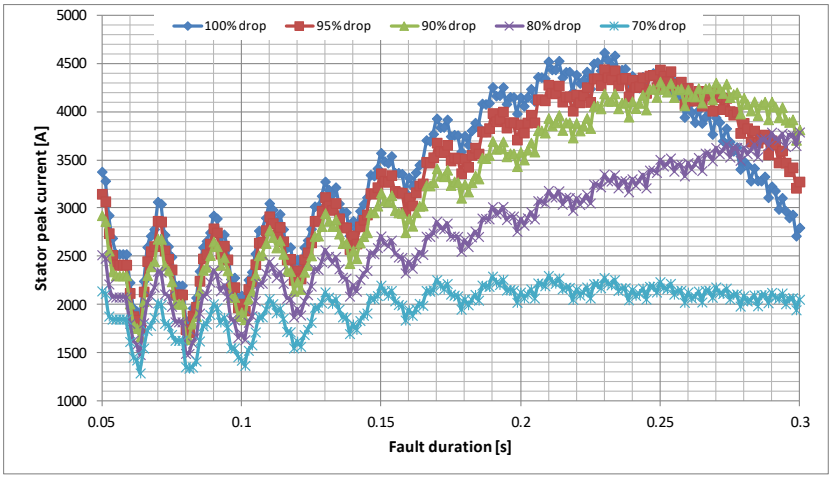


Figure 4. 20: Stator peak current variation against fault duration for different retained voltage, pre-fault power factor - 0.8 over excited, pre-fault terminal voltage 1.0pu and step voltage changes

Finite gradient terminal voltage variation: Voltage recovery during LVRT heavily depends on the characteristics of the grid in terms of effective inductance, capacitance and resistances of the transmission line. In addition, characteristics of the breaker that clears the fault also influence the shape of the voltage recovery.

Modeling the exact shape of voltage recovery using Simpowersystem is highly unreliable. Therefore, a simple approach has been considered in this section by forcing the voltage return to follow a predefined ramp rate. Figure 4.33 shows a typical voltage variation during an LVRT and the ramp rate of the voltage change is around 20ms.

Figure 4.21 shows the influence of finite voltage gradient on reducing the peak current for 100% voltage drop and 0.8 over excited power factor. Similarly, 70% voltage drop with different ramp rate return is given in Figure 4.32.

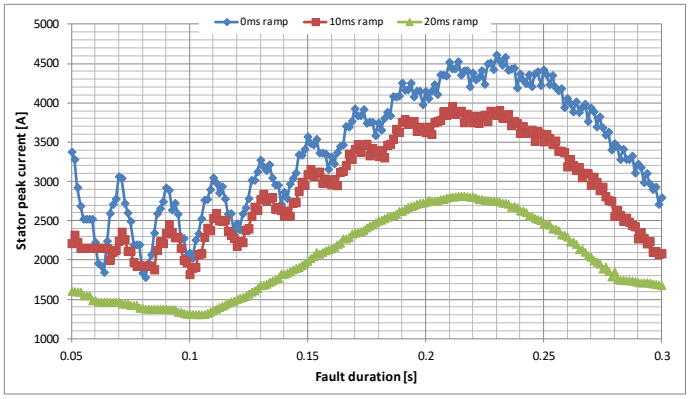


Figure 4. 21: Stator peak current variation against fault duration for different return ramp voltages, pre-fault power factor - 0.8 over excited and fault retained voltage – 0.0pu

LVRT assessment for German grid

The German electricity grid requires generators to ride through 70% voltage drop (0.3pu retained voltage) [19]. Therefore, several combinations of operating scenarios were investigated for LVRT performance with 0.3pu retained voltage.

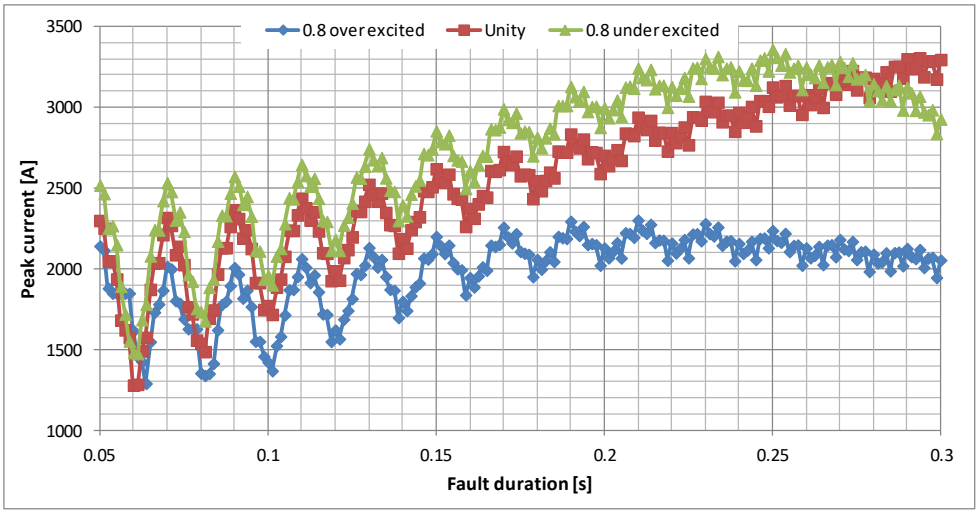


Figure 4. 22: Stator peak current variation against fault duration for different power factor. Pre-fault terminal voltage 1.0pu, fault retained voltage - 0.3pu

Figure 4.22 shows the variation of stator peak current against fault duration for different power factors. It is interesting to observe that the over excited power factor helping the generator to ride through easily. Over excited power factor operation generates significantly lower peak current than the unity or under excited power factor cases. Over excited power factor indices high internal voltage and thus enabling to transfer more active power to the grid. This helps in reducing the rotor accelerations when comparing against the unity or the under excited power factor. Time series results are given for all these three power factors from Figure 4.23 to Figure 4.24.

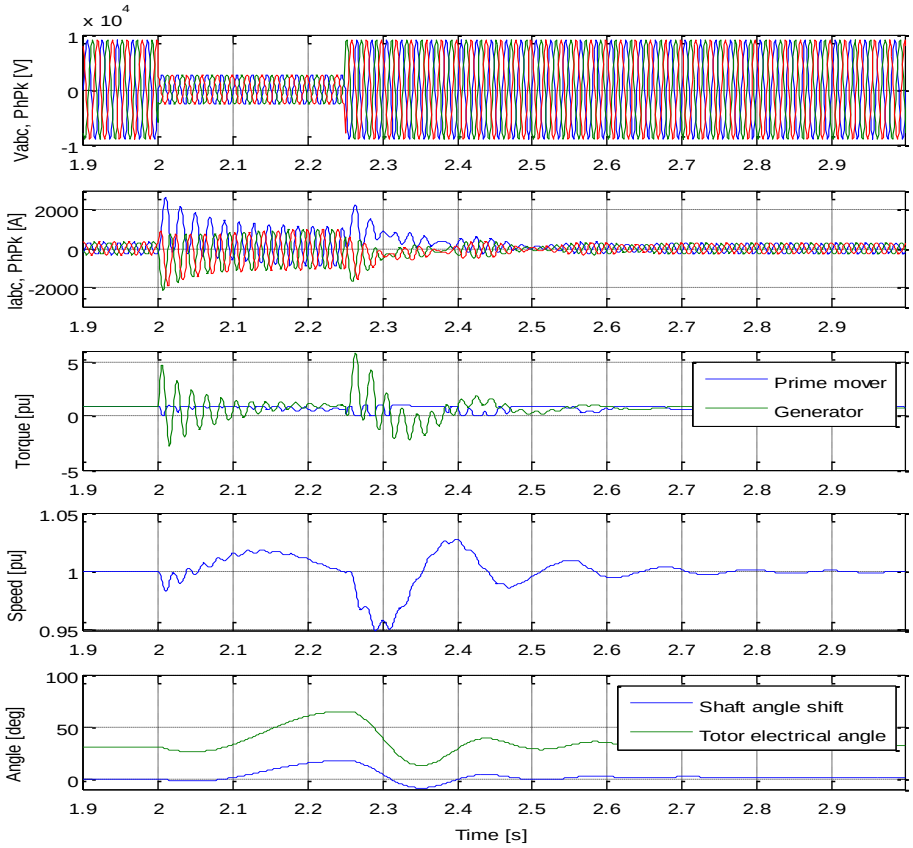


Figure 4. 23: LVRT performance: retained voltage during fault – 0.3pu, fault duration – 250ms, pre-fault terminal voltage – 1.0pu, pre-fault power factor - 0.8 over excited

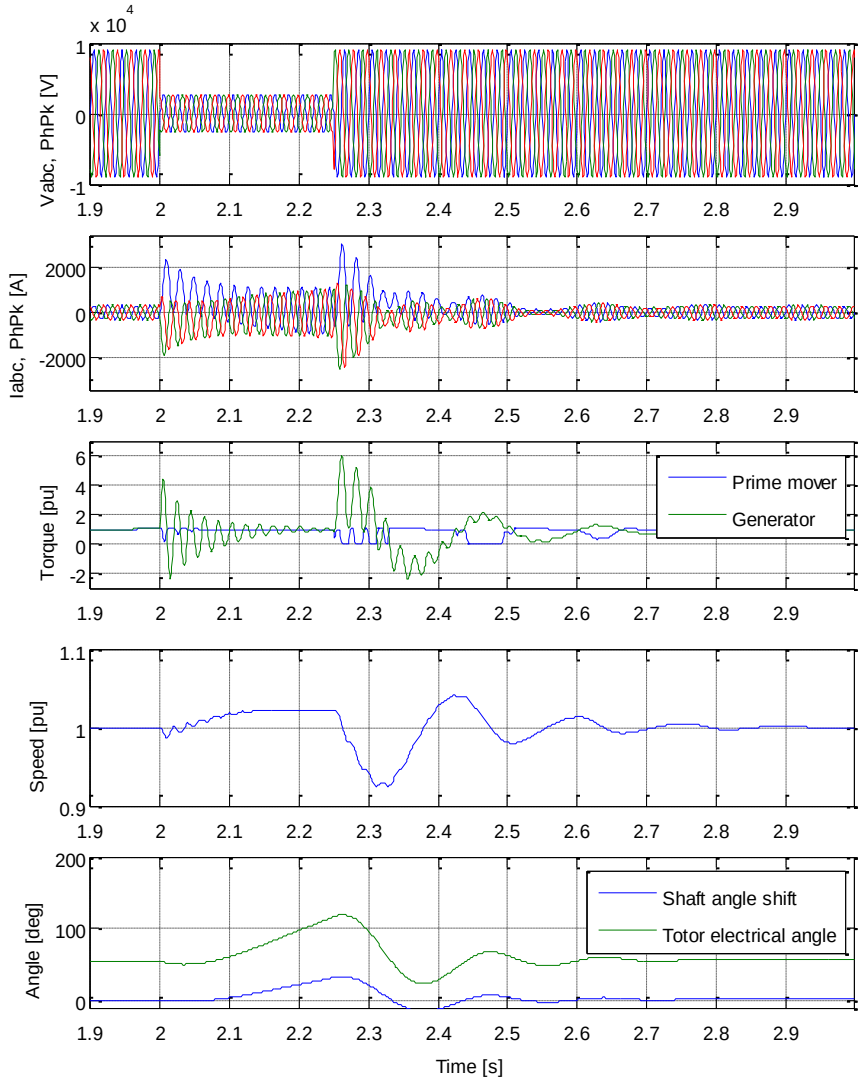


Figure 4. 24: LVRT performance: retained voltage during fault – 0.3pu, fault duration – 250ms, pre-fault terminal voltage – 1.0pu, pre-fault power factor - unity

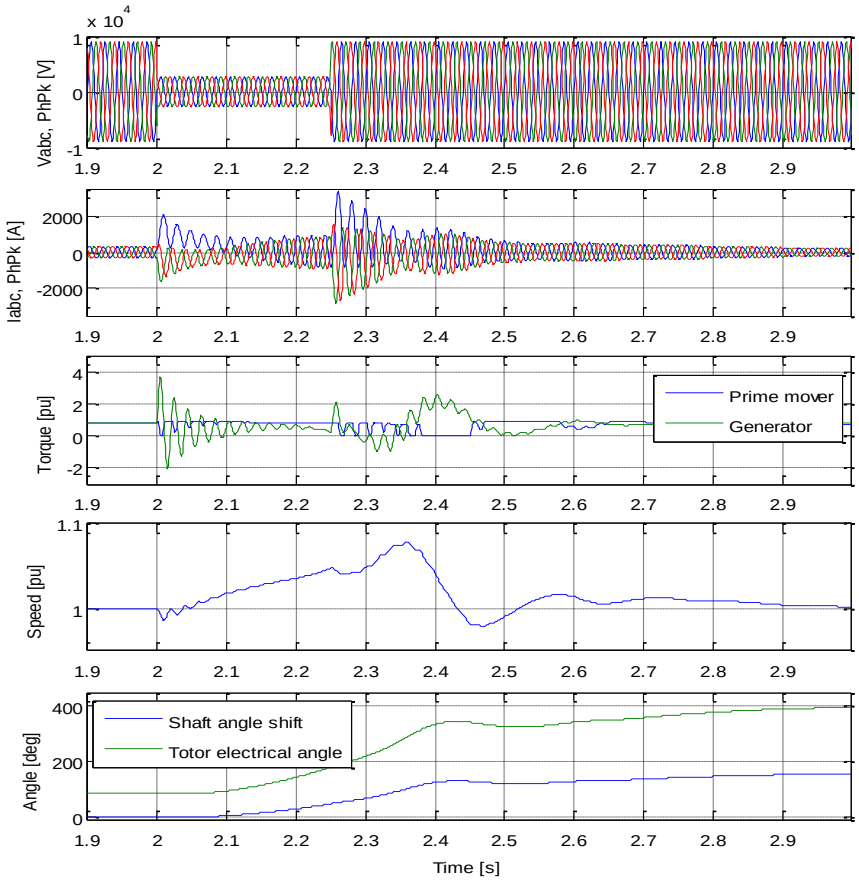


Figure 4. 25: LVRT performance: retained voltage during fault – 0.3pu, fault duration – 250ms, pre-fault terminal voltage – 1.0pu, pre-fault power factor - 0.8 under excited

RMS average values during and post-fault

Rms variation of stator current, power at the terminal and the electromagnetic torque are shown in Figure 4.25 to Figure 4.26 for 0.3pu retained voltage.

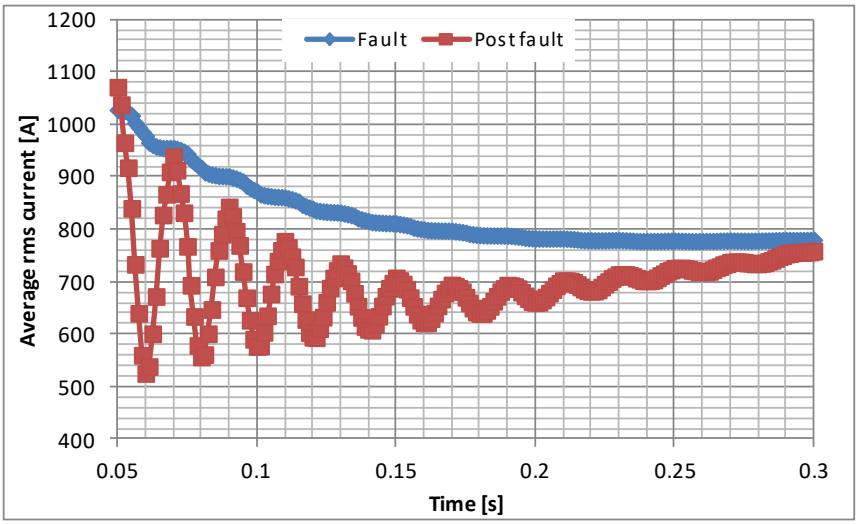


Figure 4. 26: Stator rms average current during fault and post-fault condition against fault duration, pre-fault terminal voltage – 1.0pu, retained voltage during fault – 0.3pu, step voltage changes and pre-fault PF – unity

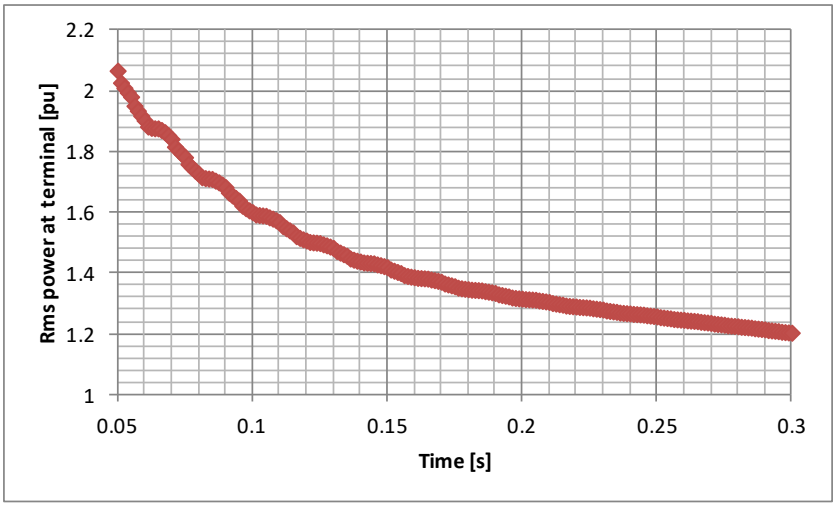


Figure 4. 27: Stator rms power at the terminals during fault and post-fault condition against fault duration, pre-fault terminal voltage – 1.0pu, retained voltage during fault – 0.3pu, step voltage changes and pre-fault PF – unity

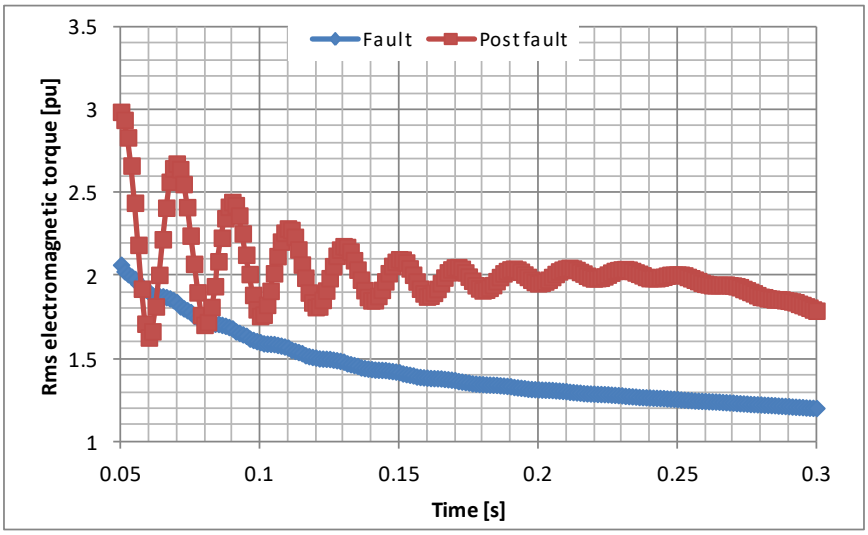


Figure 4. 28: Electromagnetic rms torque during fault and post-fault condition against fault duration, pre-fault terminal voltage – 1.0pu, retained voltage during fault – 0.3pu, step voltage changes and pre-fault PF – unity

1.1pu pre and post-fault grid and 0.3pu retained voltages

Higher terminal voltage before and after the fault always induces high peak current as the change in voltage during the LVRT is high. Figure 4.26 shows the variation of stator peak current against fault duration for different power factors. Over excited power factor is not considered in this scenario as the generator is not normally operated at over exciting while the terminal voltage is high. Figure 4.26 and Figure 4.27 shows the performance of the generator during an LVRT with pre and post terminal voltage of 1.1pu.

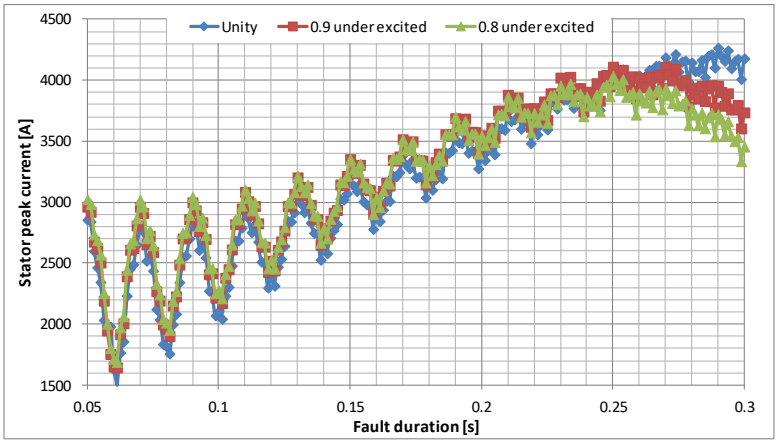


Figure 4. 29: Stator peak current variation against fault duration for under excited and unity power factors: pre and post-fault terminal voltage 1.1pu, retained voltage during fault – 0.3pu

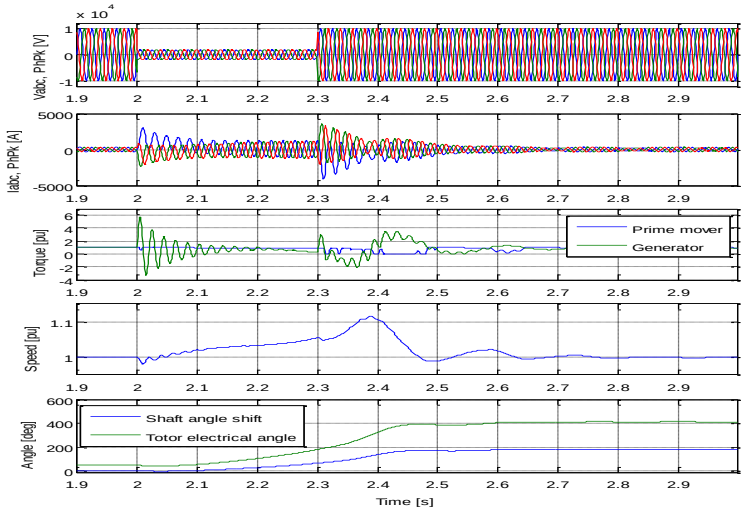


Figure 4. 30: LVRT performance: pre and post-fault terminal voltage – 1.1pu, retained voltage during fault – 0.3pu, pre-fault power factor - unity

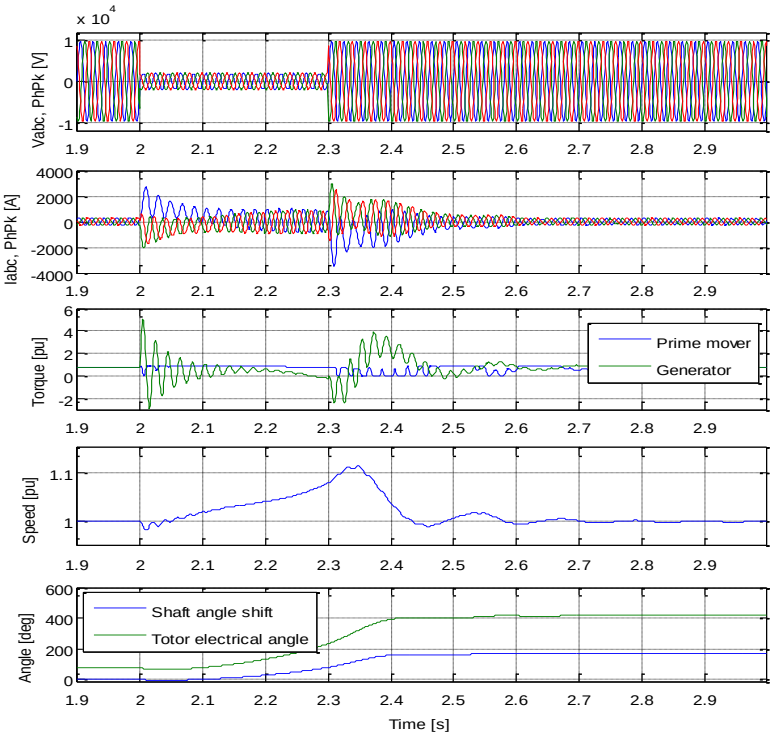


Figure 4. 31: LVRT performance: pre and post-fault terminal voltage – 1.1pu, retained voltage during fault – 0.3pu, pre-fault power factor - 0.8 under excited power factor

0.9pu pre and post-fault grid and 0.3 retained voltages

Contrarily to the previous case study, lower terminal voltage before and after the fault helps in reducing the stator peak current as the change in voltage during the LVRT is low. Figure 4.32 shows the variation of stator peak current against fault duration for different power factors. Under excited power factor is not considered in this scenario as the generator is not normally operated at under exciting while the terminal voltage is low. Figure 4.29, Figure 4.30 and Figure 4.31 shows the

performance of the generator during an LVRT with pre and post terminal voltage of 0.9pu.

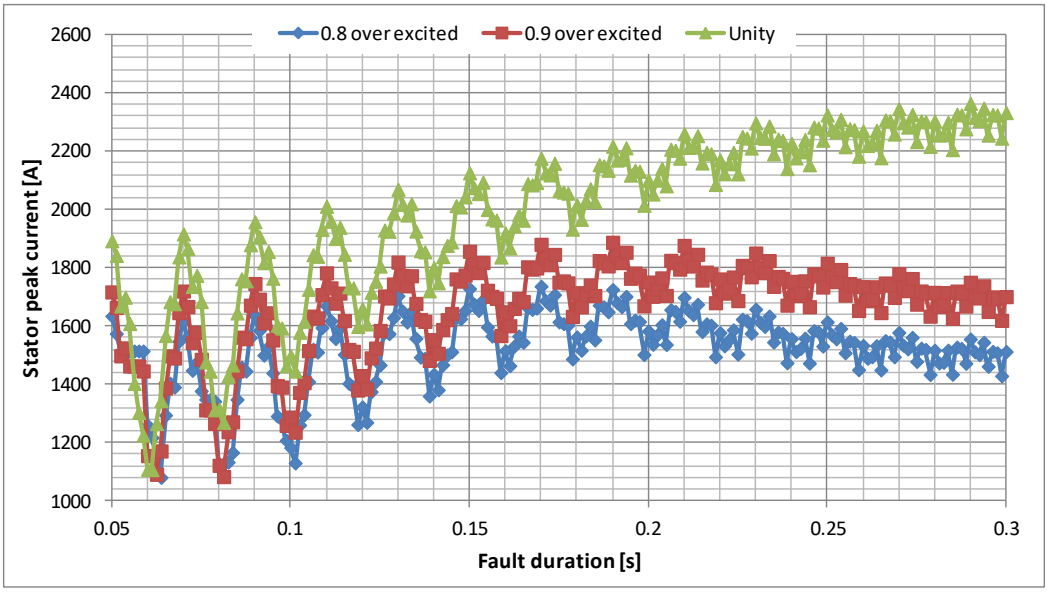


Figure 4. 32: Stator current variation against fault duration for over excited and unity pre-fault power factors: pre and post-fault terminal voltage 0.9pu, retained voltage during fault 0.3pu

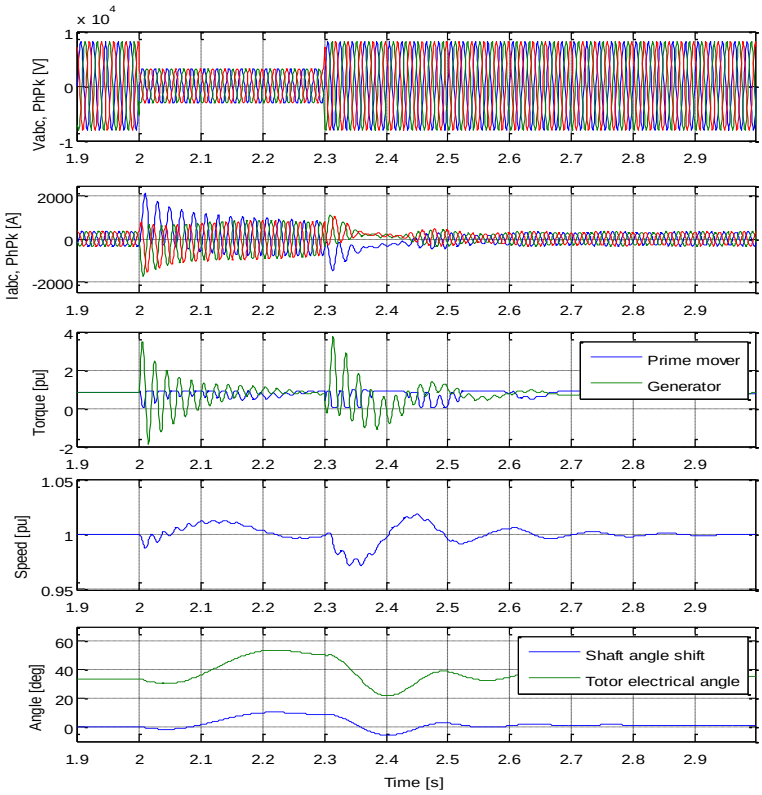


Figure 4. 33: LVRT performance: pre and post-fault terminal voltage - 0.9pu, retained voltage during fault - 0.3, pre-fault power factor - 0.8 over excited, step change in voltages

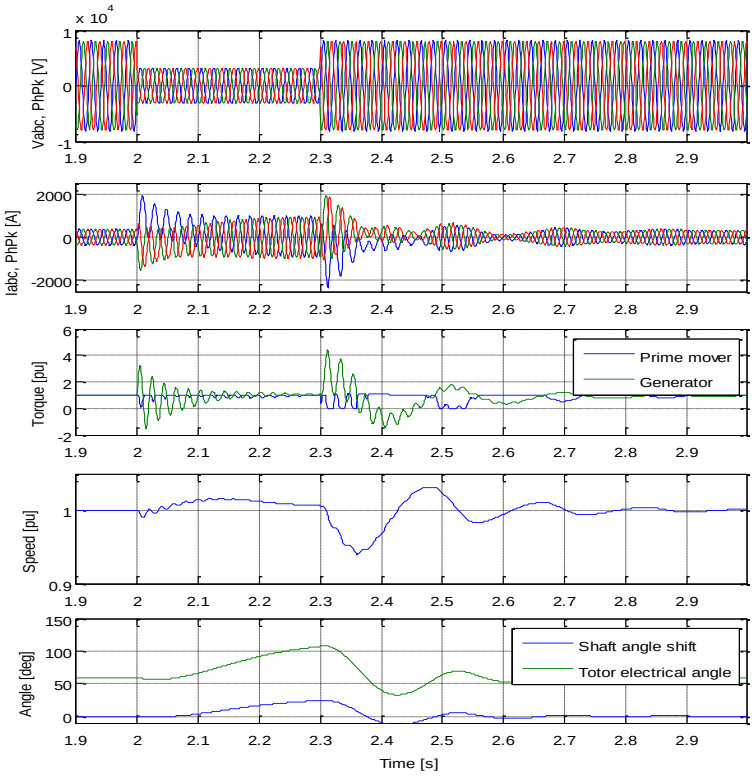


Figure 4. 34: LVRT performance: pre and post-fault terminal voltage - 0.9pu, retained voltage during fault - 0.3, pre-fault power factor – unity, step change in voltages

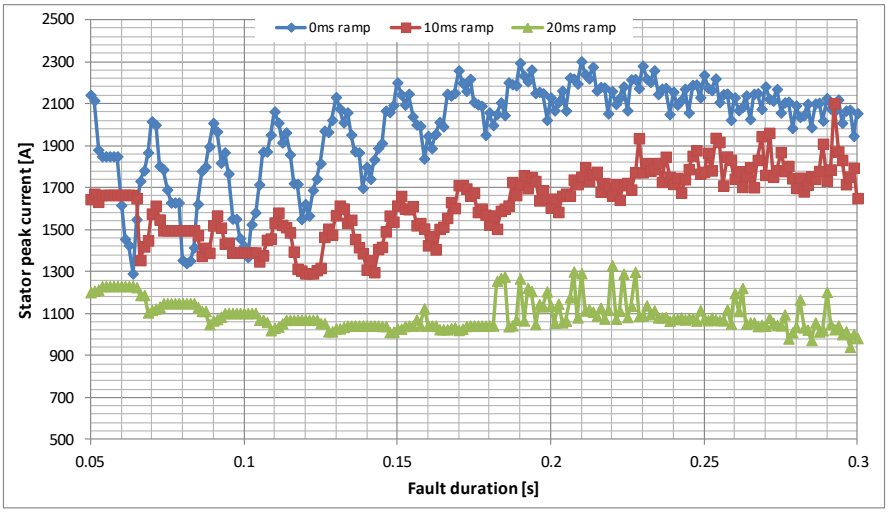


Figure 4. 35: Stator peak current variation against fault duration for different return ramp voltages, 0.8 over excited power factor and 70% drop

Effect of Slow ramp on pole-slip

Fast recovery of grid voltage induces high peak current; however, it helps to synchronize the rotor to the grid quicker. This is because the grid return establishes synchronizing torque and thus prevents further rotor accelerations. Fast resynchronization avoids any undesirable pole-slip. Definition of pole-slip during a LVRT is debatable. Formal definition according to IEEE is give as “a condition whereby a generator, or group of generators, terminal voltage angles (or phases) go past 180 degrees with respect to the rest of the connected power system”.

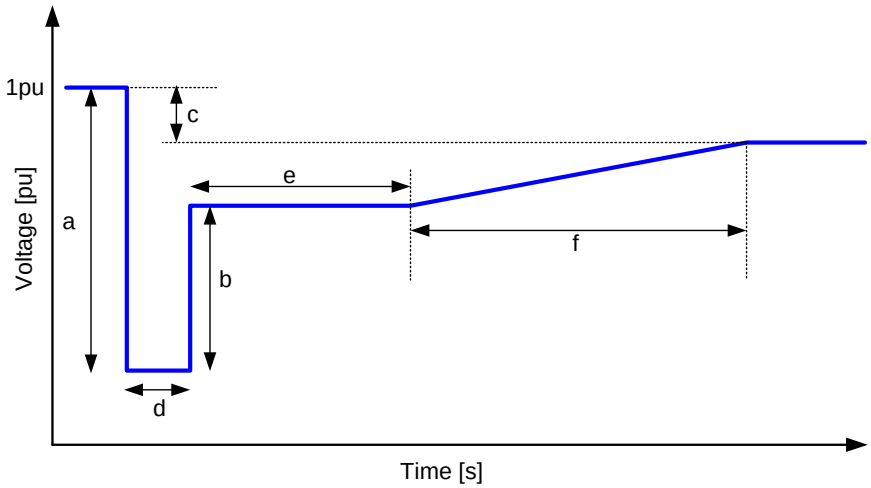


Figure 4. 36: General LVRT profile

Figure 4.33 shows the performance of the generator when a German Grid code for LVRT is applied at the terminal. Since there is a retained voltage (0.3pu) during the fault and the voltage steps up by 0.4pu, the generator can avoid any pole slips. However, when there is no retained voltage and the grid returns slowly (300ms), the rotor shaft advances by 540 degrees. That is equivalent to 3 pole slips (540/180 = 3) as shown in Figure 4.33 as the generator has 4 poles. In Figure 4.34, the prime mover has a very low controller bandwidth and thus does not alter the prime mover torque upon clearing the fault. Another set of simulations was conducted with a high controller bandwidth and the performance is given in Figure 4.35. The fast controller effectively alters the prime mover torque and manages to reduce the pole slip to only 2. This shows that the control system of the prime mover can be tuned in such a way to reduce the impact of LVRT.

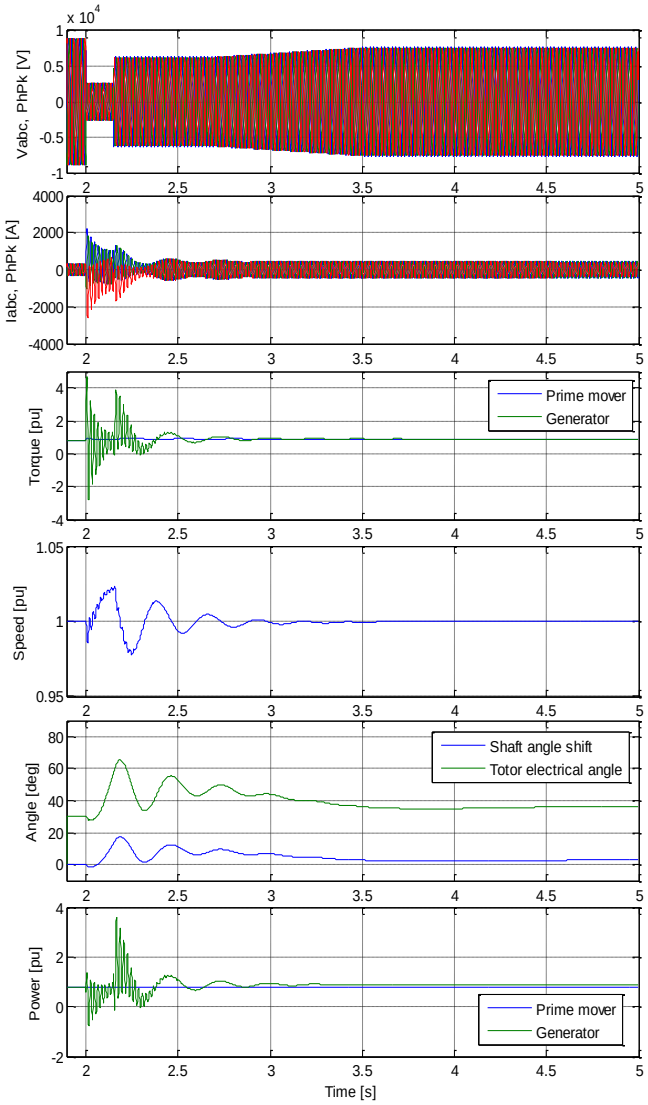


Figure 4. 37: LVRT performance with German grid code

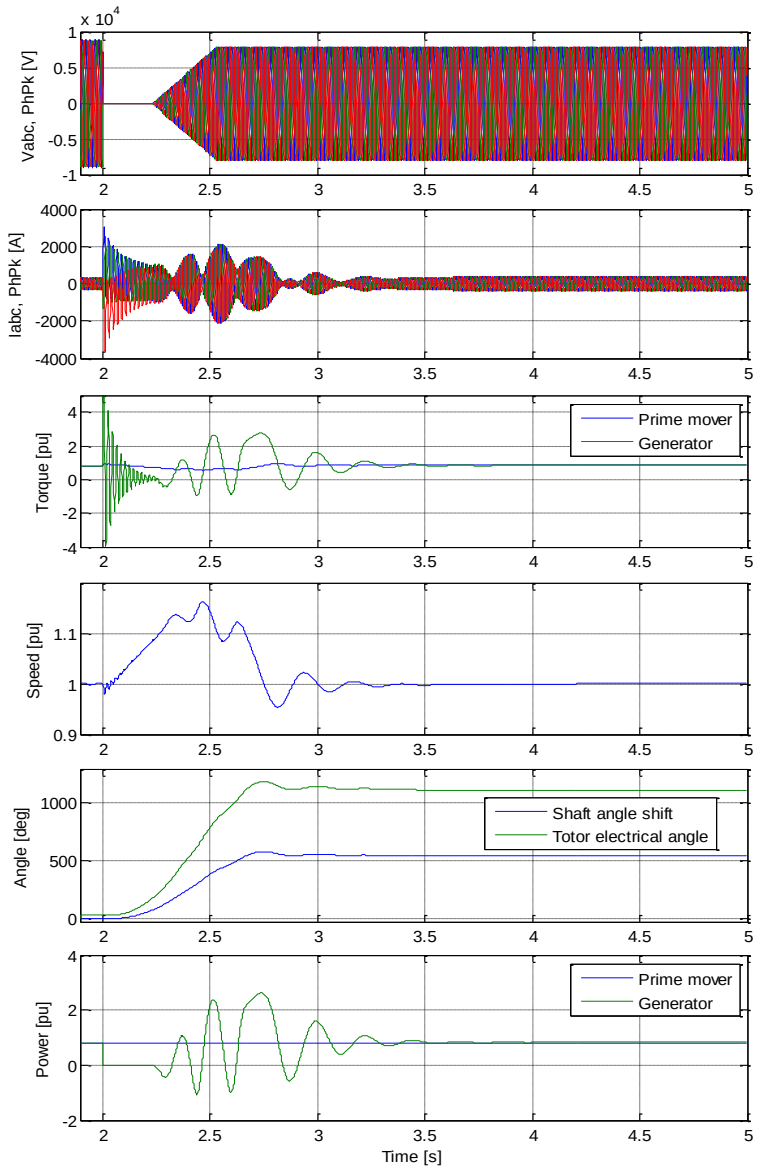


Figure 4. 38: LVRT performance with absolute worst case and slow controller

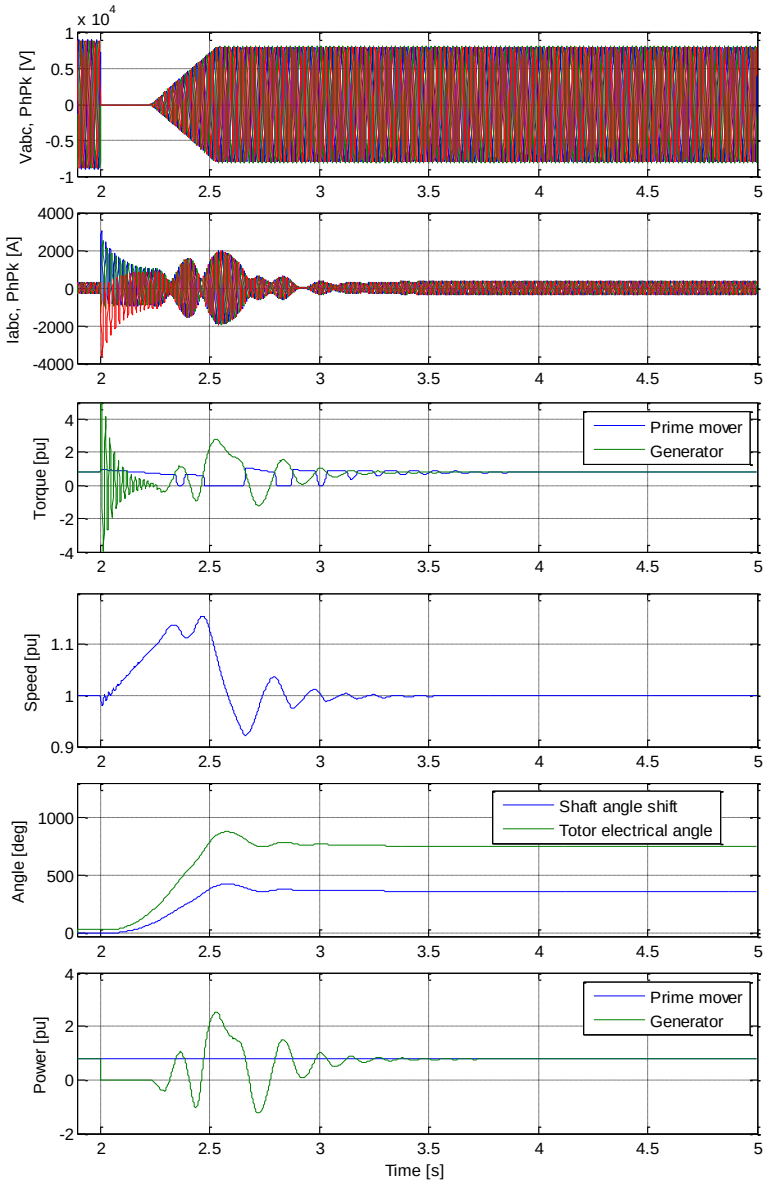


Figure 4. 39: LVRT performance with absolute worst case and fast controller

4.4 Selection of variables for power systems simulation

In chapter 3, the development of a detailed validated methodology to obtain the SG parameters was described. These parameters were then used to build a power systems simulation model of an engine driven SG connected to the grid as shown in the previous sections.

Before going into a detailed analysis using the power systems simulation model, a 4 MVA SG was used to validate the developed tool and the validation steps taken were described in the previous section. The validated model was also used to study the performance of engine driven SGs during transients on the grid and several parameters were identified as having an influence on the dynamic performance of an engine driven SG.

The power systems simulation capability / framework once validated, can be therefore applied to achieve the main objective outlined in this work, i.e. the design of a grid code compliant SG. An automated script was used to vary several quantities / inputs in various power systems simulations and the performance of the SG was monitored. The critical clearing time according to [35], [38] as the maximum fault clearing time that the SG would remain stable for any given system conditions was the output measured across all the simulations. The output from these simulations will then be processed using Neural Networks to define design criteria for grid-compliant SGs. The approach used is shown in Figure 4.40.

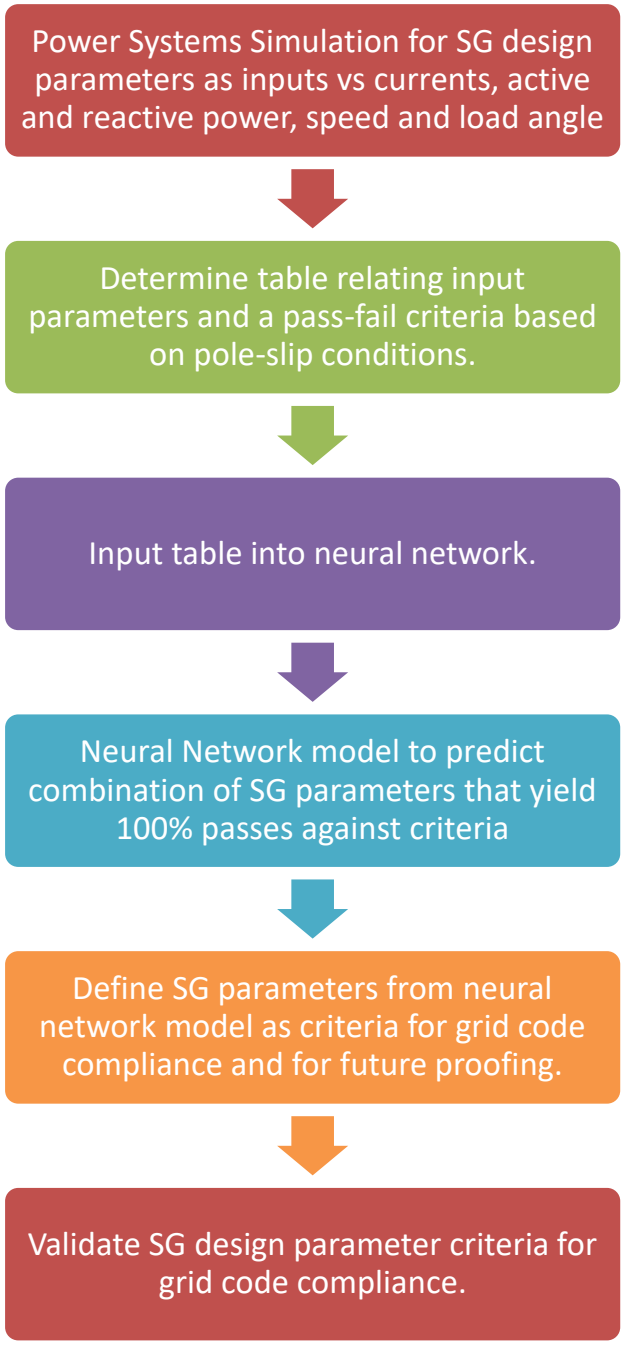


Figure 4. 40: Method to determine SG design criteria for grid code compliance

The approach to define the inputs to the power systems simulation and details on the neural network models along with results and validation with grid code tests will be addressed in the next chapter.

To run an efficient search for characteristics of synchronous machine design that contribute to grid code compliance, a simplified set of inputs were defined. A three-pronged approach was adopted as shown in Figure 4.39 to identify the input parameters to be used in the power systems simulation. Each of the three elements will be discussed in this section.

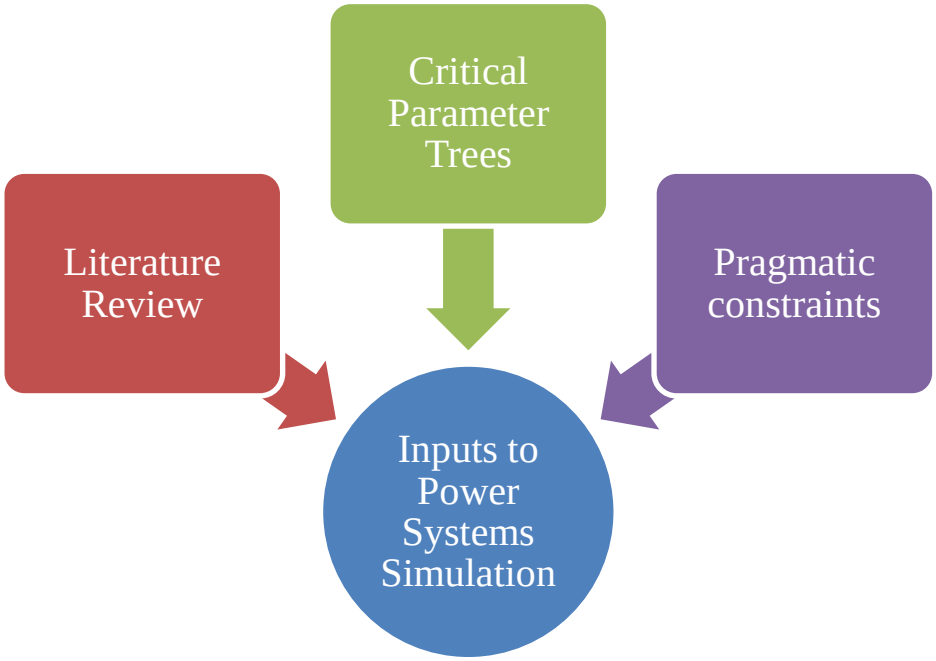


Figure 4. 41: Three-pronged approach to defining inputs to power systems simulation

4.4.1 Literature Review

[112], [113], [114], [115] through extensive discussions on grid code compliance of SGs argue that SG design parameters are the best approach to designing for grid code compliance due to impracticalities associated with knowing grid and transmission line parameters when selecting SGs for grid applications.

Additionally, [115] also argues that power electronics and any external devices would add unnecessary cost and inefficiencies to the power system. [113] shows that lower short-circuit capability of grids form the worst case in terms of dynamic stability of engine driven generating sets connected to the grid. [113] also goes on to show that typical worst-case grids are approximately three times the short-circuit power of that of the genset.

4.4.2 Critical parameter trees

Figure 4.41 illustrates the critical parameter tree for the steady state load angle. A critical parameter tree breaks down any quantity into its fundamental constituents. The steady state load angle that defines the pre-fault condition of the SG depends on the SG reactances, transmission line parameters and nature of load, including voltage at point of common coupling, power factor and kVA.

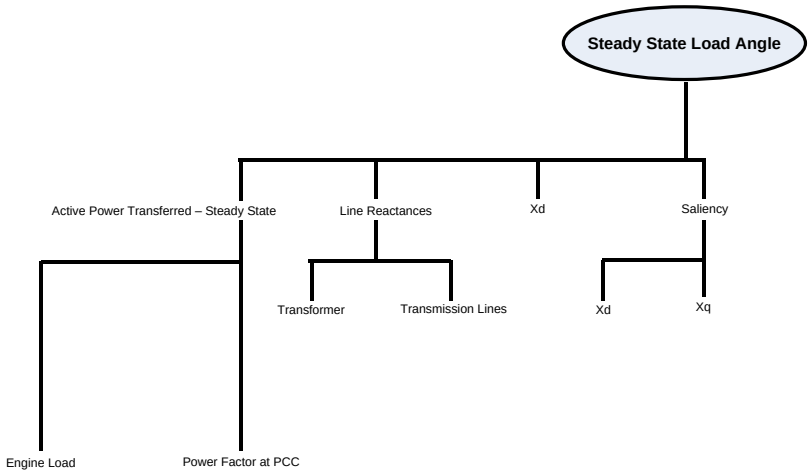


Figure 4. 42: Critical parameter tree for Steady State Load Angle

Figure 4.38 similarly breaks down acceleration of the shaft during a transient event and shows the acceleration depends on inertia of the genset, the transient torque

which depends on transient and sub-transient reactances and short-circuit capability of the grid.

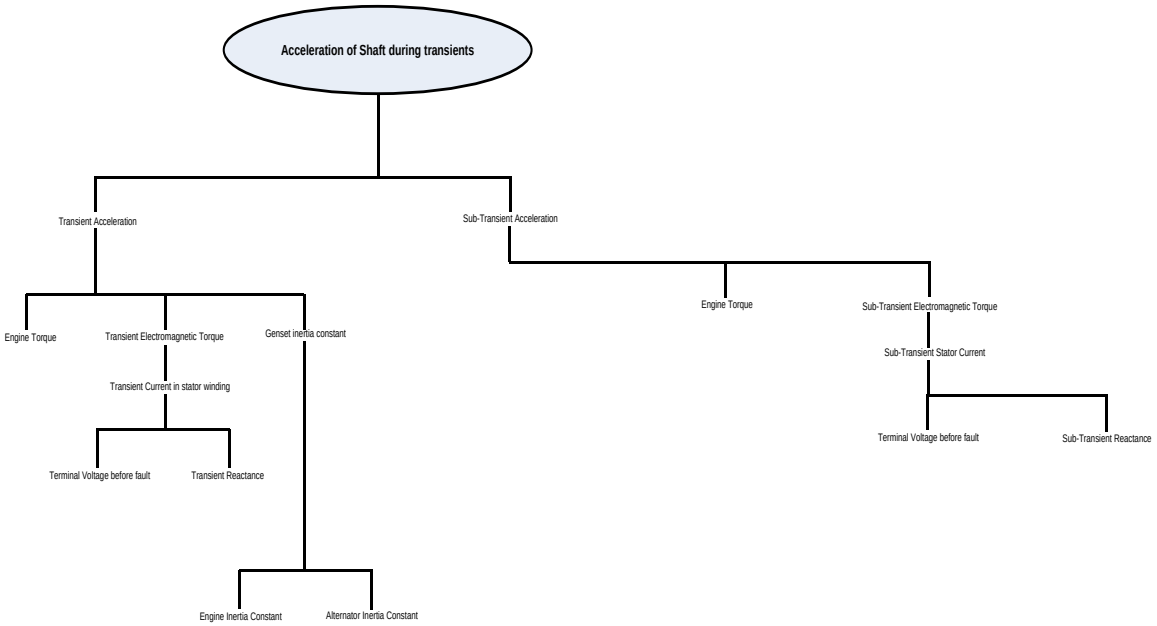


Figure 4. 43: Critical Parameter Tree for shaft acceleration during transients

4.4.3 Pragmatic constraints

The work presented in [116], [117], [118] show extensively the impact of transformer reactances on the dynamic stability of generators connected to the grid, specifically, lower the transformer reactance, more the SG needs to depend on its own stability capabilities to remain connected to the grid. Typically, the transformers used with 1400 kVA SGs have a reactance of 6% per unit [122]. Since 6% per unit is the lower limit of all transformers used with products made by Cummins Generator Technologies [122], the same value was also set as a generic transformer reactance. [117], [119], [120] demonstrate the impact of the grid short-circuit capability on dynamic stability. The authors show that high short-circuit

capability grids create a more stable connection for the SGs. Typical low values are also defined at 3 times the short-circuit capability of the SGs they are connected to. The recommendations of [117], [119], [120] were used to set the grid in the simulation to 3 times the short-circuit capability of the SG as a worst-case design constraint. [16], [17], [18], [19], [20], [21], [22], [23], [24], [25], [26], [27] list out the pass / fail criteria for static and dynamic stability as stated in the grid codes.

4.4.4 Inputs to power systems Simulation

The 3-pronged approach discussed above was used to define the inputs and constraints used in the power systems simulation as shown in Table 4.1. Additionally, to align with business and cost constraints discussed in Chapter 6, X_d and H were the only SG design parameters selected to be varied based on a hypothesis that a solution space for grid code compliance can be found by varying only these two design quantities.

Table 4. 1: Input variables and limits set in simulation

Pre-fault load (% rated load)	25%, 50%, 75%, 100%
Power Factor	0.9 lead, 0.9 lag, 0.8 lag, unity power factor
Low Voltage Ride Through Curve(s)	France, Germany, Italy

X_d	1.5 per unit, 1.6 per unit, 1.7 per unit, 1.8 per unit, 1.9 per unit, 2 per unit, 2.1 per unit, 2.2 per unit, 2.3 per unit, 2.4 per unit, 2.5, 2.6 per unit, 2.7 per unit, 2.8 per unit, 2.9 per unit and 3.0 per unit per unit
H	0.25 s, 0.5 s, 0.75 s, 1 s

4.4.5 Pole slip prediction

[35] and [38] define Critical Clearing Time as the time after which a generator that is riding through a fault will become unstable without being able to return to stability upon return of pre-fault conditions. Critical Clearing time depends on SG design parameters and the power system quantities and defines how long a SG can ride through a fault and was therefore selected as the output to be measured. A fault that lasts beyond the critical-clearing time leads to a pole-slip condition and therefore to 'measure' the transient stability of an engine driven SG under grid code conditions, predicting pole-slip and recording the pole-slip condition as a fail and a pass otherwise would be a robust approach.

An automated script was written using the principles set-out in [127] to predict pole-slip and record a '0' for a fail. The script utilizes two criteria shown in (4.1) and (4.2), where, P is the value of active power measured at a discrete time t (the

instantaneous value at a time t in the simulation), $P_{pre-fault}$ is the value of active power before the fault, Q is value of reactive power at a discrete time t and Q_{dyn} is calculated dynamically (the quantity Q_{dyn} is being averaged in a time-stepping simulation by considering the value of Q at various time steps – averaging considering a moving window) by (4.2), where, X_d is the direct axis synchronous reactance and V_{avg} is the arithmetic average of the three-phase voltage.

Since the approach is predictive and not reactive, the methodology of determining transient stability of the SG has a built-in safety margin.

$$P(t) > P_{pre-fault} \tag{4.1}$$

$$Q(t) < Q_{dyn}(t)$$

$$Q_{dyn}(t) = V_{avg}\, X\, V_{avg}^{pre-fault} X \frac{1}{X_d} \tag{4.2}$$

4.5 Prediction of critical parameters for grid code compliance with neural networks

4.5.1 Approach

The power systems simulation tool that was developed in the previous section lends itself to requiring specialist knowledge relative to matlab and simpower systems and needs extensive case by case setup and simulation that is both time consuming and cumbersome. Typically selecting generators for an application needs to be completed within 24 hours of a request being made. This means that a more

simplified simulation tool that can be used by a wider population and one that is flexible enough to work with the changing grid codes was needed. To accomplish the objectives of this thesis and to have a generic model to test for grid code compliance, a neural network approach to simplifying the power systems simulation tool developed in the previous chapter as shown in Figure 4.41.

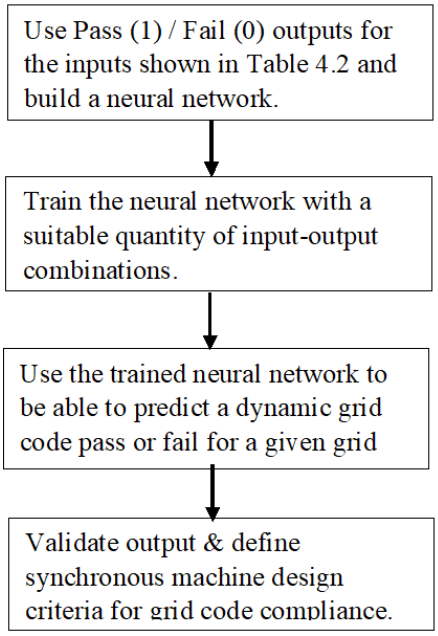


Figure 4. 44: Process to define SG design criteria using neural network.

4.5.2 Model setup & findings

For the purpose of this thesis, the 'nntool' within MATLAB was used to simplify the process of neural network creation, training and validation.

Through numerous trials, a two-layer feedforward network with sigmoid hidden neurons and linear output neurons are used. The SG d-axis reactance and inertia

constant, the load condition (percentage of rated load and power factor), Voltage at terminals of generator as a percentage of rated voltage and the grid code fault ride through curves are used as inputs to the neural network and a Pass (1) or Fail (0) from the power systems simulation results are used as outputs. Using the results from the neural network, the maximum values of reactance and minimum value of inertia constant that lead to a 100% pass for the simulated conditions are selected as the target design parameters that need to be achieved.

The neural network simplification of the power systems analysis results in a scenario where when the d-axis synchronous reactance needs to be no more than 2.1 per unit and inertia constant needs to be at-least 0.5 seconds to comply with the transient stability requirements of the required grid codes.

4.6 Grid Code Testing

To validate the findings of the neural network, a LVSI804S generator is tested using the method described in this section. Compliance testing is performed by certified test laboratories, to prove compliance of the equipment with national, international, or industry standards The most common test approach used is based on the voltage divider proposed in standard IEC 61400-21[121] and shown in Figure 5.5 below.

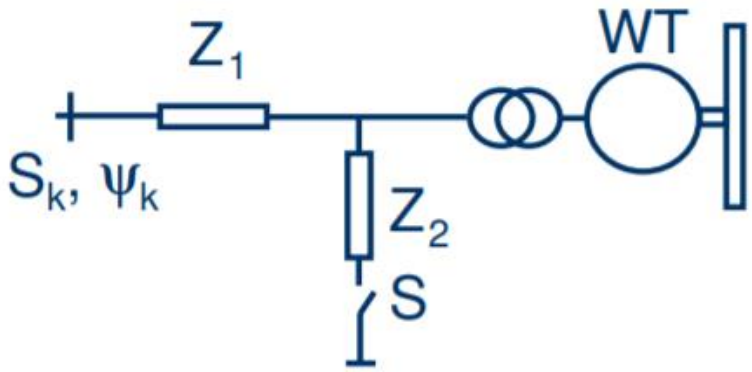


Figure 4. 45: IEC 61400-21 method of testing for grid code compliance [121]

in Figure 4.45, Z2 represents the fault impedance. The voltage dip is initiated by closing the circuit breaker S. Inductors are used as impedances because to minimize losses. Moreover, inductive fault impedance is more demanding in terms of reactive support to be provided by the generator. The impedance Z1 is needed to limit the influence of the voltage dip in the supplying grid. To be able to select the remaining voltage level during the dip (according to the grid code requirements), the impedance values must be adjusted accordingly. In most grid codes, FRT conditions are specified at the Point of Common Coupling (PCC). Testing procedures usually prescribe the same retained voltage levels as required at PCC also at the generator terminals. Indeed, this would indicate that the generator is fully compliant.

Figure 4.46 below shows the test setup for the LVSI804S driven by a Cummins QSK60 diesel engine connected to an '*Energy to Quality'* box that simulates the test method described in IEC 61400-21. The SG is subjected various grid code

conditions. The opportunity is also taken at this stage to compare results of the power systems simulation from Chapter 4 and this comparison is shown in Figure 4.47 that shows the results for a 70% voltage drop and Figure 4.48 that shows the results for a 30% voltage drop; a good correlation is observed between simulation and the tests. Also, the tests completed confirm the findings of the neural network as when the LVSI804S was tested at a rating that provides a d-axis reactance of 2.1 per unit and inertia constant of 0.5 seconds, it passed all the grid code curves.



Figure 4. 46: Grid code test setup for the LVSI804S generator with a Cummins QSK60 engine

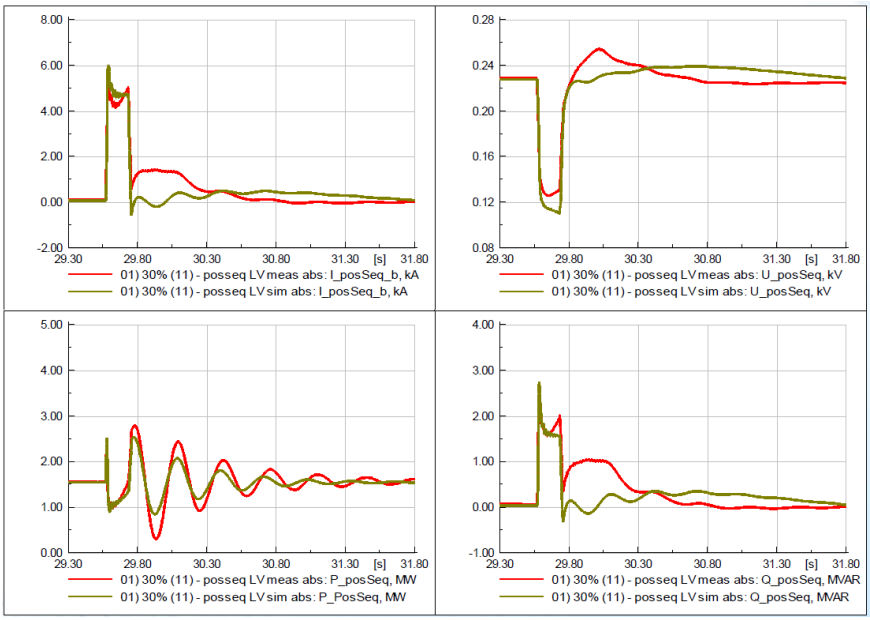


Figure 4. 47 Comparison of simulation (green) vs test (red) at a 70% voltage drop

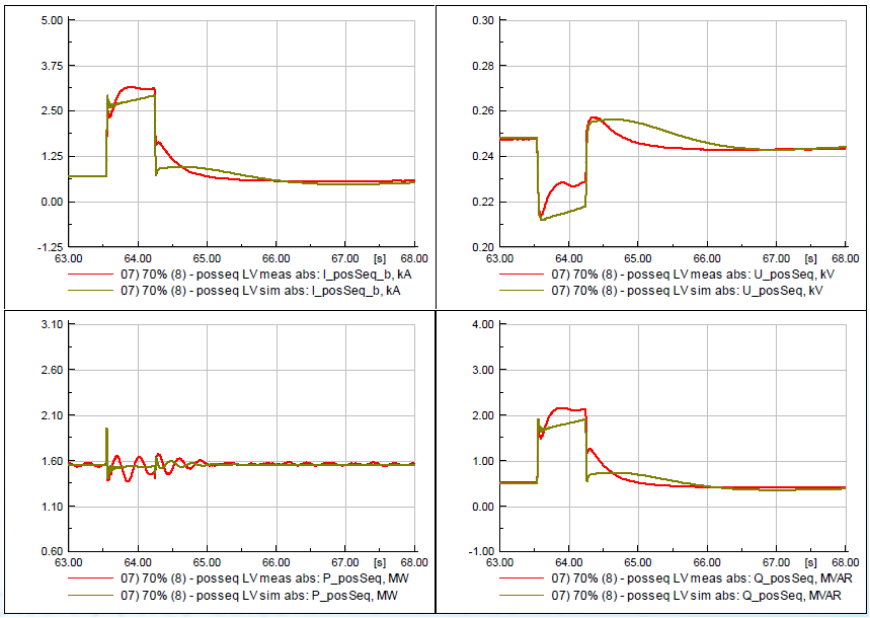


Figure 4. 48 Comparison of simulation (green) vs test (red) at a 30% voltage drop

4.7 Conclusion

A very comprehensive power systems simulation model was developed and validated. The model was also used to make some initial assessments on critical parameters that impact dynamic performance of SGs connected to the grid. The findings combined with a comprehensive literature survey, high level analysis of requirements and pragmatic considerations were used to define inputs to the power systems simulations model that will be shown to simulate a variety of grid conditions with different SG parameters using an automated script which were analyzed further using a neural network model. The power systems model also uses validated synchronous machines data derived from a finite element model that was built and validated in Chapter 3. Combined, the FE model and the power systems simulation models alone provide the capability to design SGs with a comprehensive understanding of grids, i.e. the means to design SGs with an understanding of the application and the ability to study its performance in the application prior to launching to market.

When a customer makes a request to select a SG, the decision is made by the Applications Engineering team within 24 hours of a request being made. This prompts the need for a quick response tool, especially in the absence of a readily available product. The Neural Network tool described in the chapter has simplified the process of defining a criterion for a SG to be grid code compliant, it has also laid the foundation for a tool that can be adapted to the ever-changing grid codes and diversified application conditions and requirements. Within the tool, the inputs

like reactance, inertia constant and LVRT curve can be adjusted without having to build cumbersome power systems simulation models. The resulting output is also a simple pass (1) or a fail (0) and therefore can be used by even a new employee with minimal training. This provides a competitive edge through being able to provide technically competent responses to customers in a very short-window of time. In addition to using a diverse collection of modern tools to enrich the work contributing to this thesis, this was the reason to create a neural network tool that was generated using data from a validated power systems simulation model and validated using approved grid code certification tests. The results of the neural network simulation provide selection criteria for an engine driven SG to be dynamic grid code compliant while the tool described in Appendix 4 can be used to select a SG for static grid code compliance. While both tools allow to de-rate or oversize SGs to fit the identified criteria to comply with grid codes, it is still crucial to go through a design exercise to confirm the benefits of over-sizing over designing for grid-codes or vice-versa. The design for grid codes has been described in Chapters 5 and 6 and the findings conclude that for the target SG, designing for grid code compliance is the most cost-effective solution.

CHAPTER 5

SENSITIVITY ANALYSIS

Chapter 4 described the development and validation steps of a model used to identify the system level parameters that influence the ability of an engine driven SG to be grid code compliant. In order to meet the requirements summarized in Chapter 2, the engine driven SG needs to meet the following criteria:

- d-axis synchronous reactance: X_d <= 2.1 pu for short-term gains and X_d<=1.8 pu for future-proofing for grid codes.
- Inertia constant: H ≥ 0.35 sec for engines with torque control and
- Inertia constant: H ≥ 0.5 sec for engines without torque control

Chapter 4 also described the need to re-design the 1400 kVA SG being used for this work. In addition to meeting the above requirements, the SG had to meet the constraints related to the CGT's business needs, including

- No increase in cost of the machine. i.e. achieve grid code compliance requirements with same cost.
- Reliability of SG should be identical or better than existing product.
- No change to the rotor outer diameter or stator outer diameter as this will lead to a significant change to the tooling.
- No (cost and time intense) change to the tooling used in the manufacturing and assembly processes.

Due to the nature of the business constraints, an iterative process to design the SG by performing an appropriate sensitivity analysis of the geometrical parameters is recommended.

5.1 Introduction to Sensitivity Analysis

'Sensitivity analysis is the study of how the uncertainty in the output of a mathematical model of system can be apportioned to different sources of uncertainty in its inputs' [61] [62].

A sensitivity analysis is used to improve the performance according to set objective functions by varying one variable at a time in any system; it is typically used too:

- Understand relationship between inputs and outputs.
- Test robustness of results.
- Uncertainty reduction in predictions.
- Calibrating models with large number of parameters

Considering the above, a sensitivity study can be used to analyze the impact of changing various geometrical features of a SG on the key target parameters X_d and H.

To perform a sensitivity analysis on the SG, a process shown in Figure 5.1 is defined. The following sections describe the journey taken to identify the geometrical parameters within the targeted 1400 kVA SG to achieve the design targets within the business constraints defined.

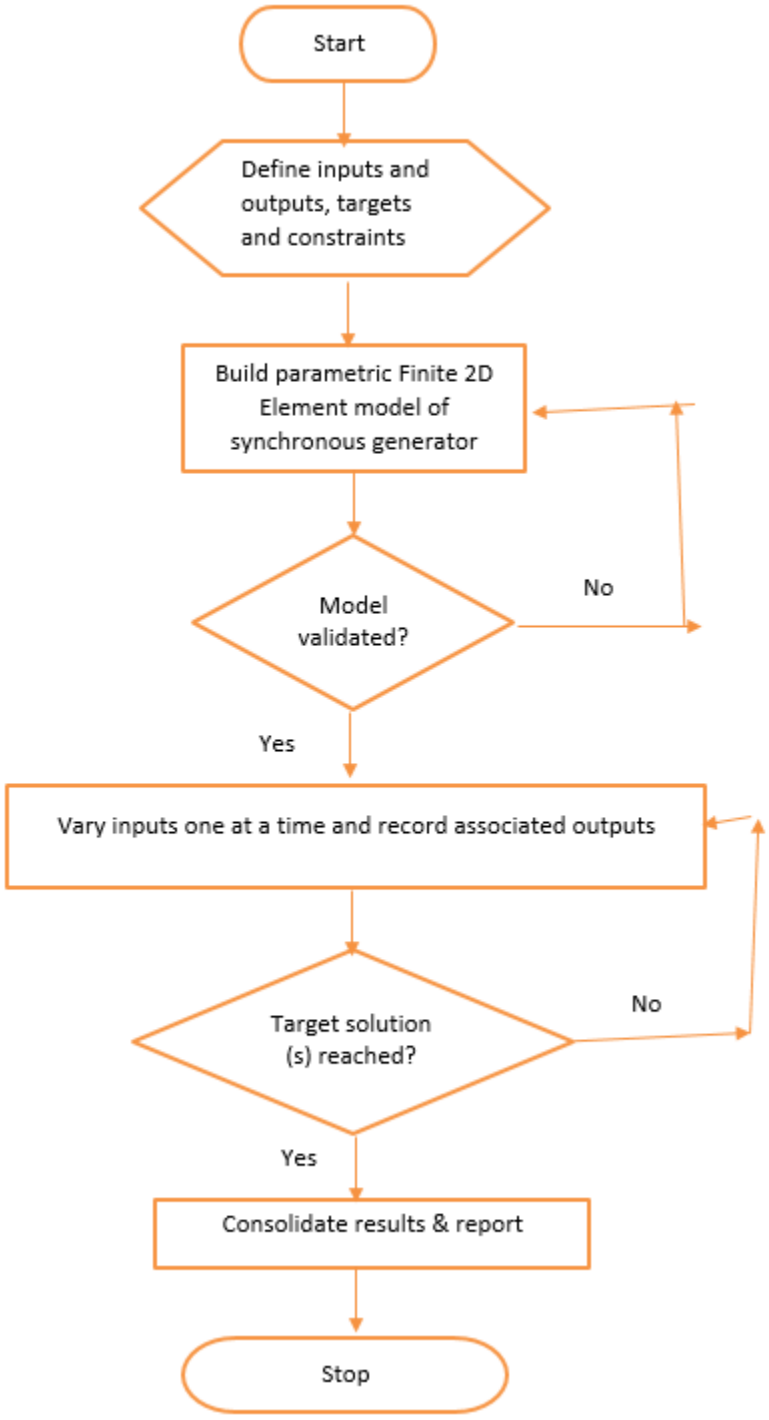


Figure 5. 1: Model setup approach

5.2 Model Setup

5.2.1 Selection of model for parametrization

The finite element model of the P7C that was developed and validated to predict its parameters was shown in Chapter 3. This model is parametrized to be used for sensitivity analysis.

5.2.2 Selection of Parametric Variables

The geometrical features of the synchronous generator that are parametrized are selected using a combination of critical parameter flow approach and first principle analytical equations that describe the various quantities we are looking to optimize.

Equations 5.1 [147], 5.2 [140][141] [147] and (3.2) together describe the d-axis reactance X_d as a function of the synchronous generator geometrical features.

$$X_d = X_{ad} + X_l \tag{5.1}$$

Where, X_d is the d-axis synchronous reactance which is a combination of the armature reactance X_{ad} and the leakage reactance X_l.

$$X_{ad} = \frac{k f_w I_n N_s}{P B_g g_{eff}} \tag{5.2}$$

Where, X_{ad} is the armature reaction reactance, k is a constant that is dependent on the permeability and therefore predominantly on the type and quantity of steel used, f_w is the winding co-efficient, In is current, N_s is the number of turns in stator, P the

number of poles, B_g the effective air gap flux density and g_{eff} the effective air gap given by Equation (5.3).

$$g_{eff} = C\ g \tag{5.3}$$

Where, C is the carter co-efficient given by equation (5.4) [147] and g is the rotor-stator air gap length.

$$C = f\left(\frac{w}{l_g}\right) \tag{5.4}$$

Where, w is the slot width and l_g is the air gap length. The carter co-efficient is a function of the slot width and air gap length and is therefore a function of the tooth design.

Equation (5.5) describes the inertia constant H in seconds.

$$H = \frac{0.5\ J\ \omega^2}{S} \tag{5.5}$$

Where, J is the moment of inertia of the spinning mass of the synchronous generator, ω is the nominal angular frequency in rad/sec and S is the rated power of the synchronous generator in kW.

The critical parameter flow approach breaks down a key requirement / performance parameter into controllable, measurable quantities. For the scope of this thesis, the critical parameter flows were created using the equations (5.1) through to (5.5) and equation (3.3). Figure 5.2 shows a critical parameter flow diagram for the steady state load angle of a wound field SG showing the high-level dependent variables into measurable independent variables.

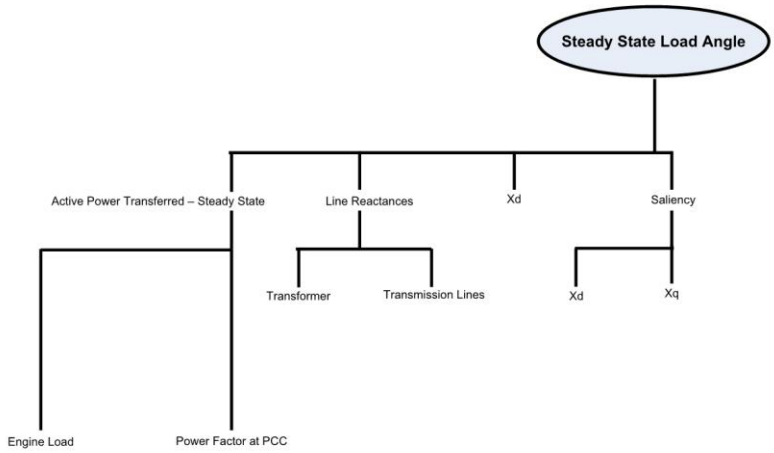


Figure 5. 2: Critical Parameter Flow Down for Steady-State Load Angle

The lowest level 'child' variables identified in Figure 5.2 – engine load, power factor at PCC, transformer, transmission lines and the synchronous reactances can be used as levers to vary the Steady State load angle. Critical Parameter Flows are developed for X_d and H as shown in Figure 5.3 to determine the variables to be parametrized in the finite element model of the target SG.

One of the key constraints of the project is to not increase rotor / stator diameter and hence increasing diameter of rotor will not be pursued in this thesis. Additionally, due to the winding method used in the manufacture of the SG, the number of turns and strands of wire per slot are mostly constrained except to fine-tune the design.

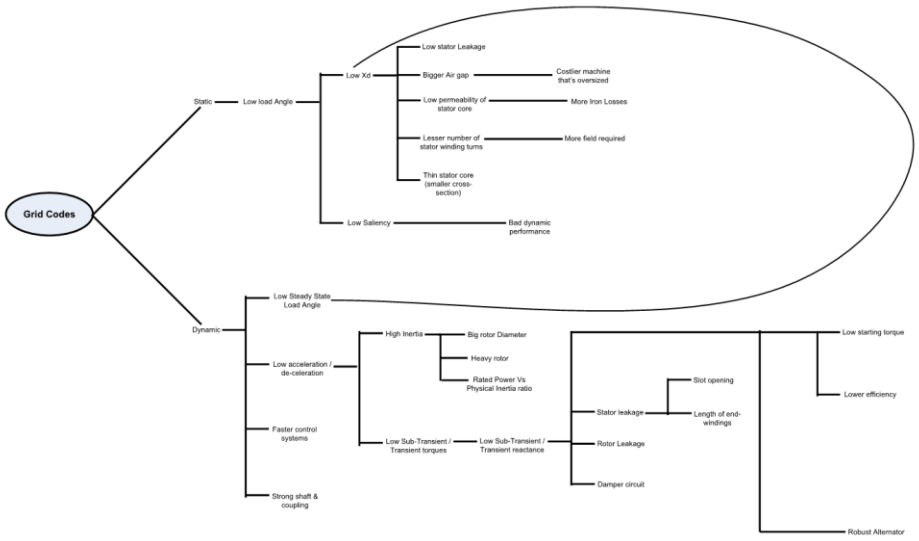


Figure 5. 3: Critical Parameter Flow for Reactance and Inertia Constant

From Figure 5.3, it can be observed that the parameters required to be modified are the following for X_d and H respectively

X_d: Air-gap, slot opening, tooth tip length and electrical steel permeability.

H: Weight of rotor (increased diameter of rotor and higher density steel), lower KVA for same volume (de-rate).

The inertia requirements of the project will be achieved using a new cast iron fan, the design and validation of which are described in detail in Chapter 6. The focus of this section and the rest of this chapter will be the aspects of the design that will be used to determine the best approach to fine tune the d-axis reactance of the target machine. The finite element model developed in Chapter 3 is parametrized to be able to vary the following quantities: Air-gap, slot opening, tooth-tip length and steel grade (steel permeability). The values of the 'selected' variables shown in Table 5.1 were controlled using a script file written to run the finite element analysis

simulations. The results of the sensitivity analysis are used as the beginning to an iterative process that has been used to design the grid code compliant SG.

5.3 Results & Analysis

All the identified parameters are shown in Table 5.1. All the parameters are varied keeping the remaining base design quantities fixed. The results are analyzed based on the sensitivity of X_d to each of these parameters.

6.3.1 Effect of Air-gap on X_d

The FE analysis confirms a 'well known' relationship between air-gap and X_d. Figure 5.4 below shows an almost linear curve. The X_d varies between approximately 3.5 and 2 per unit. At this stage, the air-gap thickness appears to be a parameter that can be modified to deliver the target value of X_d. Also, Figure 6.4 shows that the air-gap value that is required to achieve a value of $X_d < 2.1$ per unit is equal to 8 mm.

Table 5. 1: Limits of variables for sensitivity study

	Base design	Physical limits of current lamination	
		min	max
Slot opening [mm]	5	1	9
Air-gap [mm]	5	5	9
Tooth tip length [mm]	2	1	5
Electrical Steel Grade	M470-65 AP		
Core-length (mm)	550		

A larger air-gap reduces the reactance of the machine, has a detrimental effect on the rotor and increases rotor loading and therefore increasing rotor losses and reducing rotor insulation life. It is therefore required to ensure that the design is not entirely dependent on an air-gap change.

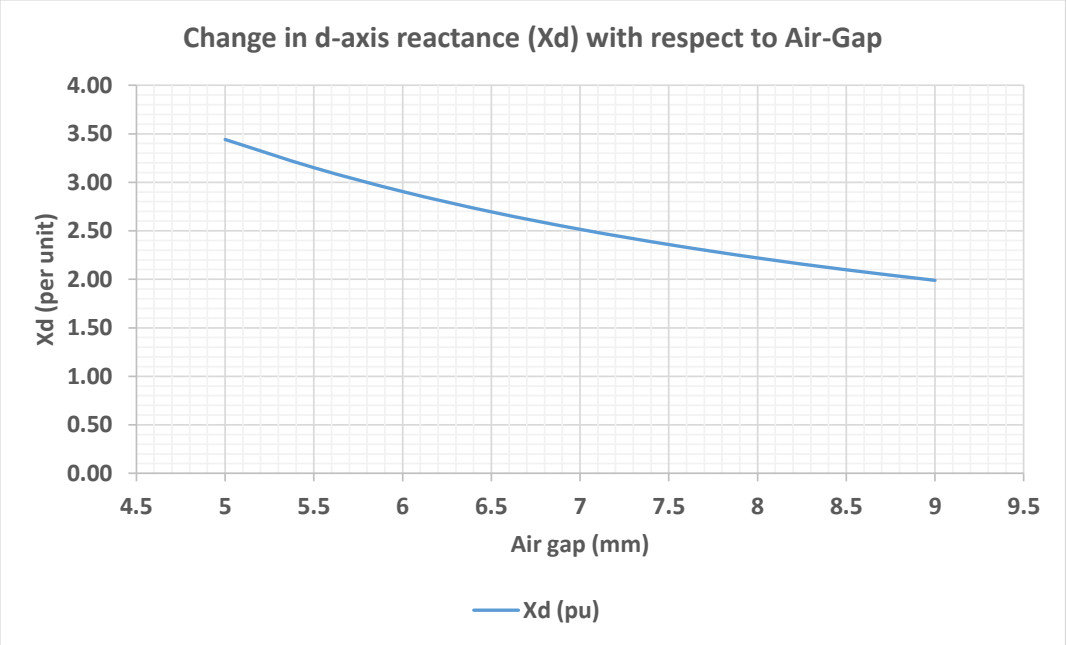


Figure 5. 4: Change in X_d with respect to Air-gap

5.3.2 Effect of Tooth tip length on X_d

The tooth tip length as shown in Figure 5.5 represents a critical part of the path of the flux lines that characterize the machine. The effect of the tooth tip length prior to the analysis was thought to have a significant effect on the reactance of the SG and that with a reduction in tooth tip length would lead to a reduction in X_d. However, analysis of the SG design shows that the tooth tip length variation leads to almost negligible impact on the X_d value as shown in Figure 5.5 b. This is due to the greater significance of the other variables like air-gap and number of turns in the machine and the fact that the geometry of the tooth tip length even with a high number of slots is not large enough to have a measurable impact on the X_d. Tooth tip length will therefore not be varied to achieve a grid code compliant SG design.

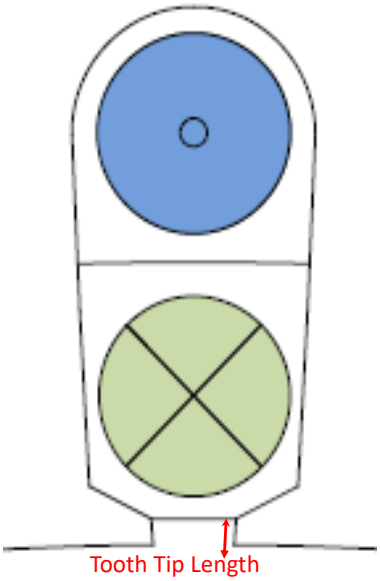


Figure 5. 5 a: Tooth Tip Length

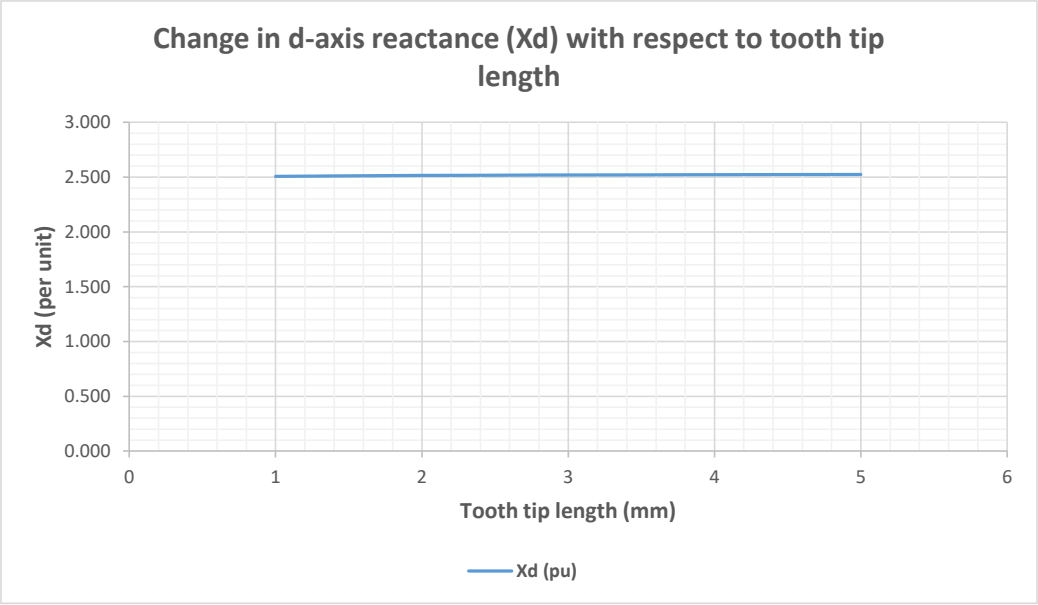


Figure 5.5 b: Change in X_d with respect to tooth tip length

5.3.3 Effect of Slot opening

The stator slot opening effect on X_d is investigated in this Section. This is due to the variation in the flux leakage around the slot opening. The bigger the slot opening, the larger is the leakage and vice-versa. The X_d of a SG depends on two key reactances – the armature reaction reactance (X_{ad}) and the leakage reactance (Xl). The slot opening impacts X_d by changing the leakage around slot openings. The analysis shown in Figure 5.6 shows that while there is a noticeable change in X_d from changing the slot opening, the variation itself is not significant enough to be considered as a design parameter that can be modified to design a grid code compliant SG.



Figure 5. 6: Change in X_d with respect to Slot opening

5.3.4 Effect of Electrical steel grade

Electrical steel is manufactured by varying the amount of silicon and carbon used in steel production to provide the core-loss and permeability characteristics needed by steels used in electrical machines [64]. The name of the electrical steel grade provides the reader information about watt-loss and permeability characteristics of the electrical steel. For example, in Figure 5.7a and 5.7b plot the permeability of various standard grades of electrical steel as a function of magnetic flux density. The M470 – 65 grade steel is a 4.7 W/Kg steel and comes in sheets of 0.65 mm thickness. The A at the end of M470 indicates non- grain oriented, fully processed steel while the P in AP that follows M470-65 indicates high permeability steel.

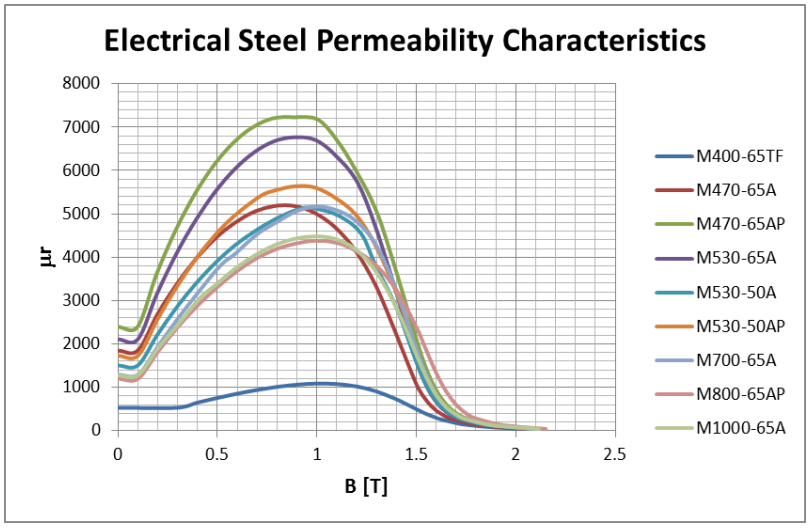


Figure 5. 7: Electrical Steel Permeability as a function of Flux Density for various steel grades [63]

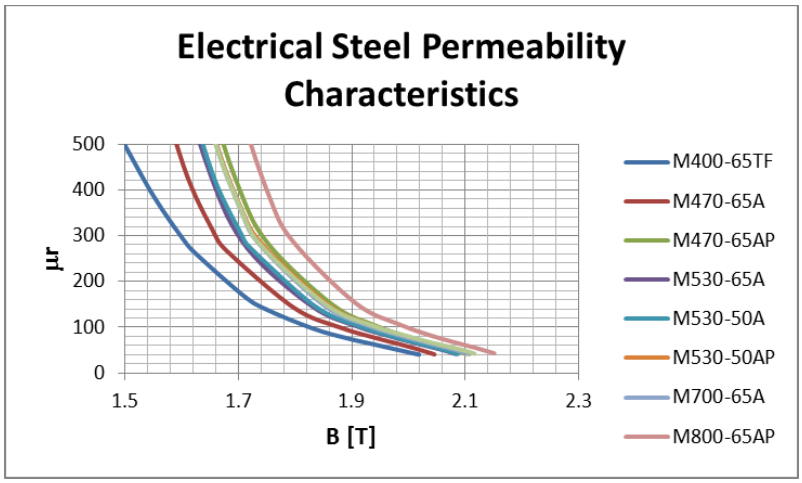


Figure 5.7b : Electrical Steel Permeability as a function of Flux Density for various steel grades at typical operating magnetic flux density range 1.5 T – 2.2 T [63]

Permeability is a key factor in determining the X_d of a SG. Figure 5.8 shows that there is a very minimal impact on X_d due to the permeability differences across the different steel grade. The steel B-H curve was obtained using a validated proprietary test method and setup described in [65], and the observed result is shown in Figure 5.7b. Figure 5.7b shows the electrical permeability for various magnetic flux densities for different commercially available types of steel. The electrical permeability defines the rotor current required to setup the desired magnetic flux densities in the air-gap to maintain the rated voltage across the stator terminals. The target SG at and close to its operating limits is running at magnetic saturation levels of the electrical steel used. At these saturated levels, the impact of

the permeability on X_d is reduced and the difference between various steel grade permeabilities at high magnetic flux densities is low.

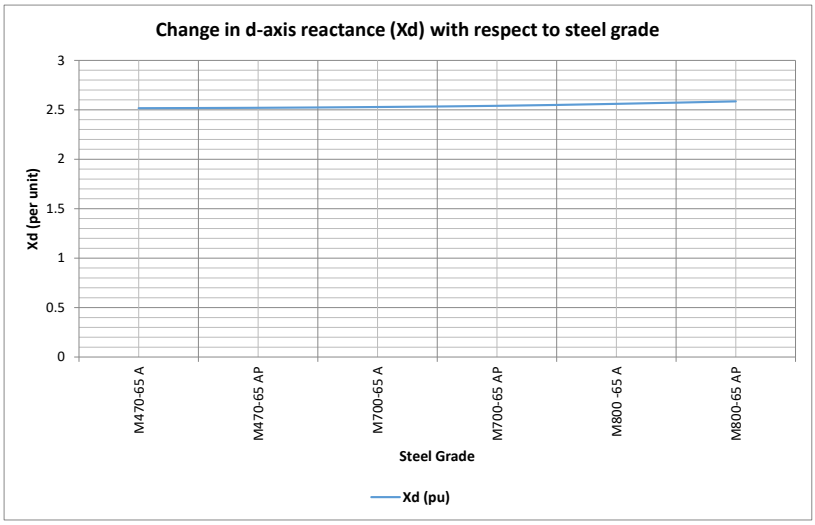


Figure 5. 8: Effect of steel grade (electrical steel permeability) on d-axis reactance

5.4 Conclusion

A sensitivity analysis of the machine design parameters that mostly affect the grid requirements and the business constraints of the SG under analysis was performed and its results shown in this chapter. The analysis results showed that the air-gap thickness plays the most important role for achieving the target X_d value. Caution must be exercised in increasing the air-gap, as it can significantly impact the rotor diameter constraint, the overall performance and the lifecycle cost of the SG.

CHAPTER 6

SYNCHRONOUS MACHINE DESIGN

6.1 Introduction

Chapter 5 summarized the approach that was used to determine the critical parameters that would enable a design that met the performance criteria to meet the various grid codes listed in the previous chapters. In this chapter, the design and validation of the 1400 kVA SG that meets the reactance and inertia targets will be discussed.

The reactance target will be mostly met with the air gap and optimized through a combination of core-length selection and winding design and the inertia requirements will be met with a special fan design.

6.2 Design Specification

Table 6. 1: Summary of design specifications

Rated Voltage (RMS)	400
Rated kVA	1400
Rated Frequency	50
Rated Speed (RPM)	1500
Direct Axis Synchronous Reactance (X_d per unit)	< 2.1
Inertia Constant (sec)	0.5
Efficiency (%)	> 95.3
Insulation Life (hours)	> 60000
L10 Bearing Life (hours)	> 20000

6.3 Design Constraints

To minimize the impact on product cost, reliability and manufacturing processes, the following design constraints were established:

- Generator to keep existing geometry as a standard design with the exception of the airgap length and armature slot design. These changes can be implemented with simple modifications to the existing tool.
- Armature windings will be concentric winding design with single turn. This is to improve the reliability of the windings by eliminating the risk due to inter-turn winding faults.
- Use a combination of machine rating and fan design to achieve the required inertia constant. The rating used will also enable the insulation system design life target of 60,000 hours. For clarity, based on practical experience, in a continuous application, the generator runs 8,000 hours per year and 60,000 hours is equivalent to 7.5 years. 60,000 hours is also the time for a major engine overhaul and therefore any change to the alternator needs to be aligned with this.

6.4 Baseline current product capabilities

To ensure minimum design effort and product change, the entire lineup of the P7 product range is reviewed against reactance, ratings and efficiencies to select a suitable starting point for re-design to meet grid code compliance based on the requirements outlined in Chapter 5.

Figure 6.1 identifies all the P7 products with respect to X_d and power range also the design specification for X_d and power are shown in the figure. From this, we can conclude that a P7E or P7G with the appropriate de-rate meets the X_d = 2.1 pu upper-limit requirement.

The Class H [66] and 85 percent ratings for the standard P7 products can be seen in Figure 6.2; the 1400 kVA requirement is also shown. This identifies that P7D, P7E, P7F and P7G meet the requirement for insulation life [67]. The P7D/F would require considerable re-design to meet the X_d requirements and the P7G would not be utilizing its active material and therefore the only option available for using as a base design is the P7E.

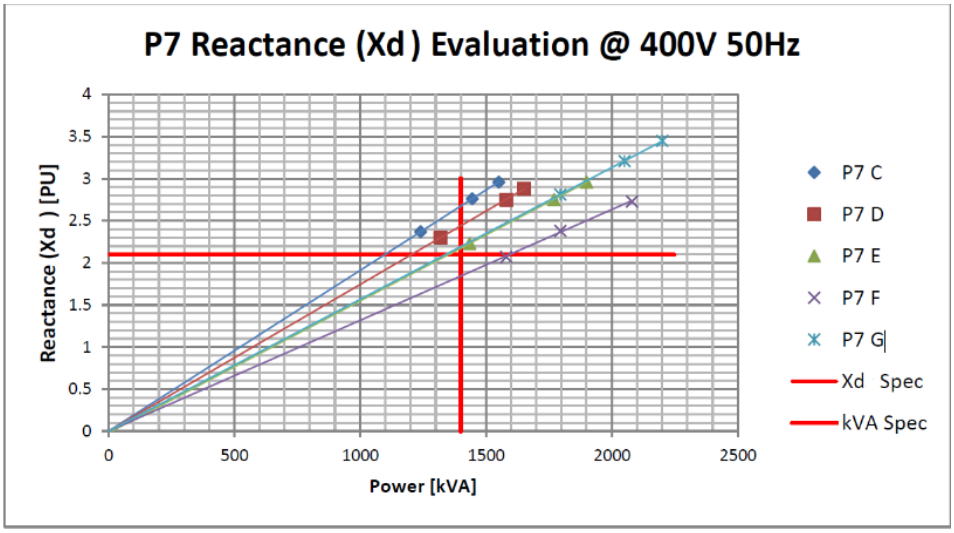


Figure 6. 1: Baseline of current product X_d capabilities

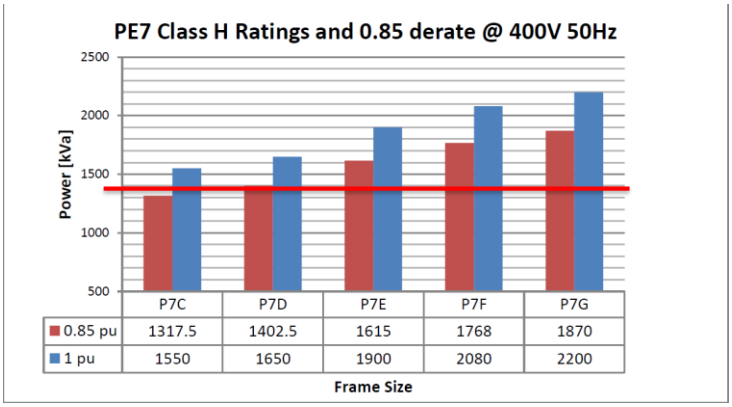


Figure 6. 2: Baseline of current product kVA capabilities

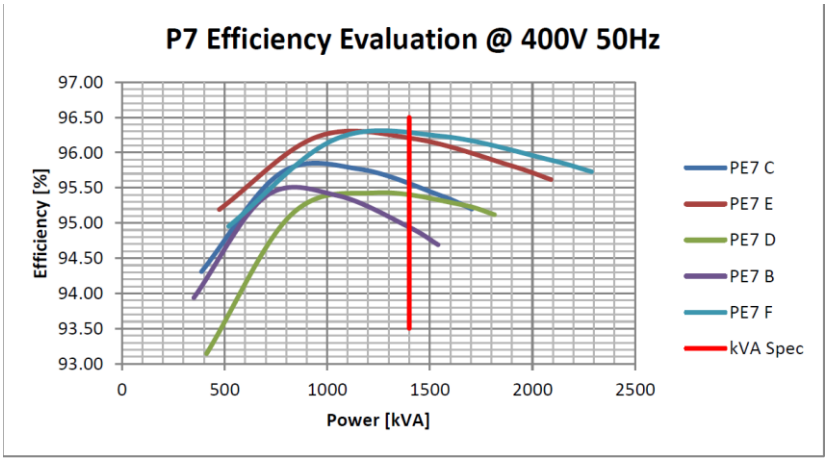


Figure 6. 3: Baseline of current product efficiency capabilities

Figure 6.3 confirms that the P7E provides one of the best efficiencies at 1400 kVA and therefore the grid machine design starting point is the P7E stator design. This winding already has a single turn lap winding which can easily be converted into a concentric winding using existing manufacturing tools and processes.

6.5 Calibrating the design tool

The design tool developed in Chapter 3 is used to design, model and analyze the grid code compliant SG. Prior to starting the design, the tool was calibrated by build models of 3 different variants of the P7 and compared to tests – 2 standard P7 models and 1 test variant that is used to confirm the capability of the design tool. Table 6.2 below summarizes the results from simulation and testing on the 3 machines models that were used.

Table 6. 2: Summary of simulation vs test data on 3 P7 model variants

			Test Results				Design Tool Predictions			
Machine model	Rating (kVA) at 0.8 lag pf	Core Length (mm)	Xd saturated (pu)	X''d (pu)	Rotor current at open circuit , 400V on stator (A)	Rotor current at short circuit and rated current in stator (A)	Xd saturated (pu)	X''d (pu)	Rotor current at open circuit , 400V on stator (A)	Rotor current at short circuit and rated current in stator (A)
Standard P7C	1550	550	3.239	0.1523	15.5	50.2	3.315	0.1588	14.96	49.59
Standard P7E	1900	700	2.381	0.18	19	44.7	2.3094	0.189	19.323	44.625
Test Design P7Grid	1400	620	3.259	0.1363	14.99	48.85	3.37	0.143	14.387	48.552

The results shown above in Table 6.2 confirm that the output of the SG simulated using the tool developed in Chapter 3 as compared to the test results are between 3% and 5% which is well within the measurement tolerances allowed by IEC 60034 [66]. The tool is therefore confirmed that it can be used to design the grid code compliant SG.

6.6 Grid code compliant SG design

In this section, the tool calibrated above will be used to design the SG to obtain the target reactance and a new fan design using cast iron will be proposed to meet the inertia constant requirements set out in the previous chapters.

6.6.1 Electromagnetic Design

The works of [39] and [68] discuss in detail the equations and first principles involved with the design of SGs. Therefore, this section will only summarize the outcome of the design exercise completed using the design tool developed to achieve the target synchronous reactance X_d.

6.6.1.1 Stator Design

The P7 standard lamination is used as a baseline to minimize the impact of the change in machine design on existing manufacturing capability. To modify the air gap change necessary to achieve the target synchronous reactance X_d, the stator internal diameter is reduced by 4 mm and therefore increasing the airgap by 2 mm to 7 mm compared to the existing air gap of 5 mm. A 96-slot configuration is used with the slot depth increased from 39.39 mm on the standard P7 to 40 mm; the standard skew factor of 1 stator slot skew is maintained. The new core-length proposed is 700 m. The effective change proposed to the new stator design would only require a new notching tool, a module that can be easily replaced in the presses that produce the stator laminations.

6.6.1.2 Rotor Design

Since the proposed stator lamination design achieves the target synchronous reactance, no changes were proposed to be made on the rotor. The design was

checked to ensure that the harmonics were not impacted with the new stator design.

6.6.1.3 Simulation on proposed design

The new 1400 kVA SG design is proposed to be called PG7S, where S denotes the core-length. The no-load field maps in Figure 6.4 below shows the difference between the standard 96 slot design and the PG7S design. The open circuit characteristics show a higher saturated design for the PG7S but this is expected due to the airgap increase and reduction in back iron for the same output voltage. This produces an increase of approximately 32% in field current. In the load case it is apparent that there is less armature reaction effects on the PG7S due to the increased airgap and therefore the saturation is higher from the standard design. But this only causes an increase in field current of approximately 9%. Thermal performance is not a concern with rotor current density of 3.822 A/mm^2 and main armature of 5.36 A/mm^2 being so low when compared to current design levels. The saturated synchronous reactance achieved using the proposed design is simulated to be 1.9 pu. The following sections will describe how the simulation results compare with test results.

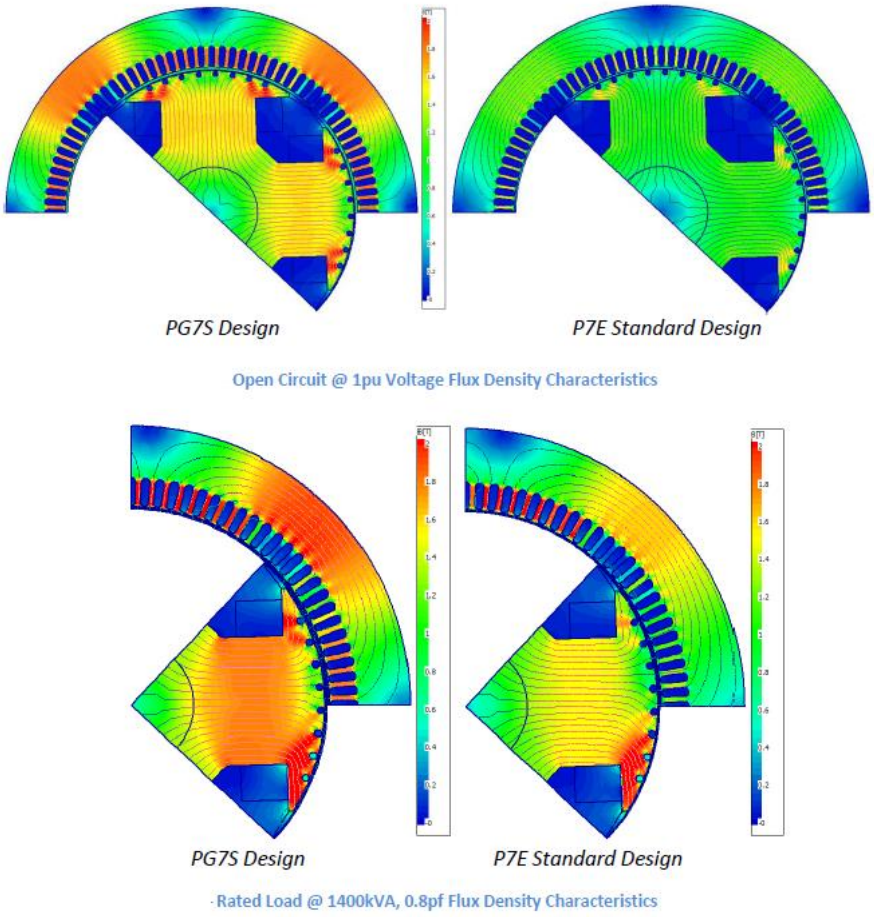


Figure 6. 4: Comparison between standard P7E baseline machine and the PG7S

6.6.2 Achieving the inertia time constant target

6.6.2.1 Design

Inertia constant (H) is the kinetic energy stored in the rotating components of an electrical machine for a given kVA rating delivered. The unit of inertia constant is in seconds [35]. For the standard P7 range, the inertia constant was calculated to be between 0.2 s and 0.4 s. On the PG7S design based on the electromagnetic design

above, the inertia constant is calculated to be 0.39 s. Inertia constant can be modified by either changing the rotor inertia or by adding mass to the rotor or by derating. To achieve a target of 0.5 s on the 1400 kVA PG7S that is being developed, 3 options were reviewed and scored based on pros and cons relative to capability of solution and cost / manufacturing constraints. Table 6.3 below summarizes the findings.

Table 6. 3: Summary of options for increasing inertia constant on PG7S

	Option1: No design change, only de-rate.	Option2: Change rotor diameter.	Option3: Add inertia disc to rotor.
Cost of solution	High	High	Moderate
Impact on manufacturing	Low	Low	Low
Effectiveness of solution	High	High	Moderate

To ensure a scalable and repeatable solution, Option 3 was selected, and an inertia disc was designed to be fitted to the fan to increase the inertia constant. Figure 6.5 below shows the fan-inertia ring assembly that was developed.

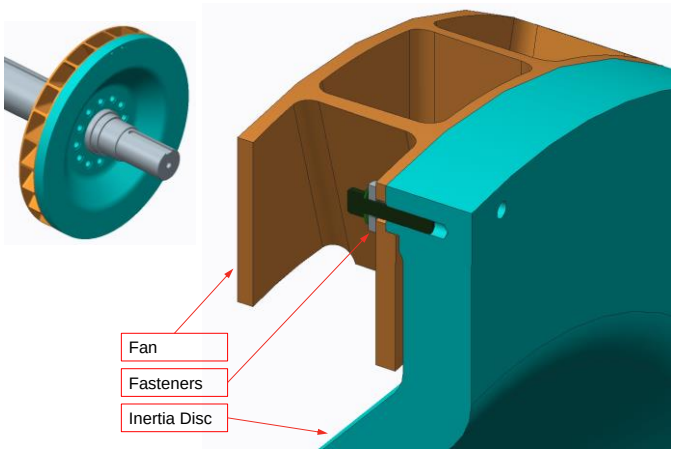
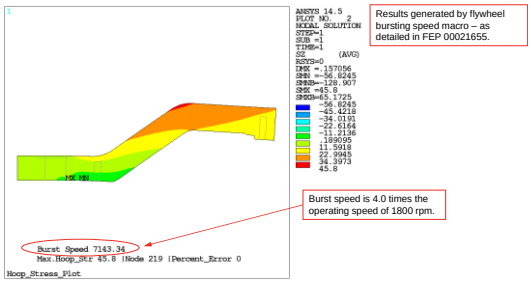


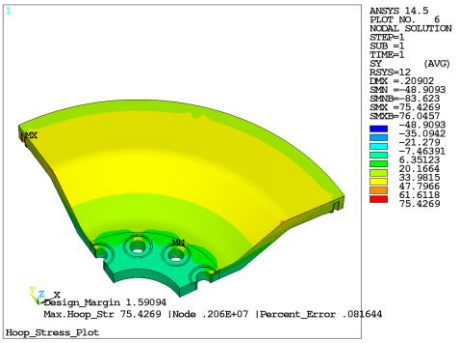
Figure 6. 5: New PG7 Fan-inertia ring assembly drawing

6.6.2.2 Analysis

Since the PG7S can be used in 50Hz (1500 rpm) and 60Hz (1800 rpm) applications, all the mechanical analyses are completed at 1800 rpm to represent worst case on the fan - inertia disc assembly. The burst speed and fatigue stress levels are checked to be below the levels indicated by FEP 00021655 [69]. Figures 6.6 (a) and 6.6 (b) demonstrate the capability of the fan-inertia disc system to meet the burst speed and fatigue requirements respectively.



(a)



(b)

Figure 6. 6: (a) Burst Speed Analysis (b) Fatigue Analysis

If the Fan and Inertia disc mating faces are not flat, then assembly stresses will be induced. Assuming an axial displacement of 0.1mm, the maximum stress in the spigot radius is shown to be less than 40 MPa (max principle stress) in Figure 6.7 below which is again in accordance with [69].

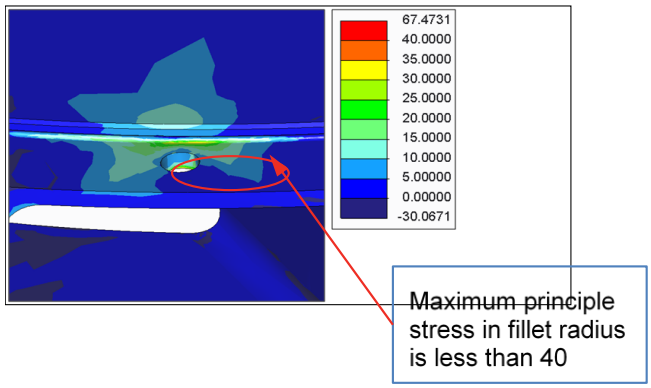


Figure 6. 7: Maximum Principle Stress due to a 0.1 mm axial displacement of one of the fasteners.

Maximum radial clearance between Fan and Inertia Disc spigot = 0.2mm. Therefore, the maximum radial slippage between the Fan and Inertia Disc is also = 0.2mm. This slippage will occur at the fasteners. To ensure no significant loss of joint integrity, Belleville washers and high-grade cap screws were specified. Loctite 2700 was also recommended to be used to prevent any relaxation of the fasteners.

Figure 6.8 below shows the maximum principle stress induced in the fan due to the centrifugal loading (1800rpm) and the resistance to the thermal expansion of the fan provided by the fasteners. The stress is shown to be less than 30 MPa which is within acceptable limits specified by [69].

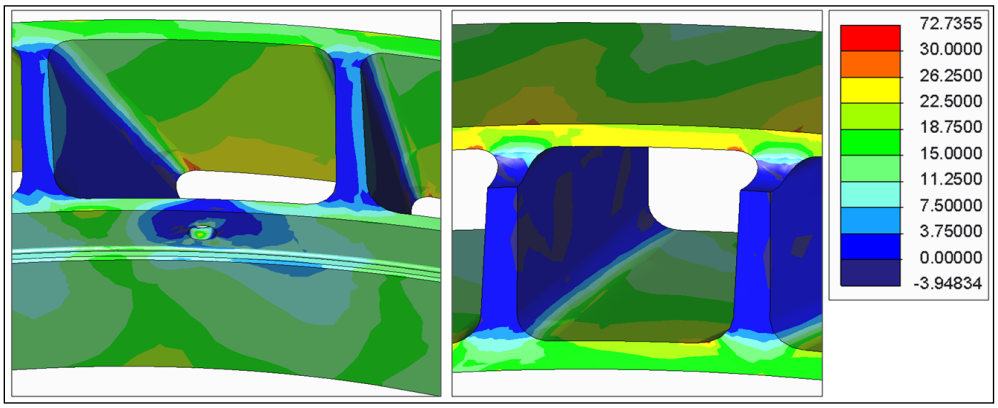


Figure 6. 8: Maximum Principle Stress at 1800 rpm due to thermal expansion

In addition to the static loading and thermal expansion effects, the integrity of the fan-inertia disc assembly was also studied under LVRT events. The LVRT events were represented through a maximum measured acceleration of 2000 radians/s^2. Figure 6.9 shows the mean stress on the assembly with LVRT loads. The maximum simulated stress was 36.2 MPa (23 MPa due to rotational velocity and 13.2 MPa

due to the acceleration during LVRT) which was well within the material yield strength. The total mean stress on the various location of the fan-inertia disc assembly was also plotted on a Goodman diagram shown in Figure 6.10 to ensure that the life of the assembly was not impacted due to the high levels of stresses seen with typical LVRT events.

Based on the above analysis, the fan design was deemed to meet requirements. The fan-inertia disc design increased the inertia constant of the PG7S to 0.5 s at 1400 kVA. Figure 6.11 shows the various inertia constant and reactances that the PG7S delivers at different kVA ratings.

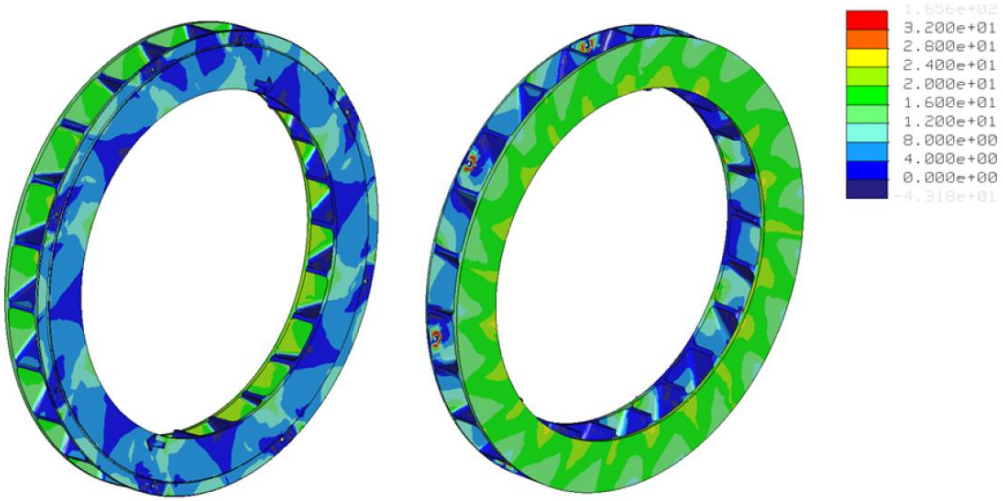


Figure 6. 9: Mean Stress at 1800 rpm with LVRT loads

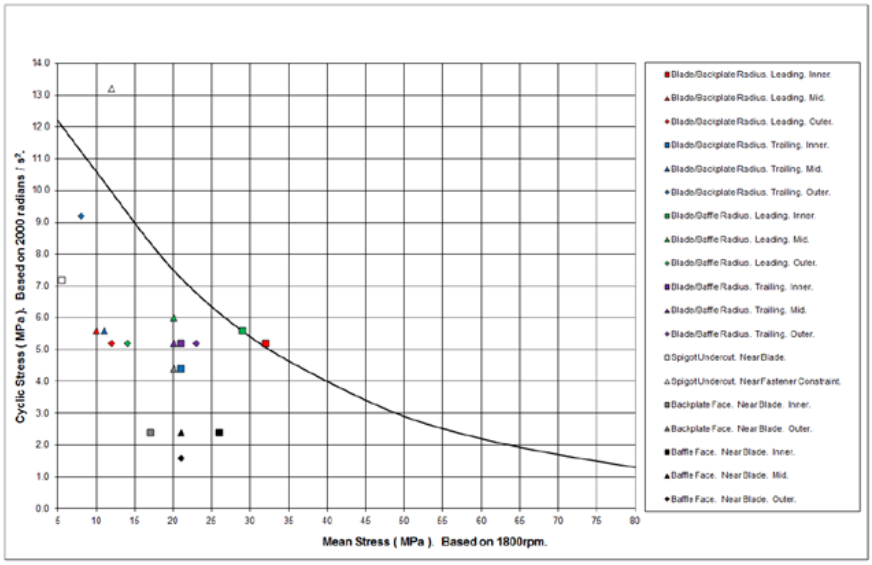


Figure 6. 10: Goodman plot for Mean Stress at 1800 rpm (MPa)

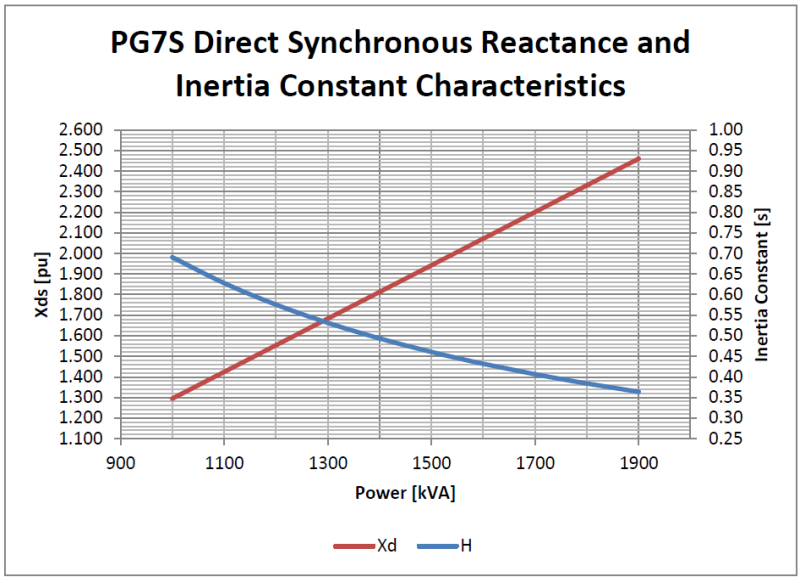


Figure 6. 11: Relationship between kVA, inertia constant and direct synchronous reactance for the PG7S

6.7 Validation of the PG7S

6.7.1 Waveform Analysis

The waveform analysis calculates the individual harmonics and consequently, the THD (Total Harmonic Distortion) of the line to line voltage on No-Load. Table 6.4 illustrates the THD for the PG7S. Figure 6.12 shows the individual harmonic components that are present in the no-load line to line voltage of the generator. The THD value measured is less than the maximum allowed THD according to [66] and therefore meets the associated requirement.

Table 6. 4: THD for the PG7S

	Line-Line (%)	Line-Neutral (%)
THD	0.41	0.4

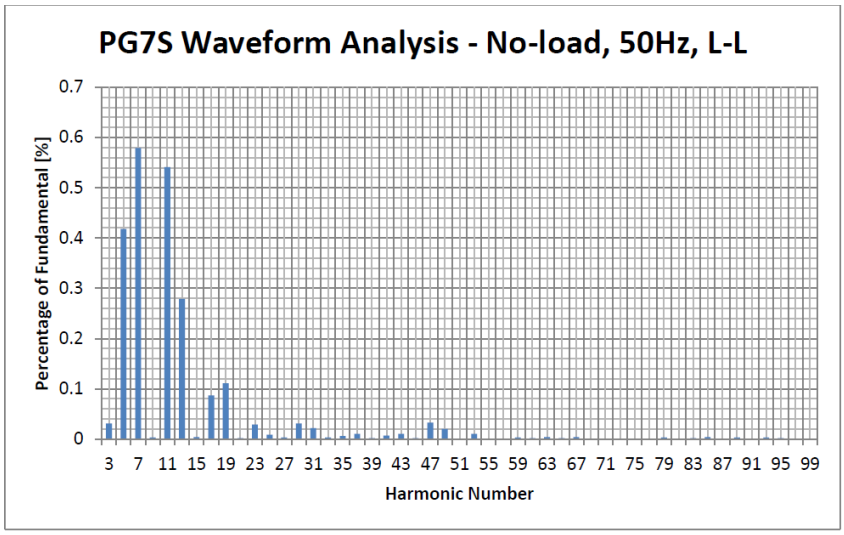


Figure 6. 12: Harmonic analysis of the PG7S

6.7.2 Open Circuit and Short-Circuit characteristics

The experimental open circuit and short circuit characteristics are illustrated in Figure 6.13 with the simulated curve. The simulation correlates well with the test results. Table 6.5 also compares the field currents and reactances between the simulation and test data and confirms a good correlation between simulation and test.

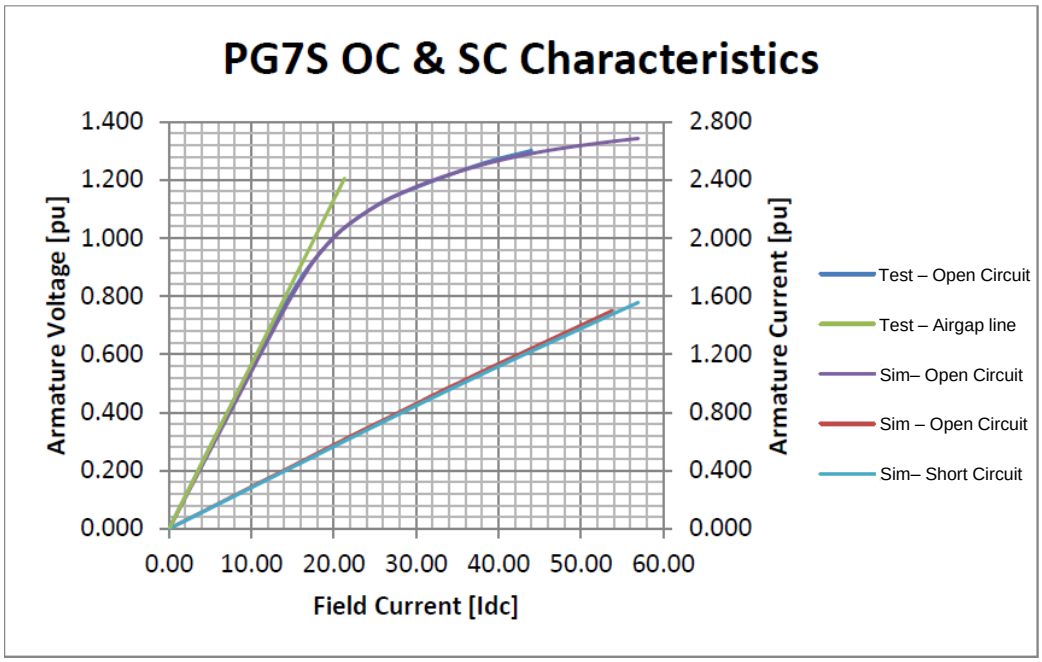


Figure 6. 13: Open Circuit and Short-Circuit characteristics of the PG7S

Table 6. 5: Comparison of Field currents and reactances of the PG7S between simulation and test

Field Current at Open Circuit Test at 400 V (A)		Field Current at Short-Circuit and rated current at 1400 kVA (A)		Xd (pu)	
Simulated	Test	Simulated	Test	Simulated	Test
19.93	35.04	19.95	35.63	1.79	1.76

6.7.3 Losses and Efficiency

The no load losses and short-circuit losses are illustrated in Figure 6.14, which is followed by Table 6.6 defining the losses at machine rating. The overall efficiency is comparable to the standard PE7. Figure 6.15 shows the efficiency characteristics at various power factors.

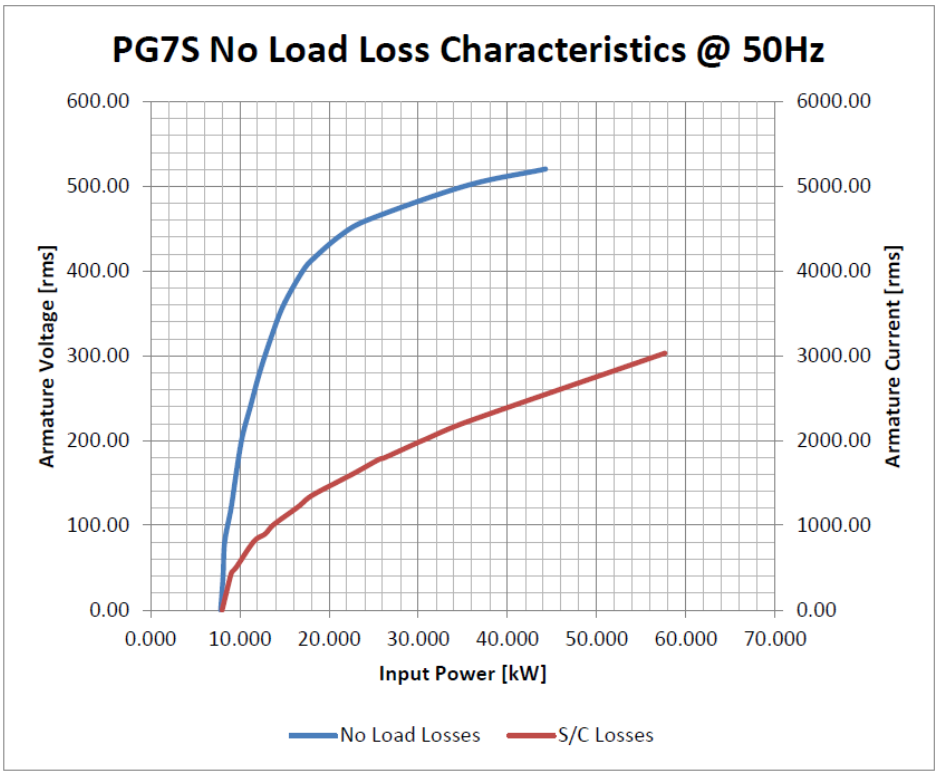


Figure 6. 14: No Load and Short-Circuit loss characteristics of the PG7S

Table 6. 6: Breakdown of losses in the PG7S

Windage & Friction	Iron	Stator Copper	STRAY	Rotor Copper	Rated Load Efficiency
[kW]	[kW]	[kW]	[kW]	[kW]	[%]
7.86	8.23	15.73	4.27	9.54	96.09

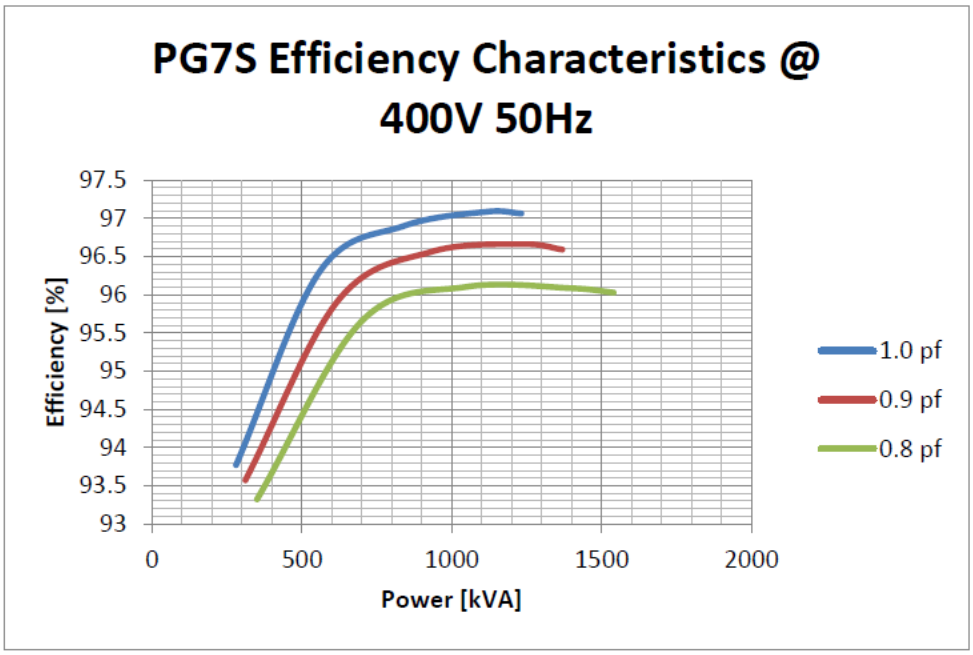


Figure 6. 15: Tested efficiency curves of PG7S at various power factors

6.7.4 Reactances and Time Constants

The PG7S was used to develop new testing methods that were later added to the Cummins Generator Technologies internal test standard DD15596 [57] for 'test procedures and product approval'. This data was used to create/validate new design procedure in the simulation tool developed. The new methods include the 'Applied voltage test with rotor in direct and quadrature axis', 'Voltage recovery' and 'DC decay test at standstill', which are described in [70]. The applied voltage test is used to validate X''_d, X''_q and the armature end leakage. Voltage recovery gives X''_d, X'_d, $T''do$ and $T'do$ time constant. The dc decay test can be performed in the direct and quadrature axis enabling the calculation of X'_d, X'_q, X_2, T'_d, T'_{do}, T''_{do}, T'_q, T''_q, T'_{qo}, T''_{qo} and the frequency response characteristics for both axes.

Figure 6.16 illustrates the classical three phase sudden short-circuit armature currents at rated voltage and frequency. The calculated results for the 3 phase Sustained short-circuit are shown in Table 6.7.

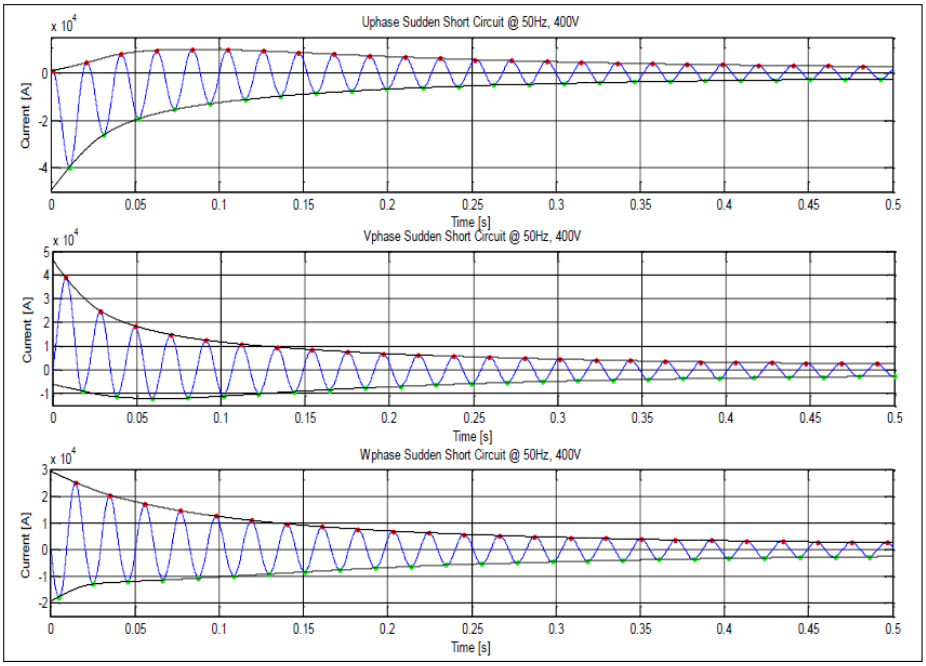


Figure 6. 16: PG7S 3 phase sudden short-circuit at 400V, 50Hz

Table 6. 7: PG7S reactances and time constants – test results

	Reactances			Time Constants			
	X''_d	X'_d	X_d	T''_d	T'_d	T'_{do}	T_a
	pu	pu	pu	sec	sec	sec	sec
Uph	0.1132	0.1534	1.7948	0.0126	0.1725	3.4014	0.0334
Vph	0.1086	0.1431	1.7873	0.0109	0.1619	3.4027	0.0266
Wph	0.1168	0.1453	1.7841	0.0096	0.1623	3.4046	N/A
Average	0.1129	0.1472	1.7887	0.011	0.1655	3.4029	0.03

6.8 Simulation of the PG7S

To conclude the design process of the PG7S, a simulation using the power system tool described in Chapter 4 is done to ensure that the PG7S meets the grid code requirements, specifically, the low voltage ride through requirements.

Figure 6.17 shows the matlab model of the PG7S coupled to an engine and connected to a power system.

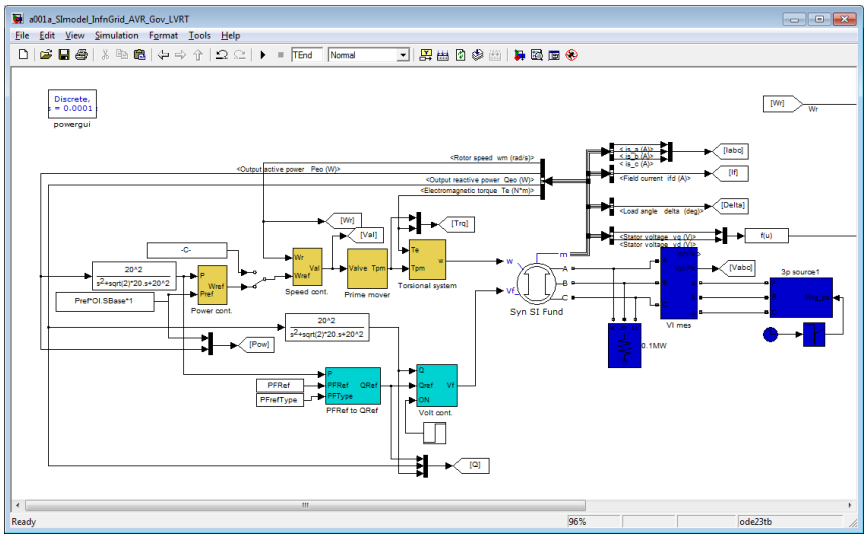


Figure 6. 17: Power system model with PG7S

An extensive analysis of the PG7S performance under extreme grid conditions, including check for pole slip during the worst case Low Voltage Ride Through conditions are completed. Figure 6.18 below shows the simulation results of a Low Voltage Ride Through simulation on the PG7S.

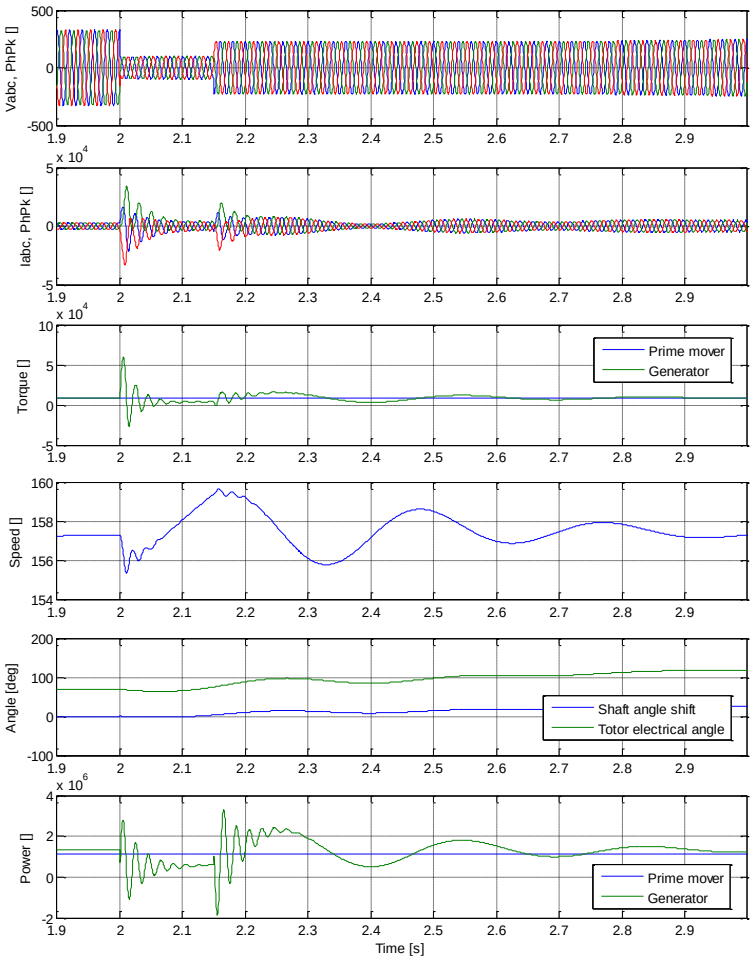


Figure 6. 18: Low Voltage Ride Through simulation on the PG7S

The simulations confirmed that the PG7S does not pole slip during the Low Voltage Ride Through operation, thereby meeting the grid code requirements set out in Chapter 2. Additionally, the stability analysis using the analytical tool developed in Chapter 4 is also completed to demonstrate capability to meet Static Stability requirements as well.

7.9 Conclusion

In this chapter, it was shown that the PG7S grid machine meets the stated inertia and reactance requirements. The PG7S has a direct axis synchronous reactance of 1.76 pu at 1400kVA and offers a flexible operating range for customers to select the appropriate synchronous reactance and inertia constants. In addition to designing and testing the PG7S, simulations aimed at checking the reliability requirements were carried out and the results are described in Chapter 7. The machine designed in this chapter demonstrates that despite the challenging conditions imposed by the various grid codes, a solution space can indeed be found and that a SG that meets the stipulated criteria can be designed and as shown in Chapter 8, the designed generator is cheaper than existing generators.

CHAPTER 7

Reliability of SGs for grid code compliance

7.1 Introduction

In Chapter 6, the design of a synchronous generator to meet the criteria set out in Chapter 4 was described. In addition to posing a challenge to the stability of engine driven generating sets, the dynamic conditions set out in the grid codes also induce high levels of stress on various components of the SG. It is therefore necessary to understand these stresses and design the SG to ensure any risk to the life / durability of the SG is not compromised whilst designing for grid code compliance. In this chapter, the SG designed in chapter 6 is reviewed at a component level in terms of reliability and a design for reliability process is applied.

As part of any new product development program, it is essential to understand the risks associated with the product, especially those specific to the application or the usage of the product. The Design Failure Mode Effects and Analysis (DFMEA) [71] is a tool that is traditionally used to identify these risks relative to the product design and performance requirements and proposes a validation or mitigation plan for each of these risks. The DFMEA itself is derived from a boundary diagram that maps out interactions at the interfaces between the SG and the application. Figure 7.1 shows a boundary diagram for the bracing rope to retain the end windings of a SG and Figure 7.2 is the associated DFMEA for the boundary diagram.

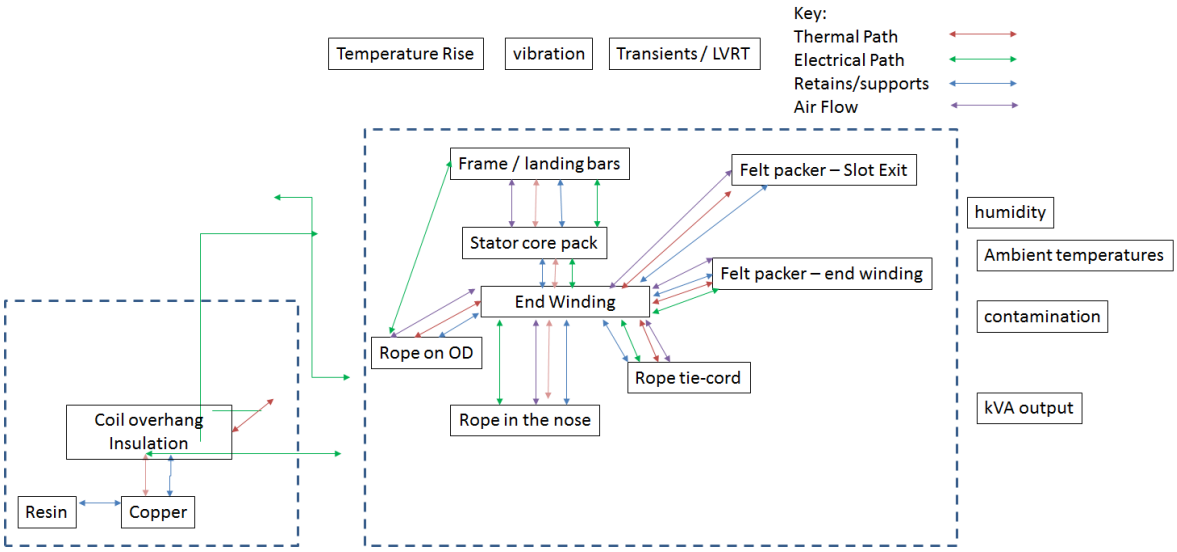


Figure 7. 1: Boundary diagram for the bracing rope showing interactions

An extensive DFMEA analysis was completed for the design presented in Chapter 6 along with the requirements defined in Chapters 4 and 6 and the following areas of focus were identified as being critical to designing a reliable SG for grid code compliant applications.

1) Temperature rise on the stator: Temperature rise in excess of typical operating conditions at a 0.8 lagging power factor on the stator due to high leading power factor loads contribute to accelerated insulation degradation thereby impacting the

ITEM / FUNCTION	POTENTIAL FAILURE MODE	POTENTIAL EFFECTS OF FAILURE	Severity of Effect(s) of Failure	Class	POTENTIAL CAUSES OF FAILURE	Probability of Cause Occurring	CURRENT DESIGN CONTROLS	Probability Controls Will Detect or Prevent Failure	RPN	Identified Control Characteristic (Tick Box if Characteristic deemed as Critical and requires control). Examples of items defined as critical would be:Safety Critical (Driven from the DFMEA) Critical Characteristic (As I/D by design, torque settings etc..) Process Characteristic (identified via the work flow diagram and PFMEA, affects capability of future operation	RECOMMENDED ACTION (Record Action Taken)	RESPONSIBILITY AND TARGET COMPLETION DATE	ACTIONS TAKEN	Severity of Effect(s) of Failure	Probability of Cause Occurring	Probability Controls Will Detect or Prevent Failure	RPN
Bracing back to the Frame / Landing bars removed from design (Risks = Thermal expansion, Prototype blocks cracking and equally spaced bracing points)																	
Resist movement	Dia 25 Rope on OD will break	debris in m/c	3		Vibration	2	none	10	60		None based on risk assessment.						
			3		elect. forces larger than predicted	7	Estimated forces	9	189		Confirm mechanical forces	O.Jackson/S.Narayanan					
			3		Thermal expansion	2	Existing product experience	9	54		None						
		lose constraint position	5		Vibration	2	None	9	90								
			5		elect. forces larger than predicted	7	Estimated forces	9	315								
			5		Thermal expansion	2	Existing product experience	9	90								
			5		Cracking from stress raisers	2	Existing product experience	9	90								
	lacing ropes snap	debris in m/c	3		elect. forces larger than predicted	4	Estimated forces	9	108								
			3		Incorrect material	1	Mat. Specification	9	27								
			3		Thermal expansion	1	Mat. Specification	9	27								
		lose constraint position	5		elect. forces larger than predicted	7	None	9	315								
			5		Incorrect material	1	Mat. Specification	2	10								
			5		Thermal expansion	1	Mat. Specification	2	10								
	lacing ropes come loose	lose constraint position	5		elect. forces larger than predicted	2	None	9	90								
			5		incorrect material	1	Mat. Specification	9	45								
			5		Thermal expansion	1	Mat. Specification	9	45								
	Coil / insulation breaks	Loss of primary function	8		Fatigue	3	Existing experience	10	240								
			8		Vibration	3	Existing experience	10	240								
			8		Stiffness to high	2	Existing experience	10	160								
			8		No damping	2	Existing experience	10	160								
	Felt packers crush	lose constraint position	5		elect. forces larger than predicted	2	None	10	100								
		Debris in m/c	3		elect. forces larger than predicted	2	None	10	60								
	Felt packer detaches	lose constraint position	5		elect. forces larger than predicted	7	Visual control	5	175								
			5		Thermal expansion	2	Visual control	5	50								
		Debris in m/c	3		elect. forces larger than predicted	2	Visual control	5	30								
			3		Thermal expansion	2	Visual control	5	30								
		Fretting	5		elect. forces larger than predicted	7	Estimated forces	5	175								
			5		Thermal expansion	2	Visual control	2	20								
Fine tune natural frequency of overhang (including damping, stiffening, strain, displacement)	Hit resonant frequency	Fretting of insulation	8		coil shapes	2	Proven design std Best practice	1	16		Launch corporate project to investigate	P.Bend/J.Matthews					
			8		Thermal expansion	2	Proven design std Best practice	1	16		Launch corporate project to investigate	P.Bend/J.Matthews					
			8		Load	5	Estimated forces	5	200		Launch corporate project to investigate	P.Bend/J.Matthews					
			8		vibration	7	None	8	448		Launch corporate project to investigate	P.Bend/J.Matthews					
			8		Tightness of lacing ropes	5	Visual control	5	200		Launch corporate project to investigate	P.Bend/J.Matthews					
			8		Quality of impregnation	2	Process Control	1	16		Launch corporate project to investigate	P.Bend/J.Matthews					
			8		Ambient condition	2	Process Control	2	32		Launch corporate project to investigate	P.Bend/J.Matthews					
		Fatigue failure	8		coil shapes	2	Proven design std Best practice	1	16		Launch corporate project to investigate	P.Bend/J.Matthews					
			8		Thermal expansion	2	Proven design std Best practice	1	16		Launch corporate project to investigate	P.Bend/J.Matthews					
			8		Load	5	Estimated forces	5	200		Launch corporate project to investigate	P.Bend/J.Matthews					
			8		vibration	7	None	8	448		Launch corporate project to investigate	P.Bend/J.Matthews					
			8		Tightness of lacing ropes	5	Visual control	5	200		Launch corporate project to investigate	P.Bend/J.Matthews					
			8		Quality of impregnation	2	Process Control	1	16		Launch corporate project to investigate	P.Bend/J.Matthews					
			8		Ambient condition	2	Process Control	2	32		Launch corporate project to investigate	P.Bend/J.Matthews					
		debris in m/c	8		coil shapes	2	Proven design std Best practice	1	16		Launch corporate project to investigate	P.Bend/J.Matthews					
			8		Thermal expansion	2	Proven design std Best practice	1	16		Launch corporate project to investigate	P.Bend/J.Matthews					
			8		Load	5	Estimated forces	5	200		Launch corporate project to investigate	P.Bend/J.Matthews					
			8		vibration	7	None	8	448		Launch corporate project to investigate	P.Bend/J.Matthews					
			8		Tightness of lacing ropes	5	Visual control	5	200		Launch corporate project to investigate	P.Bend/J.Matthews					
			8		Quality of impregnation	2	Process Control	1	16		Launch corporate project to investigate	P.Bend/J.Matthews					
			8		Ambient condition	2	Process Control	2	32		Launch corporate project to investigate	P.Bend/J.Matthews					

Figure 7. 2: DFMEA for the boundary diagram shown in Figure 7.1

insulation life and ultimately impeding the ability of the design to meet a 60,000-hour design life on the insulation system [72]. It is therefore essential to define the temperature rise limits on the windings with a view of insulation life characteristics.

2) Forces on end windings: Large transient loads during the Low Voltage Ride through Event leads to forces in the end windings that could potentially lead to degradation of the insulation system due to micro-movements. Managing the forces in the end-windings is therefore essential to ensure alternator reliability. [73], [74],

[75] discuss forces in SG windings extensively and this chapter will therefore only elaborate on the efforts taken towards understanding the design of the end windings for the grid code compliant generator designed in Chapter 6.

3) Limiting rotor current transients during LVRT: The LVRT tests described in Chapter 5 demonstrated that during a LVRT, rotor transient voltages up to 1.2 KV can be induced. On a low voltage SG like the one designed in this thesis, these transient rotor voltages exceed the capability of the insulation system and therefore could contribute to accelerated degradation of the rotor insulation system thereby reducing the life of the insulation system and consequentially the life of the product. [76], [77], [78] describe the experiences of the authors with respect to rotor transient during LVRT events on DFIGs while this thesis will focus on the rotor transient during LVRT on SGs.

4) Bearing life due to increased loading on the SG during transient events: During the LVRT tests described in Chapter 5, mechanical torque of up to 15 times the rated torque was recorded in the shaft of the SG used for testing. It is essential to ensure that the bearing and all mechanical systems connected to the shaft can withstand these loads.

This chapter will provide an elaborate summary of the work completed as part of the design exercise to mitigate the risks related to the four critical areas described above.

7.2 Design for Reliability

7.2.1 Temperature rise on the stator

The thermal rating of electrical machines is based on the life of the insulation system which is defined using the Life curve of the insulation system that is derived using methods defined by the Underwriter's Laboratory (UL) [79]. Every generator manufacturer needs to complete ageing tests on their insulation system complying with the IEC 60034-18-31 standard [80]. In this test, 10 motorettes comprising of the copper wire and insulation system used in the windings as shown in Figure 7.3 is exposed to three different temperatures 200 deg C, 220 deg C and 240 deg C followed by cold shock to -20 deg C, mechanical stress of 1.5G through 0.008'' displacement at a frequency of 60Hz plus 100% moisture tests at 23 deg C for 48 hours. This is then followed by a diagnostic test on the motorettes where a 600V phase to phase and phase to ground and 120V turn to turn voltages are applied to determine end of life failure. Failure is defined to be when the insulation resistance of the motorettes drop to 50% or less than the initial value. The time to fail is noted as the life of the insulation system and an Arrhenius rate of reaction approach [81] is used to derive the life curve of the insulation system.



Figure 8. 3: A motorette sample specified by UL

Figure 7.4 shows the life curve of the insulation system used on the P7 broadly and specifically on the PG7S that is the focus of this thesis. Using the curve, it is predicted that for a design life of the insulation system, a maximum temperature on the windings of 155 deg C at a 40 deg C ambient needs to be achieved.

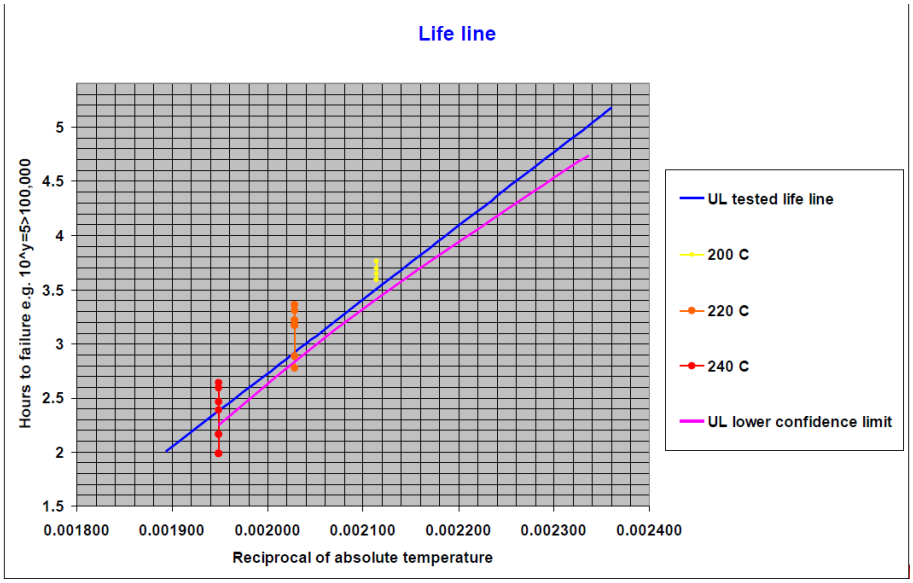


Figure 7. 4: Life curve of insulation system used in PG7S

To confirm if the PG7S designed in Chapter 6 at 1400 kVA meets the required 60,000-hour design life on the insulation system, a PG7S with a total of 58 RTDs was built to measure temperatures at various locations in the alternator, specifically focused on the stator. Figure 7.5 below shows the axial distribution of the temperature rise along the length of the machine as measured from the non-drive end; this shows that along the length of the machine all the recorded temperatures are well within the required thermal limit set out to meet the insulation system life requirements.

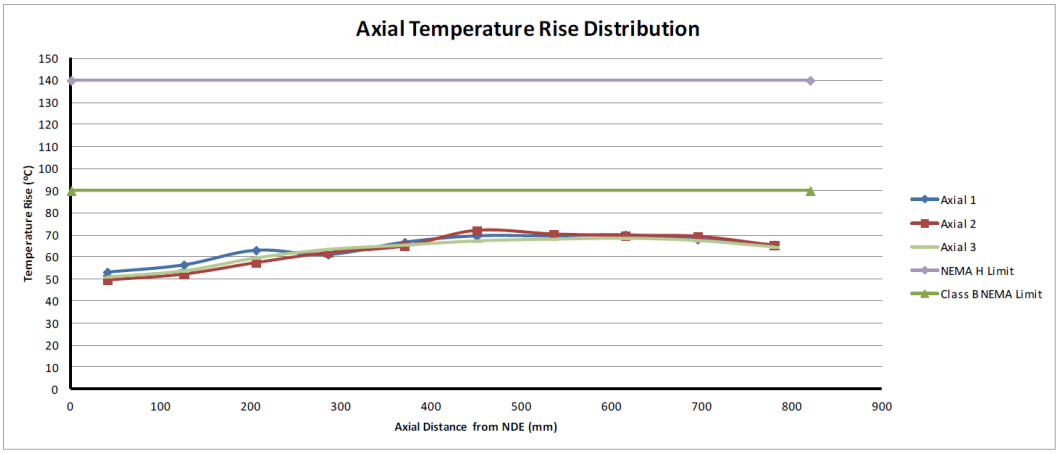


Figure 7. 5: Axial temperature distribution on the PG7S

Additionally, Figure 7.6 below also demonstrates that circumferentially, the temperature in the stator and various locations on the alternator are within the thermal limits defined.

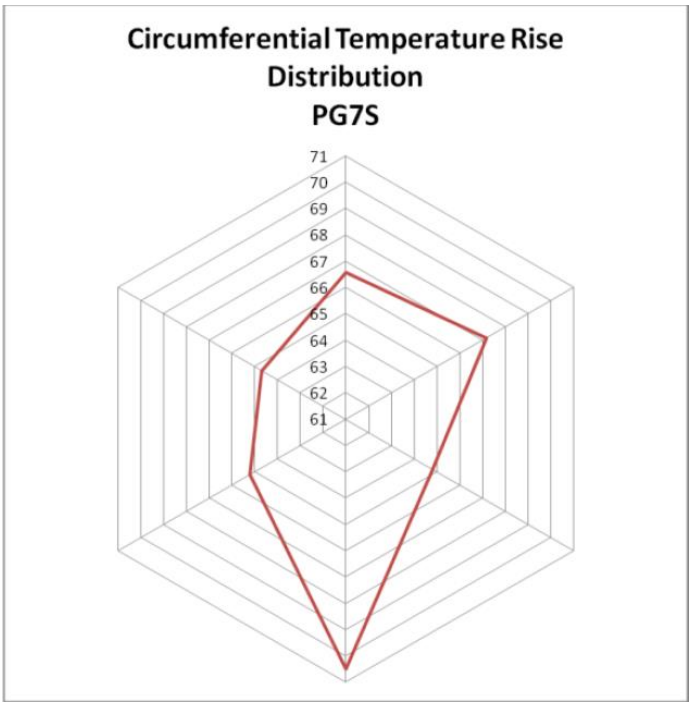


Figure 7. 6: Circumferential temperature distribution on PG7S

In summary, the PG7S as it was designed in Chapter 6, at the rated load of 1400 kVA operates thermally well below the required limits. Although, thermally the ratings can be increased, for reasons of meeting the reactance requirements, the decision was made to retain the 1400 kVA rating on the PG7S.

7.2.2 Forces on end-windings

The works in [73], [74], [75] discuss in detail the forces and stresses in stator end-windings due to the currents induced during steady-state and transient operations. Figure 8.7 breaks down the forces in the end-windings of an electrical machine. All the forces on the end-windings translate into mechanical components.

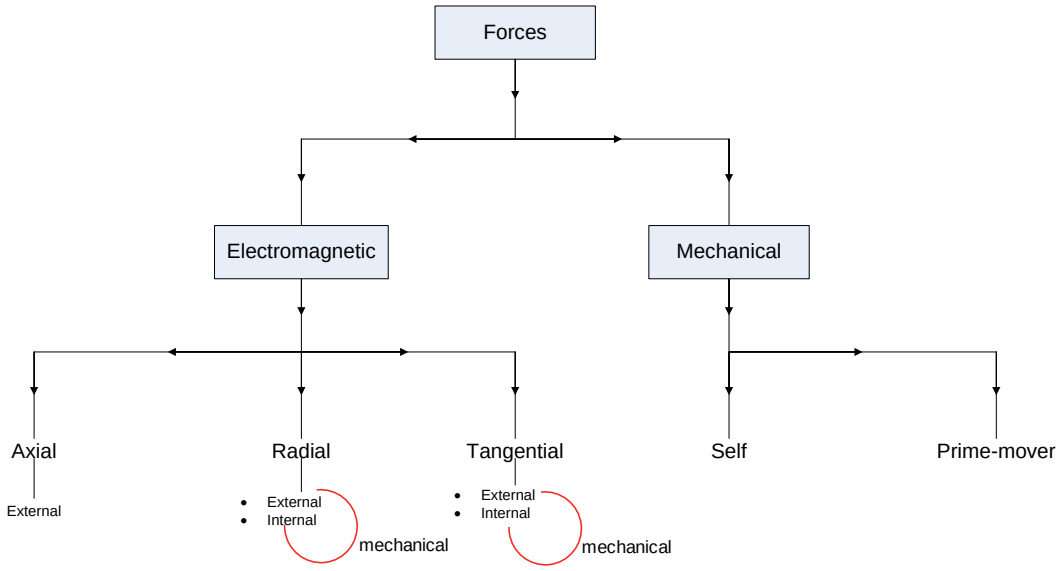


Figure 7. 7: Forces in windings of electrical machines

Of interest to the thesis were the electromagnetic forces induced in the windings under normal and fault conditions; under fault conditions, the windings experience high transient currents that induce forces that are orders of magnitude stronger than electromagnetic forces on the windings under normal operating conditions. Electrical machine stator windings are broadly of two types – formed windings and random winding. Formed windings as shown in Figure 7.8 have coils neatly formed into a well-defined geometry and inserted into the stator slots. Random wound generators have several strands bundled together and held in place by the resin that is used in the impregnation of the stator and rotor and is shown in Figure 7.9. The PG7S designed in this thesis has a random wound stator. Since most of the windings are in slots and therefore constrained from moving by the stator structure, the end-windings / overhangs in the stator are subject to the forces induced and are therefore the focus of any study on the impact of electro-magnetic forces on windings. In

[73] - [75] and [82]-[86], a summary of the results relative to the study of forces on end-windings in machines with formed winding is given. These learnings can be broadly applied to random windings, however with these windings there is a challenge related to the assembly process used. This is mainly related to several unquantifiable variations in the forces on the windings when such windings are used. This was confirmed by the work presented in Appendix 4 on developing an approximate numerical model to predict end-winding movement in SGs. To address the problem of articulating the reliability of the windings on the stator, a study of the currents in the stator windings during various LVRT conditions was simulated using the tool developed in Chapter 4. These currents were then benchmarked with the existing P7 capability to define measures to improve reliability of the PG7S end-windings.



Figure 7. 8: Formed coils in the stator

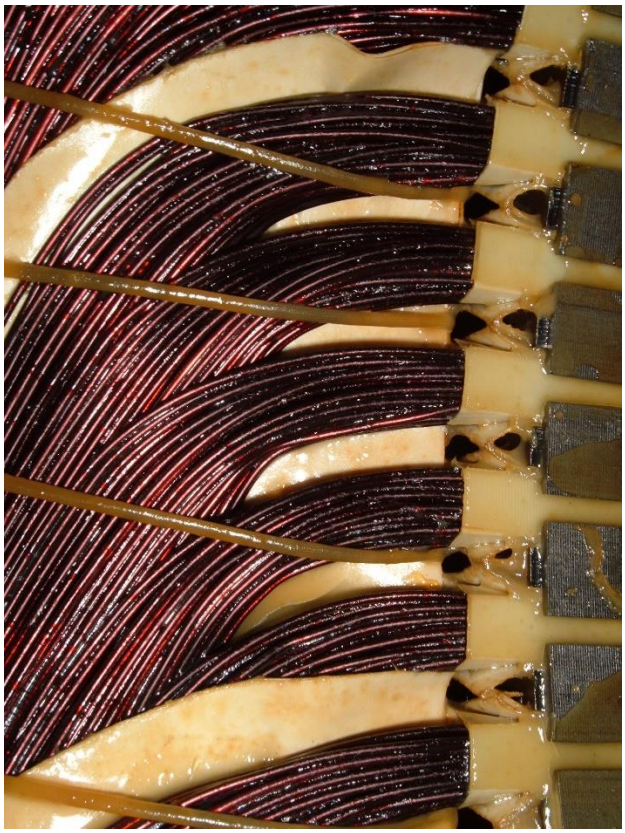


Figure 7. 9: Random winding inserted into the stator the PG7S

Figure 7.10 shows the plot of stator peak currents during LVRTs of varying duration and with the PG7S operating at 0.8 leading power factor (under-excited), 0.8 lagging power factor (over-excited) and Unity power-factor prior to the fault being induced. The currents observed in all the scenarios do not exceed the short-circuit current of the PG7S and the short-circuit currents in the standard P7 products. Since the electromagnetic forces are proportional to square of current, the PG7S is not likely to experience electromagnetic forces stronger than short-circuit on the windings. Over the life of the product (60,000 hours), the customers of Cummins Generator Technologies expect 100 LVRT events on the generating set.

It is therefore essential to ensure that the windings on the PG7S are capable of lasting for 100 short-circuits at least.

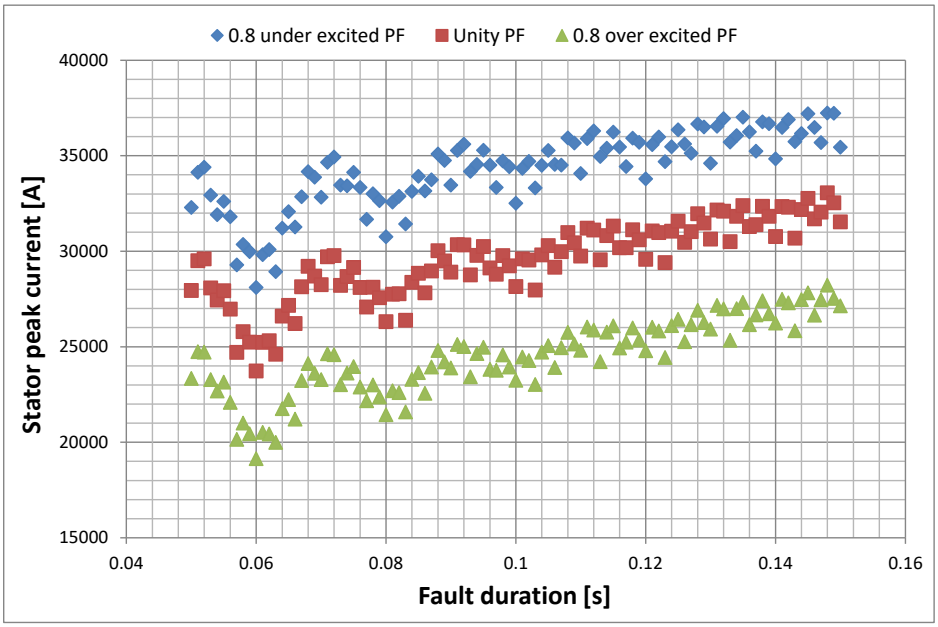


Figure 7. 10: Stator current during LVRT for various fault duration and power factors.

Since the short-circuit current of the PG7S is the biggest magnitude of current that will be experienced by the stator windings, a 100 short-circuits simulated on a PG7S followed by inspection and standard tests on the PG7S would highlight any issues with the capability of the PG7S to meet the requirement of surviving 100 LVRT events. Figure 7.11 below shows the test rig where 100 short-circuits were applied to the PG7S followed by a visual inspection of the windings, extended hours running of the PG7S and an end-winding resonant frequency check before and after the short-circuits to ensure the integrity of the windings.

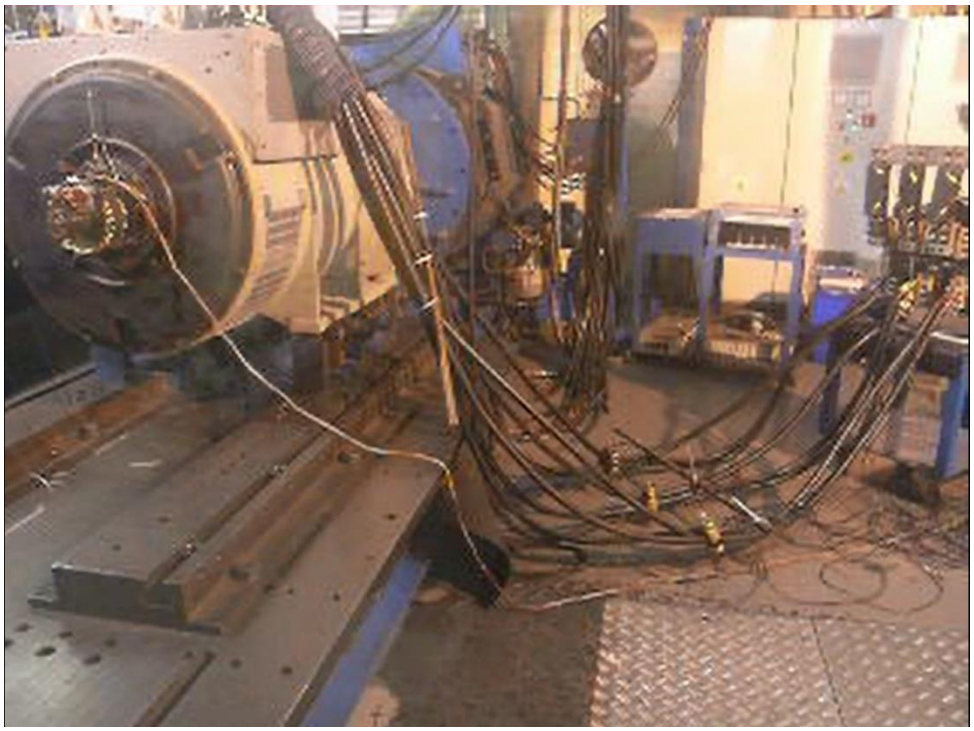


Figure 7. 11: Short-circuit test on the PG7S

The analysis of the PG7S results from 10 the 100 short-circuits confirm that the PG7S winding design as it stands can meet the requirement of withstanding 100 LVRT events.

In addition to the methodology described above, an attempt to reduce the fault currents induced by increasing the sub-transient reactance of PG7S was also investigated. A retrofit-able solution to increase sub-transient reactance by increasing leakage in the stator by adding an extension to the stator core-pack was investigated. The results were promising and allowed a reduction in the fault current of up to 20% thereby reducing the forces in the windings by up to 40%. Figure 7.20 shows the structure that was designed and investigated to increase the sub-transient reactance. This method was also filed for a granted patent GB2494166. Since

modifying sub-transient reactance impacts the transient response of the SG and since the work described above showed that no additional solutions were needed, this idea was not implemented in the product.

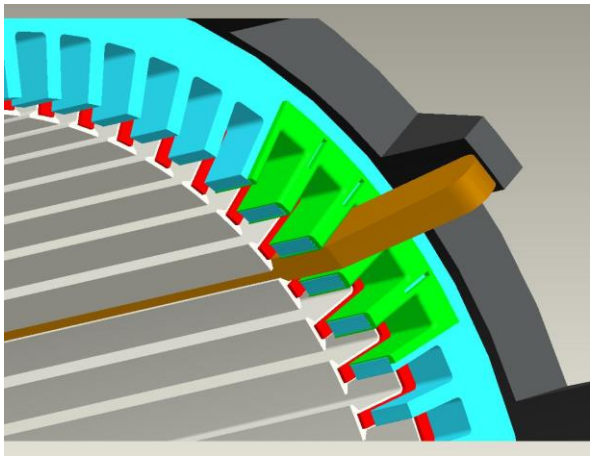


Figure 7. 12: Extension to stator core-pack to increase sub-transient reactance

7.2.3 Limiting rotor currents during LVRT

During the LVRT tests described in Chapter 4, the rectifiers used on the rectifier had to be frequently replaced due to thermal events on the rectifiers. To identify the root-cause of this problem and solve it, a rotor current, voltage and temperature measurement system was fitted to the LVRT test machine. Figure 7.13 below shows the rotor voltage during a LVRT. In this figure, the voltage peaks of up to and beyond 1 KV can be observed. This voltage is a result of the voltage induced in the rotor due to the large transient currents flowing in the stator during the fault on the grid.

These transient voltages on the rotor winding damage the rectifier thereby impacting the overall reliability of the product. While, [76], [77] and [78] describe electronics / power electronics-based methods to limit rotor voltage transients during LVRT, in conventional engine driven SGs, these technologies contribute to a significant increase in the cost of the overall product. A simpler and cheaper solution is therefore preferred to ensure that the product continues to remain competitive. Snubber resistors connected in parallel to the main rotor windings was proposed as a method to reduce the voltage transients induced in the rotor during LVRT. As the snubber resistors contribute to losses in the machine during steady state conditions, it is essential to size the snubber resistor suitably to minimize losses whilst maximizing the protection offered to the rotor winding and the rectifier circuit.

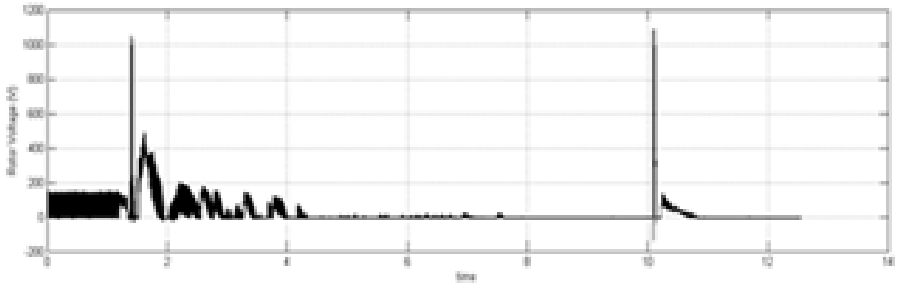


Figure 7. 13: Rotor voltage during LVRT

Since the design of snubber resistors itself is not new, the sizing / optimization exercise that was used to select the snubber resistor to reduce the rotor voltage transients during LVRT will not be discussed. Four 120 Ω, 100W resistors were connected as shown in Figure 7.14 below to achieve the attenuation required in the

rotor field winding circuit as shown in Figure 7.14, while Figure 7.15 shows the snubber assembly as it is seated onto the exciter. Figures 7.15, 7.16, 7.17 show the rotor voltage with no snubbers and various degrees of attenuation in the rotor voltage during a simulated fault condition that is replicated in house for different values of snubber resistor respectively. Combining the data, the net attenuation in rotor transient voltage spike during faults is plotted against a ratio of snubber resistance to field winding resistance as shown in Figure 8.18. This multiplication factor can be used in the initial selection of snubber resistors for any product size. This will then be followed by a validation of efficiencies and temperature rises to ensure the snubber resistors do not degrade machine performance whilst offering protection to the field winding and the rotating dioides

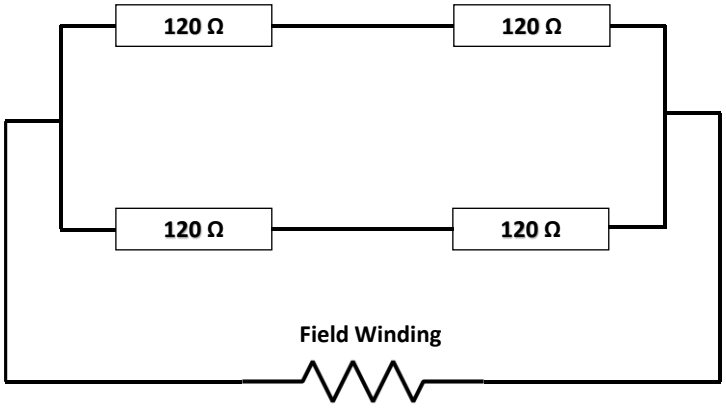


Figure 7. 14: Snubber circuit on the PG7S

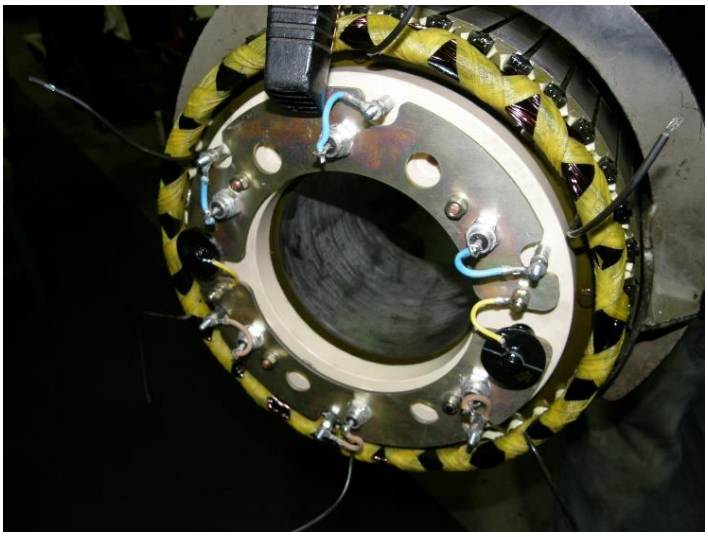


Figure 7. 15: Snubber Assembly (blue wires) attached to the exciter and rectifier (yellow wires) assembly

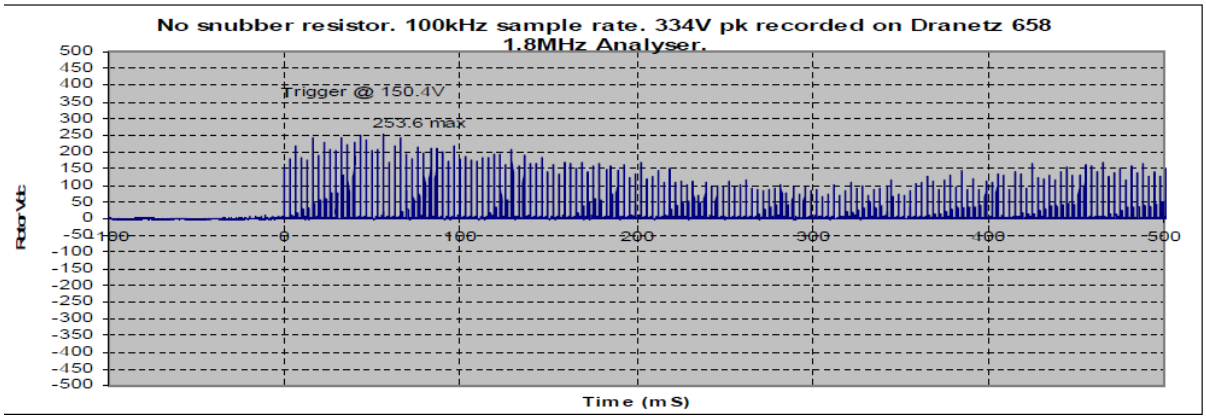


Figure 7. 16: Voltage transients in rotor without snubber resistor in a simulated fault in an in-house test environment

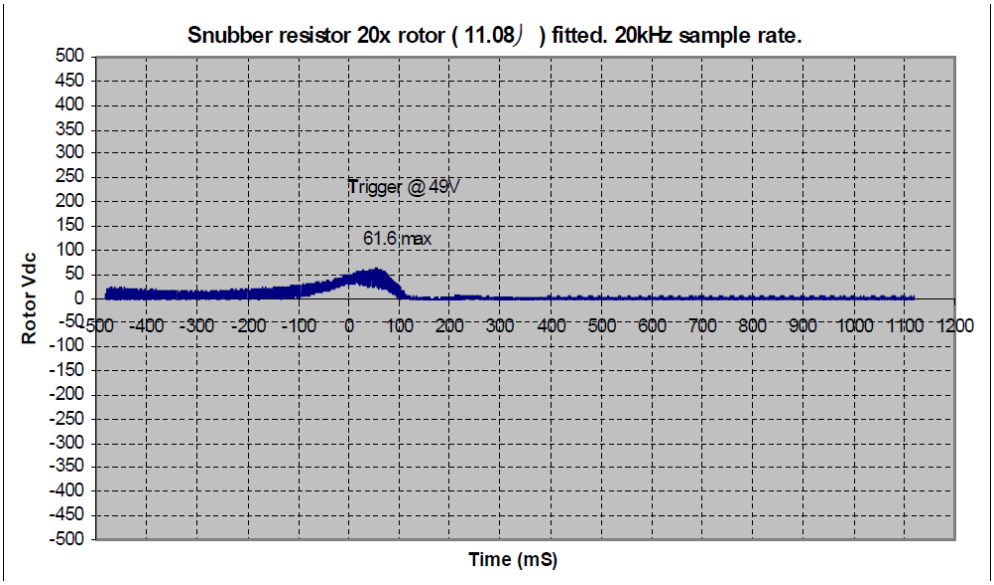


Figure 7. 17: Attenuation in rotor transient with snubber resistance 20 times field winding resistance

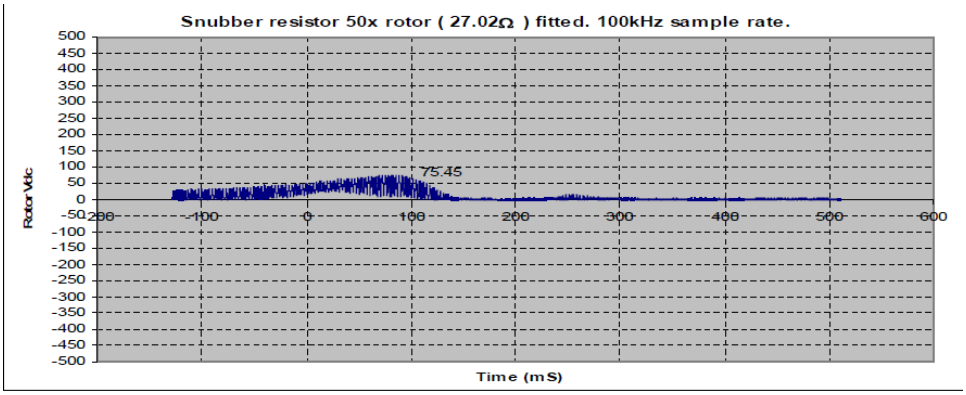


Figure 7. 18: Attenuation in rotor transient with snubber resistance 20 times field winding resistance

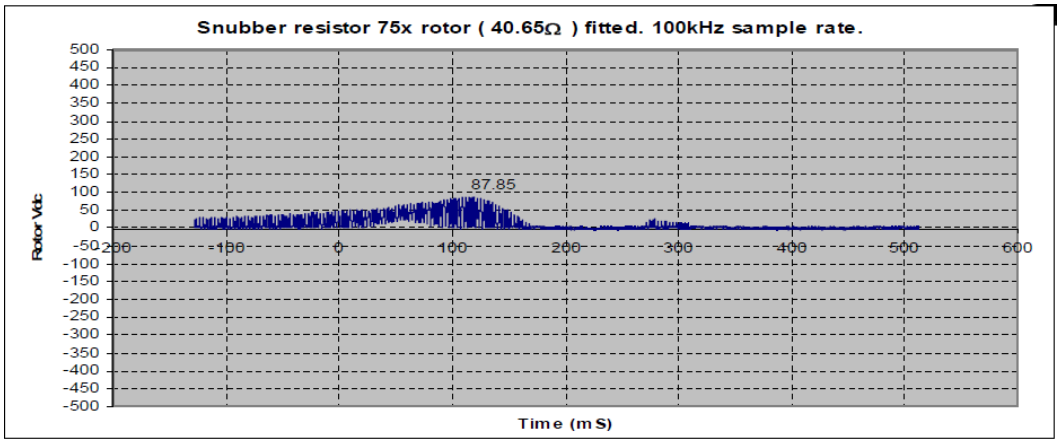


Figure 7. 19: Attenuation in rotor transient with snubber resistance 20 times field winding resistance

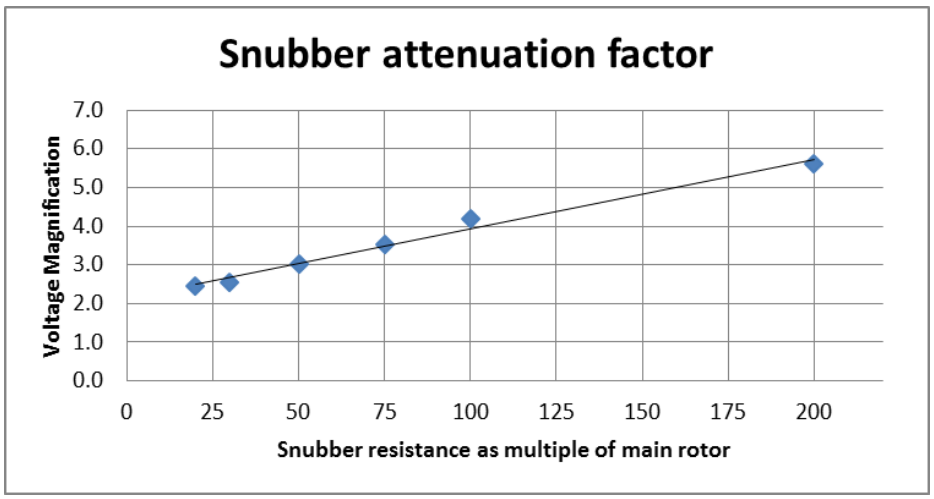


Figure 7. 20: Attenuation in rotor transient with snubber resistance 20 times field winding resistance

The snubber solution designed above was implemented on to the PG7S and the LVRT test in Chapter 4 was repeated again. Figure 7.19 compares the plots of rotor field winding voltage with and without the snubber resistors. The snubber resistors used on the PG7S are approximately 120 times the field winding resistance and

provide an attenuation of approximately 6 times reducing the rotor voltage transient voltage to approximately 150 V. Figure 8.18 predicts an attentuation of 4 times for a snubber resistance to rotor winding resistance of 120. The additional attentuation observed during the LVRT testing is likely due to the additional line impedances that are used in the test. Due to the effectivness of using snubbers for reducing rotor voltage peaks during LVRT, an internal standard was developed by CGT to design snubbers for SGs.

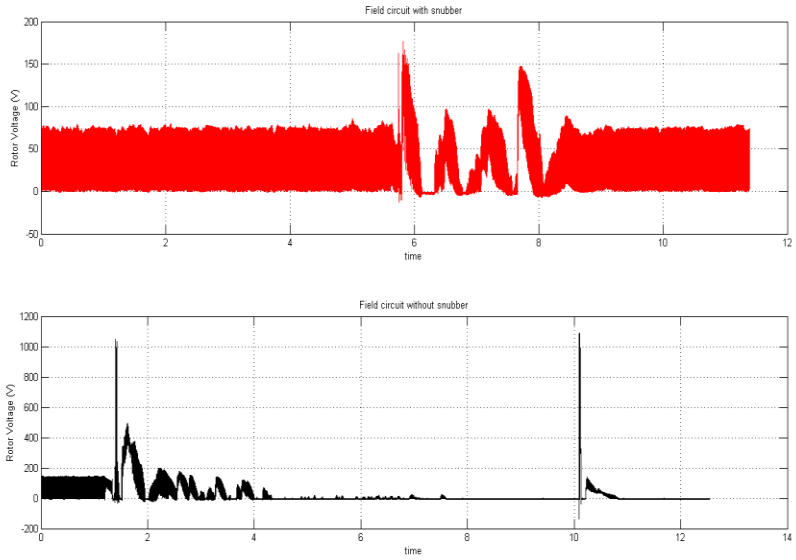


Figure 7. 21: Rotor winding voltage with and without snubbers during LVRT

7.2.4 Bearing life

The addition of the high inertia disc at the drive end of the PG7S rotor shaft combined with the torques induced during LVRT events will have an influence on the bearing life. The bearing life must remain above 20,000 hours and it is therefore

necessary to understand the risk to the bearings and mitigate any concerns. Bearing life is typically referred to with the L10 life number. L10 life is defined as the number of operating hours after which 90% of the bearing in operation are functional [87]. The L10 life of a bearing is dependent on the alternator rating, voltage, air-gap, shaft dimensions, inertia of the alternator and bearing design including grease used, contamination, stresses in application that are represented by an application factor. The L10 bearing life calculated is over 25,000 hours and therefore it is determined that no design changes are required to improve the bearing life.

7.3 Conclusion

In addition, designing the PG7S to meet the design parameters that make it grid code compliant, extensive work was also completed to ensure the desired reliability levels were met on the grid code compliant SG. Internal standards were developed as a result of this work to design SGs for grid code compliant applications. These internal standards included rating and selection of the generator for stability and thermal life and included design of snubber resistors to attenuate the rotor field winding voltage transients. Bracing design for end-windings was recommended using ratios of currents induced in the stator relative to normal operation and the limits on current rations were set using the tool developed in Chapter 4.

CHAPTER 8

CONCLUSION

In this project, a multi-physics approach aimed at designing a grid-compliant SG was proposed and validated on a 1.4MVA, SG case study. The proposed process considers both the application (i.e. required performance) and the reliability aspects of the generator whilst addressing a real-life design for regulatory compliance.

The work presented in this thesis was used to deliver three high level objectives:

1) Define the SG requirements to meet the grid code compliance requirements for a broad range of generating sets. An extensive analysis was completed of all the grid codes that exist globally and were translated into requirements specific to SGs.

2) The identified requirements identified were used to select the right products for grid code compliant applications. It was proven that there exists a solution space in which the SG design parameters can be optimized to make it grid code compliant. A simple rule that was developed for selecting / designing SGs for grid codes. This list was also validated through customer led certification of grid code compliant generating sets.

3) Design an engine-driven, 1400 kVA engine driven grid code compliant SG.

At a more detailed level, the work presented has led to a comprehensive product whose feature meet the requirements for all the grid codes presented in the thesis. At the time this work presented in this thesis started, the power generation industry in Europe had been inundated with regulatory documentation on grid codes and all

the criteria that power plants would have to meet to be able to connect to the Transmission and Distribution networks; through the work that this thesis delivered, an extensive understanding of the performance and capability of SGs in these applications was derived in addition to an understanding of design needs for SGs for grid code applications. The entire P7 range of products at Cummins Generator Technologies were redesigned to be capable of complying with grid codes without any detrimental impact to performance, cost and reliability. Figure 8.1 below shows the low voltage grid code product offering of Cummins Generator Technologies that resulted entirely because of this work [128], [129], [130], [131], [132].

Additionally, the tools and knowledge developed through this work has also resulted in internal standards for designing SGs for grid code compliant applications and several training materials that have been used at workshops delivered to generating set assemblers and power plant / power system owners.

Figure 8.2 shows the cost/kVA across different products offered by Cummins Generator Technologies in the grid code compliant low voltage product range. It can be observed that the newly designed grid code compliant PG7 product series has a significant reduction in cost/kVA compared to the standard PE7 series grid code compliant product (PEG7) that was de-rated using the sizing rules developed in this thesis.

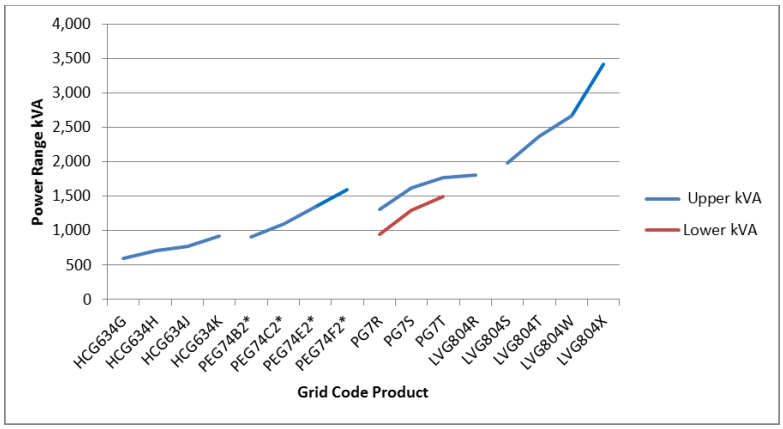


Figure 8. 1: Low Voltage Grid code compliant products offered by Cummins Generator Technologies

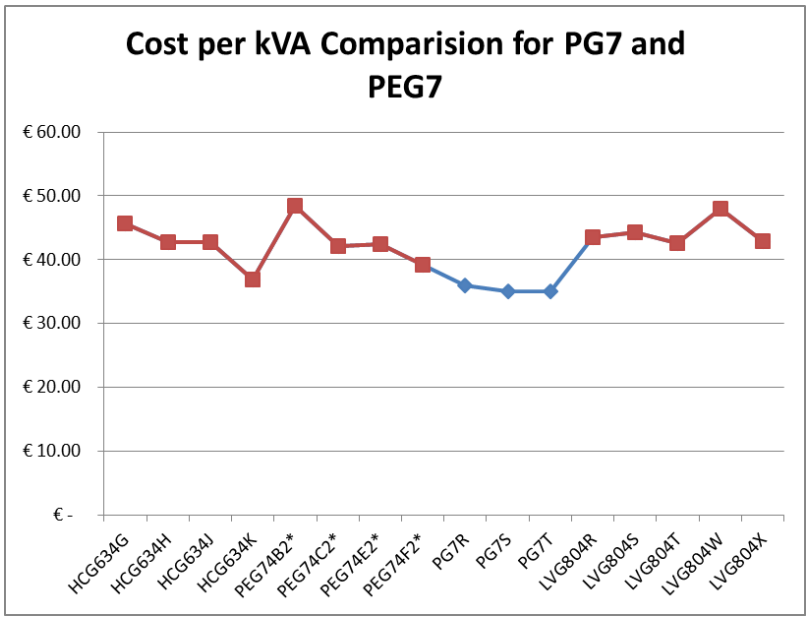


Figure 8. 2: Cost per kVA comparison across all low voltage grid code compliant products offered by Cummins Generator Technologies.

Additionally, the various risks to reliability arising from connecting SGs to harsh grid conditions have also been addressed, increasing the reliability of the products in grid connected applications.

- A snubber resistor circuit was developed to protect the rotor windings from voltage spikes induced during Low Voltage Ride Through and the methodology was generalized to create an internal standard for testing and validating snubber resistors including the rationale for incorporating snubber resistors into the design.
- Several internal projects were launched to understand the impact of current transients on the windings of random wound and form wound SGs that resulted in detailed models that helped define the winding design for all SGs manufactured by Cummins Generator Technologies. A novel method to increase the sub-transient reactance and consequentially reduce the fault currents in the stator and therefore the forces on end-windings of the SG using a retrofit-able stator 'ring' was also developed and is a granted patent.
- A detailed approach towards designing SGs for design life is presented describing the impact of designing for kVA and designing for a target temperature rise that meets insulation system life targets.
- The impact of transient loads on bearings is considered and the L10 life calculation is introduced as an approach used to confirm bearing capability relative to application conditions.

As a commodity traded in future markets, electricity pricing depends on capital costs (initial investment, cost of equipment, etc.,) and operating costs (cost of fuel, servicing and repair costs) [90]. Combined with the cost/kVA benefits shown in Figure 8.2, an enhanced product reliability offered by the PG7 product series lowers the lifecycle cost of the SG. This leads to a lower initial cost due to reduced cost/kVA and lower maintenance costs due to increased reliability thereby contributing to a lower electricity price.

In summary, the contributions of this thesis are:

- The importance of adopting a system-level design approach has been emphasized throughout the thesis. Such a system-level design approach has been used for the first time to define design requirements of SGs with a view of an arduous application (grid code compliance).
- The grid codes relevant to engine driven SGs are reviewed and a comprehensive study of their impact on the SG performance and reliability are discussed.
- A computationally efficient finite element algorithm is developed to accurately calculate the SG parameters is developed and validated.
- A simple analytical tool that can be used to define design requirements for an engine driven SG to meet the ‘static grid code’ requirements has been created and presented.

- A model of an engine driven generating set connected to the grid is created and is used to define critical design parameters that need to be met for an engine driven generating set to be grid code compliant. It is also shown that these parameters are independent of the size of the SG or that of the generating set.

- The results obtained from the above described models, have shown that inertia is not the most commercially viable and practical solutions to achieve grid code compliance of an engine driven generating set. On the other hand, it is shown that an optimum synchronous reactance can be used to minimize the need for extremely high inertia.

- The impact of a grid code type environment on the SG's robustness is discussed and relevant solutions are presented.

- The economic aspects of the proposed SG design for grid code compliance are discussed.

FUTURE WORK

The work presented in this thesis opens exciting avenues of further research, specifically combining modern tools to study how the SGs behave in various applications aiming to identify competitive advantages.

- The finite element analysis tool can be combined with the power systems simulation to avoid multiple simulation stages. A single tool that directly uses the output from the power systems simulation tool and feeds into a

power systems model would be capable of making more accurate predictions. Such a tool would also allow the exciter to be modelled in finite element analysis tool thereby providing a better mechanism to understand the effect of exciter time constants on the system stability during transients.

- While formed coils are easier to model in finite element tools and therefore easier to study the effect of stator winding forces, random wound coils are a lot more complex due to the geometry and the variability in the resin fill and effect of stator winding temperature on the mechanical properties of the random wound coil structure. Extensive work can be done in the future to study the behavior of random wound coils during transients.
- *Backswing,* the initial slowing of the rotor immediately after a fault is crucial. Damper cage design is crucial to impacting *backswing*. Further work to study damper cage design specific to backswing whilst preserving overall performance would prove effective in designing SGs that are stable during transients.
- The work presented in the granted UK patent GB 2494166 needs to be tested on a wide range of generators under various load conditions to optimize the design of the ‘leakage ring’ presented in the same patent. The effect of the ring during transients also needs to be determined using experiments.

References

[1] Kaplan.S.M (2009), *Smart Grid, Electric Power Transmission: Background and Policy Issues.*The Capital.Net, Government Series. Pp. 1-42.

[2] A. Ishchenko, *Dynamics and stability of distribution networks with dispersed generation*, PhD Thesis, Eindhoven University of Technology, Netherlands, 2008.

[3] CIRED preliminary report of CIRED working Group 04, *Dispersed Generation,* CIRED conference, Nice, June, 1999.

[4] Hossain. J, Mahmud. A (eds), *Renewable Energy Integration, Green Energy and technology*, DOI: Springer Science & Business Media, Singapore, 2014.

[5] *World Bank, Addressing the Electricity Access gap*, 2017 report.

[6] ZPRYME, *Power Systems of the future: The case for energy storage, distributed generation, and microgrids,* IEEE Smart grid, November 2012.

[7] Cummins Generator Technologies, *International Grid Codes with Stamford | AVK Rev2.0,* 2013.

[8] Wikipedia - http://www.wikipedia.com

[9] Ivan Machado, Itzel Arias, *Grid Codes Comparison,* Masters Thesis, Chalmers University of Technology, Sweden, 2006.

[10] *IEEE Std 1547- Standard for Interconnecting Distributed Resources with Electric Power Systems,* IEEE Std. July 2003.

[11] *Appendix 1 – Standard Definitions, Ontario Power Authority (OPA), Ver 1.3.1*, July 2010.

[12] *Distributed Generation Technical Interconnection Requirements: Interconnections at Voltages 50 kV and below, 1st ed*, HydroOne Networks Inc, February, 2010.

[13] Gregory Joseph Kish, *Addressing Future Grid Requirements for Distributed Energy Resources,* Masters Thesis, University of Toronto, 2011.

[14] V.Van Thong, J. Driesen, R.Belmans, *Using distributed generation to support and provide ancillary services for the power system*, International Conference on Clean Electrical Power, 2007.

[15] P. Strauss, T. Degner, W. Heckmann, I. Wasiak, P. Gburczyk, Z. Hanzelka, N. Hatziargyriou, T. Romanos, E. Zountouridou, and A. Dimeas, *International white book on grid integration of static converters*, 10th International Conference on Electrical Power Quality and Utilization, September, 2009.

[16] *IEEE Std 929 – Recommended Practice for Utility Interface of Photovoltaic Systems*, January 2000.

[17] FGW, *Technische Richtlinien für Erzeugungseinheiten und –anlagen, Teil 3*, Rev. 2, 2012

[18] *BDEW, Technische Richtlinie Erzeugungsanlagen* am Mittelspannungsnetz, 2008

[19] *BDEW, Regelungen & Übergangsfristen für bestimmte Anforderungen in Ergänzung zur technischen Richtlinie*, 2012.

[20] *JOURNAL OFFICIEL DE LA RÉPUBLIQUE FRANÇAISE, Commission de régulation de l'énergie*, French Grid Code, December, 2013.

[21] *ENTSO-E, Draft Network Code for Requirements for Grid Connection applicable to all Generators*, 2012.

[22] *Technical Regulation for Thermal Power Station Units of 1.5 MW and higher, Regulation for grid connection TF 3.2.3* , October, 2008

[23] *Regola tecnica di riferimento per la connessione di Utenti attivi e passivi alle reti AT ed MT delle imprese distributrici di energia elettrica*, Italian Grid Code, CEI-0-16, December, 2012.

[24] *Australia National Electricity Rules*, Version 45, July 2011.

[25] *PROCEDIMIENTO DE OPERACIÓN 12.3: REQUISITOS DE RESPUESTA FRENTE A HUECOS DE TENSIÓN DE LAS INSTALACIONES EÓLICAS*, Spanish grid code, Red Electrica De Espana, 2013.

[26] *Netcode Elektriciteit*, Holland grid code, 2014.

[27] *THE GRID CODE, ISSUE 5, REVISION 7*, National Grid Electricity Transmission Limited, UK, March, 2014.

[28] Sridhar Narayanan, Gary Berridge, Andreas Biebighauser, Neil L.Brown, *Fault Ride Through Effects on Alternators*, Proceedings of Powergen Asia, 2011, Kuala Lumpur, Malaysia, September, 2011.

[29] Narayanan. S, Brown,N.L, Mebarki. A, Anpalahan. P, Gerada, D, Biebighaeuser. A, Vrihriaelae. H.T, *An analytical tool to check for static grid code compliance of generating sets*, Proceedings of the 45th International Universities Power Engineering Conference (UPEC), Cardiff, 2010

[30] J. H. Walker, *Operating characteristics of salient-pole machines*, Proc. Inst. Elect. Eng, vol. 112, 1953

[31] J.Machowski, J.W.Bialek, J.R.Bumby, *Power Systems Dynamics, Stability and Control*, 2nd Ed. John Wiley & Sons, Ltd

[32] Sridhar Narayanan, *Critical Parameters of a synchronous alternator for a grid code compliant generating set*, Proceedings of Powergen Europe 2012, Cologne, June 2012.

[33] Prabha Kundur, *Power System Stability and Control*, ISBN: 0-07-035958

[34] Bernard Herzmaier, Herwig Renner, Jose Gomez, *Low Voltage Ride Through Capability of Gas Engine Driven Units*, CIRED, 22nd International Conference on Electricity Distribution, Stockholm, June, 2013.

[35] Jan Machowski, Janusz W. Bialek and James R. Bumby, *Power System Dynamics: Stability and Control, Second Edition*, ISBN: 9780470725580.

[36] Jacob Klimstra, *Fault ride-through capability of engine-driven power plants,* Proceedings of PowerGen Europe, Cologne, May 26-28, 2009.

[37] Zeljko Spoljaric, Kresimir Miklosevic & Vedrana Jerkovic, *SG Modelling Using Matlab,* SiP 2010 28th International Conference Science in Practice / Mester, Gyula (ur.).

[38] S.Jagannathan, Dr S.Palaniswami, R. Adithya, M. Naresh Kumar, *SG Modelling and Analysis for a Microgrid in Autonomous and Grid Connected Mode,* International Journal of Computer Applications, Vol 13-No.5, January 2011.

[39] Ion Boldea, *SGs (The Electric Generators Handbook),* CRC Press, Nov, 2005, ISBN: 978-0849357251.

[40] P.C. Krause, *Analysis of Electric Machinery*, McGraw-Hill, 1986, Section 12.5.

[41] Kamwa, I., et al., *Experience with Computer-Aided Graphical Analysis of Sudden-Short-Circuit Oscillograms of Large Synchronous Machines,* IEEE® Transactions on Energy Conversion, Vol. 10, No. 3, September 1995.

[42] Tilman Weckesser, Hjortur Johannsson, Jacob Ostergaard., *Impact of Model Detail of Synchronous Machines on Real-Time Transient Stability Assessment,* IREP Symposium-Bulk Power System Dynamics and Control - IX August 2013.

[43] Bianchi N, *Electrical Machine Analysis Using Finite Elements*, CRC Press, 2005, ISBN 978-0849333996.

[44] Sheppard J, *Finite Element Analysis of Electrical Machines*, Springer, ISBN: 978-0-7923-9594-2,1995.

[45] Juha Pyrhönen, Tapani Jokinen, Valéria Hrabovcová, *Design of Rotating Electrical Machines*, John Wiley & Sons, Ltd. 2008.

[46] A.B.J. Reece,T.W.Preston, *Finite Element Methods in Electrical Power Engineering*, Oxford University Press, ISBN:978-0-19-856504-8,2000.

[47] C.N. Ashtiani,D.A. Lowther, *Simulation of the Transient and Subtransient*

Reactances of a Large Hydrogenerator by Finite Elements. IEEE Transaction on Power Apparatus and Systems, Vol. PAS-103, No.7, July 1984.

[48] Drago Ban, Damir Zarko, Zlatko Maljkovic, *The Analysis of Saturated Reactancesof the 247 MVA Turbogenerator by Using the Finite Element Method.*

[49] Kolondzovski Zlatko, *Evaluation of Methods for Calculation SG Reactances*, International PhD Seminar: Computation of Electromagnetic Fields, 23-28 September 2004, Budva/Serbia & Montenegro.

[50] Silvio I. Nabeta, Albert Foggia, Jean-Louis Coulomb and Gilbert Reyne, *A Non-Linear Time-Stepped Finite element simulation of a Symmetrical Short-Circuit in a Synchronous Machine*, IEEE Transaction on Magnetics, Vol. 31, No. 3, May 1995.

[51] Prof. JJ. Simond and collective, *Automatic Determination of Laminated Salient-Pole Synchronous Machines parameters Based on the Finite Element Method*, Swiss Federal Institute of Technology, Electrical Engineering Department.

[52] D.Y.Park, H.C.Karmaker, G.E.Dawson, A.R. Eastham, *Standstill Frequency Response Testing and Modeling of salient-pole Synchronous machines*, Queens University, Canada,, IEEE transaction on Energy Conversion, Vol.13,No.3, September 1998.

[53] Arieh L. Shenkman, *Transient Analysis of Electric Power Circuits Handbook*, Springer, 2005, ISBN 0387287973.

[54] M.V.Bakshi, U.A.Bakshi, *Electrical Machine III*, Technical Publications, Pune.

[55] Ion Boldea, *SGs (The Electric Generators Handbook)*, CRC Press, 1st Edition.

[56] Martin Ranlof, *Electromagnetic Analysis of Hydroelectric Generators*, PhD thesis, 2012, Uppsala University.

[57] DD15596 – Cummins Generator Technologies, Internal test procedures & standards.

[58] The National Grid Company, '*Grid Codes',* Issue 3.

[59] Andreas Karlsson, *Evaluation of Simulink / SimpowerSystems and other commercial simulation tools for the simulation of machine system transients.*

[60] https://powersuite.cummins.com *Natural gas generator set QSK60 series engine*

[61] Cruz, J. B., editor, (1973) *System Sensitivity Analysis*, Dowden, Hutchinson & Ross, Stroudsburg, PA.

[62] Cruz, J. B. and Perkins, W.R., (1964), *A New Approach to the Sensitivity Problem in Multivariable Feedback System Design*, IEEE TAC, Vol. 9, 216-223.

[63] Thyssenkrup Electrical Steel (TKES) Electrical Steel Database 2014.

[64] www.aksteel.com

[65] Alexander J. Clerc, Annette Muetze, *Measurement of stator core magnetic characteristics*, 2011 IEEE International Electrical Machines & Drives Conference.

[66] IEC 60034-1:2010: Rotating Electrical Machines.

[67] ANSI/IEEE C57.12.56-1986, IEEE Standard Test Procedure for Thermal Evaluation of Insulation Systems for Ventilated Dry-Type Power and Distribution Transformers.

[68] M.G.Say, *Alternating Current Machine.*

[69] FEP 00021655, Cummins Generator Technologies Engineering Standard Work.

[70] BS EN60034-4:2008 Rotating electrical machines. Methods for determining synchronous machine quantities from tests.

[71] Flavio Roberto Souza dos Santos, Sandro Cabral, *FMEA and PMBOK applied to project risk management,* Journal of Information Systems and Technology Management.

[72] Sumilawska.M et.al, *The impact of thermal degradation on electrical machine winding insulation,* IEEE 10th International Symposium on Diagnostics for Electrical Machines, Power Electronics and Drives.

[73] Richard, N. *Calculation of electromagnetic forces on large generator end windings under fault conditions using a three dimensional finite element method.*

[74] A Gruning, S.Kulig, *Electromagnetic Forces and Mechanical Oscillations of the Stator End Winding of Turbo Generators.*

[75] A Binder, *Forces in big synchronous machines.*

[76] Shuying Yang, *Analytical Method for DFIG Transients during Voltage Dips,* IEEE Transaction on Power Electronics, Volume: PP, Issue:99.

[77] Fang Liu, Mingwei Mei, Juntao Pan, *A Control method of the low voltage ride through in the doubly-fed induction generator wind turbine,* Control Conference (CCC), 2013, 32nd Chinese.

[78] Wen Juan Zhang, Zhi Xia Han, *Rotor current analysis on Transient Performance of Low Voltage Ride-Through of Doubly Fed Induction Generator,* Advanced Materials Research Volumes 945-949.

[79] *Electrical Insulation Systems: UL 1446, Understanding, Specifying and Evaluating Electrical Insulation Systems for UL Certified Applications.*

[80] Rotating electrical machines - Part 18-31: Functional evaluation of insulation systems - Test procedures for form-wound windings - Thermal evaluation and classification of insulation systems used in rotating machines.

[81] *Fundamentals of HALT / HASS Testing,* White Paper, Tektronix.

[82] A. Stermecki et al, Analysis of SG End-Winding Deformations Using 3-D Time-Harmonic FEM, XIX International Conference on Electrical Machines, ICEM 2010, Rome.

[82] A.Merkhouf et al, *Generator end windings forces and natural frequency analysis,* Electrical Machines and Drives Conference, 2003, IEMDC.

[83] Raffaele Albanese et al, *Electromechanical analysis of end windings in turbo generators,* COMPEL-The international journal for computation and mathematics in electrical and electronic engineering, Vol 30, Iss: 6, pp 1885-1898.

[84] Ariadne Ann Tampion, *Double-Frequency Stator Core Vibration in Large Two-Pole Turbogenerators*, PhD thesis, University of Southampton, Aug 1990.

[85] Ranran Lin et al., *End-Winding Vibrations Caused by Steady-State Magnetic Forces in an Induction Machine,* IEEE Transactions on Magnetics, Vol 46, No 7, July 2010.

[86] M.M.A Rahman and Jesse Jackson, *Generator End-winding vibration Analysis – A Capstone Experience,* School of Engineering, Grand Valley State University, Michigan, 2014.

[87] SKF, *Bearing life and load ratings,* www.skf.com.

[88] P. M. Anderson and A. A. Fouad. *Power System Control and Stability*, Second Edition. John Wiley and Sons, Inc., New York, New York, 2003.

[89] IEEE Std 421.5-2005, *IEEE Recommended Practice for Excitation System Models for Power System Stability Studies.*

[90] U.S. Energy Information Administration, *Levelized cost and Levelized Avoided cost of New Generation Resources in the Annual Energy Outlook 2016,* eia, Aug 2016.

[91] Hydro-Quebec, TransEnergie Technologies, *Simpower Systems.*

[92] Sridhar Narayanan et al, *Low Voltage Ride Through performance of a 4MVA SG* – measurements and simulations, Proceedings of 2014 conference on Power Electronics, Machines and Drives (PEMD).

[93] Gayek, H. W, '*Transfer characteristics of brushless aircraft generator system'*, IEEE Transactions on Aerospace, Vol. 2, No. 2, 1964 5. Wang, X-F., at all: Modern Power.

[94] Wang, X-F., et al: '*Modern Power System Analysis'*, 2009 Springer, Heidelberg, Germany, ISBN 978-1-4419-4451-1.

[95] M.G.Lloyd, P.G.Anew, *'The Regulation of Potential Transformers and the Magnetizing Current'.*

[96] Fernando L. Alvarado, Claudio Canzares, '*Synchronous Machine Parameters from Sudden-Short Tests by Back-Solving',* IEEE Transactions on Energy Conversion, Vol 4, No 2, June 1989.

[97] F.S.Sellschopp, M.A.Arjona, *'Semi-Analytical method for determining d-axis SG parameters using the DC step voltage test',* IET Electric Power Applications, Volume 1, Issue 3, May 2007.

[98] Bargallo.R et al, '*Main Inductance determination in rotating machines. Analytical and Numerical calculation: A didactical approach'*, International Conference on Modern Electrical Power Engineering, July 2016.

[99] Jacek F.Gieras et al, '*Calculation of Synchronous Reactances of small Permanent-Magnet Alternating-Current Motors: Comparison of Analytical Approach and Finite Element Method with Measurements'*, IEEE Transactions on Magnetics, Vol 34, September 1998.

[100] Akbar Beik Khormizi et al, *'An Analytical Method to Parameter Estimation by Dynamic Performance Evaluation'*, International Journal of Energy and Power, Volume 2, Issue 1, February 2003.

[101] Mohamed Labib Awad, *'Modeling of Synchronous Machines for System Studies',* PhD Thesis, University of Toronto, 1999.

[102] Alexander Zaritskiy, '*Mathematical Models and Stability Analysis of Three-Phase Synchronous Machines',* PhD Thesis, University of Jyvaskyla, 2013.

[103] *'IEEE Guide for SG Modeling Practices in Stability Analyses',* IEEE, March 21, 1999.

[104] P.J.Turner et al, *'The DC Decay Test for determining synchronous machines parameters, measurement and simulation*', IEEE Transactions on Energy Conversion, December 1989.

[105] M.Hasni et al, *'Synchronous Machine Parameter Identification in Frequency and Time Domain',* Serbian Journal of Electrical Engineering, June 2007.

[106] J.M.Ramirez, '*Power System reduced model by Artificial Neural Networks'*, Proceedings of 2005 IEEE International Joint Conference on Neural Networks.

[107] C.R.Minussi, M.doC.G.Silveria, *'Electric power systems transient stability analysis by neural networks'*, Proceedings of the 38th Midwest Symposium on Circuits and Systems, 1995.

[108] Jerzy Tchorzewski, *'Capabilities of Matlab and Simulink related to Modelling of Polish Power Exchange'*, Information Systems in Management, 2016.

[109] A.R. Bahmanyar, A.Karami, '*Power system voltage stability monitoring using artificial neural networks with a reduced set of inputs'*, Electrical Power and Energy Systems 58, 2014.

[110] Karami. A, '*Power System transient stability margin estimation using neural networks'*, International Journal of Electric Power Energy Systems 2011; 33(4): 983-91.

[111] Vakil-Bagmisheh MT, Razmi H, ' *Dynamic Voltage Stability Assessment of power transmission systems using neural networks',* Energy Convers Manage 2008; 49; 1-7.

[112] Anthony R.Thorne, Thomas H. Sloane, '*Engine Generators in Outside Plant Applications',* Alpha Technologies, White Paper, October 1998.

[113] C.Blome, M. De Bortoli, G. Stanic, '*Grid Fault Ride-Through capabilities of diesel-electric systems'*, International Conference on Electrical Machines (ICEM), 2010.

[114] L. Diez-Maroto, L. Rouco, F. Fernandez-Bernal, '*Fault ride through capability of round rotor SGs: Review, analysis and discussion of European grid code requirements',* Electric Power Systems Research 140, 2016.

[115] H. Johal, R. Konopinski, J.P.Skliutas, M. Eitzmann, D.J. Leonard, '*Solutions to Improve Grid Code Compliance of Synchronous Generation'*, CIGRE US National Committee, 2014 Grid of the Future Symposium.

[116] Sung Don Cho, '*Parameter estimation for transformer modeling',* Michigan Technological University, Dissertation Master's Thesis, 2002.

[117] N. Essl, H. Renner, *'LVRT Retardation-Device for Decentralized Power Plants'*, Electric Power Quality and Supply Reliability Conference, 2014.

[118] N. Essl, H. Renner, '*Influence of LVRT Test Equipment Characteristics on the Dynamic Performance of a Power Generation Unit'*, CIRED, 23rd International Conference on Electricity Distribution, June 2015.

[119] Anna Goelieva, '*Low Short Circuit Ratio Connection of Wind Power Plants'*, Master of Science Thesis, TU Delft, DTU, NTNU.

[120] Malin Sjolund, '*Study of Grid Code Compliance – Thanet Wind Farm'*, Uppsala Universitet, 2012.

[121] IEC 61400-21: International Standard, Wind turbines, part 21, '*Measurement and assessment of power quality characteristics of grid connected wind turbines'*, IEC, 2008.

[122] Applications Guidance Notes, Cummins Generator Technologies.

[123] Matthew Sands, Richard Feynman, '*The Feynman Lectures on Physics',* 1964.

[124] A.Binder, '*Forces in big synchronous machines', Darmstadt technical University.*

[125] A. Grüning, S. Kulig, *'Electromagnetic Forces and Mechanical Oscillations of the Stator End Winding of Turbo Generators'*, University of Dortmund.

[126] vonRoll, 'Low Voltage *Insulation Training Material',* vonRoll publication, 2011.

[127] J. Krata, A.Burek, J.Altonen, '*Modern approach to pole slip protection'*, International conference on power system transients, 2013.

[127] '*Neural Network Toolbox',* MATLAB.

[128] '*Cummins Generator Technologies grid code-ready alternator range*, Power Engineering International, September, 2014.Powergen International (PEI)

[129] '*Ready to Meet New Grid Code Challenges'*, Generating Insight, Edition 1, www.stamford-avk.com.

[130] '*Cummins Generator Technologies Announces Support for Grid Code Compliant Generating Sets',* Diesel and Gas Turbine Guide, April 23, 2012.

[131] '*Cummins ships Grid Code Compliant gensets*, Data Centre Dynamics, January 14, 2015.

[132] '*Cummins first with grid code Compliant gensets',* Asian Power, 12th June, 2012.

[133] '*QSK60',* www.cummins.com/generators/qsk60.

[134] Olivian Chiver, Liviu Petrean, Liviu Neamt, Zoltan Erdei, '*Study regarding end winding inductance of three phase A.C.windings in a single layer'*, Proceedings of the International Conference on ENERGY and ENVIRONMENT TECHNOLOGIES and EQUIPMENT.

[135] A.Schramm, D.Gerling, '*Analytical calculation of the end winding leakage inductance based on the solution of Neumann integrals'*, Proceedings of the IEEE International Symposium on Industrial Electronics, 2005. ISIE 2005.

[136] P.Chmelicek, '*Synchronous Genrator Reactance prediction using FE analysis'*, Masters Thesis, Brno University of Technology, 2010.

[137] '*Blackout of November 2006:important lessons to be drawn',* European Commission, Press release database.

[138] R.H.Park, '*Two-Reaction Theory of Synchronous Machines, Generalized Method of Analysis – Part 1'*, Transactions of the American Institute of Electrical Engineers, Volume 48, Issue 3, July 1929.

[139] P.L.Alger, *'The Calculation of Armature Reactance of Synchronous Machines',* Transactions of the American Institute of Electrical Engineers, Volume 47, Issue 2, April 1928.

[140] R.H. Park, R.L.Robertson, '*The Reactances of Synchronous Machines',* Transactions of the American Institute of Electrical Engineers, Volume 47, Issue 2, April 1928.

[141] R.H.Park, '*Two-Reaction Theory of Synchronous Machines - Part II'*, Transactions of the American Institute of Electrical Engineers, Volume 52, Issue 2, July 1933.

[142] C.J.Fechheimer, '*Some Factors Affecting Temperature Rise in Armatures of Electrical Machines',* Electrical Engineering, Volume 52, Issue 1, Jan 1933.

[143] M.Stone, '*Parallel operation of A-C generators – Action of governors and damper windings',* Electrical Engineering, Volume 52, Issue 1, Jan 1933.

[144] Harold E. Edgerton, Kenneth J. Germeshausen, Gordon S. Brown, Ralph W. Hamilton, '*Synchronous Motor Pulling-Into-Step Phenomena'*, Transactions of the American Institute of Electrical Engineers, Volume 52, Issue 2, June 1933.

[145] I.Boldea, S.A.Nasar, '*A General Equivalent Circuit (GEC) of Electrical Machines Including CrossCoupling Saturation and Frequency Effects'*, IEEE Transactions on Energy Conversion, Vol 3, No.3, September 1988.

[146] A.M. El-Serafi, J.Wu, '*Determination of the Parameters Representing the Cross-Magnetizing Effect in Saturated Synchronous Machine'*, IEEE Transactions on Energy Conversion, Vol 8, No.3, September 1993.

[146] L.Chedot, G.Friedrich '*A cross saturation model for interior permanent magnet synchronous machine. Application to a starter generator'*, IAS 2004.

[146] Truls Even Hestengen '*Design Optimization of Hydropower Generators'*, Masters' Thesis, June 2016.

APPENDIX 1

Feasibility Studies on using various technologies towards Grid Code Compliance of Engine Driven SGs

A1.1 Introduction

To define the primary path of investigation and to justify the work presented in this thesis, the feasibility of using commonly available technologies / obvious solutions to comply with grid codes was carried out. The below sections describe the various technologies / obvious solutions investigated and the associated findings.

A1.2 Investigation into available technologies / obvious solutions

A1.2.1 High Inertia

The initial investigation focused on understanding how much inertia was required to meet the stringent dynamic response requirements of grid codes. A 1.5 MVA, 400V, 50Hz, generator was simulated. The generator is driven by an engine with a typical inertia constant and is connected to an infinite bus through a transformer. The inertia constant of the generator was varied and its effect on critical clearing time was plotted. Figure A1.1 below shows the graph between inertia constant of the generator. Increased inertia is found to be an effective solution relative to being able to increase the critical clearing time of the generator. However, to achieve a critical clearing time of 250 ms, the generator inertia constant must be closer to 1

second. A typical 1.5 MVA, 400 V generator has an inertia constant of 0.3 seconds and therefore, the required inertia constant requires an increase in inertia by 3 times. While it is shown that an inertia value can be defined, the practicality of such a high increase in inertia is questionable. Figure A1.2 shows the effect of increasing inertial mass on the bearing life. In addition to reducing bearing life, the generator also becomes prohibitively expensive.

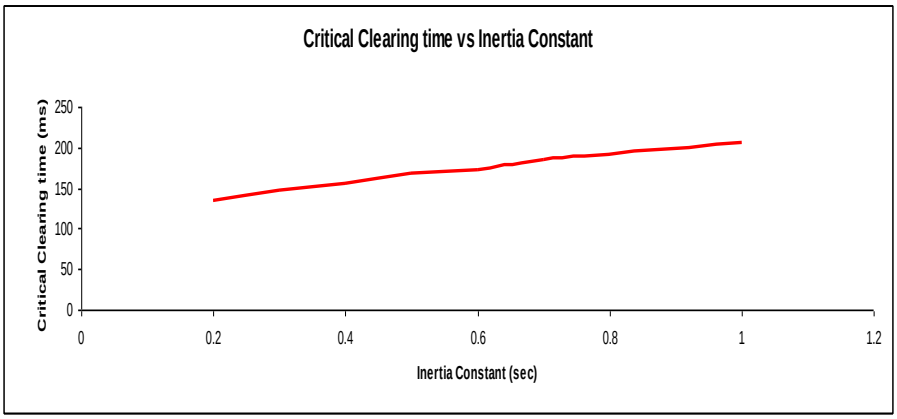


Figure A1. 1: Inertia constant vs Critical Clearing Time

A1.2.2 Transformer Reactance

The generator used in A1.2.1 was also studied to understand the effect of varying transformer reactance on critical clearing time. Figure A1.3 below shows that there is a very small change in critical clearing time for a large increase in transformer reactance. Since transformers are a critical part of the total cost of ownership, it is not practical to select a high reactance transformer only to get a small improvement in system stability.

The transformer reactance therefore like the inertia constant while improves critical clearing time is not a viable solution.

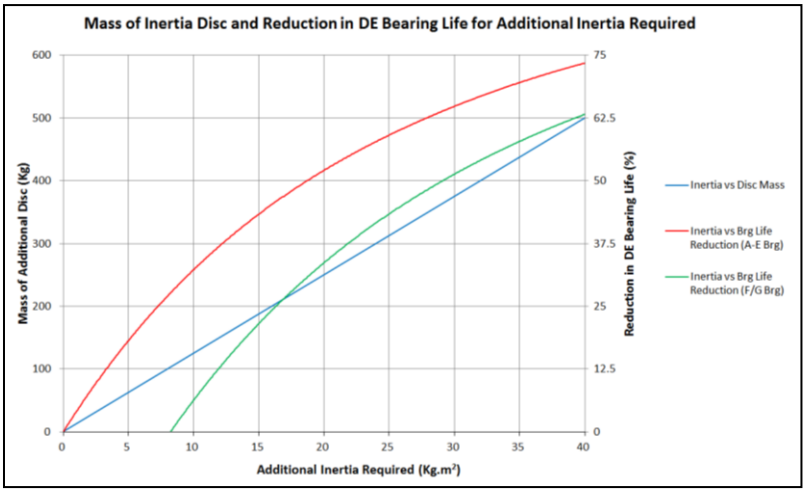


Figure A1.2: Impact of increased inertia on bearing life

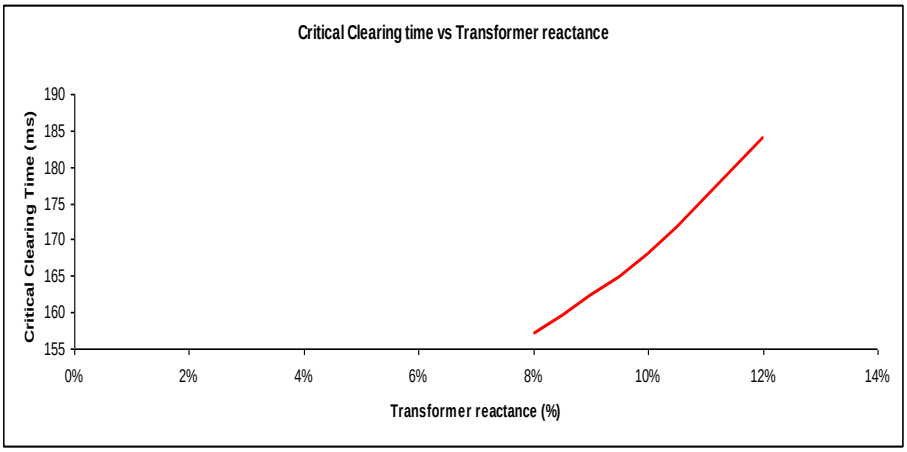


Figure A1. 2: Effect of transformer reactance on critical clearing time.

A1.2.3 Other solutions

A1.2.3.1 Power Electronics

Full power converters have always been used in wind farms to improve the stability of the system. However, in applications that use diesel generators, low initial cost of installation is key. A 1.5 MW full power converter costs approx. $ 250,000, almost 70% of the cost of 1 generating set and therefore making it difficult to justify using full power converters in grid installations with diesel generating sets.

A1.2.3.2 Braking resistors

Braking resistors – series or parallel have been known to provide braking capabilities to grid installations. When connected continuously to the diesel generating set they increase the losses in the system and when switched in to introduce braking only during a transient, leads to undesirable voltage transients that reduce the life of insulation used in the generator. Again, the braking resistors are not a practical solution to improving critical clearing time.

A1.3 Conclusion

From the work completed in this section, it is seen that no conventional solution can be used to achieve grid code compliance practically. Therefore, it is essential to define a set of targets and constraints to find the solution space for a grid code compliant generator.

APPENDIX 2

Exciter Modelling

The excitation system model, as adopted from [89], might be subdivided into three functional sub-systems, representing Automatic Voltage Regulator (AVR), an exciter, and a three-phase uncontrollable rectifier, supplying DC voltage *EFD* to the field winding of a SG such as. The rotor field current *IFD* is fed back to reflect demagnetizing effect of the armature reaction in the exciter rotor. The rotor winding as a load connected to the exciter is predominantly of inductive character, causing the armature reaction flux in the exciter to be aligned in the d-axis of its magnetic circuit. The voltage regulator aims to match the terminal voltage of the alternator with reference voltage value

The discussed AC8B excitation system illustrates Figure A2.1 below.

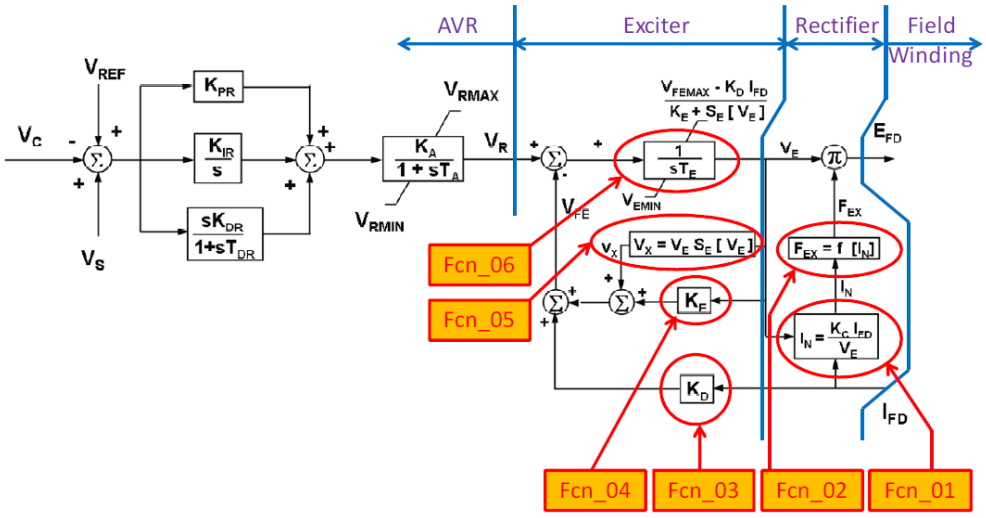


Figure A2. 1: AC8B model of the excitation system with sub-components defined

The uncontrollable three-phase rectifier is modelled by functional blocks “Fcn_01” and “Fcn_02”, followed by four functional blocks from “Fcn_03” to “Fcn_06” responsible for the exciter alternator, and eventually the AVR performing the control action and supplying the exciter field voltage. Variables in terms of their abbreviations follow Figure A2.1, so that they correspond to valid international standards [89].

A2.1 Description of the functional block “Fcn_01”

The functional block “Fcn_01” normalizes the rotor field current I_{FD} vs. the short-circuit current of the three-phase rectifier I_{SC} as the variable I_N.

$$I_N = \frac{I_{FD}}{I_{SC}} \tag{A2.1}$$

The short circuit current of the rectifier *ISC* is defined according to Equation (A2.1) as a ratio of the exciter induced voltage V_E and commutation reactance X_C.

$$I_{SC} = \frac{V}{X_C} \tag{A2.2}$$

The commutation reactance of the rectifier X_C also represents the coefficient K_C according to Figure (A2.1). The commutation reactance X_C (Ω) is frequently assigned to be equal to the transient reactance of the exciter (Ω), if the machine has no amortisseur windings [93]. This is the case for the exciter generator as a part of the excitation system. The commutation reactance may be modelled with a greater level of accuracy as a function of commutation angle δ and sub transient reactances X''_{dE} (Ω) and X''_{qE} (Ω) of the exciter machine, since short circuit in fact occurs during commutation of diodes in the rectifier circuit as shown in Equation (A2.3).

$$X_C = \frac{X''_{dE} - X''_{qE}}{2} \cos\delta \quad \text{(A2.3)}$$

Eventually, the normalized current ratio *IN* is by substituting Equation (A2.2) into Equation (A4.1) defined for base values as shown in Equation (A4.4).

$$I_N = \frac{X_C I_{FD}}{V_E} \quad \text{(A2.4)}$$

Equation (A2.5) characterizing a steady state operation of a three-phase rectifier [94].

$$E_{FD} = \frac{3\sqrt{2}}{\pi} V_E - \frac{3X_{dE}}{\pi} I_{FD} \quad \text{(A2.5)}$$

A4.2 Description of the functional block "Fcn_02"

The functional block "Fcn_02" transduce the normalized current into voltage $F_{EX} = f(I_N)$ according to the rectifier characteristic illustrated on Figure A4.2 below.

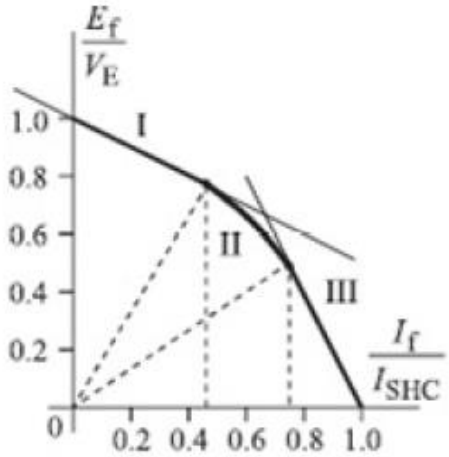


Figure A2. 2: Normalized Volt-Ampere characteristic of uncontrolled rectifier [93]

The above depicted V-A characteristic of the uncontrolled rectifier reflects its three distinct conduction modes [94] depending on the commutation angle of rectifier diodes. Then the main field voltage E_{FD} may be calculated by multiplying the exciter terminal voltage V_E with thus obtained F_{EX}.

A2.3 Description of the functional block "Fcn_03"

The parameter *KD* in the functional block "Fcn_03" represents the armature reaction feedback coefficient, in other words proportionality of the rotor field current I_{FD} to the input of the rectifier [94].

$$K_D = \frac{X_{dE} - X'_{dE}}{k.E_{EB}} I_{FDB} \quad \text{(A2.6)}$$

Where X_{dE} (Ω) and X'_{dE} (Ω) are d-axis reactance and d-axis transient reactance of the exciter respectively. Coefficient $k = 2\sqrt{3}/\pi$ characterizes relation between the AC input rectifier current and the output DC current, hence the field current.

A2.4 Description of the functional block "Fcn_04"

The functional block "Fcn_04" describes the self-excitation coefficient K_E of the exciter. Hence, it is obtained from the no-load curve of the alternator as unity p.u. voltage for zero current in exciter field winding. The value of *KE* ranges $0 < K_E < 1$ in p.u. system.

A2.5 Description of the functional block “Fcn_05”

The saturation characteristic of the exciter describes the functional block “Fcn_05” through functional dependency of the saturation factor *SE* on the exciter AC voltage *VE*. The procedure for calculating *SE* is illustrated on Figure A2.3 below.

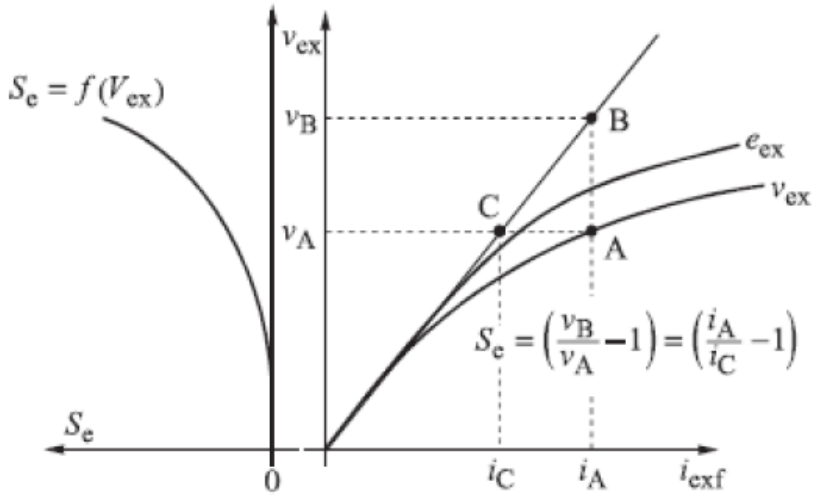


Figure A2. 3: Exciter Saturation Characteristics [93]

Then the exciter saturation factor is calculated as shown in Equation (A4.7).

$$S_E[V_E] = \left(\frac{V_B}{V_A} - 1\right) = \left(\frac{i_A}{i_C} - 1\right) \quad \text{(A2.7)}$$

The B and C are read from *exciter* no-load curve, similar to the main field no-load curve of the alternator. The no load curve must be measured additionally.

A2.6 Description of the functional block “Fcn_06”

The functional block “Fcn_06” contains time constant of the exciter T_E. Hence, it determines response in terms of the exciter rotor voltage V_E. To a step change of a

regulator output voltage V_R, applied to a field winding of the exciter. The exciter field time constant is the ratio of the exciter stator resistance and stator inductance.

APPENDIX 3

An Approximate Numerical Model of End-Winding in SGs

A3.1 Introduction

From an electromagnetic perspective, fault conditions in synchronous machines are transient events that impose loads onto the end winding structure proportional to the square of the instantaneous currents flowing through the end winding. This can be clearly deduced from the Lorentz force equation [123].

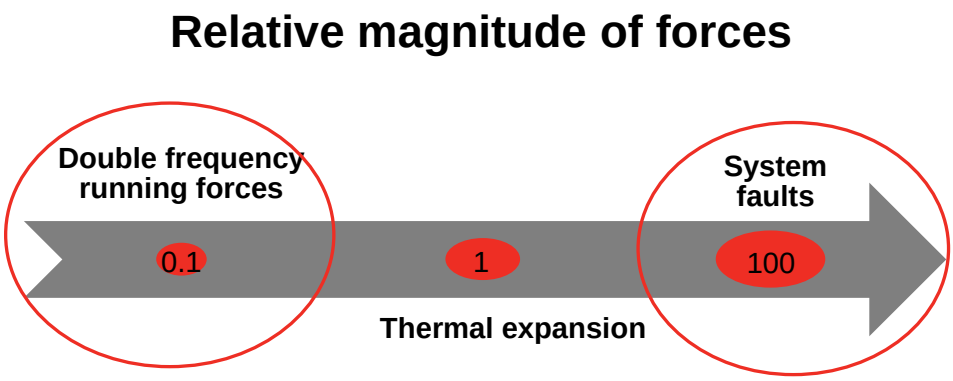


Figure A3. 1: Relative magnitude of forces on SG windings

$$\Delta F = I \times B\Delta L \text{ ---------- (A3.1)}$$

where:

F is the electromagnetic force induced on the current carrying conductor [N]

I is the current flowing through the wire [A]

B is the magnetic field acting on the current carrying conductor [T]

L is the length of the wire considered [m]

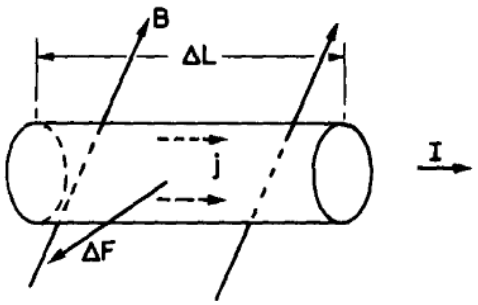


Fig.1 The magnetic force on a current carrying wire is the sum of the individual moving charges [123]

Now, the magnetic field acting on a current carrying conductor from an adjacent wire in the stator end winding can be expressed as (Feynman, 1964):

$$B = \frac{1}{4\pi\varepsilon_0 c^2} \cdot \frac{2I}{r} \quad \text{----------} \qquad [A3.2]$$

where:

ε_0 is the permittivity of free space

c^2 is the relativistic electromagnetic constant = 1

r is the distance between current carrying conductors [m]

Substituting A5.2 in A5.1 gives

$$\Delta F = I \times \left\{ \frac{1}{4\pi\varepsilon_0 c^2} \cdot \frac{2I}{r} \right\} \cdot \Delta L \qquad \text{----------} \qquad (A3.3)$$

Thus:

$$\Delta F \propto I^2 \qquad \text{----------} \qquad \text{(A3.4)}$$

Hence for a synchronous machine going through a short circuit event, with short circuit currents of twelve times nominal [124], this would give electromagnetic forces on the end windings of one hundred and forty-four times nominal. The mechanical implications of such instantaneous shock loads are severe relative to the durability and life time of the synchronous machine.

Furthermore, with the decentralization of power generation to smaller power nodes distributed in the grid (such as for wind, combined heat and power), grid codes are being drawn up which demand grid stability, forcing synchronous machines to remain online during such transient events and thus ensuring a non-intermittent electricity supply to customers.

Similar harsh operating conditions are experienced in emerging countries, where large numbers (40) of small synchronous machines (1.5MVA) are connected in parallel to supply multi-megawatt power in support to inherently weak national grids.

For the requirements of grid connect synchronous machines to be achieved and increase the reliability of the stator end windings, one can:

a) Consider the implementation of power electronics onto the genset to protect the electrical machine from such large transient current spikes
b) Make the windings more robust to withstand the large electromagnetic forces and thus increasing the durability of the winding. This implies that

the windings will be absorbing the energy from the transient event by design.

In both options above, the preferred way forward for implementation on current products should be dictated by a business case for the particular machine. About option (b), the rest of this report shall be dedicated to highlight the work that has been done in this regard

A3.2 Characterizing the behavior of end-windings under transients

To quantify the effects of transient events (in mechanical terms) on the end windings of synchronous machines, one must define:

1. End winding geometry (bar wound/random wound)
2. Electromagnetic loads on the end windings under transient event in consideration
3. Material properties
4. Boundary conditions

An overview of each of the above shall now be given.

A4.2.1 End winding geometry

About geometry used for analysis, synchronous machines can be either bar wound (Figure A3.3) or random (Fig.A3.2) wound. This is largely dictated by the power rating of the machine, synchronous machines designed for prime power tend to be bar wound (e.g. AvK) while standby units (e.g. Stamford) are generally random

wound. Then again, this is also largely dictated by the application at hand and the unit cost of the machine being designed.

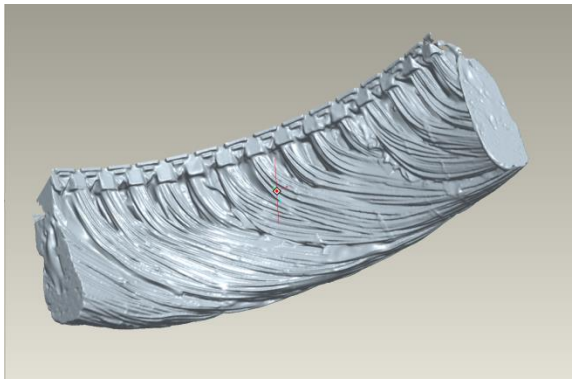


Figure A3. 2: P7 end windings – random wound machine

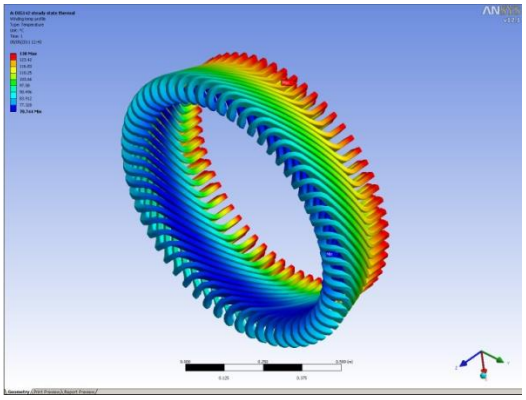


Figure A3. 3 DIG142 – bar wound machine

As shown in Fig.A3.2 and Fig A3.3, random wound machines are inherently more complex to analyze and laser scanning techniques have been used to define the topology of the end regions.

A3.2.2 Electromagnetic loads on the end windings under transient event in consideration

A finite element (FE) analysis of a DIG142 has been carried with short circuit currents. The electromagnetic FE analysis has been carried out using Opera. Due to the three dimensionality of the magnetic field, three force components are present, listed below in order of calculated magnitude:

i. Radial 5kN
ii. Axial 4kN
iii. Tangential 300N

This is consistent with the force magnitudes of these three components computed by Gruning *et al [125]*. In the work presented in [125]. have carried out both finite element analysis and experimental work on a 170MVA air-cooled turbo-generator to deduce deflections of end windings under short circuit conditions. The force components are as per Fig.A3.4 below.

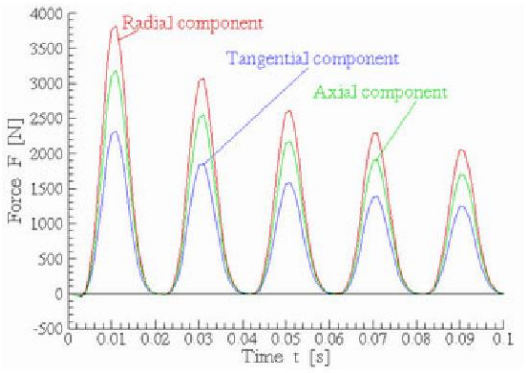


Figure A3. 4: Forces on end-winding under fault conditions [125]

A3.1 Introduction

A critical part in defining this FE problem across the electromagnetic – mechanical domain is the definition of the loads on the mechanical model as a function of the electromagnetic loads under short circuit.

Since electromagnetic forces act on each electron in the copper bars, the most suited way of representing this load in mechanical terms would be in terms of nodal forces. Ideally the same mesh should be used for both electromagnetic and mechanical FE analysis.

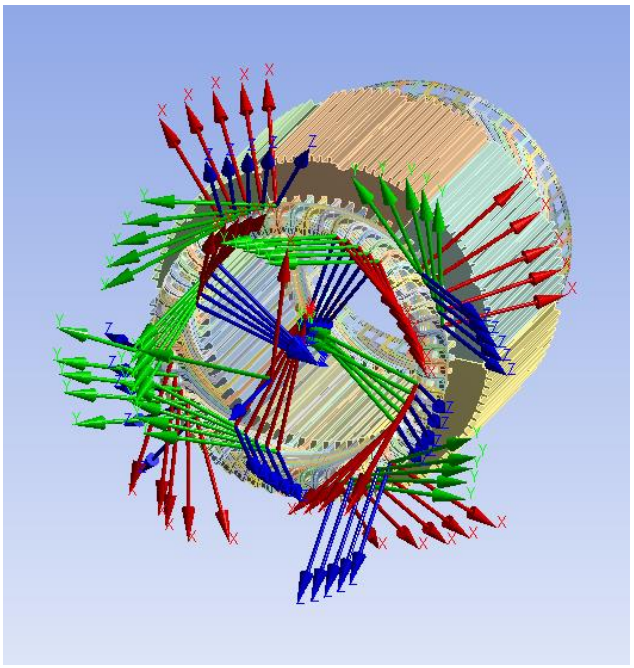


Figure A3. 5: Defining local coordinate systems on individual conductors. Axial, radial & tangential

In the absence of a link between the electromagnetic FE solver (Opera) and ANSYS Mechanical, local coordinate systems were defined on each current carrying conductor and the three forces components were defined.

Also, a full mechanical dynamic analysis for the end windings should be carried out for this transient event. This should be preceded by a modal analysis to determine the natural frequencies of the end winding basket. Then again, the validity of these results should be validated experimentally since the FE geometry neglects a number of mechanical components such as felt pads which contribute to damping of the end winding basket.

In this analysis a first-cut approximation to the mechanical deflection was calculated simply by applying steady state loads to the model.

Furthermore, a load history could be applied to the winding by modeling a unit load on the winding and then applying time history data.

A3.2.3 Material properties

The key to understanding the mechanical behavior of end windings lies in understanding the behavior of different components of the end windings *individually* as well as *collectively*. In both bar and random wound machines, one can identify the following materials:

a) Copper wire/bars
b) Enamel coatings on current carrying conductors
c) Resin / Impregnation liquid (generally a thermosetting polymer)
d) Nomex-Mylar-Nomex phase insulation paper
e) Banding tapes
f) Tie cords

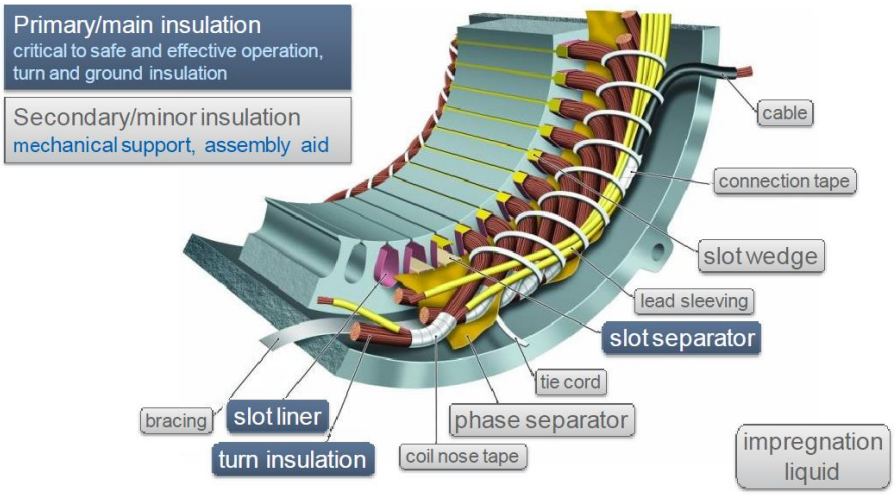


Figure A3. 6 Primary and secondary insulation on random wound machines [126]

It is thus clear that from a material scientist's perspective, the end winding is essentially a composite material. Furthermore, the mechanical properties of the matrix (resin impregnation material) vary significantly as a function of temperature.



Figure A3. 7: Banding tapes used on bar wound machines [124]

Thermosetting polymers typically used for impregnation purposes on random wound machines are usually epoxy based resins, having a glass transition temperature. The glass transition temperature of a thermosetting polymer marks the transition between a glassy state to a rubbery state with inferior mechanical

properties. Fig. A3.8 below shows a Dynamic Mechanical Analysis (DMA) using a Trition Trictec 2000, characterizing the Young's Modulus as a function of temperature. DMA is a standard method of determining the glass transition temperature of a thermosetting polymer.

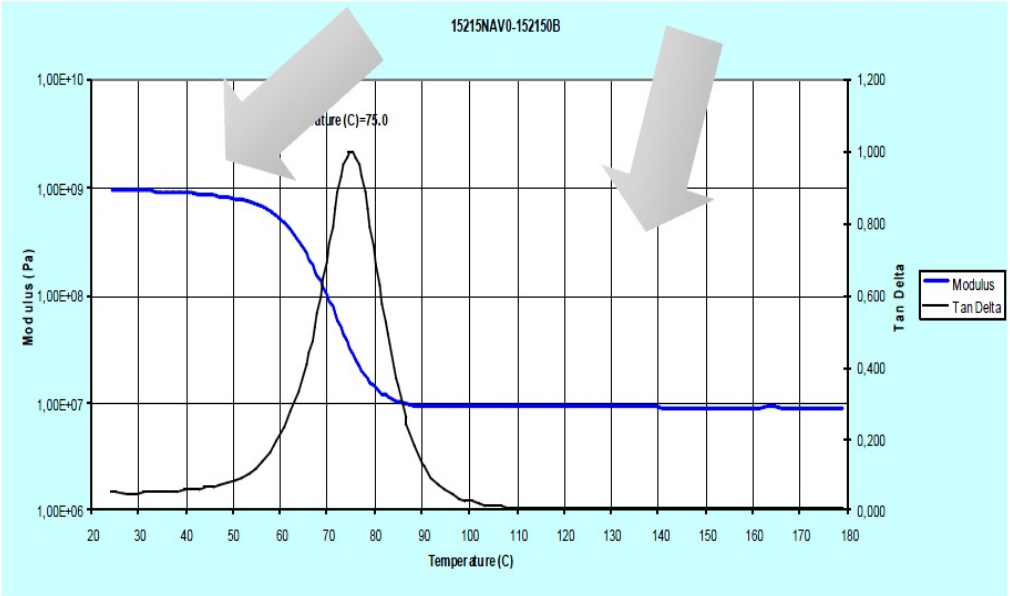


Figure A3. 8: Variation in Young's Modulus as a function of temperature [126]

As shown Figure A3.8, the Young's modulus for an epoxy resin that has gone through the glass transition temperature (at circa 75degC) is two orders of magnitude (100 times) lower than that of the same resin at a temperature below this glass transition temperature.

It is thus clear that a careful characterization of the mechanical properties of impregnating resins is essential to fully understand the deflection of end windings under transient conditions.

Also, Gruning *et al* [125], have carried out experimental work to determine the mechanical properties of a bar wound machine in a servo-hydraulic test facility. This paper summarises inter-disciplinary research between mechanical and electrical engineers over a period of five years to match FE work to experimental deflections gathered from actual machines under test. Gruning *et al* [125], "The bars of the stator winding consist of multiple twisted conductors, each covered with insulating varnish. These are enclosed by epoxy resin impregnated glass silk tape. To obviate the modelling of such a complex structure the bars of the stator end winding were modelled as massive bodies of comparable mass distribution, stiffness and damping characteristics. To determine the stiffness parameters, bending tests were accomplished. Dynamic parameters were estimated by additional oscillation tests. Beside the measurements a detailed mechanical finite element model of a stator bar was implemented and used to compute the parameters of different stator bars numerically. The stiffness parameters of the bandages were determined by conducting static and dynamic tests in a servo hydraulic test facility. Tests at different temperatures showed a significant dependency of the stiffness of the bandages on the temperature."

A rigorous test program has been initiated with Elantas to determine the thermo-mechanical properties of six different resin systems, one of which is the widely used EIP5070. Since the resin is essentially the matrix of the composite body being analysed, an in depth understanding of this insulation component is required.

A3.1 Introduction

The approach that was investigated at Cummins Generator Technologies was the homogenization approach. In this method, the composite material was reduced into a singular body having equivalent mechanical properties.

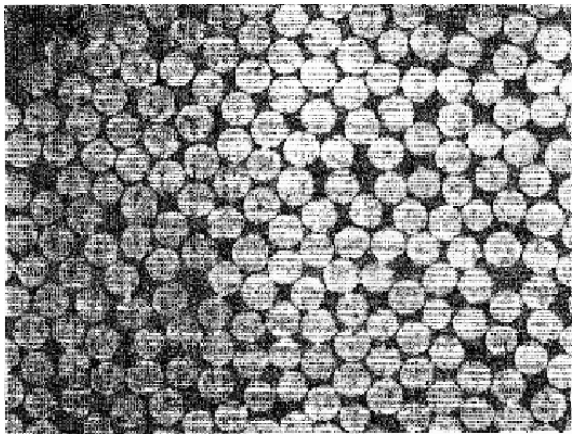


Figure A3. 9 A multi-strand composite material, matrix and fibrous components. Chang Yan (2003)

An equivalent Young's Modulus and Poisson's ratio was deduced from the rule of mixture Chang Yan [127].

$$E_{equivalent} = \left(E_{fibre} \cdot V_{fibre}\right) + \left(E_{matrix} \cdot \left(1 - V_{fibre}\right)\right) \text{ ---------- (A3.5)}$$

$$\upsilon_{equivalent} = \left(\upsilon_{fibre} \cdot V_{fibre}\right) + \left(\upsilon_{matrix} \cdot \left(1 - V_{fibre}\right)\right) \text{ ----------(A3.6)}$$

where

E is the Young's Modulus [MPa]

υ is Poisson's ratio

V_{fibre} is the volume fraction of fibers in the composite body

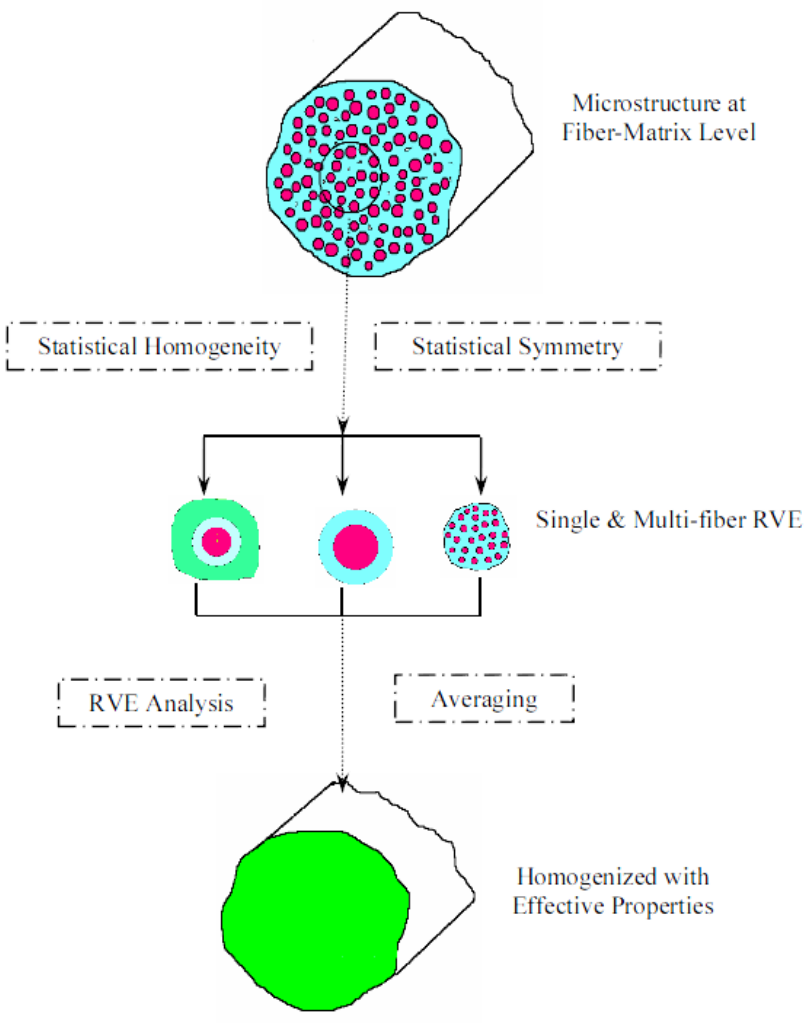


Figure A3. 10 Homogenization approach for composite materials. Chang Yan (2003) [127]

A3.2.4 Boundary conditions

As with all FE work, boundary conditions dictate the accuracy of FE models to real life situations. In the DIG142 analysis, the end winding basket was given a fixed support at the interface between the end winding and the stator core pack.

A3.1 Introduction

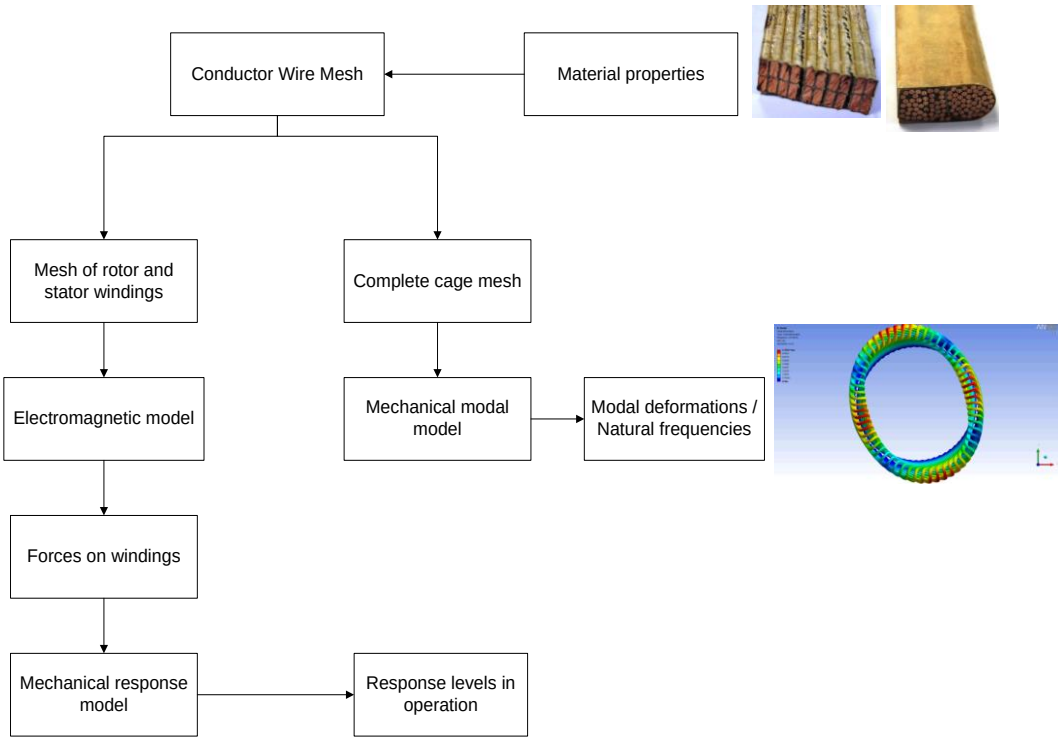


Figure A3. 11: Method of simulation of end-winding movement

The results for the end winding deflections of DIG142 under short conditions are displayed below:

A3.1 Introduction

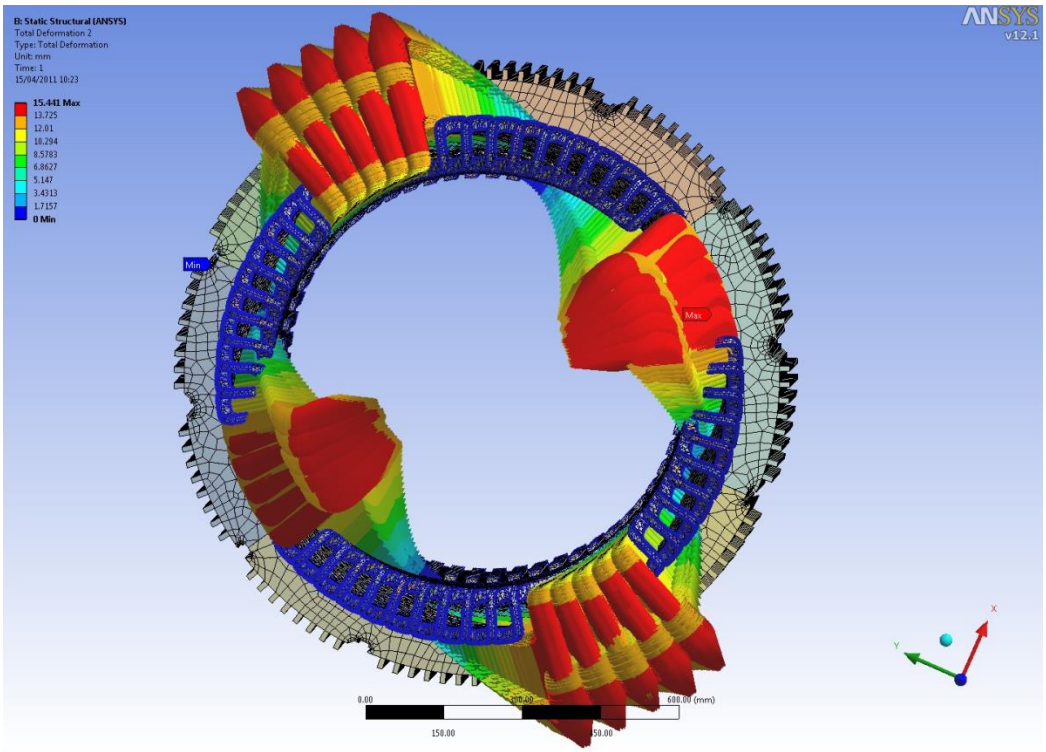


Figure A3. 12 DIG142 deflections under short circuit

These results have been obtained with the following assumptions:

I. Conductor bars are pure copper

Young's modulus = 110 GPa

Poisson's ratio = 0.34

Yield stress = 280 MPa

Ultimate tensile stress = 430 MPa

II. Electromagnetic forces loaded with local coordinate system

These assumptions give the model a low fidelity ranking, and the maximum deflection calculated (15mm) is surely not the case in practice. About the deflected

shape of the end winding, the shape that the model has assumed is consistent with result obtained by Gruning *et al*[125]. (Figure A3.13)

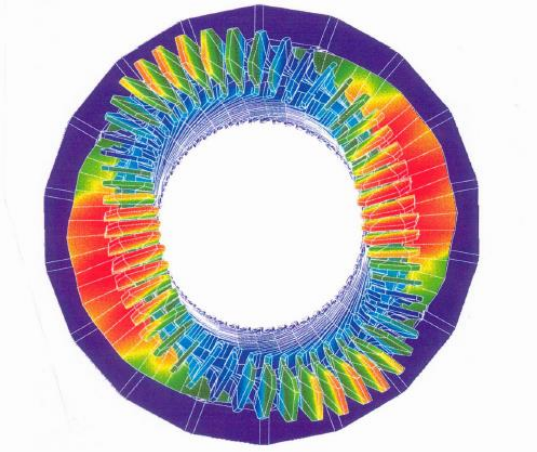


Figure A3. 13 Deflected end winding basket under short circuit conditions.

Gruning *et al*[125].

Location of coil nose	Displacement			
	Computed		Measured	
	Tangential [μm]	Radial [μm]	Tangential [μm]	Radial [μm]
3 h	934	1216	–	1174
6.75 h	1059	1055	558	1215
7.5 h	1344	1220	–	877
9 h	931	1159	879	934
9.75 h	925	1103	–	1502
10.5 h	874	1021	1068	1644
11.25 h	1003	989	–	993

Figure A3. 14 Computed and measured values for end winding deflection.

Gruning *et al* [125].

As can be seen from Figure A3.14, the end winding deflection for a 170MVA machine under short circuit is circa 1mm. This further proves the assumption (I)

taken in the DIG142 analysis to be incorrect. Furthermore, Gruning *et* al [125]. confirm in their work the need for accurate characterization of the end windings as a function of temperature in the previous section.

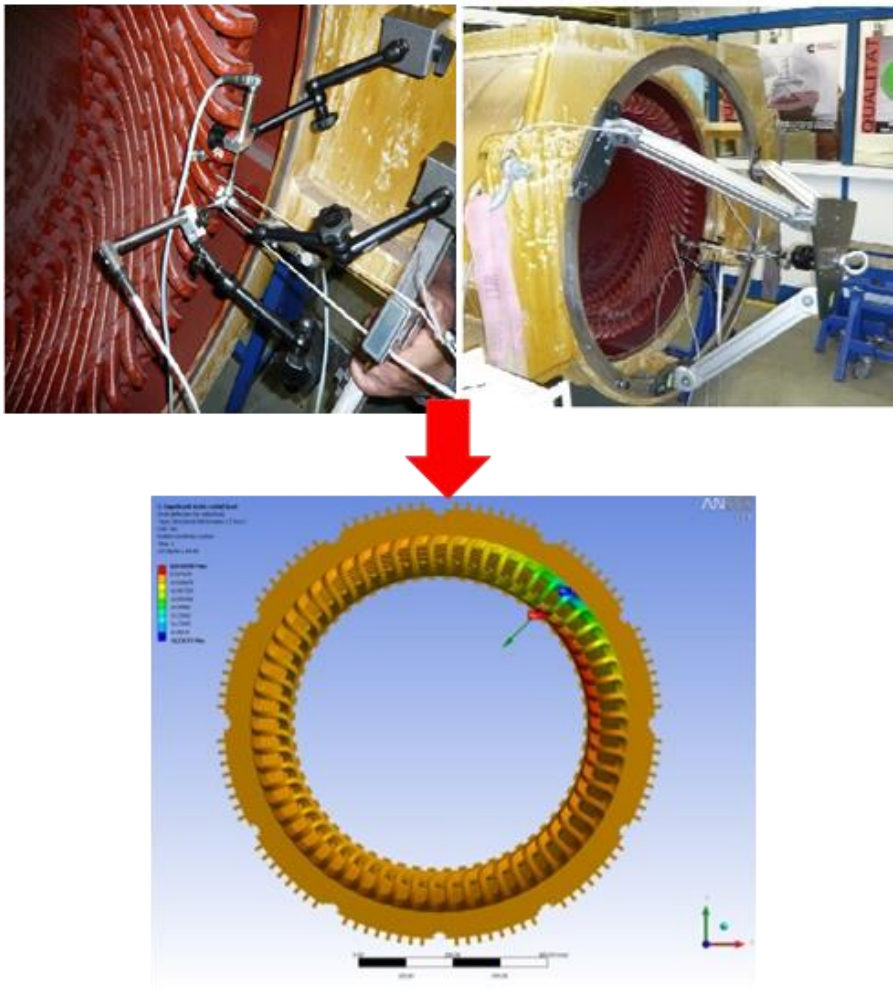


Figure A3. 15: Test method developed to measure coil mechanical properties at various temperatures.

APPENDIX 4

An Analytical Tool to predict steady state stability of SGs

A4.1 Introduction

A prime mover drives the rotor of the SG and exerts a mechanical torque T_{mech}. The machine develops an equal, but opposing, electromagnetic torque T_{em} that is defined by the load (and therefore the current) on the SG stator windings. The electromagnetic torque induced due to the interaction between the stator and rotor magnetic fields keeps the speed of the SG constant. The air-gap mmf can be resolved into its constituent stator and rotor components. These mmfs are similar to two magnets rotating with the same speed trying to align their magnetic fields. The electromagnetic torque Tem between the stator and rotor is given by (A4.1).

$$T_{em} = \frac{\pi}{2}\varphi_f F_r \sin\delta_{fr} + \frac{\pi}{4}F_r^{\,2}\frac{R_q - R_d}{R_q R_d}\sin 2\delta_{fr} \qquad \text{---------- (A4.1)}$$

Where, δ_{fr} is the torque angle, Fr is the air-gap mmf and R_d and R_q are the d and q axis reluctances respectively and Φ_f is the main field flux.

Fig. A5.1 is Phasor diagram representing a salient-pole SG. Vg is the terminal voltage and I is the current. The suffixes d and q represent the d and q axis quantities respectively. From Figure A4.1, the load angle δ_g is given by Equation (A4.2).

$$\delta g = \arctan\left(\frac{\cos\varphi_g}{\frac{V_g}{IX_q} - \sin\varphi_g}\right) \qquad \text{---------- (A4.2)}$$

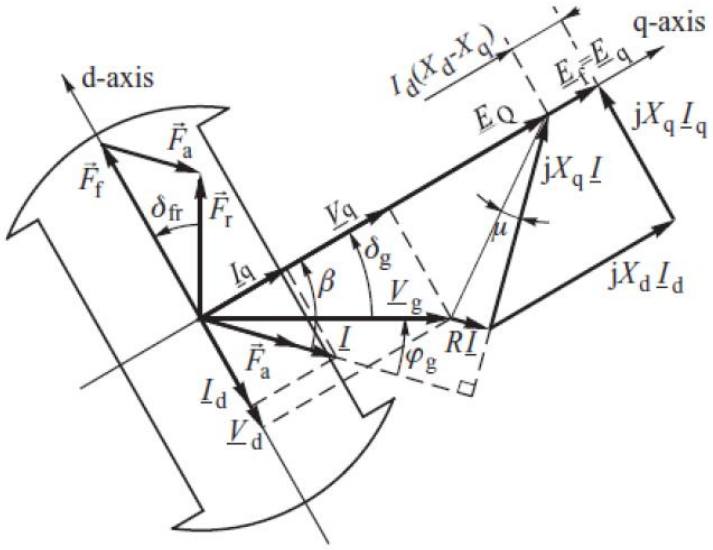


Figure A4. 1: Phasor diagram for salient-pole generator

and using similar assumptions, the internal emf E_f is given by

$$E_f = IX_d \sin(\delta_g - \varphi_g) \quad \text{---------- (A4.3)}$$

From Equation (A4.3) and Fig.A4.1, φ_g is calculated as

$$\varphi_g = \delta_g - \arctan\left[\frac{X_q}{X_d}\right]\left(\frac{E_f}{V_g \sin\delta_g} - \frac{1}{\tan\delta_g}\right) \quad \text{---------- (A4.4)}$$

From Equation (A4.2), the value of I is derived.

$$I = \frac{V_g}{X_q}\left(\frac{1}{\frac{\cos\varphi_g}{\tan\delta_g} + \sin\varphi_g}\right) \quad \text{---------- (A4.5)}$$

A4.2 Tool Development

Equations (A4.1) – (A4.5) completely describe the steady-state operation of a salient-pole SG.

We shall use the load angle as an indicator of the stead-state performance. If the load angle crosses the 'stead-state limit', the machine is unstable for the given load condition. The other requirement we will be enforcing is that at the worst-case condition, the alternator has 10% reserve left, so any further increase in mechanical power can be compensated by the electromagnetic torque. With these assumptions in mind, we shall describe the steps involved in calculating the load angle and the amount of reserve left at the worst case.

	A	B	C	D	E	F	G	H
1	**Input(s)**							
2								
3								
4	U/Un	0.9	pu			Power Rating	1.55	MVA
5	S/Sn	0.58	pu			Voltage(ph-ph RMS)	0.4	KV
6	p.f	0.9	lead			Zbase	0.103225806	ohms
7	Xdsat (calculated)	1.99062	pu			Xdsat (datasheet)	2.78	pu
8	Xqsat (calculated)	1.27457	pu			Xqsat (datasheet)	1.78	pu
9						Ld (original)	0.000913447	henry
10						Lq (original)	0.000584869	henry
11	**Calculation**					wn	314.1592654	rad/sec
12						H	0.5	sec
13	SCR	0.50236				f	50	Hz
14	PHI	0.45103	radians	25.84193276	degrees	Ld (original - fixed)	0.000913	henry
15	Ireal	0.64444	pu			Lq (original - fixed)	0.000585	henry
16	Iim	0	pu			Adjusted Base Power	Reduce Power	MVA
17	I/In	0.64444	pu					
18	Edeltareal	0.54197	pu					
19	Edeltaim	0.73925	pu					
20	Edeltamag	0.91663	pu					
21	delta	0.93818	radians	53.7537751	degrees	load angle		
22	theta	0.48715	radians	27.91184234	degrees			
23	Ef	1.13265	pu					
24								
25								

Figure A4. 2: Snapshot of analytical tool developed to predict static stability

1. Inputs – grid voltage (as a % of rated voltage), power demand (% rated kVA), power factor at the point of common coupling, rated power, voltage of the alternator, X_{dsat}, X_{qsat}.

2. Calculate current from load and voltage.

3. Real component of internal emf is calculated using Figure A4.1.

4. Imaginary component of internal emf is calculated using Figure A4.1.

5. The magnitude of the net internal emf is then the vector sum of the real and imaginary parts and the angle theta would then be the angle θ between the real and imaginary parts.

6. The sum in case of lagging power factor (difference in case of leading power factor.) of θ and the power factor angle is the load angle.

7. Map load angle versus total torque developed, reluctance torque and electromagnetic torque.

8. Using the table from above, find the maximum Torque and the corresponding value of load angle.

9. Calculate ratio of torque at given load to maximum torque possible – must be greater than 10% [30].

10. If both the load-angle and torque reserve conditions are fulfilled, the alternator is grid-code compliant, otherwise, de-rate.

A4.2 Tool Validation

The rating of the alternator has been listed in Table. A4.1. The reactance values of the alternator were determined using Finite Element Analysis (Fig. A4.3a. and Fig.

A4.3b). These values were then used in the Excel tool developed (Fig. A4.2). The alternator is assumed to run at rated load and the load angle at which the pull-out torque occurs is calculated using the above tool. An experiment to verify the results of the tool shown in Figure A4.2 was completed. The load angle when the test alternator pole-slipped was measured. The results of the test as compared against the calculation are listed in Table. A4.2.

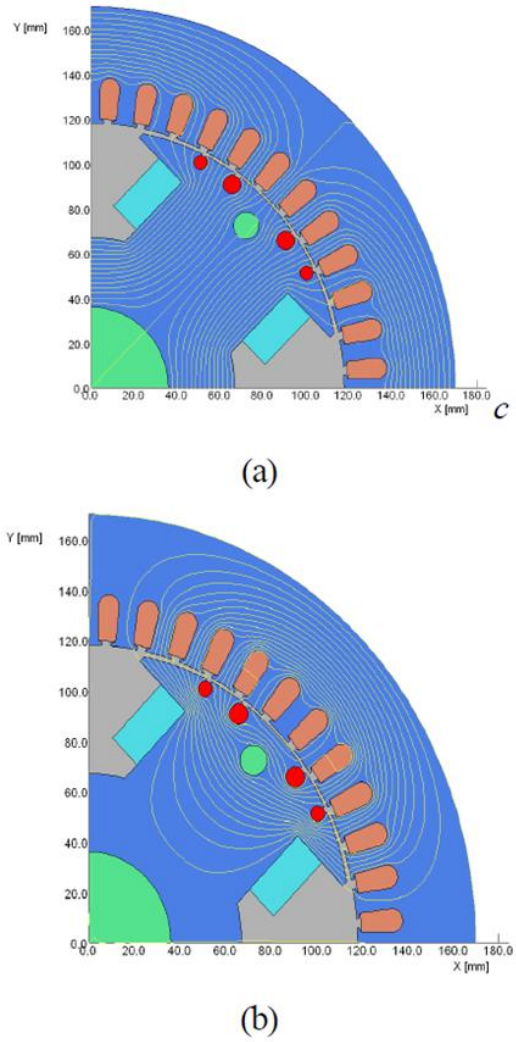


Figure A4. 3: Finite element models to predict reactance.

A4.2 Tool Validation

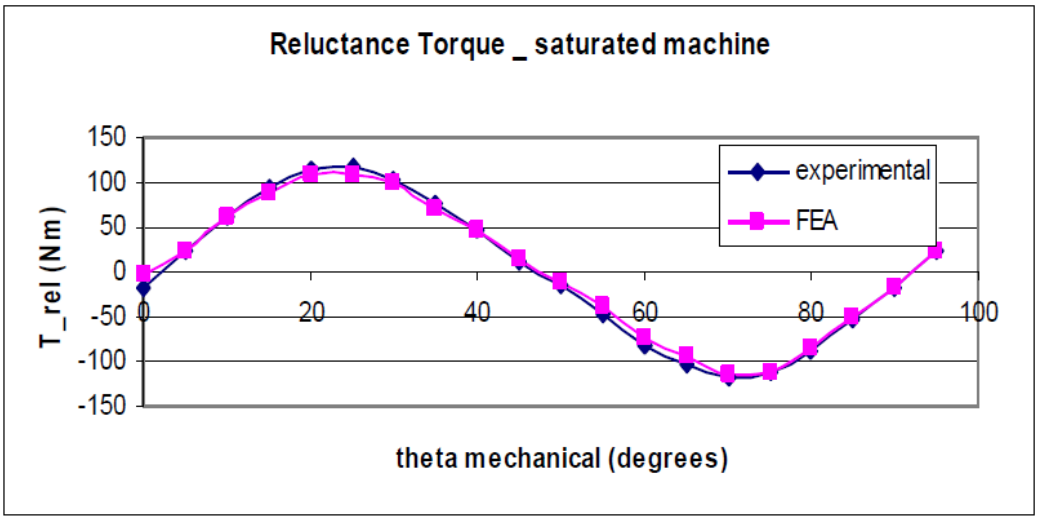


Figure A4. 4: Reluctance torque predicted vs tested

Table A4. 1: Data for test machine

Quantity	Value with units
Power	42.5 KVA
Voltage (ph-ph RMS)	380 V
X_{dsat} (from FEA)	2.11 pu
X_{qsat} (from FEA)	1.14 pu

Table A4. 2: Validation of tool predictions

Load Angle at 'Pull –Out' Point	Value (degrees)
Calculated	70
Measured	72

A4.3 Discussion

The tool thus developed was used to determine the stability of a SG under steady state grid code conditions. Using the tool various static grid code conditions were studied and the observations have been summarized below.

a. A salient-pole SG has better pull-out torque than a cylindrical rotor equivalent, so the chance of unstable steady-state operation is lower.

c. The alternator operating at a terminal voltage lower than rated voltage at a leading power factor condition at the point of common coupling is the worst from a static stability perspective.

d. As a rule, $X_{dsat} \leq 2.22$ pu or a short-circuit ratio $(1/X_{dsat}) \geq 0.45$ helps an alternator to remain stable.

e. It is seen that an oversized alternator that meets the above minimum short-circuit ratio criteria can meet the grid-code requirements. It is also interesting to note that some grid codes have placed a lower limit of 0.45 on the short-circuit ratio.